The University of Nottingham

UNITED KINGDOM · CHINA · MALAYSIA

Therapeutic intracellular delivery using magnetic fields, nanoparticle technology and enhanced cell penetrating peptides

Lia Andrea Blokpoel Ferreras, MSc

Thesis submitted to the University of Nottingham for the degree of Doctor of Philosophy

September 2018

Abstract

The aim of this project was to develop a platform technology for the delivery of Magnetic Nanoparticles (MNPs). The delivery system is based on the incorporation of newly formulated multi domain delivery peptides termed GET (Glycosaminoglycan Enhanced Transduction) to biocompatible dextran coated iron oxide nanoparticles. GET synergistically combines a cell penetrating domain with a heparan sulphate binding unit and it has been previously demonstrated to efficiently deliver a wide range of cargoes without the disadvantages of a cell penetrating peptide such as cytotoxicity or low functionality of the delivered cargo.

This technology was initially optimised for the delivery of MNPs as a theranostic complex with application to *in vivo* relevant environments and then tailored for magnetically mediated gene transfer for its application on modified cell therapies.

Significant advancement has been made in the last couple of years in the development of MNP based therapies. Their applications rely on their physicochemical and magnetic properties and range from drug delivery systems for targeting therapeutics, to contrast agents for Magnetic Resonance Imaging (MRI), including their use in hyperthermia, cell and protein sorting or direct iron delivery. The most frequent application of MNPs in the clinic is in MRI with several MNP formulations already approved by the Food and Drug Administration (FDA).

MNPs as gene delivery vectors allow for targeted gene transfer to a specific area by means of an external magnetic field (magnetofection). Although the potential of MNPs as drug/gene targeting agents has been consistently reported *in vitro,* their

performance in preclinical studies has not been as successful. The main challenges that have prevented the incorporation of MNPs as targeted delivery systems include on the one hand, the alteration of the physicochemical properties of MNPs when they enter in contact with biological environments which makes it difficult to predict their behaviour *in vivo*. On the other hand, the lack of systems capable to generate a precise magnetic field capable to concentrate particles on a specific area against blood flow has restricted successful uptake in the targeted area *in vivo*. Since magnetic force is a function of the distance between the particle and the source of the magnetic field, this task becomes more complex the deeper the organ is inside the body. Asides from improving biomedical magnetic field settings, current efforts are focused on the formulation of stable (resistant to modification by interaction with biological matrixes) and long circulating MNPs that favour the fast cellular uptake at the target site, in order to reduce the need of long retention times at the target site.

GET was able to safely mediate sustained intracellular transduction of MNPs even in the presence of plasma proteins.

In order to exploit the ability of GET to promote the intracellular transduction of MNPs for gene delivery purposes, a modified version, able to efficiently condense DNA was conjugated with MNPs to develop a magnetic gene delivery vector.

GET-MNPs mediated magnetofection significantly improved gene transfer speed achieving transfection efficiencies compared to commercially standard reagents in 1 hour. Additionally, external manipulation of the MNPs after delivery by the application of an external magnetic field, further enhanced transfection efficiency.

Overall the two formulations of GET-MNPs were able to efficiently and safely deliver their cargo *in vitro*. With further development GET-MNPs could provide a flexible and tuneable platform technology for MNPs therapeutic delivery *in vivo*.

Outputs

Publications

Anastasios Spiliotopoulos, **Lia Blokpoel Ferreras**, Ruth M. Densham, Simon G. Caulton, Ben C. Maddison, Joanna R. Morris, James E. Dixon, Kevin C. Gough and Ingrid Dreveny. **Discovery of USP11 peptide ligands targeted to a novel ubiquitin-like domain binding site**. Journal of Biochemical Chemistry. Accepted July 2018.

Hareklea Markides, Karin Newell, Heike Rudorf, **Lia Blokpoel Ferreras**, James Dixon, Robert Morris, Martin Graves, Joshua Kaggie, Frances Henson and Alicia El Haj ***In vivo* MRI Cell Tracking of Autologous Mesenchymal Stem Cells in an Ovine Osteochondral Defect Model**. (2017). Stem Cell Research & Therapy. Submitted July 2018.

Publications in preparation

Lia Blokpoel Ferreras, Hareklea Markides, Daniel Scott, Robert Layfield, Saul Vazquez Reina, Scott Young, Kevin M. Shakesheff and James E. Dixon, **Enhanced cellular transduction of nanoparticles resistant to rapidly-forming plasma coronas.** Manuscript complete/awaiting submission.

Poster Presentations

pH-inducible GET peptides for delivery of therapeutics to tumours. Drug Delivery Workshop Children with Cancer, 2016, London, UK.

pH-inducible GET peptides for targeted intracellular delivery of Theranostics. Britain Israel Research and Academic Exchange (BIRAX) in Regenerative Medicine, 2016, Oxford, UK.

Magnetic and pH inducible targeting of pediatric tumours. Centre of Doctoral Training (CDT) Cross Cadre meeting, 2016, Loughborough, UK.

Characterising the enhanced intracellular delivery of Magnetic Nanoparticles by GET. CDT Joint Conference, 2016, Manchester, UK.

pH-inducible GET peptides for targeted intracellular delivery of Theranostics. Tissue and Cell Engineering Society (TCES), 2016, London, UK.

Enhanced delivery of Magnetic nanoparticles by GET. CDT Cross Cadre meeting, 2017, Keele, UK.

Enhanced delivery of Magnetic nanoparticles by GET. Tissue Engineering and Regenerative Medicine (TERMIS EU), 2017, Davos, Switzerland.

Oscillating magnetic fields post-transfection promotes enhanced transgene expression for GET-mediated transfection. British Society for Gene and Cell Therapy (BSGCT), 2017, London, UK.

Oral Presentations

Characterising the Enhanced Intracellular Delivery of Magnetic Nanoparticles by GET. Future Investigators in Regenerative Medicine (FIRM), 2016, Girona, Spain.

Enhanced Delivery of Magnetic Nanoparticles by GET and its applications. CDT Cross Cadre meeting, 2018, Nottingham, UK.

Oscillating magnetic fields post-transfection can promote endosomal escape and enhanced transgene expression for GET-mediated transfection TERMIS World Congress, 2018, Kyoto, Japan.

Acknowledgements

I would like to first thank my first supervisor Dr James Dixon for all the support and guidance throughout this project. He has basically tought me pretty much everything I know about cell biology. His passion and determination have encouraged me to work hard and make the most of my PhD. His support and guidance have been constant and has has gone out of his way to help me, even when I was far far away and there was little he could really do. I would also like to thank my secondary supervisor Professor Kevin Shakesheff for his input into the project. Thanks to all my colleagues at the RMCT group for helping me out whenever I needed. I would like to express my gratitude to Professor Gerardo Fabian Goya for welcoming me to his laboratory at Universidad de Zaragoza and for his support afterwards, most of all the physics and magnetism I know has been all his doing. Special thank you to Dr Jon Dobson and his team for also initally welcoming me to his laboratory at the University of Florida and then prolonging my placement further. In particular I would like to thank Olivia Lanier, for her love to magnetic nanoparticles and Obiora Azie for his help out of hours. The most special thank you goes to my family for all their constant emotional and finantial support. Thanks to my parents Margarita and Christiaan for putting up with me like nobody else does. To my abuelito Cayo because he was always there for a chat and to my abuelita Curra for the meals that powered my writing. I would like to also thank my friends, in particular Alicia Perez, because without her support I would not have been able to cope and my partner Kevin, because life outside the laboratory is as important, and without them I would not have enjoyed the process as much as I have. Lastly I would like to thank Skittles, Pixie and Wendy for their love and attention.

Acknowledgements

This thesis is dedicated to all my family members, particulartly to my parents Margarita Ferreras and Christiaan Blokpoel and my brother Marco Blokpoel Ferreras. I would not have been able to do this without you.

Appendix

List of Figures

List of Tables

Glossary

AAV	Adeno-associated virus
ADA	Adenosine Deaminase
AMF	Alternating Magnetic Field
ATCC	American Type Culture Collection
AUC	Area Under the Curve
BCA	Bicinchoninic acid
BIRAX	Britain Israel Research and Academic Exchange
Bp	Base pair
BSA	Bovine Serum Albumin
BSA	Bovine Serum Albumin
BSGCT	British Society for Gene and Cell Therapy
CAR	Chimeric antigen receptor
CDT	Centre of Doctoral Training
CLSM	Confocal laser scanning microscopic
CME	Clathrin mediated endocytosis
CMV	Cytomegalovirus
CPP	Cell Penetrating Peptide
CRE	CAMP Response Element
DCs	Dendritic cells
DLS	Dynamic light scattering
DMEM	Dulbecco's modified Eagle´s media
DNA	Deoxyribonucleic acid
DPSS	Diode-pumped solid-state
DTS	DNA Targeting Sequence
EBNA-1	Epstein–Barr virus nuclear antigen 1
EBV	Epstein–Barr virus
EDTA	Ethylenediaminetetraacetic acid
EGF	Epidermal Growth Factor
EIPA	5(N-ethyl-N-isopropyl) amiloride
FACS	Fluorescence activated cell sorting
FCS	Foetal Calf Serum
FCS	Flow Cytometry Standard
FDA	Food and Drug Administration
FGF	Fibroblast Growth Factor
FIRM	Future Investigators in Regenerative Medicine
FLR	FGF2B-LK15-8R
Fmoc	Fluorenylmethyloxycarbonyl chloride
FTIR	Fourier-Transform Infrared Spectrometry
GAG	Glycosaminoglycan
GET	Glycosaminoglycan Enhanced Transduction
GFP	Green Fluorescent Protein
GLuc	Gaussia Luciferase
GMP	Good Manufacturing Practise

HBD	Heparin Binding Domain
HBSS	Hank's Balanced Salt Solution
HEPES	4-(2-hydroxyethyl)-1-piperazineethanesulfonic acid
HIV	Human Immunodeficiency Virus
hMSCs	Human Mesenchymal Stem Cells
HSE	Health and Safety Executive
HTA	Health Technology Assessment
ICP-MS	Induced Coupled Plasma Mass Spectrometry
IMS	Industrial Methylated Spirit
LB	Luria broth
LC-MS	Liquid Chromatography-Mass Spectrometry
LHRH	Luteinizing hormone releasing hormone
LPLD	Lipoprotein Lipase Deficiency
MBCD	methyl-B-cyclodextrin
MHT	Magnetic Hyperthermia
MNPs	Magnetic nanoparticles
mRFP	Monomer Red Fluorescent Protein
MRI	Magnetic Resonance Imaging
MSC	Mesenchymal Stem Cells
N/P ratio	Ratio between amine (NH_2) groups in a vector and phosphate (PO_3) groups in DNA
NC	Nanocrystals
NEB	New England Biolabs
NPs	Nanoparticles
NSAF	Normalized Spectral Abundance Factor
PBS	Phosphate-buffered saline
PDI	Polydispersity Index
PE	Phycoerythrin
PEG	Poly(ethylene glycol)
PFA	Paraformaldehyde
PLGA	Poly(lactic-co-glycolic acid)
PPR	Protein Peptide Research
PR	P21-8R
PR-T	P21-8R-TAMRA
PTD	Protein Transduction Domain
PVA	poly(vinyl alcohol)
PVP	Poly (vinylpyrrolidone)
RFU	Relative Fluorescent Units
RGD	Arginine glycine aspartic acid
Rh-DNA	Rhodamine-labelled DNA
RISC	RNA-induced silencing complex
RLU	Relative Light Units
RMCT	Regenerative Medicine and Cell Therapy group
RNA	Ribonucleic acid
RUNX2	Runt-related Transcription factor 2
S/MARs	Scaffold/Matrix Attachment Regions

SCID	Severe Combined Immunodeficiency
SDS-PAGE	Sodium Dodecyl Sulphate-Polyacrylamide Gel Electrophoresis
SFM	Serum Free Media
SOC	Super Optimal broth with Catabolite repression
SOP	Standard Operating Procedure
SPIONs	Superparamagnetic Iron Oxide Nanoparticles
SSR	Sum of Squared Residuals
SV40	Simian Virus 40
TAMRA	Carboxytetramethylrhodamine
TAT	Transactivator of Transcription
TCES	Tissue and Cell Engineering Society
TEM	Transmission Electron Microscope
TERMIS	Tissue Engineering and Regenerative Medicine
TGA	Thermogravimetric Analysis

1 Introduction

The development of new therapeutic molecules with novel targets and sites of action compared with conventional drugs, requires for enhanced delivery systems. In order to be able to efficiently translate these delivery systems into the clinic, it is important to fully understand the requirements of a specific therapy and assess how that could be achieved starting with the currently existing technologies.

This introduction will provide a brief overview on two recently developed delivery systems that are currently under optimisation but have so far not achieved translation to the clinic: Magnetic Nanoparticles (MNPs) and Cell Penetrating Peptides (CPPs) with specific interest on their current clinical applications, their strengths and limitations and their applications to gene delivery.

1.1 Magnetic Nanoparticles (MNPs)

Nanomedicine uses nano-sized tools for the diagnosis, prevention and treatment of disease, in addition to improving the understanding of underlying pathophysiology. In this context, nanoparticles (NPs) are defined as particles with a size between 1 and 1000 nm (i.e. on a nanometre scale)[1], their small size makes them suitable for penetrating biological barriers, concentrating in tumours and mediating intracellular delivery. In the past few decades a wide range of NPs have been developed for their use in medicine.[2] Special interest has been paid to MNPs. MNPs physicochemical properties like size, surface area, adsorption kinetics and biocompatibility, can be finely tuned by means of their synthesis.[3] Additionally, their magnetic properties allow for external manipulation with an applied magnetic field. This option has been

exploited for applications *in vivo* such as concentration of MNPs on a specific site or localised heating through the application of an alternating magnetic field The latter was, in fact, the first biomedical application of magnetic particles back in 1957 where micron sized magnetic particles were used to heat metastatic lymphatic nodes.[4]

1.1.1 Magnetism

Every atom is formed by a positively charged nucleus surrounded by negatively charged electron(s) creating an atomic magnetic dipole between the nucleus and each individual electron. When all these dipoles in an atom cancel out, the atom is said to have no magnetic dipole, however, if these individual dipoles do not cancel out their combination forms a permanent magnetic dipole. How strong that magnetic dipole is, is called the dipole moment and can be simplistically described as the capacity of the dipole to align with an external magnetic field (H). The alignment of the magnetic moments within a material causes a net magnetic moment defined as magnetization(M) which is proportional to the magnetic field applied.[5]

$$M = \chi H \qquad (1)$$

Where χ is defined as the magnetic susceptibility constant of a particular material. Based on their susceptibility magnetic materials can be classified as ferromagnetic, diamagnetic, paramagnetic and superparamagnetic. Ferromagnetic materials present a very large positive susceptibility whereas diamagnetic materials exhibit weak repulsion in the presence of a magnetic field with negative susceptibility constants.[6]

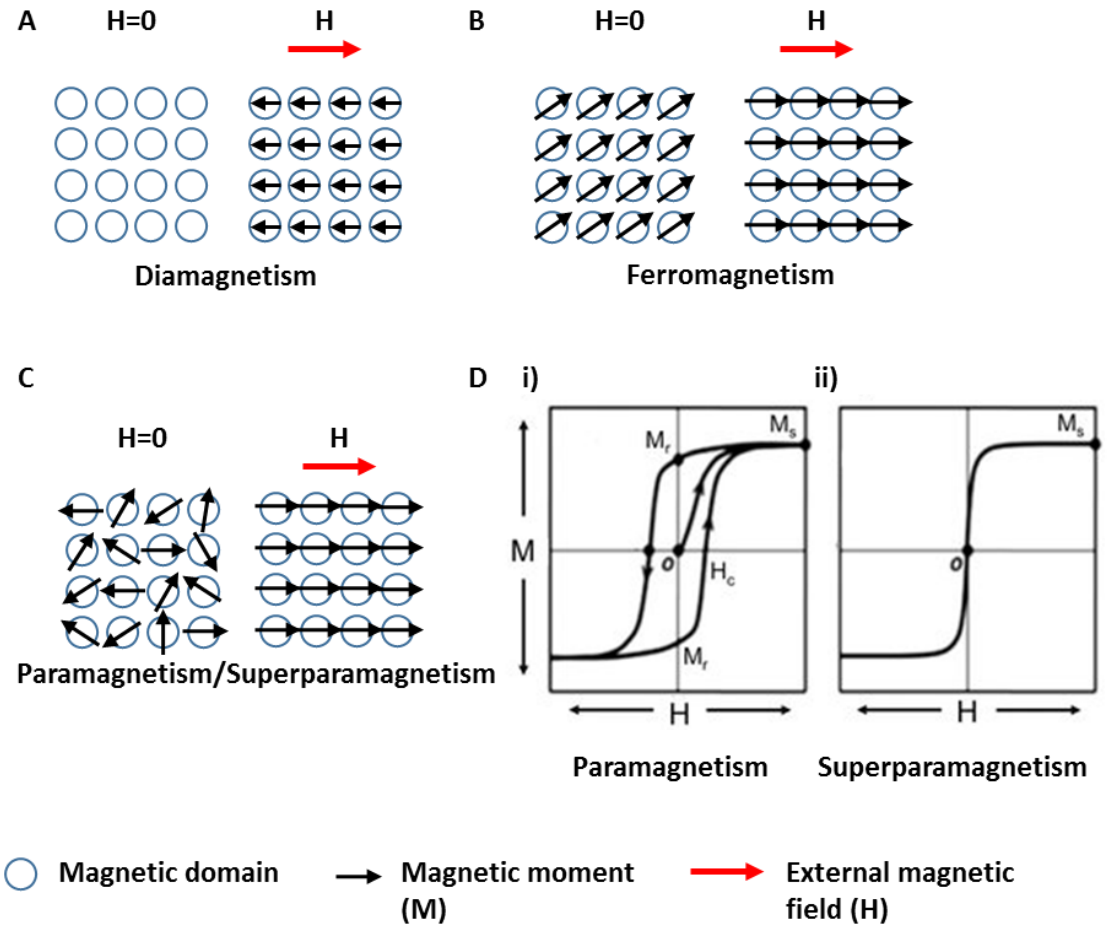

Figure 1.1 Schematic of behaviour of magnetic materials in the presence of an external magnetic field.

Illustration of the effect of an external magnetic field on the magnetic moment of A) diamagnetic materials; B) ferromagnetic materials and C) paramagnetic and superparamagnetic materials. D) Schematic of typical magnetisation curves generated by an applied field on paramagnetic (i) and superparamagnetic (ii) materials. Magnetisation curves from taken from Jeong et al.[7]

The atoms in a paramagnetic material fluctuate randomly in response to the thermal energy resulting in changes in their magnetic moments and causing a net magnetisation of zero. When an external magnetic field is applied, the magnetic moments of each atom aligns and produces a net crystal magnetisation. If the magnetic material is small enough, then random fluctuation affects the magnetic moment of entire crystallites (as opposed to single atoms). This behaviour is characteristic of superparamagnetic materials. Similarly to what happens in

paramagnetism, in the absence of a magnetic field, the magnetic moments of individual crystallites compensate for each other resulting in a null magnetisation. When a magnetic field is applied the magnetic moment of entire crystallites align with the field and generates a net magnetisation. In paramagnetic materials the formation of domain walls prevents the return of the individual atoms to the initial disorganised state. In superparamagnetic particles, the formation of domain walls is not energetically favoured and the individual crystals return to the initial state of null magnetisation (Figure 1.1). For applications *in vivo*, the dissipation of the magnetisation when the external field is removed is essential to prevent the formation of agglomerates and therefore clot formation or particle sedimentation.[8]–[10]

1.1.1.1 Magnetic force

MNPs can transform an external magnetic field to a mechanical force, the magnitude and direction of which is determined by the applied field. When MNPs are subjected to a magnetic field gradient, their magnetic moments experience a force that pulls them toward the region of higher field density. This force is defined by the magnetic moment 'm' of the particle and the field gradient 'B' applied as described in Equation (2)

$$F = (m \cdot \nabla) B \qquad (2)$$

When there is only one magnetic field applied in one direction then Equation 2 can be expressed as:

$$F = M M_S \frac{dB}{dr} \qquad (3)$$

Where 'M' represents the magnetic mass of the particle, 'Ms' the particle magnetization and 'dB/dr' the field gradient in one dimension.[9], [11], [12]

This magnetic force experienced by a magnetic nanoparticle represents the basis of MNPs biomedical applications such as drug targeted delivery or magnetic cell separation.

1.1.2 Formulations

MNPs are formed of a magnetic core (inorganic) and a biocompatible coating to provide stability and allow for further functionalisation of the particles (Figure 1.2).The formulation of MNPs for biomedical applications must be tailored for their specific application. This can be done by altering their different components.

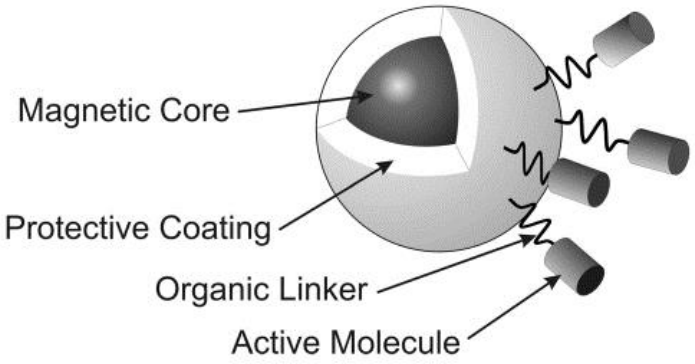

Figure 1.2 Typical design of a magnetic nanoparticle for biotechnology.
Adapted from McBain et al.[13] *With permission from the author.*

1.1.2.1 Magnetic core

Colloidal iron oxide NPs have been the most widely investigated for biomedical applications. Their magnetic properties are a consequence of the electron hopping between the Fe^{2+} and Fe^{3+} irons present in the crystalline structure. Furthermore, iron oxide is biocompatible and biodegradable with the degradation products being incorporated into the organisms iron stores. [14]

Metallic NPs (made of cobalt, nickel, iron or a combination of more than one metal, like FePt NPs) represent a very attractive alternative to iron oxide particles due to their high magnetisation, however they are in general more unstable and difficult to synthesise. [2], [15], [16]

1.1.2.2 Biocompatible coating

The coating on MNPs serves multiple purposes: provides stability to the magnetic cores, avoiding leaching into the system. Coating materials also improve colloidal stability and prevent particle aggregation as well as prolonging the particle half-life *in vivo.*[17] Importantly, MNPs coating allows to control for their size, shape and charge, parameters that play a very important role on particle biodistribution and cell uptake.[18] Finally, coating allows for particle functionalisation which could be achieved by further interaction or modification of reactive functional groups in order to couple the therapeutic cargo or by encapsulation of biomolecules of interest within the coating matrix.[19]

Polymeric and molecular coatings include synthetic like poly (vinyl pyrrolidone) (PVP), poly(lactic-co-glycolic acid) (PLGA), poly(ethylene glycol) (PEG), poly(vinyl alcohol) (PVA) or natural polymer systems like dextran, chitosan or gelatine.[14], [20]–[22] These coatings prevent nanoparticle aggregation and in some cases like PEG they have demonstrated extended circulation times and avoidance of macrophage interactions.[23] To date, the most commonly used coating for clinical preparations is the natural polymer dextran. Dextran is a natural polymer of glucose (α-1,6 glycosidic linkages for linear dextran and α-1,3 linkages for branched polymers). Dextran presents different structures and properties (i.e., molecular weight, solubility, branching). The reason dextran is such a suitable candidate for particle coating is

primarily due to its high biocompatibility (low molecular weight dextran has been broadly used as plasma expander) and high affinity for iron oxide, minimizing the chemical manipulation of the iron oxide. Additionally, ease of chemical derivatization of dextran enables tailoring of the surface properties and incorporation of functional groups to the nanoparticle. [2], [24]–[26]

Liposomes and micelles described as phospholipid blazered membrane vesicles have been broadly exploited to encapsulate and deliver drugs, contrast agents or DNA. Some liposomal formulations have been already tested in the clinic with particular focus on cancer therapy.[27] As well as incorporating therapeutic agents, liposomes can encapsulate MNPs creating multimodal platforms that allow for efficient combination of therapeutic agents and diagnostic tools.[28]

Finally, core-shell structures in which the magnetic core is encapsulated on a gold or silica matrix have also been researched for their applications in Magnetic Resonance Imaging (MRI) or magnetic drug delivery. These shells present great stability *in vivo*, protect the magnetic core, and allow for further functionalisation or incorporation of a therapeutic within the matrix.[19], [29], [30]

1.1.2.3 Functionalisation

One of the main hurdles that has hindered the clinical application of NPs is their complex and unpredictable pharmacokinetics. In this context, functionalisation of MNPs has been researched as a means to control and tailor their biodistribution and cellular uptake.

Ligand/receptor targeting has been widely exploited for active drug targeting and has been recently applied to enhance MNPs therapeutic potential in specific cell

types/organs.[31] Targeting agents such as folic acid/folate[32], [33], arginine glycine aspartic acid (RGD) peptide from collagen[34] or luteinizing hormone releasing hormone (LHRH)[35] amongst others have been incorporated onto MNPs to target cell surface markers expressed in tumour cells. Non-cell specific ligands such as transferrin (and derivate) and ceruloplasmin[36], [37] have also been used to enhance MNP-cell interaction. Enhanced MNP uptake mediated by CPPs will be discussed later in section 1.3.3.

Further development of biomaterials and ligands have allowed for incorporation of responsive polymer based coatings that allow for selective display of the ligand, only mediating cellular uptake under the desired physiological conditions.[38]

1.1.3 Applications in biomedicine

1.1.3.1 Magnetic Resonance Imaging (MRI)

The main clinical application of MNPs is currently in magnetic resonance imaging (MRI).[39] MRI relies on the relaxation times T1 and T2 of protons in a given sample after the application of a linear magnetic field gradient in addition to a main static field. These relaxation times are characteristic to each type of tissue. [11] Tissues with short longitudinal relaxation times T1 generally present greater image intensity. Paramagnetic materials facilitate the relaxation time T1 of nearby photons increasing the signal in that particular region.[40], [41] Superparamagnetic particles on the other hand, are magnetically saturated at the magnetic field strengths used in MRI scanners, stablishing a perturbing dipolar field, which shortens T2 to T*2 relaxation time producing a hypo intense region on T2 or T2*-weighted images.[26], [42]

Increasing progress in the development of cellular therapies for immune or regenerative therapies has made the field focus on monitoring the progress of the therapeutic cells in the organism. The same characteristics that have made iron oxide particles a very suitable candidate contrast agent for MRI in the clinic (including biocompatibility and degradability into non-toxic metabolites), makes them an excellent candidate for cell labelling and *in vivo* cell tracking (Figure 1.3).[39], [42]–[48].

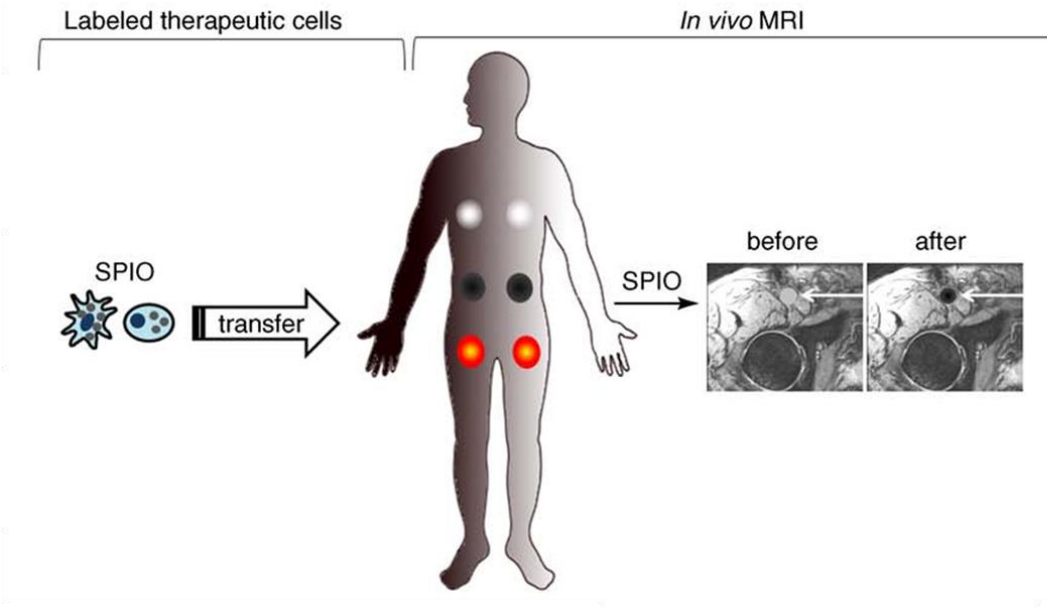

Figure 1.3 Schematic on MNPs cell labelling for in vivo cell tracking using MRI. *Adapted from Srinivas et al.*[49]

Despite the limitations presented in clinical studies in patients such as loss of signal by cell division, or potential transfer of the magnetic label to macrophages or other cells in the surrounding tissue, studies have been able to track the cells in preclinical studies in humans up to several weeks post transplantation, providing strong evidence of the clinical potential of tracking cells with MRI.[50]–[56] Past and current clinical trials regarding the use of MRI for tracking of implanted cells include dendritic cell vaccines and stem cells for multiple sclerosis and tissue reconstruction.[57]–[61]

As with other theranostics approaches, the use of MNPs as contrast agents for MRI of implanted cells has certain limitations, aside from the previously mentioned signal dilution by cell division and differentiating between life and dead labelled cells, MRI cell tracking is not suitable in cases that involve a traumatic injury with haemorrhage, since the some of the blood derivatives, such as methemoglobin, present hypointensity on T2-weighted MR images, making it difficult to detect the loss of signal induced by SPIONs. Additionally, certain tissues such as the lungs display a hypointense signal or areas on T2-weighted MR images that make the detection of SPIO labelled cells very challenging. [52], [62]

1.1.3.2 Hyperthermia

Their ability to efficiently convert dissipated magnetic energy into thermal energy, makes MNPs a focus of interest for the use in hyperthermia treatment.[1], [63]–[66]

When MNPs are subjected to an alternating magnetic field (AMF), the magnetic moments of the particles couple with the oscillating field, absorbing energy and transforming it into heat by a thermally assisted relaxation process. The frequency region of the applied electromagnetic radiation used in magnetic hyperthermia (10^5-10^6 Hz) has negligible effect on living matter so heating effects of magnetic hyperthermia (MHT) can be restricted to a certain area *in vivo* as long as the magnetic particles are confined to the target tissue. This characteristic makes MHT suitable for treatment for solid localised tumours. Tumour treatment can be achieved either by direct cytotoxic effects of high temperatures (above 42^{o}C) or by partial heating of tumour cells, making them more sensitive to other treatments, maximizing the efficiency of chemotherapy and radiotherapy. [66]–[69]

1.1.3.3 Drug/gene delivery

It is a common drug development principle that for a drug to have maximum efficiency it should be able to concentrate on the target site at effective concentrations and minimise off target effects. Magnetic drug targeting was first reported in 1978, when a cytotoxic drug Adriamycin was first conjugated to magnetic carriers to target solid tumours *in vivo*.[70] Just over two decades later Mah et al[71] reported the first attempt for targeted gene delivery by means of a magnetic vector and an applied external magnetic field, this new approach for gene delivery was termed "magnetofection".

Magnetic drug and gene delivery have mainly been aimed at solid tumours or inflammation sites. However, despite the potential of this technology, success has rarely been reported for their application *in vivo* [72]–[77]with only a few clinical trials performed to the date. [78], [79] A more detailed discussion on Magnetofection will be provided later in this chapter *(1.2.2.1 Magnetofection).*

1.1.3.4 Others

With the recent and rapid development of regenerative medicine and cell therapies, MNPs have gained significant interest as a means to non-invasively manipulate cell fate *in vivo*. Most preclinical trials have reported significantly enhanced retention of the MNPs/cells in the target tissue in the presence of an external magnetic field. [80]–[83] Similarly, magnetically labelled macrophages have also been targeted *in vivo* using magnetic resonance to target otherwise difficult to access tumours.[84]

Other applications include remote cell actuation, cell separation, protein separation and iron delivery for the treatment of iron deficiency in patients with anaemia. [48], [85]–[87]

1.1.3.5 Clinical applications

Three SPION drug formulations have been approved by the FDA: Feraheme (ferumoxytol, AMAG Pharmaceuticals, developed as gastrointestinal contrast agents (Ferumoxil, Abdoscan), Feridex (specifically approved for liver imaging), and GastroMARK (particularly efficient for imaging of the stomach and small intestine); however, the latter two have been withdrawn from the market. [79], [88] More recently a new SPION formulation (Magtrace™) has been approved for the imaging of sentinel lymph node detection in breast cancer. [55]

Additionally, some of these SPION formulations have been tested for cell tracking purposes in early stages clinical trials in cell therapy treatments of Multiple Sclerosis, brain trauma and spinal cord injury. [51], [54], [89], [56]

Only one magnetic nanoparticle based product has been approved to the date for hyperthermia treatment in glioblastoma, Nanotherm® (MagForce).[69]

Finally, there is a wide range of magnetic nanoparticle formulations approved for the delivery of iron for iron deficiency in chronic kidney disease such as Ferrlecit®, INFeD® (Sanofi Avertis) or Venofer®(Luitpold Pharmaceuticals).[26], [39], [90]

1.1.4 Limitations

Current clinical trials involving the use of MNPs are mostly limited to expanding the application of MNPs as contrast agents for diagnosis or hyperthermia.[91], [92] These applications mostly rely on the differential uptake of the particles by certain cells/tissues or on the direct injection of the particles to the target site but do not take advantage of the targeting possibility provided by the MNPs. This suggests that although very promising as a concept, current therapies involving MNP targeting have yet to come to fruition in the clinic. Magnetic fields need to be strong enough to retain MNPs on a target tissue against the blood flow. Since magnetic force is a function of the distance between the particle and the source of the magnetic field, this task becomes more complex the deeper the organ is inside the body.[8] Commercially available magnets are only capable to penetrate a couple of centimetres into the skin so their use would only be successful for superficial targets.[93] Targeting of MNPs to other organs would require expensive and complex external magnetic field set ups, complicating their implementation in the clinic. Further improvement in biomedical magnetic field settings as well as the formulation of stable and long circulating MNPs that favour the fast cellular uptake on the target site are set to significantly improve the applications of MNPs. [94], [95]

1.2 Gene therapy

Gene therapy is a unique therapeutic approach suitable to treat both inherited and acquired diseases by replacing a distorted or missing gene to express the correct phenotype.[96] Gene therapy has also been used to promote a process that doesn't naturally happen (i.e. induce expression of growth factors to direct cell fate).[97]

1.2.1 Gene delivery

As with most drugs, nucleic acids, must reach their site of action in order to produce a therapeutic effect. Unlike conventional drugs however, the target site of nucleic acids is inside the cell (normally cytoplasm for RNA or the nucleus for DNA) meaning nucleic acids must at the very least traverse the cell membrane in order reach their target site. The cell membrane is a dynamic structure of a predominantly lipophilic nature, which restricts the entrance of large charged molecules into the cell. Genetic molecules are normally hydrophilic or charged as well as relatively large in size making it very difficult for them to cross the cell membrane on their own. Therefore in order to achieve successful gene therapy, a delivery system capable of packaging and ferrying the genetic material inside the cell is paramount. Additionally, if the uptake route involved entrapment of the nucleic acids inside intracellular vesicles, the delivery system should enable trafficking of the nucleic acids outside the vesicle into the cytoplasm.[98] Furthermore, for nucleic acids like DNA to express the protein of interest, they have to enter the cell nucleus in order to be transcribed into RNA (mRNA) (Figure 1.4).[99]–[101] For clinical translation and commercialisation, the ideal gene delivery system should also be; easy to produce at a large scale, immunologically inert, tissue or cell specific and able to tailor the gene expression to meet the therapeutic need, i.e. permanent vs transient expression.[102] All these factors should be considered when developing a new gene delivery system.

This introduction will mainly focus on the challenges and opportunities achieved on DNA delivery, since its delivery is significantly more complex. However, some examples of successful RNA mediated therapies will also be provided. For simplicity

the term “vector” will be used moving forward to describe a nucleic acid delivery system, unless otherwise specified.

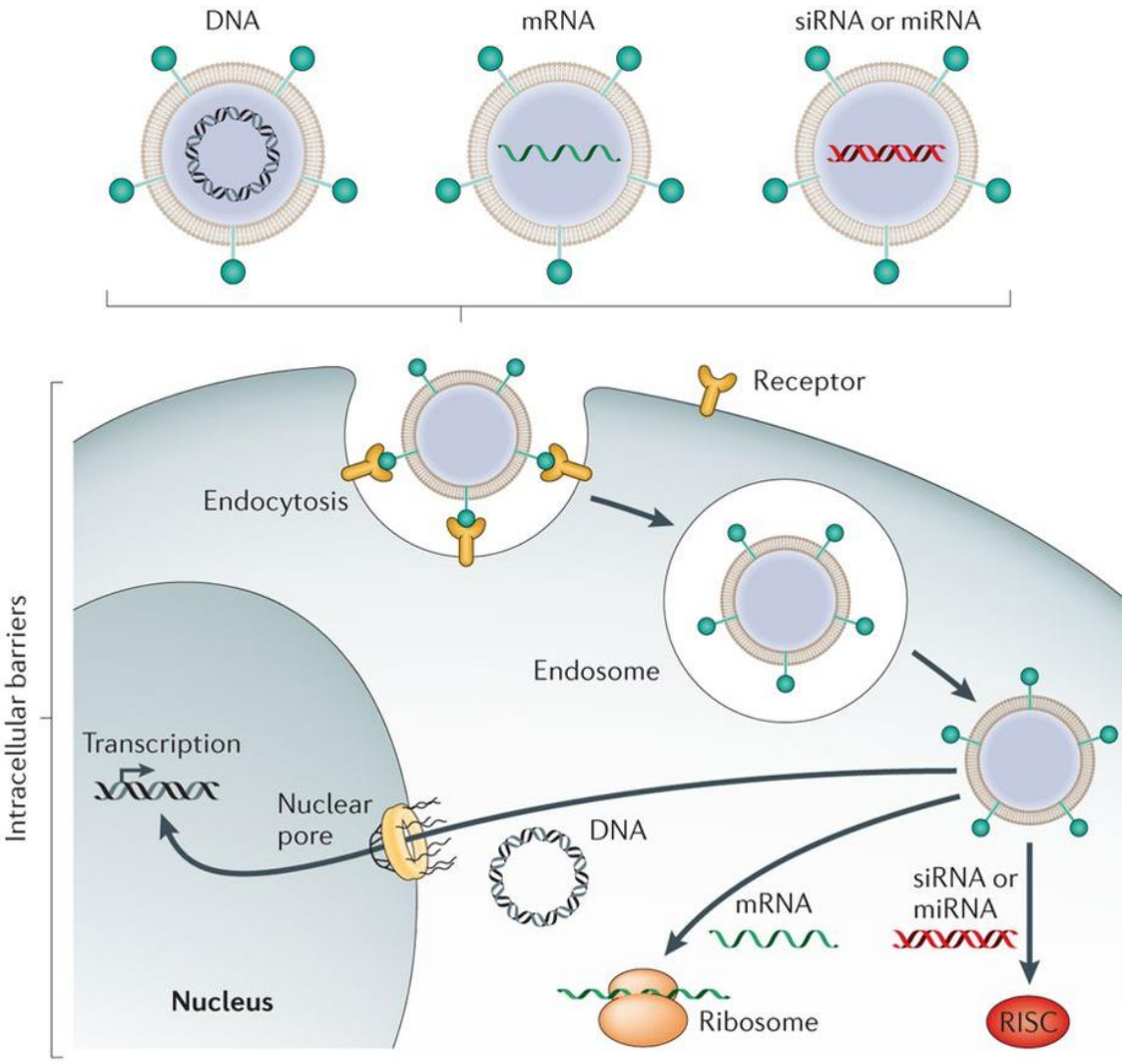

Figure 1.4 Schematic of non-viral nucleic acid delivery to the cell.
Different types of nucleic acid have different targets on the cell. SiRNA and miRNA mimics must be loaded into the RNA-induced silencing complex (RISC), whereas mRNA must bind to the translational machinery. DNA has to be further transported to the nucleus to exert its activity. Adapted from Yin et al.[101]

1.2.1.1 Viral vectors

Viral vectors are derived from viruses by replacing their genetic components (either DNA or RNA) by the therapeutic gene. Additionally, viruses can be modified so that the vectors mediate transient short-term (non-integrating) and permanent long-term

expression (integrating). To date, the most commonly used DNA viral vectors include: integrating retroviral, lentiviral or adeno-associated viral (AAV) vectors and non-integrating adenoviral vectors. [101], [103]

Viral vectors for gene delivery suffered a tremendous setback in 1999, when Jesse Gelsinger became the first patient to die in a Phase I gene therapy clinical trial. His death was directly related to the vector used in the treatment (AAV).[102] The exact cause of Jesse's death was never clear, but some theories pointed to the possibility an immune response to the treatment.[104]

Aside from the potential risk of high immunogenicity, viral vectors present other disadvantages such as carcinogenesis, limited packaging capacity and difficulty in reproducible production.

Despite their limitations, extensive work has been carried out on improving their safety profiles and to date, they still account for more than 70% of the clinical trials approved and all the clinically approved products for gene delivery thus far.[105]

1.2.1.1.1 Commercially available gene therapy: viral vectors

The world of gene therapy experienced a massive revolution in 2017 whereby the Food and Drug Administration (FDA) approved the first two therapies with chimeric antigen receptor (CAR)[106] T cells for immunotherapy in cancer treatment (Kymriah™ for acute lymphoblastic leukaemia and Yescarta for B-cell lymphoma) . Ever since the first patient successfully treated with autologous T cells (modified to express a CAR specific to the B-cell antigen CD19)[107], there have been hundreds of patients treated in similar clinical trials that have shown significant remission rates in

treatment of leukaemia or lymphoma. Current work is also focusing on the use of CAR T cell therapy on more difficult to treat tumours, such as glioblastoma.[108] Furthermore, in 2017, the FDA approved the first AAV gene therapy for the treatment of Leber's congenital amaurosis, a genetic retinal dystrophy (Voretigene neparvovec-Luxturna™).[109]

There are other gene based therapeutic products that have been approved for therapeutic applications in Europe: Glybera, AAV-based gene therapeutic treatment of rare inherited disease Lipoprotein Lipase Deficiency (LPLD).[110] Strimvelis ex vivo stem cell gene therapy to treat patients with ADA-SCID (severe combined immunodeficiency due to adenosine deaminase deficiency).[111] Finally, Imlygic is a modified form of the herpes simplex virus for the treatment of unresectable cutaneous, subcutaneous and nodal lesions after initial surgery in patients with melanoma. Estimation of cost effectiveness has resulted on the withdrawn of Glybera from the market.[112] Strimvelis and Imlygic have so far not been withdrawn from the market but they are currently facing challenges within their applications (e.g. Strimvelis treatment is restricted to one site in Italy) and coverage by the different healthcare systems.[111]

1.2.2 Non-viral vectors

Non-viral approaches for DNA delivery use mostly plasmid DNA as expression vectors. Plasmid DNA gets transferred into the cell directly by physical methods such as electroporation or gene gun (not so efficient for *in vivo* applications) or encapsulated or complexed with liposomes, peptides or polymers complexes (chemical methods).[113] Non-viral vectors offer advantages such as easy characterisation,

simplicity and reproducibility of production, larger packaging capacity and reduced immunogenicity. However, in general, they show significantly less gene transfer efficiency compared to viral systems.[101]

The main challenges encountered by the non-viral vector include: low accumulation efficiency at the tissue of interest, cellular internalisation, endosomal escape and transport into the nucleus. This later obstacle is a rate limiting step of non-viral vectors and presents a major disadvantage compared to viral vectors, which have evolved to readily enter the cellular nucleus. Another potential disadvantage of non-viral gene delivery vectors is their transient expression.[99] Although this characteristic of non-viral vectors could be seen as an advantage for certain therapeutic applications that require transient gene expression, particularly in the field of regenerative medicine (i.e. cell induced differentiation).[114]

However, for those applications that do require a more stable expression, recent advancements in the field have enabled a more permanent expression of the gene. This can be achieved by: self-replicating plasmids and harbouring Epstein–Barr virus (EBV) nuclear antigen 1 (EBNA 1) gene derived from the EBV. Another approach consists of prolonging extrachromosomal stability of the plasmid by scaffold/matrix attachment regions (S/MAR).[115], [116]

In addition to plasmid DNA manipulations, advances in biomaterials and delivery technologies have allowed to significantly enhance the efficiency of non-viral gene delivery.[105]

Recent clinical trials have demonstrated the efficiency of a cationic liposome formulation of gene therapy on patients with cystic fibrosis, reporting stabilisation of lung function after 12 months.[117]

There is certainly potential for the application of non-viral vectors; however, further optimisation and research to understand their limitations is required.

1.2.2.1 Magnetofection

Table 1 Magnetofection therapies for non-viral nucleic acid delivery in vivo.

Ref	Year	Vector	Animal	Delivery (target)	Gene	Outcome
[118]	2002	transMAG^{PEI}	Rats	In situ (Small intestine)	Lac Z	Localized gene expression
[120]	2006	transMAG^{PEI}-Liposomal	Mice	Intranasal catheter (Nasal epithelium)	Luciferase	MNPs decreased luciferase expression compared to naked DNA Magnetic field did not enhance MNPs-mediated transfection
[122]	2007	PEI Chemicell	Cats	intratumoral (Fibrosarcoma)	Fe IL-2 Fe IFN-γ Fe GM-CSF	Magnetofection was safe
[119]	2008	transMAG^{PEI}	Cats	Intratumoral (Sarcoma tumour)	GM-CSF	Magnetofection was safe
[123]	2010	Self-assembled ternary complexes of cationic magnetic NP	Rat	Intrathecal injection (Spinal cord)	Luciferase	Localised gene expression
[124]	2015	NeuroMag	Rat	In situ (Visual cortex neurons)	EYFP	Localised gene expression
[121]	2016	SPION-PAA-PEI-pDNA	Mice	Intratumoral (Melanoma tumour)	Anti-MCAM	Increased DNA uptake at the tumour site Reduced tumour size after serial administration
[125]	2017	CPP-oligonucleotides-Fe_3O_4 NP	Mice	Systemic	Luciferase	MNPs-mediated transfection comparable to non-MNPs vector

Magnetofection has been previously mentioned in this introduction section as one of the therapeutic applications of MNPs. It is defined as any type of nucleic acid delivery under the influence of a magnetic field on nucleic acids associated with MNPs (cited from[126]). Magnetofection is a simple gene delivery approach that does not

necessarily require complicated conjugation protocols and can be adapted to deliver most types of nucleic acid or vector (viral or non-viral), provided the right binder. As it allows concentration of the therapeutic gene to a specific area, magnetofection also has the potential to reduce vector doses as well as off target effects.

Magnetofection has shown very promising results *in vitro*. The results obtained so far from its application *in vivo* are overall positive, although targeted and localised delivery are not always achieved and some studies are not very specific as to localization of plasmid DNA outside the targeted area. Table 1, summarizes some of the most representative studies so far and their outcomes, including two preclinical trials in cats, assessing for magnetofection safety.

1.2.2.1.1 Limitations

In principle, magnetofection provides a convincing solution for gene targeted delivery *in vivo*, however, despite the efforts in the field during the last two decades, magnetofection still hasn't been clinically adopted.

The same general limitations that affect MNPs apply for magnetofection, including, lack of stable formulation, lack of strong enough magnetic fields to hold the particles on the target tissue, risk of particle aggregation and clot formation, renal clearance, and cytotoxicity.

Magnetofection combines low cost of production, localisation of delivery and enhanced efficiency in short incubation times. However, this also applies to other physical methods such as electroporation, which has achieved efficient transfection in non-dividing cells, something magnetofection has not yet attained. The true appeal of

magnetofection, which other physical methods have not yet achieved, is that it can be integrated with new technologies to meet the current needs of biomedicine.[126] Some examples of the various applications of magnetofection include, combined magnetic cell separation and nucleic acid delivery for cell therapy, targeting of genetically engineered cells for tissue regeneration to specific areas by a magnetic field and theranostic systems for integrated nucleic acid delivery and multimodal medical imaging.

1.3 Cell penetrating peptides (CPPs)

CPPs or Protein Transduction Domains (PTDs) are two terms used interchangeably (in many instances) to describe peptides with membrane translocation capacities. They are typically composed of 5-30 amino acids and normally do not require specific receptors to cross the cell membrane.[127] CPPs are also able to transport compounds through biological barriers such as the skin, intestine, the blood–brain barrier or the conjunctiva of eyes.[128]

The first report of CPPs in the literature dates back to 1988 when two different groups published the efficient internalisation of the transactivator of transcription (TAT) protein of human immunodeficiency virus (HIV).[129], [130] Ever since, a wide variety of CPPs have been developed and optimised for delivery of different cargoes for applications in cancer, asthma or ischemia.[131]

1.3.1 Clinical trials and commercial products

The first CPP to ever enter a clinical trial was developed by CellGate for the treatment of psoriasis[132] but the trial was discontinued in 2003.[133] To date, a number of CPPs, particularly, TAT-peptide based CPPs have taken part in clinical trials both phase I and phase II for a wide range of applications (topic delivery of botulin toxin, prevention of keloid scaring, cancer, siRNA delivery, ischemia..).[131], [134], [135]

However, CPPs progression to later stages of clinical trials and their use in the clinic are restricted by factors such as, poor solubility, short circulating half-life or immunogenicity.[136]

CPPs-based reagents that are commercially available are mainly a combination of different CPPs or mixtures of CPPs with polymers, designed to form non-covalent complexes with a specific therapeutic cargo (peptides, protein, RNA…).[128]

1.3.2 CPPs for gene delivery

In theory, CPPs are advantageous for gene delivery compared with other non-viral vectors, because they are able to condense the plasmid DNA and mediate interaction of the nanoparticle with the cell membrane and ferry the nucleic acid cargo across into the cell. Peptides rich in lysine or arginine efficiently condense DNA by interaction of the positively charged lysine and arginine residues and the negatively charged phosphate groups in the DNA chain, forming compact and stable nanoparticles.[137] CPPs have been demonstrated to moderately enhance transfection efficiency in mammalian cells, although their activity is significantly hampered by the entrapment of the genetic material in intracellular endosomes.[138]–[142] In order to overcome

this disadvantage, CPPs have been conjugated with other molecules capable of mediating endosomal escape such as PEI. So far the results of the combination of these two vectors have been very promising both *in vivo* and *in vitro.*[143]–[146] Other non-viral vectors such as chitosan [147], PEG [148], liposomes [149] or cationic polymers [150] have also been successfully conjugated with CPPs for efficient gene transfer.

Despite the recent advances in the development and optimisation of CPPs for gene delivery, they still suffer from the same limitations as the other non-delivery vectors and further research should be conducted to ensure targeted delivery, high efficiency and low toxicity.[127]

1.3.3 CPPs for MNP delivery

Functionalisation of MNPs with specific ligands has been widely used as a platform for cancer targeting, drug delivery, magnetic resonance imaging and cell transfection as it has been previously introduced. MNP functionalisation looks to increase particle concentration on the target cell/tissue.[151]

CPPs have been demonstrated to significantly enhance MNP uptake *in vitro* with minimal effect on cell viability or cell function.[152]–[158] Efficient delivery of CPP-MNPs to cells ex vivo, allowed tracking of T cells and progenitor cells *in vivo.*[159], [160]

Wunderbaldinger et al. showed that TAT-labelled MNPs were able to penetrate vascular cells into the liver tissue when injected systemically.[161] Furthermore, Song

et al. were able to direct gene expression to the cervical spinal cord with the use of a magnetic field *in vivo* by TAT-MNPs.[162]

1.3.4 Limitations

Despite all the advantages of CPPs and the relative success achieved in the clinic, there are some limitations that still need to be addressed.

In general, CPPs present low cell, tissue or organ specificity, which could lead to delivery of therapeutic cargo outside the target tissue, resulting in undesired side effects.[133]

The other major drawback of CPP mediated uptake of therapeutic molecules such as DNA that require nuclear localisation is the entrapment of the uptaken cargo in intracellular vesicles, reducing the amount of available cargo, and therefore, its therapeutic efficiency.

Additionally, most CPPs are very susceptible to the proteolytic action of proteases present in biological fluids or even serum used for cell culture which limited their functional lifetime.[128]

1.3.5 GET system

In 2016, Dixon et al. published their work on the development of a modified PTD based delivery system termed GET (Glycosaminoglycan-Enhanced-Transduction).[163] Their aim was to improve PTD transduction efficiency by incorporating an additional sequence to enhance PTD-cell interaction. They tested a wide variety of sequences in the literature reported to interact with ubiquitously expressed molecules on the cell

membrane. The most successful candidate resulting from the screening was P21 (KRKKKGKGLGKKRDPCLRKYK) a membrane docking peptide to heparan sulphate glycosaminoglycan (GAG) extracted from the binding sequence of the Heparin Binding Domain (HBD) in Epidermal Growth Factor, HB-EGF. In combination with polyarginine residue 8R, P21 was able to synergistically enhance the transduction of recombinant protein mRFP in cells that had previously shown poor transduction with 8R only, such as mouse embryonic stem cells or induced pluripotent stem cells (Figure 1.5, C).

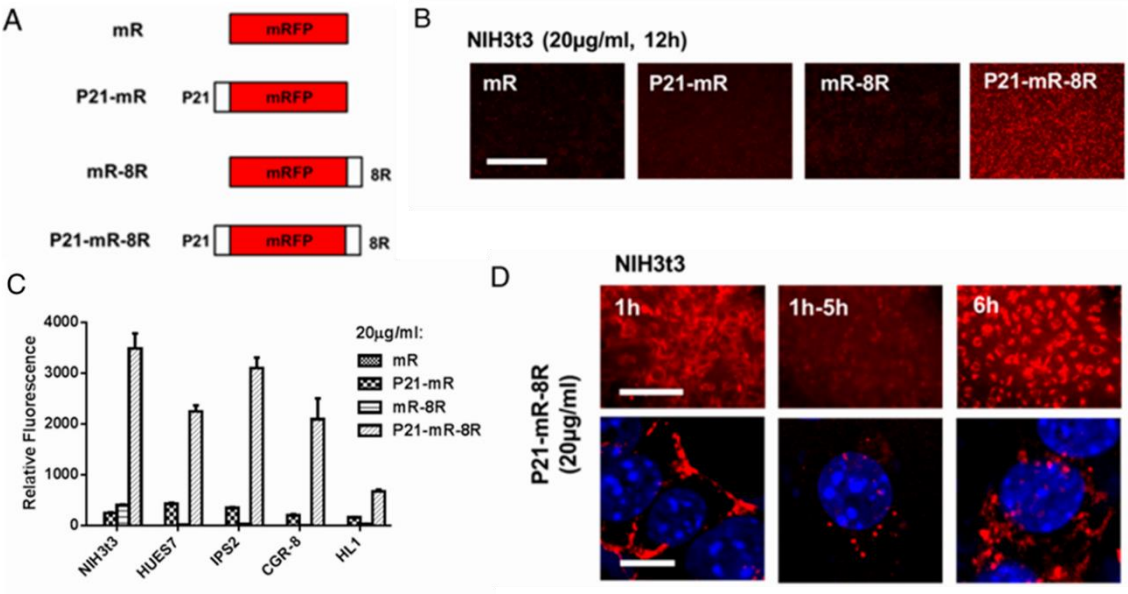

Figure 1.5 Development and optimisation of GET: GAG-(Glycosaminoglycan)-enhanced-transduction.

Figure was adapted from Dixon et al.[163] *Permission was obtained from the author. A) Schematic of the proteins created after screening domains that improve efficiency of protein delivery to cells. P21-mR is mRFP with an N-terminal fusion of the P21 domain of HB-EGF. P21-mR-8R is mRFP with N-terminal fusion of P21 and C-terminal fusion of 8R. B) Fusion of P21 to mR-8R significantly improves uptake into NIH3t3 cells. Fluorescence microscopy images of NIH3t3 cells treated with proteins (20 μg/mL) for 12 h in standard media conditions. (Scale bar, 100 μm) C) P21-mR-8R is efficiently taken into hESCs and mESCs (HUES7 and CGR-8, respectively) and hiPSCs (IPS2) and mouse cardiomyocyte cell line HL1. Flow cytometry analyses of the mR-8R inefficiently delivered cell lines treated with proteins mR-8R (20 μg/mL) for 12 h. D) P21-mR-8R initially strongly interacts with cell membranes and progressively is taken up and localised perinuclearly. Fluorescence (Top) and confocal laser scanning microscopy (Bottom) images of NIH3t3 cells treated with P21-mR-8R (20 μg/mL) for 1 h, 1 h with washes and a further 5 h incubation (in serum-free media), or 6 h treatment. Cells were preincubated for 1 h in serum-free media and transduced for the desired time in serum-free media. (Scale bars, top, 50 μm; bottom, 10 μm.)*

Dixon et al.[163] conducted an exhaustive study and analysis of the mechanism of action underlying GET enhanced delivery. They showed that GET-mediated delivery significantly increase the activity of the cargo in the cells, compared to CPP alone. In addition, they demonstrated that positive charge was a prerequisite for GET transduction, however, the synergistic effect observed by the combination of PTDs

and HBD was largely dependent on the correct sequence and structure of the HBD. Furthermore, they identified other HBDs such as Fibroblast Growth Factor (FGF2B) that were even more efficient at cell transduction in specific cell lines. They proposed that interaction of GET with membrane proteins/receptors was key for enhanced transduction. On that same paper, Dixon et al. reported MNPs enhanced delivery mediated by GET, by covalently binding the peptide to COOH dextran coated iron oxide particles.

1.3.5.1 GET applications

Since its discovery, GET system has been implemented in a wide variety of applications, including cell programming in 3D hydrogels[164] and delivery of runt-related transcription factor 2 (RUNX2) to induce osteogenic differentiation in human MSCs.[165] Additionally, Abu-Awwad et al.[166] developed a protocol for encapsulation of GET tagged proteins (exampled by mRFP) to allow for controlled and sustained release to cells over time. A variant of GET, including an amphipathic peptide (LK15) for enhanced DNA binding, was optimised for efficient lung gene delivery *in vivo* by the addition of PEG groups. [139] This GET-PEG system was able to perform better than commercial standard PEI *in vivo.*[167]

1.4 Aims

1.4.1 Results I: Enhanced cellular transduction of MNPs resistant to rapidly-forming plasma coronas.

Targeted delivery strategies for MNPs have been developed towards specific- or over-expressed receptors on disease cells by functionalising the nanoparticle surface with

proteins, antibodies or other biomolecules. These strategies efficiently enhance nanoparticle delivery to the target cells *in vitro*; however there is mounting evidence that targeting ability of functionalised particles disappears when placed in biological environments.[168]–[170]

As previously mentioned, GET system refers to a range of delivering peptides that combine a membrane docking domain and a CPP and as a result, show significantly improved intracellular uptake properties.[163] From the different GET peptides described by Dr Dixon et al. P21-8R (PR), had previously demonstrated to efficiently enhance cell transduction of MNPs in living cells in the presence of serum, when covalently bound to the MNP surface. However, in order to develop a flexible delivery system that could adapt to the different MNPs for potential biomedical applications it would be optimal that the incorporation of PR and MNPs was simplified and reduce the number of manipulation steps. Therefore the first aim of this chapter was to assess the potential of PR to electrostatically interact with MNPs and mediate MNPs uptake. If successful, this new platform will assist on various aspects of MNPs delivery: for localised delivery to the target site PR would ensure rapid interaction with the targeted cells avoiding non-specific delivery (i.e. rapid interaction with the cells surrounding the injection site). Additionally, PR-MNPs could provide a useful approach for magnetically mediated targeting of MNPs to cells *in vivo* by reducing the need of prolonged magnetic exposures.

The aims of this chapter were to:

1. Develop and optimise PR-MNPs formulation for enhanced MNP transduction.

2. Demonstrate that PR can be used to mediate sustained intracellular transduction of MNPs even in the presence of serum proteins.
3. Characterise colloidal stability, nanoparticle physical properties, toxicity and cellular uptake in the presence of serum and plasma proteins
4. Assess protein corona formation and composition over time in the presence of plasma proteins.
5. Determine haemocompatibility of PR-MNPs in the context of systemic particle delivery.

1.4.2 Results II: Optimisation of GET-MNPs for magnetically mediated gene delivery *in vitro.*

The mechanisms by which CPPs induce cargo translocation across the cell membrane are complementary to magnetofection, which effectively concentrates the genetic material on the cell membrane.[162] It was proposed that the combination of a modified version of GET containing an LK15 residue for DNA condensation [167] and MNPs would enhance speed transfection efficiency in the presence of a magnetic field. The version of GET used in this chapter will be termed FLR for simplicity purposes, unless otherwise specified.

This chapter aimed to:

1. Incorporate FLR into the previously optimised MNPs delivery system for gene transfer *in vitro*.
2. Characterise FLR-DNA-MNPs complex formation, stability, DNA binding capacity.
3. Demonstrate efficient magnetofection mediated by FLR-MNPs.
4. Investigate plasmid DNA uptake mechanisms and intracellular fate.

1.4.3 Results III: Use of GET-MNPs and Magnefect-nano^{TM} for enhanced gene delivery in dendritic cells.

The FDA approval for the use of genetically modified cells for immunotherapy in the treatment of cancer, introduces a new range of therapeutic opportunities that require *ex vivo* cell modification. Therapies including this approach currently on clinical trials include CAR-T cell therapy and dendritic cells vaccine. These new therapeutic

approaches open up the way for development of multimodal technologies like magnetofection capable of fast and efficient gene delivery in addition to providing imaging and targeting possibilities.[171]

Recent work shows that magnetically mediated gene delivery in a permanent oscillating magnetic field significantly increased transfection efficiency in a range of hard to transfect cells in short periods of time (30 min).[172]–[174]

It was suggested that magnetofection on an oscillating magnetic field (mediated by Magnefect-nano^{TM}) could further increase transfection efficiency mediated by FLR-MNPs, providing a useful tool for application in future cell therapies.

This part of the project involved the following aims:

1. Optimisation of FLR-MNPs magnetic gene transfection in dendritic cells in the context of dendritic cell vaccine.
2. Characterisation of the effect of different magnetic oscillation regimes on gene transfer efficiency in dendritic cells.

2 Material and methods

2.1 General cell culture

All cell culture work was carried out in a class II biological safety cabinet (Walker Safety Cabinets, Derbyshire, UK or Thermofisher Scientific biological safety cabinet, model 1358, USA). Cell culture work was performed under risk assessments authorised by the HSE and Standard Operating Procedures (SOP) under the HTA (Licensed premises: University of Nottingham; License number: 12265). Before starting any work in the safety cabinet, this was sterilised using 70% IMS. All equipment to be used inside the cabinet was either sterilised using 70% IMS or autoclaved. Sterile cell culture plastic ware (Costar, UK) was used. Liquids were purchased sterile or sterilised by filtering or autoclaved. Unless otherwise specified all cells were incubated at 37°C in 5% CO_2 (v/v).

2.1.1 Mammalian Cell culture

Mouse embryonic fibroblasts NIH3t3 were purchased from American Type Culture Collection (ATCC). Glioblastoma cell line U87 were provided by Dr Ruman Rahman from Children's Brain Tumour Research Centre, University of Nottingham and tested for typical pathogens. Mouse dendritic cells 2.4 (DC 2.4) were kindly provided by Dr Duane Mitchell's Lab from the University of Florida.

Cells were cultured in Dulbecco's modified Eagle´s media (DMEM; Sigma), supplemented with 10% (v/v) Foetal Calf Serum (FCS, Sigma), 4.5 g/L D-Glucose, 2 mM L-glutamine and 100 units/ml penicillin and 100 units/ml streptomycin (Invitrogen). From now on this media will be referred to as 10% FCS media. Dendritic cells media

additionally included 1% (v/v) HEPES buffer (4-(2-hydroxyethyl)-1-piperazineethanesulfonic acid, Lonza)

Bone marrow derived Human Mesenchymal Stem Cells (hMSCs) were purchased from RoosterBio Inc and cultured in xeno-free medium Rooster Nourish™-MSC-XF (KT-016) also from RoosterBio.

Cell passage was carried out using 0.05% (w/v) trypsin-EDTA (Invitrogen) at 70-80% confluency.

2.1.2 Cell viability

2.1.2.1 Cell metabolic activity

Cell metabolic activity was measured by resazurin based Presto Blue® Cell Viability Reagent (Invitrogen). Cells were washed with Phosphate-buffered saline (PBS) solution and then incubated for 15-30 min with Presto Blue® working solution, prepared according to manufacturer's instructions: Presto Blue stock solution 10% v/v in Hank's Balanced Salt Solution (HBSS, Sigma). Change in the fluorescence was measured using a plate reader with the excitation/emission wavelengths set at 530/590 nm (Synergy™ 2 Multi-Mode Microplate Reade, Biotek Instruments or Infinite® 200 PRO, TECAN). Untreated cells were used as control for 100% metabolic activity. All data sets are combined for the statistical analysis.

2.1.2.2 Trypan Blue cell viability assay

Trypan Blue cell assay was performed at least 24 hours post cell treatment. Trypsinised cells were diluted in equal volume of Trypan blue solution (Sigma Aldrich). (1:1). Viable cells were manually counted on a haemocytometer. For consecutive day proliferation analysis, cells were trypsinised every 24 hours, counted and half the cells were seeded again. Results were reported as percentage of viable cells and total number of cells per treatment group.

2.2 Particle characterisation

2.2.1 Zeta potential and size

Malvern Zetasizer Nano ZS was used to study zeta potential and size of the nanoparticles.

2.2.1.1 Dynamic light scattering.

Measurements consisted of 3 repeats (12-15 subruns per repeat) of the same sample to estimate the error in the measurements. Refractive index of the samples and absorption were approximated to 2.918 and 0.029 respectively for MNPs based vectors and 1.450 and 0.001 respectively for protein only vectors. Water viscosity was set at 0.8872 cP and refractive index of 1.3330. The measurements were recorded at room temperature. Particle size values were reported based on intensity.

2.2.1.2 Zeta potential.

Measurements consisted of 3 repeats (12 subruns per repeat) of the same sample to estimate the error in the measurements. The measurements were recorded at room temperature. Because zeta potential measurements were performed in an aqueous solution, the Smoluchowski approximation was used to calculate the zeta potentials from the measured electrophoretic motilities. Water dielectric constant was set as 78.5.

2.2.2 Conformational Assessment of Particle-Bound Proteins

Infrared analysis of surface-bound GET was conducted using a Thermofisher Scientific Nicolet iS50 Fourier-Transform Infrared Spectrometry (FTIR) Spectrometer. Spectra were recorded at 4 cm^{-1} resolution with 36 scans being averaged, smoothed by 9 point adjacent averaging and curve fitted. OMNIC software was used to identify and analyse the spectra. Briefly, adsorption band regions in the amide 1 band were estimated from the wide range of literature: alpha helix (1646-1656 cm^{-1}), Beta sheets (1628-1640 cm^{-1}, 1669-1688 cm^{-1}), unordered structures (1642-1652 cm^{-1}) and turns (1659-1681 cm^{-1}). Curve fitting was performed by Dr Paul Roach at University of Keele. Curve fitting methodologies were used as previously reported.[175] Statistical analysis performed using Benjamini, Krieger and Yekutieli t-test, with Q = 1%. N refers to repeated measurements.

2.2.3 Protein adsorption: Langmuir isotherm

2.2.3.1 PR adsorption

PR was labelled with fluorescent variant of rhodamine, 5-Carboxytetramethylrhodamine (5-TAMRA, Sigma). From this point onwards TAMRA

labelled PR will be referred to as PR-T. The following solutions of PR-T were prepared in PBS: 0.025, 0.05, 0.1, 0.2, 0.4, 1 and 2 nM PR-T. PR-T solutions were incubated with 50 µg/ml of Micromod dextran coated MNPs under constant agitation for 10 mins at RT (this incubation time was chosen based on experimental *in vitro* delivery). MNPs were then magnetically separated and supernatant was collected. Protein concentration was measured using a plate reader excitation 546 nm, emission 579 nm (Infinite® 200 PRO, TECAN). N=4, independent repeats.

2.2.3.2 BSA adsorption

Solutions of FITC- labelled Bovine serum albumin (BSA) (Thermofisher, A23015) were prepared in PBS: 6.25, 12.5, 25, 50, 100, 150 and 200 µg/ml. Solutions were incubated with 50 µg/ml of dextran coated Nanomag®-D MNPs (Fe3O4 core; 250nm; Micromod, product code 09-02-252) under constant agitation for 10 mins at RT. Protein concentration was measured using a plate reader excitation 488 nm, emission 532 nm (Infinite® 200 PRO, TECAN). N=6, independent repeats.

For PR and BSA, standard curves were prepared for the tagged protein by plotting increasing concentrations versus measured fluorescence. Background fluorescence was subtracted both from the media (PBS) and MNPs only to account for particle background fluorescence.

Isotherms were adjusted to the Langmuir equation (Eq. 4) using non-linear least-squares fitting on Excel.[176]

$$S = \frac{S_{max} K C_f}{1 + K C_f} \qquad (4)$$

Where Cf is the solute concentration remaining in solution at equilibrium, S represents the adsorbed amount of solute at equilibrium, S_{max} is the maximum concentration of

bound solute onto the MNPs and K is the Langmuir's equilibrium constant that describes the strength of interaction between solute and the particles surface.[177]

Briefly, a function was defined in Excel to minimize the value of the sum of squared residuals (SSR). In this context a residual was defined as the difference between the observed data and the experimental data calculated using the Langmuir equation. S_{max} and K were adjusted to obtain a minimum value for SSR.

2.2.4 Gel electrophoresis

For determination of plasma proteins adsorbed onto the particles (MNPs and PR-MNPs), sodium dodecyl sulphate-polyacrylamide gel electrophoresis (SDS-PAGE) using Novex 12.5% Tris-Glycine mini protein gel (Invitrogen) was used following the manufacturer's instructions. Briefly, MNPs and PR-MNPs were incubated in plasma (Sigma Aldrich, Lot#SLBL6438V) at room temperature for 10 mins. Controls for plasma, PR and MNPs were also included. After incubation, particles were thoroughly washed with PBS. In order to detach the proteins adsorbed from the particles, these were incubated with trypsin at 80^{o}C for 5 min. The solution was then loaded into the gel. The samples were run at a constant voltage of 200 V for 35 min. Gels were stained with Coomassie blue (Invitrogen) and de-stained before imaging. Gels were imaged using a CanoScan LIDE 210 (Canon).

2.2.5 Liquid chromatography–mass spectrometry (LC-MS)

Human plasma was obtained from Sigma (pooled human blood, Sigma Aldrich, Lot#SLBL6438V). MNPs and PR-MNPs were incubated in plasma for 1 min and 30 min at 37^{o}C. After incubation particles were centrifuged (5 minutes at 14000 x g) and

separated from the plasma aided by a magnet. Particles pellets were washed twice with PBS. Particles were then digested with trypsin and analysed by liquid chromatography coupled with tandem mass spectrometry (LC-MS/MS) using a 4000 Q-Trap (Applied Biosystems, Carlsbad, CA, USA) mass spectrometer.

Proteomics results were analysed with help from Dr Daniel Scott and Dr Robert Layfield from the University of Nottingham. Proteomics analysis was performed with Scaffold software. Key identification parameters were set to 95% protein threshold, minimum number of peptides 2 and peptide threshold of 95%. Quantitative analysis was done by Normalized Spectral Abundance Factor (NSAF). Proteins were then clustered based on size (molecular weight), isoelectric point (pI) and protein family.

2.2.6 Thermogravimetric analysis (TGA)

The amount of dextran polymer on the particle surface was determined by TGA (TA Instruments Q 6000 STD) in a nitrogen atmosphere. Particles were dried overnight at 80^{o}C before TGA measurements. 4-8 mg of particles were deposited into a platinum TGA pan. The sample was allowed to equilibrate inside the TGA furnace at room temperature, then was ramped to 200^{o}C at a rate of 15^{o}C/min. The sample was held at 200^{o}C/min for 5 mins, before ramping up to 600^{o}C at 15^{o}C/min. Sample was held at 600^{o}C for 5 mins before cooldown. The organic content of the sample was estimated as the mass loss occurring between 200^{o}C and 500^{o}C. The fraction of mass that evaporates before 200^{o}C is typically assumed to be low-boiling volatiles (such as solvents, adsorbed moisture, etc.) while the fact that sample mass begins to plateau around 500^{o}C is taken to indicate that the organic have combusted and only the inorganic core of particles is left behind.

2.3 Magnetic nanoparticle (MNPs) delivery *in vitro*

All particles used in this thesis were dextran coated Nanomag®-D MNPs (Fe_3O_4 core; 250nm; Micromod, product code 09-02-252), unless differently stated MNPs used were COOH functionalised dextran coated Micromod Nanomag-D MNPs. Collaborators Dr Hareklea Markides and Prof Alicia El Haj from Keele University had previously tested these particles as MRI contrast agents *in vitro* and *in vivo* and had reported positive results on imaging with minimal effects on cell viability or cell differentiation capacity.[178]

All GET versions used in this thesis were synthesized by Fmoc solid chemistry by Protein Peptide Research (PPR Ltd) provided as salts.

For MNPs delivery in serum, cells were seeded into 12 well tissue culture treated plates (Scientific Laboratory Supplies) and incubated for 24 hours.

NIH3t3 and U87 were seeded at 5.2 x 10^4 cells/cm^2. hMSCs were plated at 5 x 10^4 cells/ cm^2.

Cells were treated, with nothing (media exchange), 50 μg/ml of MNPs and PR-MNPs at a 4 nmol PR/mg of MNPs unless otherwise specified. Cells were incubated overnight unless otherwise stated.

2.4 Iron analysis

2.4.1 Induced Coupled Plasma-Mass Spectrometry (ICP-MS)

Cells were washed with PBS and trypsinised for 3 min. Cell pellets were lysed in HCl 6M-HNO_3 (concentration 65% v/v) for 2 h at room temperature for the degradation of the particles to release the Fe content. Samples were then diluted in water in order to achieve a final acid concentration of less than 2% (w/v).

Samples were analysed by ICP-MS (Thermo-Fisher Scientific iCAP-Q; Thermo Fisher Scientific, Bremen, Germany). Samples were introduced from an autosampler (Cetac ASX-520) incorporating an ASXpress™ rapid uptake module through a PEEK nebulizer (Burgener Mira Mist). Internal standards were introduced to the sample stream on a separate line via the ASXpress unit and included Fe External calibration standard (Claritas-PPT grade CLMS-2 from SPEX Certiprep Inc., Metuchen, NJ, USA), in the range 0 – 100 μg L-1 (0, 20, 40, 100 μg L-1). A collision-cell (Q cell) using He with kinetic energy discrimination (He-cell) to remove polyatomic interferences was used to measure Fe. Sample processing was undertaken using Qtegra™ software (Thermo-Fisher Scientific). Results were reported back in parts per billion (μg/L). Iron association per cell was calculated as a percentage of the total amount of iron delivered.

2.4.2 Prussian Blue staining

Cells were fixed for 20 mins with 3.7% paraformaldehyde (w/v) in water (PFA; Sigma) at room temperature. From now on and for simplicity fixative solution will be referred to as 3.7% PFA.

Prussian blue staining solution: potassium ferrocyanide (Sigma) was diluted in a solution of hydrochloric acid 2.5% (v/v) in dH_2O to a final concentration of 25 mg/mL. Prussian blue staining solution was added to the cells and incubated for one hour. Stained cells were imaged using a Nikon Eclipse TS1000 light microscope.

2.5 Transfection

2.5.1 Plasmids

The plasmid pCMV-GLuc 2 encodes for the secreted luciferase from the copepod Gaussia Pinceps as a reporter under the control of cytomegalovirus (CMV) promoter. pCMV-GLuc 2 was purchased from New England Biolabs (NEB). Plasmid map on Figure 8.4.

The plasmid pGL4.51 with a gene encoding for firefly luciferase under the CMV promoter was kindly provided by Dr Blanka Sharma (University of Florida). Plasmid map on Figure 8.3.

The plasmid pCMV-eGFP-SV40-noDTS with a gene encoding for enhanced green fluorescent protein under the CMV promoter and the simian virus (SV40) enhancer and no DNA nuclear targeting sequences (no-DTS) was kindly provided by Prof Jon Dobson (University of Florida). Plasmid map on Figure 8.5.

All plasmids were propagated in DH5α competent E. coli. and selected for antibiotic resistance on agar plates. Individual colonies were picked and expanded to maxiprep volume on LB growth media containing antibiotic (ampicillin 100 µg/ml; kanamycin 50µg/ml). Bacteria pellets were purified using Qiagen Plasmid Purification Maxi kit,

following the manufacturer's protocol. DNA was diluted in nuclease free water (Sigma). Final DNA concentration and purity were measured by Nanodrop (NanoDrop ND-1000 Spectrophotometer, Labtech International). DNA was aliquoted and stored at -20^{o}C.

2.5.1.1 Plasmid labelling

pCMV-GLuc 2 plasmid DNA was labelled at a 1:1 ratio (v/w) of Label IT CX Rhodamine reagent to nuclear acid according to manufacturer's specifications (Mirus). 5 µl of 10X Labelling Buffer A were mixed with 5 µl of 1mg/ml plasmid DNA and 5 µl of Label IT CX Rhodamine Reagent in 35 µl of DNase, RNase free water. The mix was incubated for 1 hour at 37^{o}C. Labelled DNA was purified using a G50 Microspin Purification Column. Labelled DNA was stored protected from the light at -20^{o}C. Unless otherwise specified, for *in vitro* studies 1/3 of labelled DNA was used in combination with 2/3 of unlabelled DNA (w/w) as per previously optimised in the group. DNA labelled this way will be referred to as Rh-DNA.

2.5.2 YO-PRO-1 fluorescence quenching assay

There are various fluorimetric techniques to determine the interaction of a gene vector with DNA. These techniques rely on the fact that the DNA molecule on its own is not fluorescent, however, there are certain molecules such as ethidium bromide, monomeric and dimeric cyanide dyes that emit fluorescence upon intercalation into the DNA structure. When adding a molecule in solution capable of complexing DNA, the ability of the dye to intercalate with the DNA decreases, leading to a decrease in fluorescent signal from the DNA/dye complex. YO-PRO-1 is a cyanine dye that has

previously been demonstrated to interact with DNA with minimal interference in the condensation process (Figure 2.1).[179]

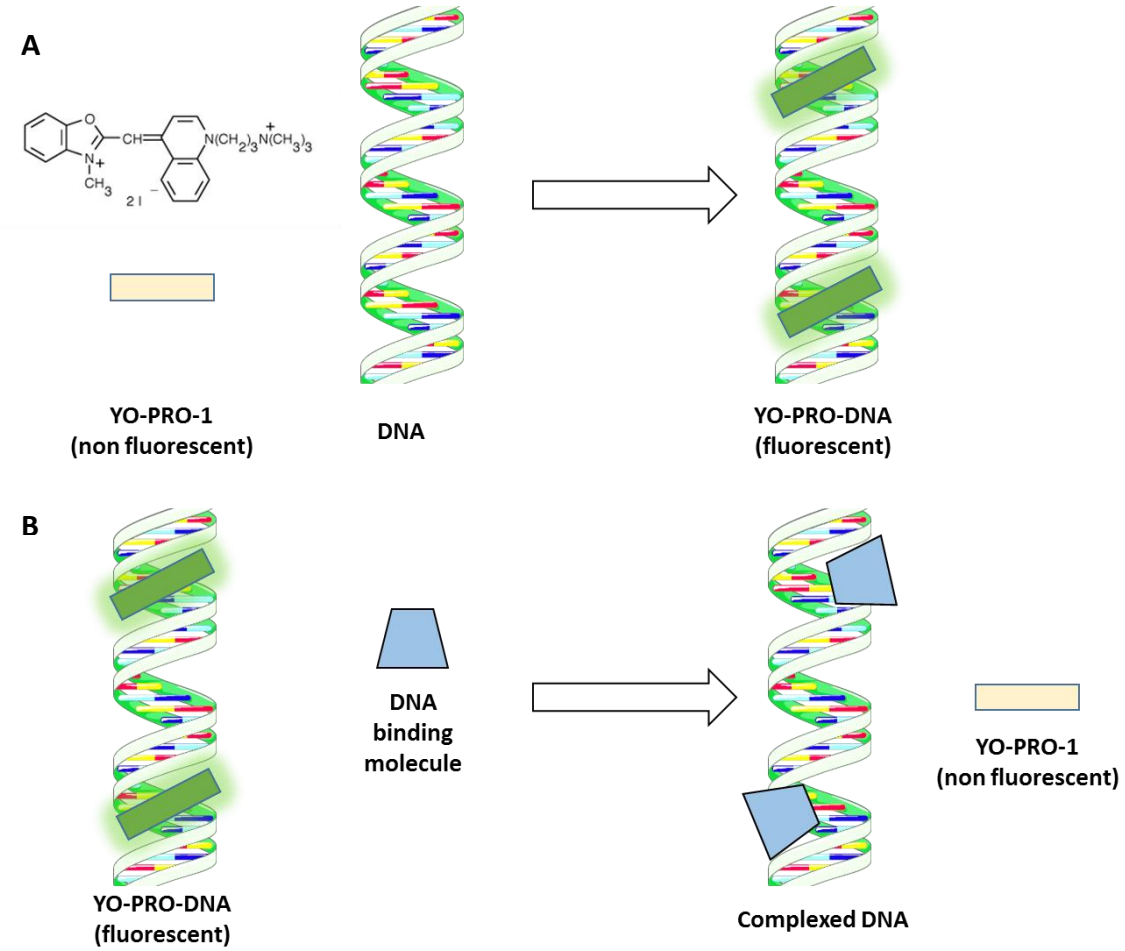

Figure 2.1 Schematics of YO-PRO-1 binding mechanism to DNA.

A) Upon binding to DNA, YO-PRO-1 becomes fluorescent (ex. 491 nm, em. 509 nm). B) When the DNA binding molecule outcompetes YO-PRO-1 of DNA based on the higher affinity, YO-PRO-1 loses its fluorescence. The loss in fluorescence is inversely proportional to the amount of complexed DNA.

Table 2 Calculation of amount to YO-PRO-1 needed to bind 1 µg of pCMV-GLuc 2.

Base pairs (bp) per pCMV-GLuc 2 plasmid	bp in 1 µg of pCMV-GLuc 2 plasmid	YO-PRO-1 molecules to bind 1 µg of pCMV-GLuc 2*	Volume of 1 mM YO-PRO-1 solution to bind 1 µg of pCMV-GLuc 2 (µl)
5800	9.3×10^{14}	1.9×10^{13}	0.03

** For optimal DNA binding, the concentration of YO-PRO-1 dye to DNA is 1 dye molecule to 50 DNA base pairs (bp).* [180]

For each individual repeat, 1 µg of DNA was diluted in 6 µl of 10 mM HEPES buffer (pH 7.4). Similarly, 0.03 µl of YO-PRO-1 1 mM were diluted in 6 µl of the same buffer. The DNA solution was added dropwise to the peptide solution and incubated for 5 hours at room temperature in foil-wrapped tubes (Table 2).

This process was scaled up proportional to the number of repeats per experiment, making up one stock solution of YO-PRO-DNA.

The YO-PRO-DNA solution was diluted to a final concentration of 10 µg/ml in 10 mM HEPES buffer (pH 7.4). An increasing amount of peptide corresponding to the desired charge ratio between amine (NH_2^+) groups in a vector and phosphate (PO_3^-) groups in DNA (N/P) (Table 3) was added to DNA-YO-PRO, followed by mixing and further incubation for 10 mins. Fluorescence intensity was measured at ex/em 480/509 nm (Infinite® 200 PRO, TECAN). Experiments were performed in triplicate and results are expressed as percentage of fluorescence of YO-PRO-DNA alone against charge ratio (N/P). YO-PRO-1 alone was used as blank.

Table 3 Volume of FLR (1 mM) in µl needed to form a peptide-DNA complex at the indicated charge ratio (N/P) for 1 µg of plasmid DNA of approximately 5800 bp.

FLR/DNA ratio (N/P)	1	2	3	4	5	6	7	8	9	10
FGF2B-LK15-8R (µl of a 1 mM solution)	0.17	0.34	0.51	0.68	0.85	1.02	1.2	1.37	1.54	1.71

N/P charge ratio was calculated based on the number positively charged amine groups of the FLR molecule (+18).

2.5.3 Magnetofection and Transfection NIH3t3 cells (*Results II*)

Table 4 FLR-DNA-MNPs complexation for 0.5 µg of DNA per transfection on a 48 well-plate format. Scalable to other well-plate formats.

MNPs (µg/µg DNA)	DNA (µg)	FLR¥/DNA incubation time (min)	OptiMEM (µl)*	MNPs (µl of 10 mg/ml stock)§	FLR/DNA + MNPs incubation time (min)	Media per well (µl)	Total transfection volume (media+ OptiMEM)(µl)
5	0.5	15	2x12.5	0.25	15	100	125
10	0.5	15	2x12.5	0.5	15	100	125
25	0.5	15	2x12.5	1.25	15	100	125
50	0.5	15	2x12.5	2.5	15	100	125

¥ Volume of FLR (1mM) added was adjusted according to N/P ratio (table 3)
** FLR was diluted to a total volume of 12.5 µl in OptiMEM. DNA was diluted to a total volume of 12.5 µl in OptiMEM. DNA solution was added to FLR solution and mixed thoroughly to facilitate particle formation.*
§ MNPs volume was added straight into the FLR-DNA solution and mixed thoroughly.

For transfection/ magnetofection, cells ($4.2x10^5$ NIH3t3 cells/cm^2) were seeded on a 48 well plate format (unless otherwise specified) 24 hours prior to treatment. Prior to transfection, media in the wells was replaced with fresh media. FLR-DNA-MNPs were formulated as described on table 4. For magnetofection, cells were placed on top of individual magnets arranged in a way such that the wells would be on top of each individual magnet. Magnet array schematic (Figure 2.2) Individual magnet dimensions, 10 mm dia x 5 mm thick, N52 Neodymium (First for Magnets, UK catalog number F645-N52-10).

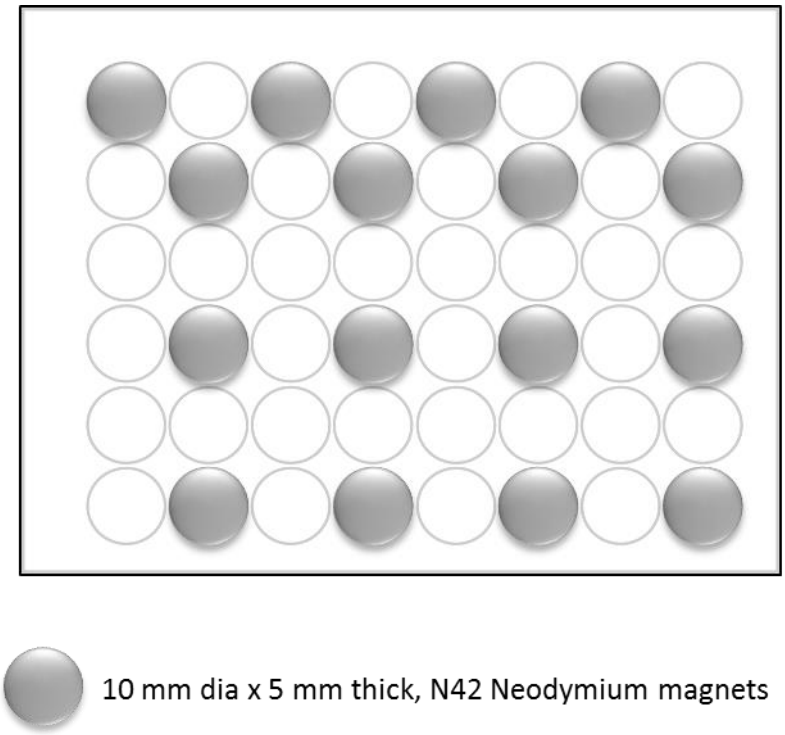

Figure 2.2 Magnet array configuration for magnetofection.
Individual magnets were arranged and fixed in a way such that they would fit wells on a 48 well-plate format. Individual magnets were N52 Neodymium, 10 mm diameter and 5 mm thick. Field strength was of 4.4 T on the magnet surface according to manufacturer's specifications.[181]

After transfection/magnetofection, cells were washed three times with PBS or heparin (first wash 100 µg/ml in PBS + two washes with PBS). PBS was replaced with growth media followed by further 24 hour incubation at 37°C in 5% CO_2.

2.5.4 Magnetofection/transfection for DC 2.4 (*Results III*)

2.5.4.1 Particle optimisation

2.5.4.1.1 PEI-MNPs

PEI-MNPs OLEIC acid nanoparticles were kindly provided by Dr Melissa Cruz-Acuña (University of Florida). Previously published optimisation of the particles[182]

reported complete DNA binding at a N/P ratio of 3. For gene delivery optimisation in DC 2.4, N/P ratios of 2.5, 5 and 10 were tested.

N/P ratio was calculated based on the number of positively charged amine groups of 25 KDa branched PEI (Sigma) (+211). PEI content of PEI-MNPs was reported to be 67% (w/w). The concentration of the PEI-MNPs solution provided was 10.93 mg/ml (table 5).

Table 5 Volume in µl of PEI-MNPs (10.93 mg/ml) needed to form a PEI-MNPs /DNA complex at the indicated charge ratio (N/P) for 1 µg of plasmid DNA of approximately 5800 bp

PEI:DNA ratio (N/P)	2.5	5	10
PEI-MNPs (µl of a 10.93 mg/ml particle solution)	0.125	0.25	0.5

Optimisation of PEI-DNA on DC 2.4 was done empirically. PEI-DNA particles were formed by combination of PEI particles and plasmid DNA at the above mentioned N/P ratios 2.5, 5 and 10 in serum free media (SFM) for 15 mins. Final concentrations of DNA 0.06, 0.125, 0.25, 0.5, 1 and 2 µg DNA/transfection were achieved by serial dilution of PEI-DNA complexes in Serum Free Media (SFM).

2.5.4.1.2 FLR-DNA-MNPs

FLR-DNA-MNPs were formulated as previously described (*Material and Methods*, tables 3 and 4). Dextran coated Nanomag-D MNPs; Fe_3O_4 core; 250nm were purchased from Micromod. Briefly, FLR-DNA nanoparticles were mixed at an initial DNA concentration of 2 µg of DNA/transfection, N/P ratio of 10 in serum free media and incubated for 15 min at room temperature[183]. MNPs were added to the following final concentrations: 10, 20 and 40 µg of MNPs/µg of DNA and incubation for a further 15 mins at room temperature.

Optimisation of FLR-DNA-MNPs on DC 2.4 was done empirically by serial dilution of FLR-DNA-MNPs to final concentrations of DNA: 0.06, 0.125, 0.25, 0.5, 1 and 2 µg DNA/transfection.

2.5.4.2 Magnetofection

2.5.4.2.1 Magnefect-nano™

Horizontal NdFeB magnet arrays, grade N42 and Magnefect-nano™ system were kindly provided by Dr Jon Dobson's lab.[184] All experiments were performed on a 96 well plate format and corresponding configuration of magnet array. The frequency and amplitude of the oscillation of the magnet array was controlled by a computerized motor system. Field strength was of 320 ± 25 mT on the magnet surface, field gradient ranges from 100-200 T/m (from the centre to the edge of the well).[185]

First, the plasmid of interest was combined with FLR at a N/P ratio of 10 in serum free media (SFM) to a total volume of 15 µl per µg of DNA. FLR-DNA mix was incubated for 15 min at room temperature (RT) after which it was combined with MNPs in SFM at a DNA: MNPs mass ratio of 20 µg MNPs/ 1 µg of DNA. FLR-DNA-MNPs were incubated in a total volume of 25 µl for a further 15 min at RT.

As a positive control FuGENE (FuGENE 6, Promega, USA) was also conjugated in parallel according to manufacturer's specifications, briefly, FuGENE was mixed with DNA at a 3:1 ratio (v/w) in SFM.[186]

Prior to transfection cell growth media was replaced with fresh media. Total transfection volume (transfection mix plus growth media) per well on a 96 well-plate format was 100 µl.

Immediately after delivery of transfection mix the culture plate was placed: on a static magnet array (static magnetofection) or on the Magnefect-nano^{TM} array sample holder at 2 Hz frequency and 0.2 mm displacement (oscillating magnetofection) [182], [187], [188]. After 1 hour, cells were washed twice with PBS and incubated in normal growth media at 37^{o}C and 5% CO_2 until collection.

2.5.5 Reporter gene expression

2.5.5.1 Gaussia Luciferase activity

Gaussia Luciferase expression was measured 24 hours post transfection/magnetofection using BioLux Gaussia Luciferase Assay Kit (New England Labs, UK), based on the reporter luciferase from the marine copepod Gaussia princeps. 10 µl of media were collected from each transfection well and added onto a white 96-well plate (Corning, UK). 50 µl of Gaussia luciferase (GLuc) assay solution were added to each well, GLuc assay solution: 1:100 dilution BioLux GLuc Substrate into BioLux GLuc Assay Buffer. Luminescence was measured using a luminometer ((Infinite® 200 PRO, TECAN), integration time 500 ms.

2.5.5.2 Firefly Luciferase activity

Measurement of firefly luciferase activity was carried out with Luciferase Assay System (Promega, USA). This kit relies on the light produced by the oxidation of luciferin to oxyluciferin, catalysed by firefly luciferase protein produced by the transfected cells.

Cells were washed twice with PBS and incubated with 1 X Cell Culture Lysis Buffer (Promega, USA) for 15 min at room temperature under constant shaking. Cells were

scraped from the wells and centrifuged at 12000 x g for 15 seconds at room temperature. The cell lysate was collected into a new tube.

Lysates were stored at -80^{o}C until luciferase activity measurements.

To measure firefly luciferase activity 10 µl of the cell lysate were transferred to a black 96 well-plate (Corning, USA). Right before measurement, 50 µl of the working solution of luciferase substrate (D-Luciferin) were prepared following manufacturer's specifications, briefly, 100x Luciferase Assay Substrate (D-Luciferin) stock was diluted on Luciferase Assay Buffer (Promega, USA) (1:100). Luminescence was measured using a luminometer, integration time 1 s (Synergy HT, Biotek instruments, Gen 5 Software).

Firefly luciferase activity was reported per mg of protein in the sample. Protein quantification was performed by Bicinchoninic acid (BCA) assay.

2.5.5.2.1 BCA protein assay

Protein content per sample was quantified using bicinchoninic acid, BCA Protein Assay (Thermo ScientificTMPierce^{TM}, US). This protein assay method is based on the reduction of Cu^{2+} to Cu^{1+} by protein in an alkaline medium. Cu^{1+} cations are chelated by BCA forming a purple-coloured complex with strong absorbance at 562 nm. Following manufacturer's specifications, 10 µl of cell lysate were mixed with 200 µl of BCA reagent in a 96 well plate and incubated at 37^{o}C. After 30 min the plate was cooled down to RT, and the absorbance was measured at 562 nm on a plate reader (Synergy™ 2 Multi-Mode Microplate Reade, Biotek Instruments, Gen 5 Software v 1.10). A standard curve of bovine serum albumin (BSA) was used to determine final protein concentration in the sample.

2.5.5.3 Green Fluorescent Protein (GFP) expression

Expression of GFP encoding reporter gene was quantitatively measured by flow cytometry.

Transfected cells were trypsinised and resuspended in 200 µl of FACS sorting buffer (2% FCS v/v in PBS). Each sample was run individually through a flow cytometer, 5000-10000 total events were recorded per sample (488 nm laser on a BD LSR Cell analyser, FACS Diva Software). Flow cytometry raw Flow Cytometry Standard (FCS) file data were gated and quantified using Weasel software (version 3.0.2). Briefly, viable cell population was gated based on side and forward scatter dot plots (Figure 2.3). Untreated DC 2.4 were used as a control for cell side and forward scatter[189]. Due to the uptake of MNPs the side scattered of the cells was significantly shifted. A gating area that would include MNP labelled and unlabelled cells was established. Next, a new dot distribution of GFP intensity against Phycoerythrin (PE) intensity was plotted to identify cell autofluorescence[190]. Only cells with a mean GFP intensity of over $1x10^3$ outside the diagonal were considered GFP positive cells.

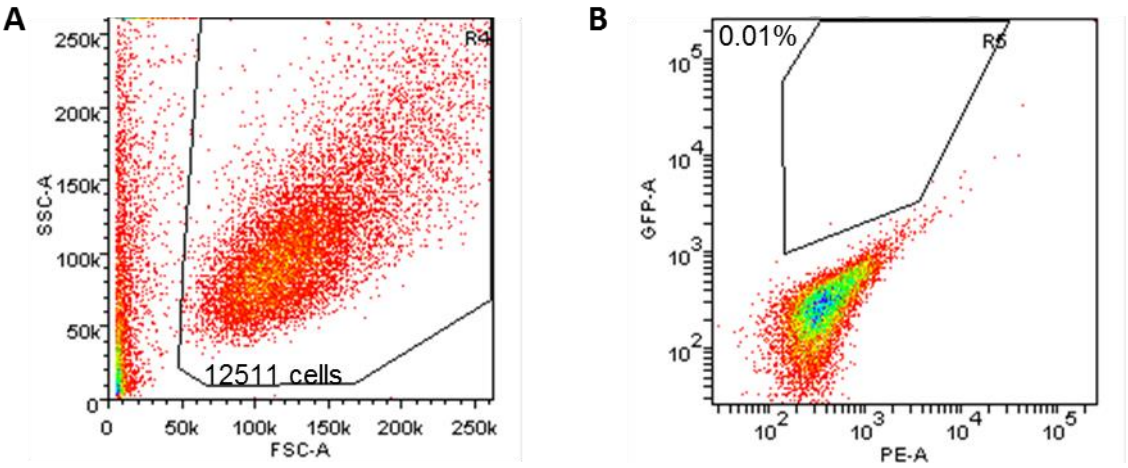

Figure 2.3 Fluorescent activated cell sorting (FACS) profiles of DC 2.4.

DC 2.4 were transfected with pCMV-eGFP-SV40-noDTS plasmid as described in Material and Methods. FLR/MNPs ratio was the same for A and B. Cells treated with FLR-MNPs were used as a control for changes in side scatter (SSC) (A). Only cells with a mean GFP intensity of over 1x10^3 outside the diagonal were considered GFP positive cells (B).

2.5.6 Cellular Uptake Inhibition Study

To study the mechanism of uptake of FLR/FLR-MNPs vectors with and without the application of magnetic field, NIH3t3 cells were prepared on 48-well plates at a 4 x 10^4 cells/well and incubated at 37^{o}C and 5% CO_2 for 24 hours. Prior to transfection cells were exposed to one of the following conditions for 30 mins: (1) incubated at 4^{o}C (as opposed to 37^{o}C), (2) addition of 0.45 M of sucrose (Sigma, S9378) [191], [192] into the cell growth medium, (3) 100 µM of 5(N-ethyl-N-isopropyl) amiloride (EIPA) (Sigma, A3085) [193]and (4) 5 mM methyl-B-cyclodextrin (MBCD) (Sigma, C4555) [194], [195] in normal growth media. Cells were then loaded with 25 µl of FLR-DNA or FLR-DNA-MNPs (formulated with Rh-DNA) and incubated for one hour with or without exposure to a magnetic field. Transfection was carried out at 4^{o}C for inhibition at low

temperature. All other transfections were carried out at 37^{o}C. Control group was transfected at 37^{o}C in normal growth media without inhibitors. After one hour cells were washed with PBS or heparin (100 µg/ml).

Plasmid cellular uptake was quantified by flow cytometry. Each sample was run individually through a flow cytometer, 5000-10000 total events were recorded per sample (Astrios EQ sorter, Beckman Coulter, US). Untreated cells were used as control.

2.5.7 Extraction of extrachromosomal DNA

After transfection/magnetofection cells were washed with PBS to remove any unbound vector. Cells were then incubated in normal growth media at 37^{o}C 5% CO_2 until collection. Collecting points: immediately after transfection (0 min), 10 min, 25 min, 55 min and 24 hours post transfection. Briefly, cells were trypsinized for 3 min at 37^{o}C, 5% CO_2 after which the trypsin was neutralized with pre-warmed media. Cells were pelleted and resuspended in 50 µl Hirt buffer (10 mM EDTA, pH 7.5, and 0.6% SDS) and incubated at 4^{o}C for 8 hours after which they were stored at -20^{o}C until DNA extraction/purification.

For DNA purification QIAprep Spin Miniprep Kit was used according to manufacturer's specifications (QIAGEN, ID 27106) briefly, 400 µl of PB buffer were mixed with the Hirt-cell suspension. The mix was then applied to a QIAprep spin column and centrifuged for 60 seconds at maximum speed (>15kxg). The eluent was discarded and the column was then washed with 500 µl of PE buffer by centrifugation (same as for PB buffer). Finally the DNA was eluted in 30 µl of ultrapure DNase free water.

DH5α competent E. coli (40 µl) were added to purified DNA (2.5 µl) and incubated for 30 min on ice. Cells were then heat shocked for 45 seconds in 42°C water bath after which the tubes were placed again on ice for 5 min. 250 µl of pre-warmed SOC recovery media were added to cells and incubated for 1 hour at 37°C, shaking at 225 rpm. After incubation 50 µl of each transformation were spread on a selective LB agar plate (100 µg/ml ampicillin). Plates were then incubated overnight at 37°C. Colonies were counted the following day.

2.6 Haematocompatibility assays

The impact of the GET-MNPs on erythrocyte aggregation and haemolysis were analysed as described. [196]

2.6.1 Erythrocyte aggregation

Human blood sample was purchased from the NHS. Blood was transferred into tubes and centrifuged at 5000xg for 5 min. The cell pellet was washed twice with PBS. To quantify aggregation, 6 x 10^5 erythrocytes were mixed to 100 µg/ml MNPs (MNPs), 0.4 nmol/ml PR (PR) and 100 µg/ml PR-MNPs (4 nmol PR/mg MNPs) in PBS or plasma. After incubation under constant shaking at 37°C for 5 and 30 min, cell aggregation was evaluated using Nikon Eclipse TS1000 light microscope. As negative control for aggregation, erythrocytes were treated with either PBS or plasma alone.

2.6.2 Haemolytic activity

Human blood sample was purchased from the NHS. Blood was transferred into tubes and centrifuged at 5000xg for 5 min. The cell pellet was washed twice with PBS. 6 x 10^6 erythrocytes were mixed to 100 μg/ml MNPs (MNPs), 0.4 nmol/ml PR (PR) and 100 μg/ml PR-MNPs (4 nmol PR/mg MNPs) in PBS or plasma. After incubation for 5 and 30 mins samples were centrifuged at 5000xg for 5 min. The supernatant was collected and haemoglobin content was analysed by spectrophotometry at 544 nm (Infinite® 200 PRO, TECAN).

2.7 Cell imaging

2.7.1 Transmission electron microscope (TEM)

To confirm the cellular localization of the MNPs, samples were fixed in 3% (w/v) glutaraldehyde in 0.1 M cacodylate buffer for one hour and post-fixed in 1% aqueous osmium tetroxide for 30 min. The samples were then dehydrated in a graded ethanol series and infiltrated with Transmit resin (TAAB, UK), then allowed to polymerise for 48h at 70°C. Semi-thin sections were cut (0.5 μm), using a Reichert-Jung ultramicrotome, and stained with 2% toluidine blue. Imaging was performed on a Tecnai 12 Biotwin TEM (FEI, USA) run at 100Kv.

2.7.2 Confocal microscope

2.7.2.1 NIH3t3 cells imaging

NIH3t3 cells were seeded on sterilized glass coverslips (Borosilicate Glass, 13 mm dia, VWR) at a density of 4.2 x 10^4 cells/cm^2 in normal growth media and incubated at 37°C and 5% CO_2 for 24 hours. Cells were loaded with 25 μl of FLR-DNA or FLR-DNA-MNPs

(formulated with Rh-DNA) in OptiMeM formulated as previously described. After 30 min, 1 hour and 24 hours of incubation cells were fixed in 3.7% PFA and permeabilised using triton X-100 for 15 minutes then washed in PBS. Actin cytoskeleton was visualised by staining with Alexa Fluor 488 Phalloidin (Thermo, A12379). The coverslips were washed and sealed onto slides with DAPI containing Fluoroshield mounting media (Sigma Aldrich, UK). Cells were imaged using a LSM880C Confocal Microscope (Zeiss, Germany). A 63x immersion objective lens was used with a 488 nm laser used for Hoechst and phalloidin stained cytoskeleton and a 561 nm Diode-pumped solid-state (DPSS) laser for rhodamine labelled DNA. Images were captured using ZEN software (Zeiss, Germany). Three-dimensional image stacks were recorded by sequential acquisition of optical sections along the z-axis with steps of 0.33-0.37 um. The acquired digital images were merged and processed by using ImageJ version 4.

2.7.2.2 Dendritic cell imaging

DC 2.4 cells were seeded on sterile coverslips at a density of $7.8x10^4$ cells/cm^2. After 24 hours the cells were transfected with FLR-DNA-MNPs with 0.5 µg fluorescently labelled Rh-DNA, N/P 10, 20 µg MNPs/ 1 µg of DNA. FLR-DNA-MNPs were delivered under a static field for 1 hour at 37^{o}C and 5% CO_2. Unbound vector was washed with PBS and cells were placed back on the incubator in normal growth media. 1 hour post-delivery cells were placed on a static magnet array (static) or on an oscillating magnet array (2 Hz, 0.2 mm amplitude) for 1 hour. At this point cells were fixed with 3.7% PFA for 20 mins at room temperature. Cells were then washed with PBS and sealed onto glass slides with Vectashield® Mounting Medium with DAPI (Vector Labs, USA)

Confocal laser scanning microscopic (CLSM) analysis of the cells was performed using Leica TCS SP8 with Leica Application Suite X Software (LAS X). A 63x immersion objective lens was used with a 488 nm laser used for Hoechst and a 561 nm DPSS laser for rhodamine labelled DNA. At least 12 random images were taken for each condition. Three-dimensional image stacks were recorded by sequential acquisition of optical sections along the z-axis with steps of 0.5 µm. The acquired digital images were merged and processed by using ImageJ version 4.0J.

2.8 Statistical analysis

For *in vitro* studies n represents the number of biological repeats. Technical replicates refer to experiments carried out with different passage cells but identical experimental conditions. Data were presented as mean ± standard deviation (s.d.) and analysed by Prism statistical analysis software (GraphPad v. 7.03). The significance of the results is denoted by "*" or "$" symbol and described for each graph as well as the comparison test used.

3 Enhanced cellular transduction of MNPs resistant to rapidly-forming plasma coronas

3.1 Introduction

Targeted delivery strategies for MNPs have been developed towards specific- or over-expressed receptors on disease cells by functionalising the NPs surface with proteins, antibodies or other biomolecules. These strategies efficiently enhance NPs delivery to the target cells *in vitro*; however there is mounting evidence that enhanced uptake and targeting ability of functionalised particles disappears when placed in an *in vivo* biological environment.[168]–[170], [197]

It is now well established that when any material surface encounters biological systems, interactions occur between the material and the biological components (i.e. proteins, lipids, DNA) forming a "protein corona". This protein corona defines the physicochemical and biological identity of the particle by altering properties such as size and charge and as a result colloidal stability. Additionally, proteins expressed on the particles surface greatly influence its interaction with the environment. Adsorbed proteins in general favour particle clearance from the body and inhibit cell adhesion and subsequent uptake.[196], [198]–[201]

As previously mentioned during the introduction, Dr Dixon's group has published the development of a peptide based system, termed GET, capable of efficiently delivering a broad range of cargoes for various tissue engineering and gene therapy applications. More importantly for the purpose of this chapter, a variant of GET, P21-8R (Figure 3.1),

was able to significantly enhance MNP uptake *in vitro*.[163] From now on in this thesis, and unless otherwise stated, P21-8R will be referred to as PR.

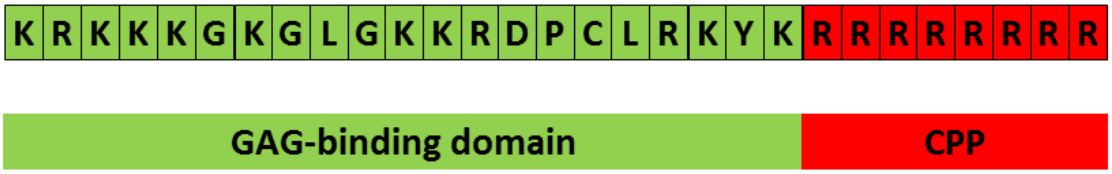

Figure 3.1 GET peptide P21-8R (PR).

PR peptide amino acid sequence. GAG-Binding Domain represented in green and Cell Penetrating Peptide (CPP) represented in red. Full amino acid chemical structure displayed in Figure 8.6.

3.1.1 Aims

The aim of this results chapter was to characterise and quantify the physicochemical properties and delivery of PR-MNPs to mammalian cells *in vitro.* PR was capable to efficiently enhance particle uptake in serum and plasma-rich conditions. As this appeared different from the published examples which use cell membrane targeting of NPs, [168], [202] the detailed structure of MNPs interface with the biological environment was investigated, including protein corona density and make-up formed on PR-MNPs over time as well as their pathobiological effects.

3.2 Chapter experimental overview

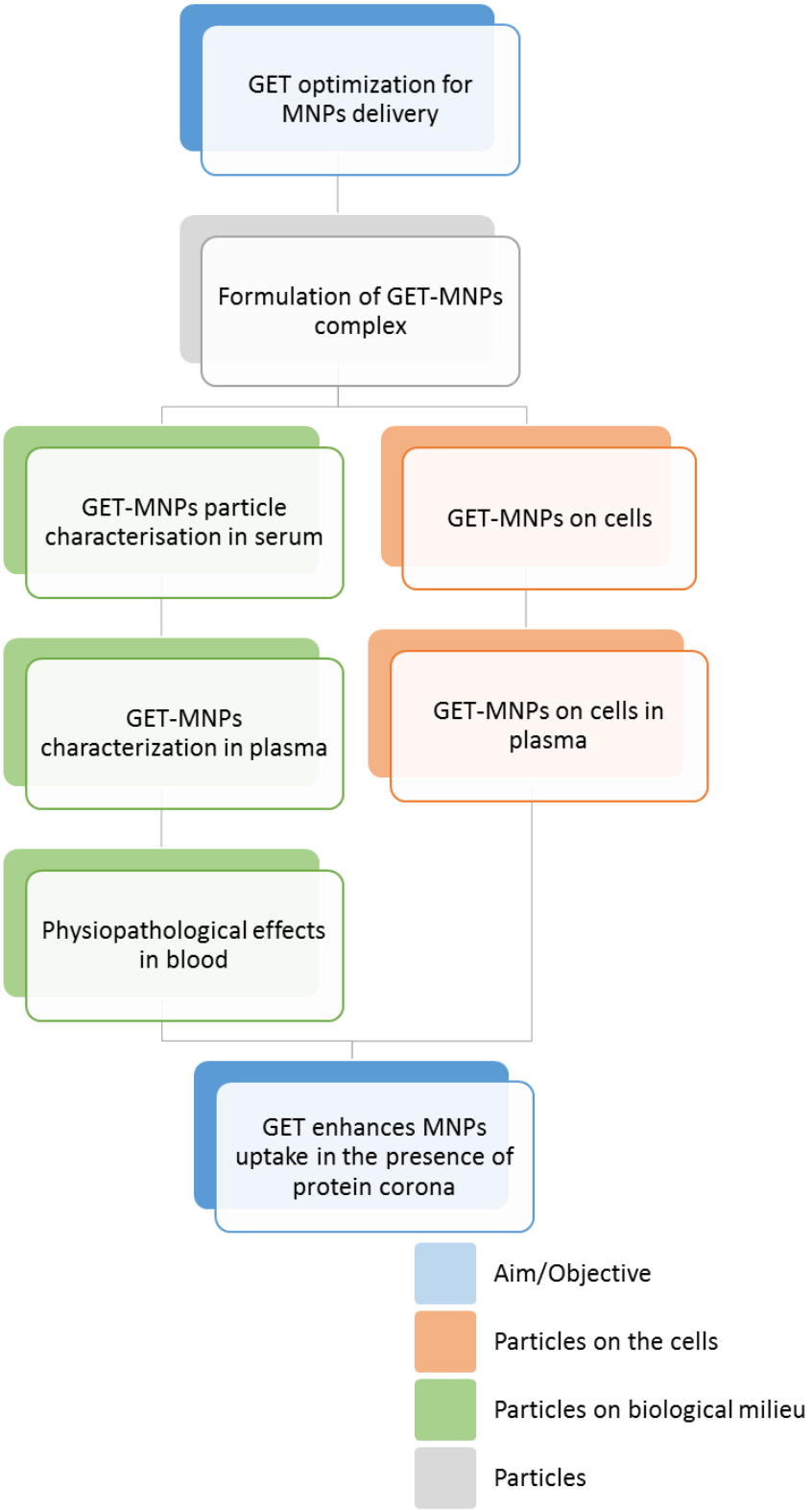

3.3 Results

3.3.1 PR electrostatically interacted with dextran coated MNPs

Currently, dextran-coated MNPs or SPIONs (containing iron oxide cores) are being used for a wide number of applications in biomedicine.[5], [73], [86], [203] In this results section and unless otherwise stated, MNPs refers to commercially available dextran-COOH coated MNPs (Micromod Nanomag-D, 250nm). TEM analysis of the magnetic core of these MNPs (250nm) showed a core size of 133 nm ± 38 nm (Figure 3.2).

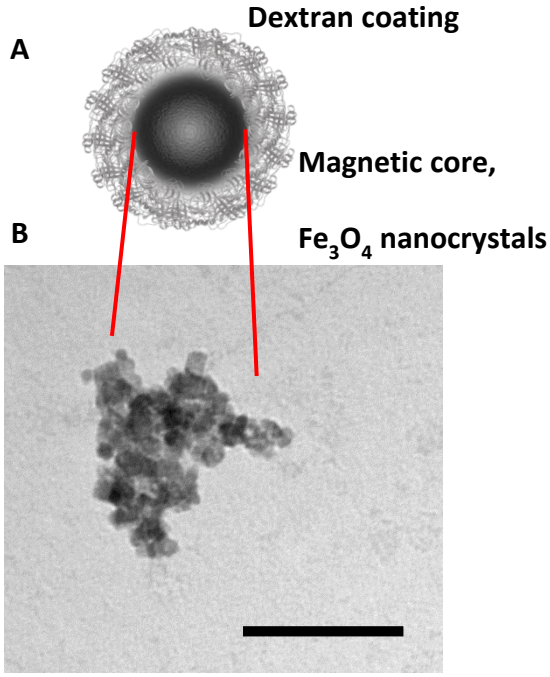

Figure 3.2 Micromod Nanomag-D MNPs.
A) Schematic representation of Micromod Nanomag-D 250 nm particles (MNPs). Formed of a magnetic core of Fe_3O_4 nanocrystals embedded in a dextran matrix functionalised with carboxyl groups. B) Representative TEM image of the Micromod Nanomag-D 250 nm particles (MNPs) showing the magnetic core formed by a cluster nanocrystals. Average core size 133 nm ± 38 nm diameter. Scale bar 100 nm. Other TEM images displayed in Figure 8.8.

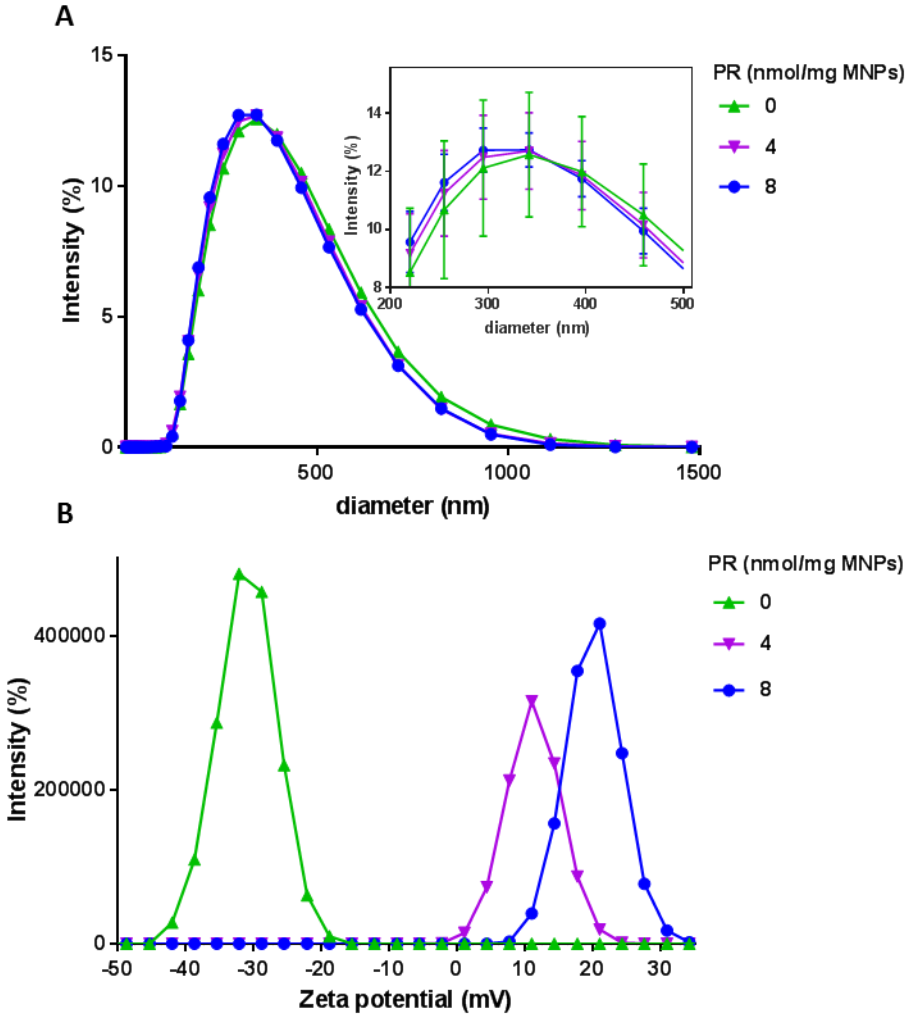

Figure 3.3 Characterisation of PR-MNPs.

A) Apparent diameter of the particles obtained by DLS for 50 µg/ml of MNPs incubated with increasing concentrations of PR (PR concentration expressed as nmol PR per mg of particles). DLS measurements were done in water. n=6 independent repeats, 3 subruns per repeat. B) Zeta potential of MNPs (50 µg) incubated with increasing concentrations of PR (PR concentration expressed as nmol of PR per mg of particles). Zeta potential was measured in water. The shift in zeta potential indicates the interaction of PR with MNPs (n=6 independent repeats, 3 subruns per repeat).

It had been previously shown that by simple co-incubation of GET peptides with MNPs intracellular uptake of the MNPs into mammalian cells was significantly enhanced. PR is a positively charged L-amino acid (pI ~12)[163] whereas Micromod Nanomag-D dextran coated particles are negatively charged. In order to assess PR interaction with MNPs, the zeta potential of the MNPs in the presence of increasing concentrations of

PR was assessed (Figure 3.3 B). The shift in zeta potential of the MNPs (-26.2 mV) compared with PR functionalised particles at 4 and 8 nmol/mg MNPs (11.7 mV and 20.3 mV respectively) indicates strong electrostatic interaction between the dextran coated particles and the positively charged PR which was proportional to PR concentration. Particle characterisation assessments demonstrated particles in the monodisperse range after functionalisation with 4-8 nmol/mg of MNPs (Table 6) with no significant changes from particle size distribution compared to naked particles.[204]

Table 6 Physical characterisation of PR-MNPs.

	DH (nm)*	**PDI¥**	**Zeta potential (mV)**
MNPs	320.9 ± 21.6	0.16 ± 0.04	-26.2 ± 6
PR-MNPs (4 nmol/mg)	310.2 ± 12.8	0.16 ± 0.03	11.7 ± 1.5
PR-MNPs (8 nmol/mg)	309.4 ± 11.7	0.16 ± 0.02	20.3 ± 0.8

The size and zeta potential of the bare and PR *functionalised MNPs in water (dH2O) were measured using Malvern Nanosizer Nano ZS. Values represent mean ± s.d. (n=6 independent repeats)*

** Z-average hydrodynamic diameter extracted by cumulant analysis of the data.*

¥Polydispersity index from cumulant analysis

PR labelled with fluorescent TAMRA, PR-T, was used to study the binding isotherms of peptide to MNPs. Langmuir's approximation (Eq 4) was used to fit the adsorption isotherms due to its ability to estimate relevant parameters for understanding the protein adsorption process such as maximum concentration of bound protein in a monolayer formation as well as the equilibrium constant for the adsorption.[177], [205]

$$S = \frac{S_{max} K C_f}{1 + K C_f} \qquad (4)$$

Where in this particular application, Cf is the PR-T concentration remaining in solution at equilibrium, S represents the adsorbed amount of PR-T at equilibrium, S_{max} is the maximum concentration of bound PR onto the MNPs and K is the Langmuir's equilibrium constant that describes the strength of interaction between PR and the particles surface. [177]

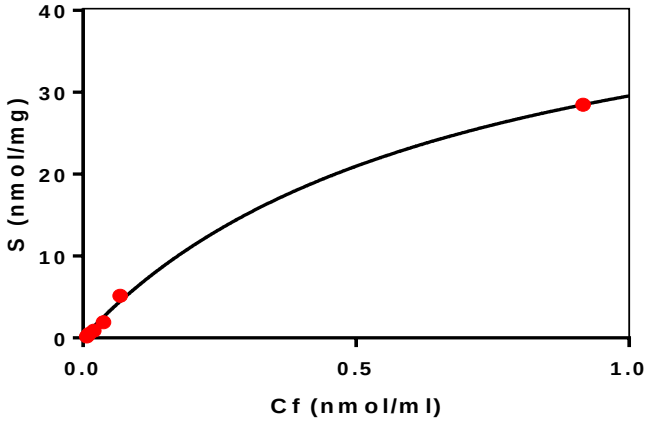

Figure 3.4 Representative Langmuir fitting curve for PR adsorption on MNPs.
Red dots represent the adsorption measured on MNPs, black line represents the non-linear fitting of Langmuir isotherm (n=1, all Langmuir fitted isotherms are presented in Figure 8.9*.*

The adsorbed fraction of PR-T was plotted versus the free concentration in solution at equilibrium and non-linear regression was fitted to the experimental data[176] (Figure 3.4). Parameters of adsorption S_{max} as well as the constant of adsorption *K* confirm high binding efficiency of PR to the MNPs (Table 7).

Table 7 Average Langmuir parameters for PR-T adsorption on MNPs (n=4, Langmuir parameters for each independent replicate are displayed on Table 15 Langmuir constants for PR adsorption on MNPs.

	S_{max} (nmol/mg)	**K (ml/nmol)**
PR-T-MNPs	44 ± 8.6	1.2 ± 0.2

The complexity of the protein adsorption process makes development of models that account for all the different binding interactions and phenomena involved very difficult. However, the estimation provided by this model was used as a reference concentration for MNPs saturation with unlabelled PR (MNPs saturated by PR at approximately 40 nmol/mg in a 15 minute incubation).

Upon adsorption onto a surface, protein molecules can experience a change in conformation and/or orientation in search of the most energetically stable arrangement. Driven by hydrophobicity and charged group interaction these structural changes can impact on protein-substrate interactions and thereby reduce efficiency.[199], [206], [207] Protein structure can be studied through the analysis of their amide I band which provides a very strong adsorption on infrared spectroscopy. This band can be deconvoluted in order to quantify secondary structure components.[175], [208], [209] Conformational changes of PR peptide upon interaction with MNPs were also studied by FTIR (Figure 3.5). PR significantly loses alpha-helical structure in favour of beta-sheet component (alpha-helix fraction decreases from 0.26 to 0.22; beta-sheet fraction increases 0.29 to 0.32). These changes suggest a certain degree of denaturation of the original PR peptide secondary structure on interaction with the MNPs. Additionally, the increase of beta-sheet component indicates a higher coordination of the different subunits of the molecule (lysine-rich P21 amino acid peptide GAG-binding domain and octoarginine 8R which is the CPP component) whereas the loss on the helical structure component would be consistent with a change of the protein onto a more organized conformation required for a stable interaction with the MNPs. [207]

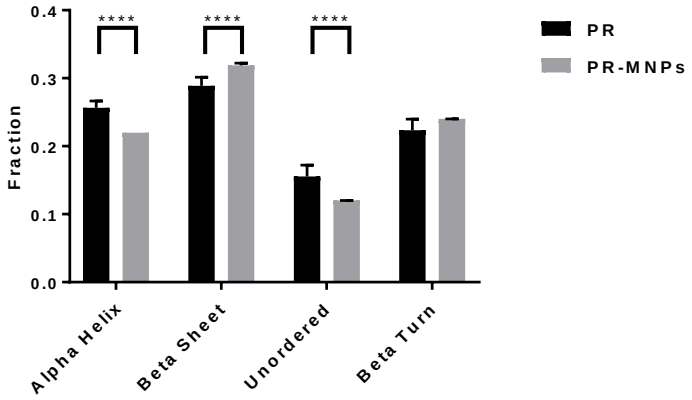

Figure 3.5. PR changes conformation upon adsorption to MNPs.
Conformational assessment of PR upon adsorption onto MNPs, showing the fraction of the protein on Alpha Helix, Beta Sheet, Unordered and Beta Turn conformations. The differences on PR secondary structure when incubated with MNPs confirms the interaction of the peptide with the MNPs. (n= 8 Sidak's multiple comparisons test, p<0.0001).

3.3.2 Low PR concentrations significantly enhances nanoparticle uptake *in vitro*

It has been previously shown by Dixon et al. that exceptional levels of cell-MNPs loading could be achieved by PR. [163] The aim of this results section was to understand the level of binding required for this activity and how this was affected by the microenvironment during delivery (serum in the media). The ability of PR to enhance particle uptake in mammalian cells (NIH3t3 cells) was assessed at increasing concentrations of PR. MNPs and PR -MNPs were delivered to cells overnight and MNP cell association was quantitatively assessed by Inductively Coupled Plasma Mass Spectroscopy (ICP-MS) (Figure 3.6).

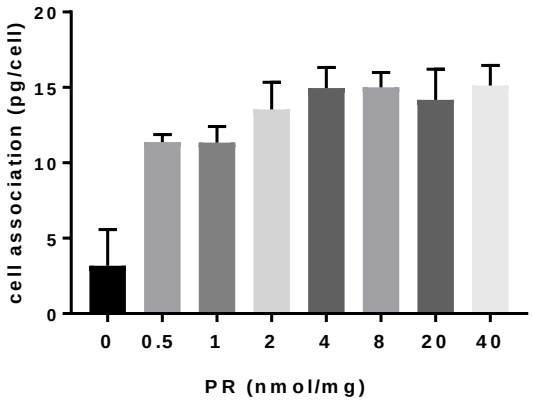

Figure 3.6 Iron cell association after delivery of PR-MNPs.
Iron-cell association in NIH3t3 cells after delivery of MNPs (50 µg) and increasing concentrations of PR (0.5, 1, 2, 4, 8, 20 and 40 nmol PR per 1 mg MNPs). MNPs were delivered overnight in serum containing media (10% FCS). Iron cell association was measured by ICP-MS. Full bars represent mean ± s.d. pg of iron per cell. n=6 biological repeats, 3 technical replicates.

PR significantly enhanced MNP-cell association (3.2 pg Fe/cell with MNPs to 15 pg Fe/cell for PR-MNPs at 4 nmol/mg MNPs), a dose that is ten-fold lower than that determined for MNPs saturation (40 nmol/mg MNPs). Uptake was progressively increased (linear trend) with no further enhancement of uptake beyond this dose (4 nmol/mg MNPs). This data demonstrates only small amounts of PR peptide coating are required for significantly enhanced MNP cell association. From now on in this results section and unless indicated differently PR-MNPs were formulated as 4 nmol of PR/mg of MNPs. This formulation was chosen because it would allow reproducible activity but if PR activity or interaction with MNPs was perturbed then even the smallest effect would be noticeable.

3.3.3 Enhanced MNP delivery mediated by PR is not due to particle aggregation

Nanoparticle size is one of the key factors that determine uptake pathways. Aggregation prior to contact with the cell membrane leads to changes in shape and size that could change the endocytic pathway of such particles. Furthermore, it has been reported that aggregation could potentially increase cell association in certain cell lines, by adsorbing onto the cell membrane providing false positives on particle delivery.[210] Assessing aggregation behaviour of nanoparticles is key to understand differences in their uptake. Aggregation occurs when the attractive forces between particles are greater than the electrostatic repulsive forces. Successive changes on MNPs by electrostatic interactions with PR and serum proteins could potentially lead to a destabilization on the particle surface and aggregation. If this was the case, then the reported enhanced delivery could be due to precipitation of aggregates instead of PR mediated interaction with the cell.[211], [212]

Particle size distribution was measured by dynamic light scattering (DLS) immediately after particle formation (day 1) and after 24 hours incubation (day 2) in an attempt to mimic the behaviour of particles over the delivery process *in vitro*. Particles were measured and incubated in 10% FCS (v/v) in water (Figure 3.7). There are no significant differences on average particle size between MNPs and PR-MNPs on day 1 (289.8 ± 21.9 nm MNPs and 302.1 ± 27.7 nm PR-MNPs) or day 2 (277.9 ± 16.4 nm MNPs and 289.1 ± 16 nm PR-MNPs).

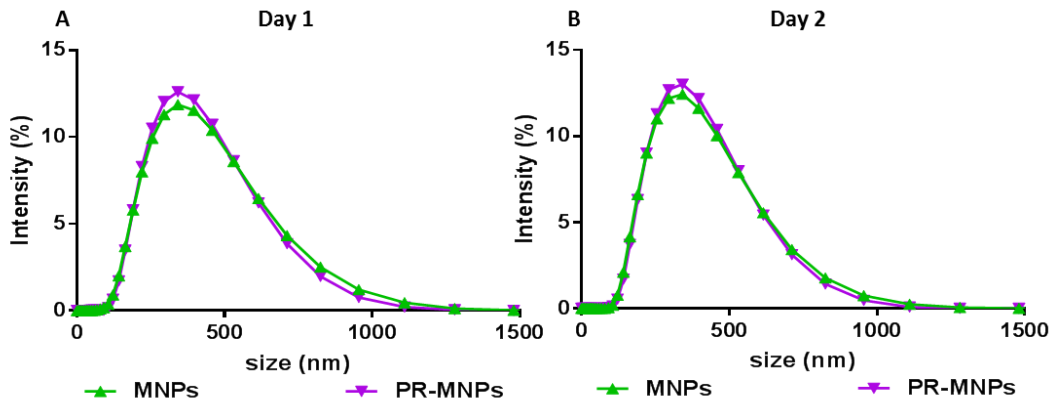

Figure 3.7 MNPs and PR-MNPs present similar size distribution in the presence of serum proteins.

Apparent diameter of the particles obtained by DLS for 50 µg/ml of MNPs and 50 µg/ml MNPs incubated with 4 nmol PR /mg MNPs in 10% FCS v/v in water. DLS was measured on day 1 (particle formation) and day 2 (24 hours after particle formation) looking to most accurately reproduce particle delivery to cells in vitro. Values represent mean intensity. n=6 technical repeats.

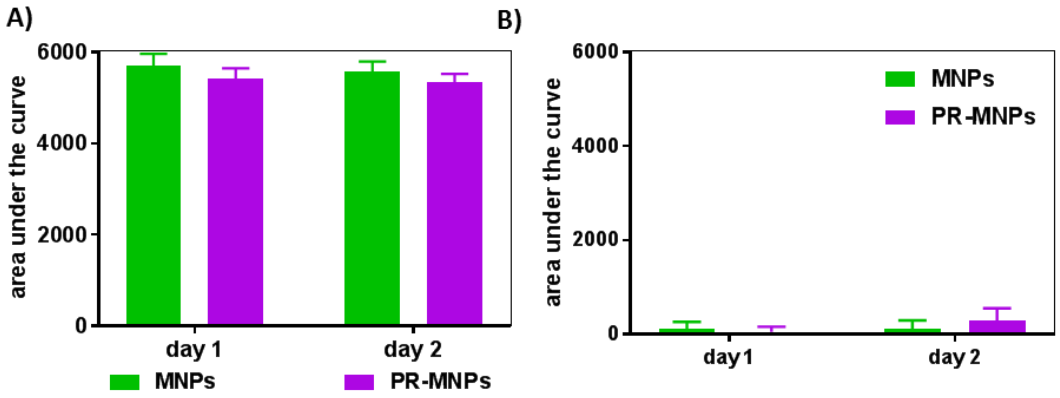

Figure 3.8 PR-MNPs do not aggregate in the presence of serum proteins.

*Area under the curve (AUC) for the size distribution of MNPs and GET-MNPs of the main peak (A) and aggregates (B). Main peak AUC calculated between 0-1600 nm (*Figure 3.7*). Aggregate area calculated between 3000-7000 nm. AUC was calculated in 10% FCS on day 1 (particle formation) and day 2 (24 hours after particle formation) looking to most accurately reproduce particle delivery to cells in vitro. Size distribution plots (*Figure 8.10*). Area under the curve was calculated by GraphPad Prism. n=6 technical repeats.*

Figure 3.8 represents area under the curve (AUC) of the size distribution of main peak (A) and aggregate peak (B) of MNPs and GET-MNPs. Aggregates account for 2-5% of the total size distribution area. There are not significant differences between aggregate formation in MNPs and GET-MNPs neither are there any differences in the size distribution of the main peak between day 1 and day 2.

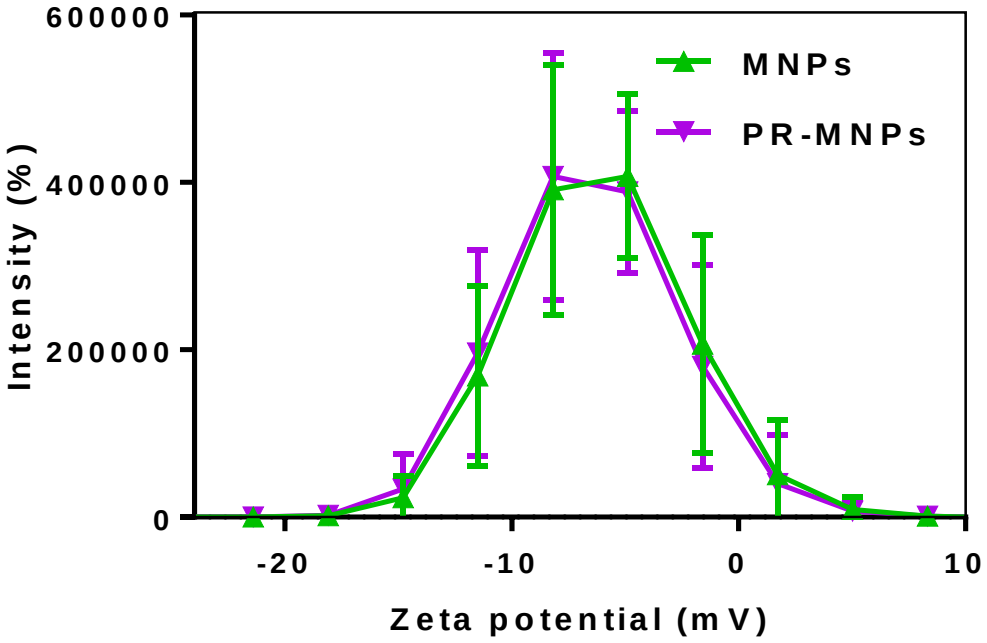

Figure 3.9 Zeta potential of MNPs and PR-MNPs becomes negative in the presence of serum.

Average Zeta potential distribution of MNPs and PR-MNPs. Zeta potential was measured in 10% FCS v/v in water using Malvern Nanosizer Nano ZS. n=6 independent repeats, 3 subruns per repeat.

In addition to particle size and aggregate formation, it was important to understand how the charge of MNPs and PR-MNPs properties changed when exposed to the complex molecular environment of serum (in cell culture) (Figure 3.9). Interestingly, MNPs and PR-MNPs showed similar zeta potential profiles, with an average zeta potential of around -8 mV. The change in charge of the two particle types was attributed to the interaction with negatively charged proteins in serum.

Together, these findings suggest that PR-mediated enhanced particle uptake was not mainly driven by differences in particle charge, size or particle aggregation between MNPs and PR-MNPs.

3.3.4 Enhanced delivery of MNPs by PR is mediated by interaction with heparan sulphate GAGs.

An uptake mechanism based on the interaction of GET with the glycosaminoglycans present on the cell membrane had already been proposed by Dixon et al.[163] They hypothesized that this interaction would trigger the start of the endocytosis process. Efficiency of MNPs delivery was assessed at increasing concentrations of heparin, which had been shown to serve as a competitive inhibitor of cell uptake mediated by GET.[213] Figure 3.10 B shows that heparin inhibits PR-mediated cell association by 93% (99.6 ± 15.2% at 0.1 µg/ml heparin to 6.5 ± 4.7% at 1 µg/ml heparin). Naked MNPs uptake remained unaffected by even the highest concentration of heparin. Prussian Blue staining confirmed the same trend and demonstrated uniformity across all cells in culture (Figure 3.10 C).

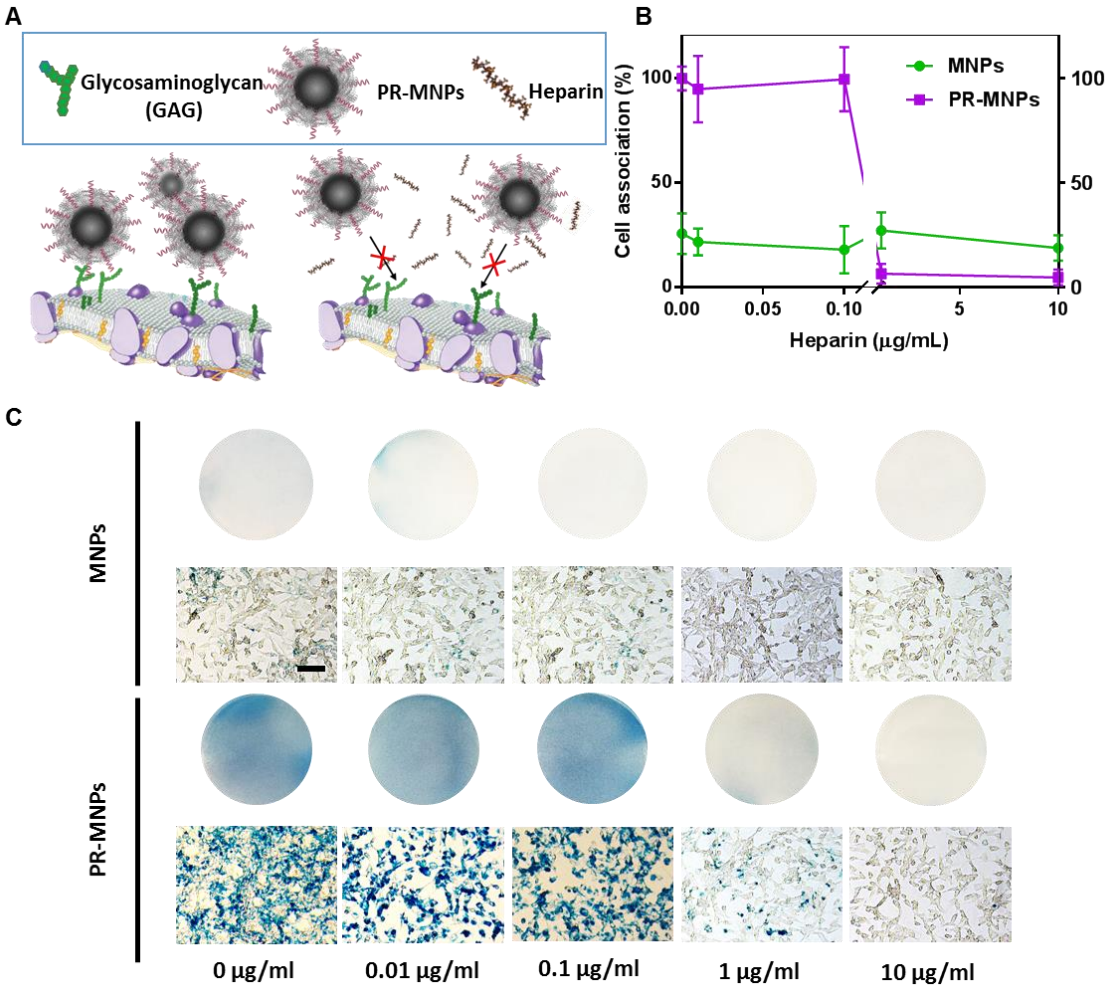

Figure 3.10 High concentrations of heparin negate PR-mediated MNPs uptake.
A) Schematic representation of heparin blocking PR-MNPs interaction with the cells. B) Percentage of MNPs cell association mediated by PR in NIH3t3 cells at increasing concentrations of heparin (0, 0.01, 0.1, 1 and 10 µg/ml heparin). Percentage of cell association was calculated taking cell association in the absence of heparin as 100%. n=6 biological repeats, three technical replicates. C) Representative light microscopy images of Prussian blue iron-stained NIH3t3 cells treated with 50 µg MNPs or 50 µg PR-MNPs at increasing doses of heparin. Circular image shows entire well. Scale bar 100 µm.

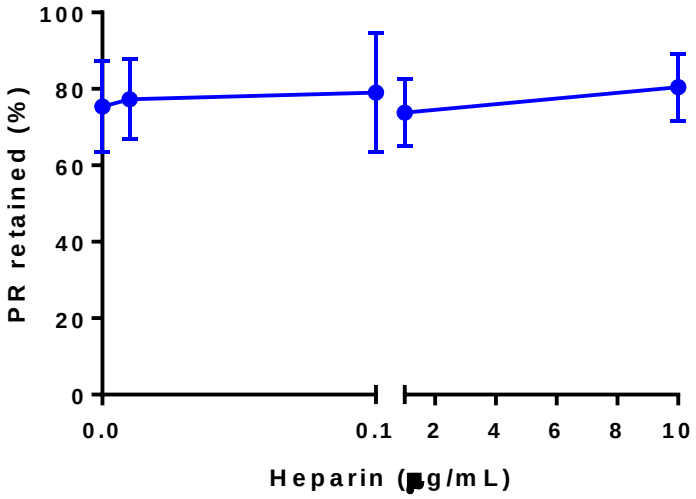

Figure 3.11 Heparin does not affect PR binding to MNPs.
Percentage of PR bound to MNPs after incubating PR -MNPs with increasing concentrations of heparin (0, 0.01, 0.1, 1 and 10 µg/ml heparin).Percentage was calculated based on total amount of peptide adsorbed (2.98 nmol/mg MNPs). n=6 technical repeats.

It was unclear whether the heparin inhibition was affecting the uptake directly or the electrostatic interaction between PR and MNPs. In order to test this, red fluorescently tagged PR (PR-T) was adsorbed onto MNPs and then incubated with increasing concentrations of heparin. The amount of unbound PR was measured by fluorimetry (Figure 3.11). Heparin did not have a significant effect on the amount of PR desorbed from MNPs compared to control (just PBS) even up to concentrations as high as 100 µg/ml which prevented any enhanced uptake in the cell assays.

Taken together these results suggest that heparin inhibits PR-enhanced uptake of MNPs at the level of the cell membrane interaction however, whether this inhibition is due to the specific binding of the heparin to the GAG binding domain of PR (P21) or whether heparin is simply interacting with the numerous positively charged residues of PR still remains unclear.[214] To gain better understanding on the mechanism

underlying PR enhanced intracellular uptake Dixon et al. [163] assessed the delivery efficiency of P21 variants including a scrambled P21 sequence and also with all but the positive residues (R&K) deleted. None of the above variants was taken up with the same efficiency as the native P21. In order to confirm the hypothesis that PR enhanced MNP uptake requires the interaction with GAGs in the cell surface and that this interaction is due to the presence of P21 and not exclusively of the positive charge of the peptide, future work should include the delivery of PR-MNPs to cells lacking GAG-receptors and compare their uptake with a similarly charged peptide, including the P21 variants previously tested by Dixon et al.

3.3.5 PR mediated enhanced particle uptake is a rapid and not cell-type specific

The next aim was to demonstrate that PR enhanced particle delivery was not cell type dependent. PR-MNPs (4 nmol/mg MNPs) were delivered to NIH3t3 (fibroblasts), U87 (glioma) and hMSCs (human mesenchymal stem cells). There were significant differences in the iron cell association between the different cell lines which could be attributed to a range of different factors, including cell type specific preferential mechanism of uptake or cell size.[215], [216] Regardless of the overall differences on MNP uptake between the different cell lines, they all showed at least 3 fold increase on particle association in the presence of PR (Figure 3.12).

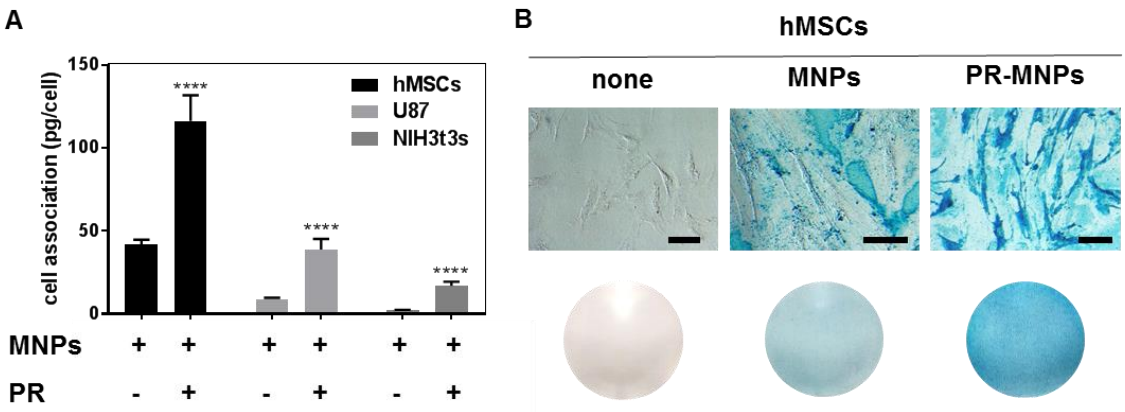

Figure 3.12 PR significantly enhances cell uptake in all cell lines tested.

A) *Iron cell association after delivery of 50 µg MNPs or 50 µg PR-MNPs (4 nmol/mg MNPs). Particles were delivered to: human mesenchymal stem cells (hMSCs), human glioblastoma cells (U87) and mouse embryonic fibroblasts (NIH3t3). Iron cell association was analysed using Inductively Coupled Plasma (ICP). Values represent mean iron association/cell ± s.d, (n=6 biological repeats, three technical replicates p < 0.0001, Sidak's multiple comparisons test). B) Representative light microscopy images of Prussian blue iron-stained hMSCs treated with 50 µg MNPs or 50 µg PR-MNPs (4 nmol/mg MNPs) for 12 hours. When MNPs are delivered without PR the iron staining is localized mainly around the cells. MNPs are taken into hMSCs most efficiently when delivered with PR (PR-MNPs). Circular image is of entire well. (Scale bar = 50 µm).*

To confirm that cell association was indeed intracellular and not membrane-associated, transmission electron microscopy (TEM) of embedded cell suspensions was used to assess MNP localisation. TEM images of NIH3t3 cells after 24 hour delivery of MNPs with and without PR (Figure 3.13) show accumulation in intracellular vesicular structures that resemble endosomes when particles are delivered with PR. Almost no particles are detected when they were delivered in the absence of PR.

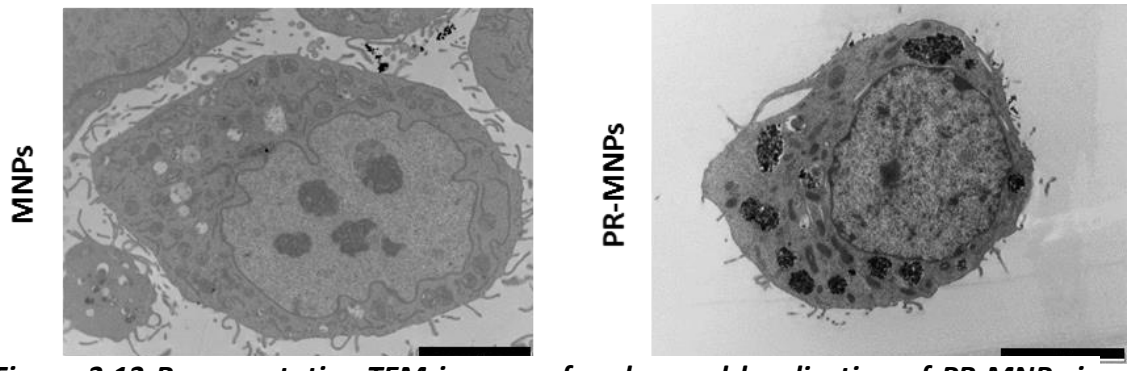

Figure 3.13 Representative TEM images of endosomal localisation of PR-MNPs in NIH3t3 cells.
Cells were treated with 500 µg MNPs (MNPs) or 500 µg PR-MNPs (4 nmol/mg MNPs). White arrow heads indicate intracellular localization of MNPs in endosomes. Scale bar 5 µm.

3.3.6 PR-MNPs uptake kinetics

Understanding the kinetics of magnetic nanoparticle uptake was considered essential to further understand the process of uptake and if protein corona effected the interaction with cells or rapidity of uptake. Iron content of the cell media and washes (non-cell associated) and iron content in the cells (after washing; cell associated) were analysed at 0.5, 2, 4, 6 and 24 hours post-delivery with MNPs and PR-MNPs (Figure 3.14).

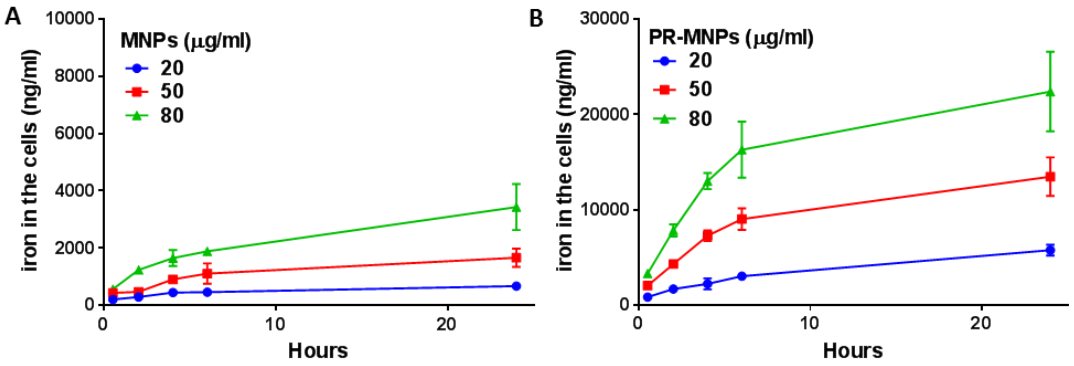

Figure 3.14 Iron uptake rapidly increases shortly after delivery.
Total concentration of iron in the cells for naked MNPs delivery (A) and PR-MNPs (B) over time in NIH3t3 cells. Increasing dosages of MNPs (20 µg, 50 µg and 80 µg) were delivered in order to assess effect of concentration on uptake. PR-MNPs were delivered at 4 nmol/mg MNPs. Iron content in the cells was analysed 0.5, 1, 2, 4, 6 and 24 hours post-delivery using Inductively Coupled Plasma (ICP). Values represent mean percentage of iron cell association ± s.d (n=6 biological repeats, three technical replicates).

Figure 3.14 shows that MNPs concentration in the cells increases linearly up until 4 hours of delivery independent of the particle type (MNPs or PR-MNPs) (Figure 8.11, Table 16). After 4 hours of delivery the concentration of particles starts to deviate from linearity towards a logarithmic fit, tending towards a plateau, where the concentration of MNPs per cell remains almost constant up to 24 hours. For MNPs and PR-MNPs particle uptake was proportional to the amount of MNPs delivery. Iron concentration in the media decreases overtime inversely proportionally to the uptake of iron by the cells (Figure 3.15).

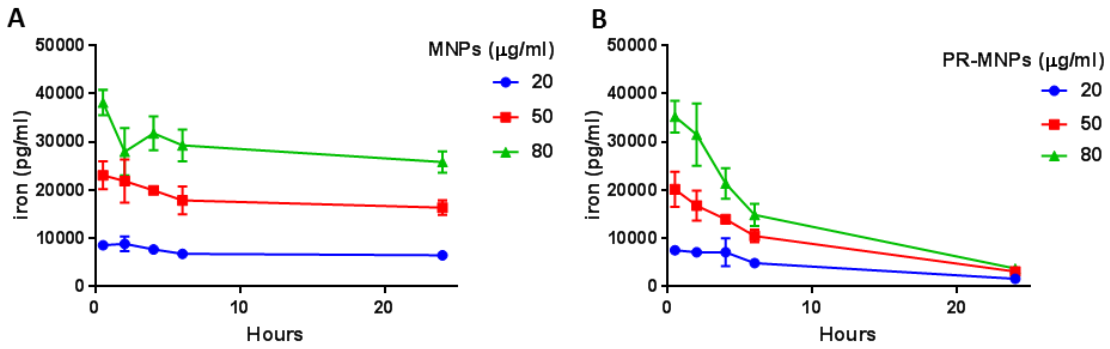

Figure 3.15 Total concentration of unbound iron in the media over time in NIH3t3 cells.

Increasing dosages of MNPs and PR-MNPs (20 µg, 50 µg and 80 µg) were delivered in order to assess effect of concentration on uptake. PR-MNPs were delivered at 4 nmol/mg MNPs. Iron content in the media was analysed 0.5, 1, 2, 4, 6 and 24 hours post-delivery using Inductively Coupled Plasma (ICP). Values represent mean percentage of iron cell association ± s.d (n=6 biological repeats, three technical replicates).

Nanoparticle uptake in cells is a process determined by several sub processes, including transport across the cell membrane towards endosomes and flux toward lysosomes. At early time points these processes are mainly concentration dependent and intracellular concentration of the particles rise linearly. However, at later time points energy depletion and decrease in the number of "endocytosis domains" from the cell surface account for linearity deviation and eventually reach a steady state of uptake concentration.[217]

3.3.7 Cell viability is not affected by enhanced MNP uptake mediated by PR

In order to assess whether enhanced MNP uptake mediated by PR had an effect on cell viability and proliferation, a 0.4% trypan blue (v/v) solution was used. It had been previously stabilised in the group that NIH3t3 doubling time was approximately 24 hours, therefore it was decided to measure cell viability after 24 hours delivery of MNPs and PR-MNPs and every day for a week post-delivery. At every time point, only

50% of the cells were seeded back in a fresh well, in order to maintain a constant number of cells and to avoid cell confluency. Enhanced cell uptake through PR does not have an effect on cell viability or proliferation (Figure 3.16).

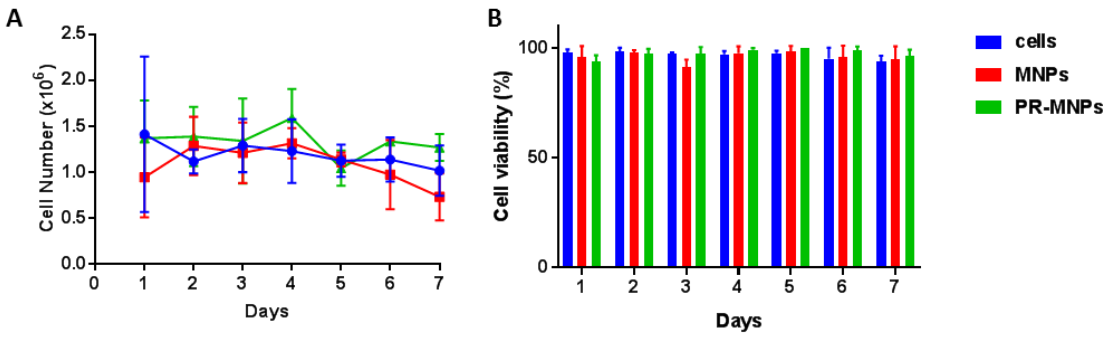

Figure 3.16 NIH3t3 proliferation and viability after incubation with MNPs and PR-

A) *Cell number count after treatment with nothing (cells), 50 µg of MNPs (MNPs) and 50 µg of MNPs with 4 nmol/mg MNPs (PR-MNPs). Values represent mean numbers of viable cells ± s.d (two technical repeats, n=6 biological repeats). B) Cell viability of untreated cells (cells), cells treated with 50 µg of MNPs (MNPs) and cells treated with 50 µg of MNPs with 4 nmol/mg MNPs (PR-MNPs). Cell viability was measured using trypan blue cell number count. Percentage of cell viability was calculated based on the total number of viable and unviable cells for each group. Overall, there are no significant differences in cell viability between the different groups. Values represent mean percentage of cell viability ± s.d (n=6 biological repeats, two technical replicates).*

3.3.8 PR enhanced nanoparticle delivery is not affected by plasma protein corona

So far, all the experiments presented in this chapter have been performed in 10% FCS media. Previous studies have confirmed that other targeting systems lose uptake efficiency, and can even be completely negated when delivered in the presence of serum compared to the same delivery in serum free media.[168], [196], [201], [218] Most of these studies treat serum and plasma interchangeably when it comes to "biological milieu". Recent research, however, has shown significant differences between plasma and serum in terms of protein corona composition.[219], [220] It was

therefore important to assess the differences between plasma (unclothed containing fibrinogen and other factors) verses serum (clotted and lacking fibrinogen).

3.3.8.1 MNPs plasma coating

Due to the nature of the dextran coating of the particles concentration or precipitation of the MNPs was not possible without obtaining a significant degree of aggregation (observational data). This made it very challenging to efficiently coat the MNPs with plasma and rapidly remove non-bound protein without affecting monodispersity. Delivery and characterisation assessments were precluded in 100% plasma as this significantly affected cell viability in cultured lines, affecting the reproducibility of the delivery. To overcome these technical issues fluorescently labelled Bovine Serum Albumin (BSA) was used to determine albumin saturation (S_{max}) on MNPs through the previously described Langmuir modelling of protein adsorption. The S_{max} of albumin on MNPs was used to extrapolate the amount of plasma needed to fully coat the MNPs. S_{max} for albumin in MNPs was calculated to be around 318 µg/mg of MNPs (Figure 3.17 and Table 17 Langmuir constants for BSA adsorption on MNPs). Albumin represents approximately 50% of the plasma protein content.[221] Taking the density of plasma as 1.025 g/ml it was estimated that in order to saturate 50 µg of particles (used for delivery) 31 µl of human plasma were required. Since once again Langmuir isotherm is a very simplified model of protein adsorption, the S_{max} value was used as an estimate. For size, charge analysis and *in vitro* delivery 50 µl of plasma (5% v/v in solution) were used per 50 µg of MNPs unless otherwise specified.

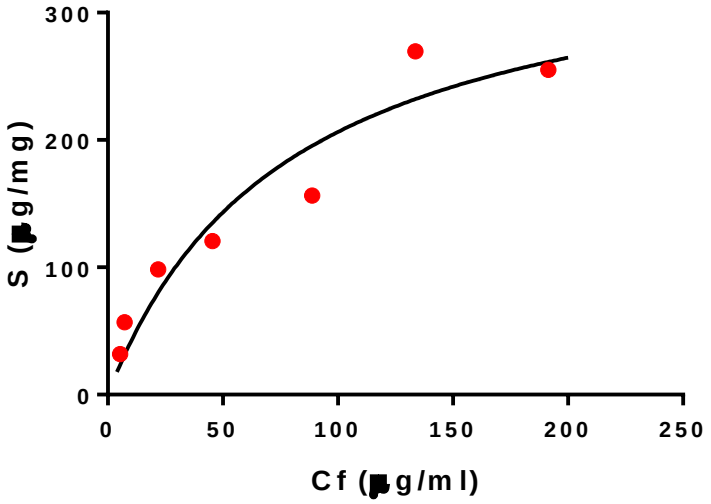

Figure 3.17 Representative Langmuir fitting curve for BSA adsorption on MNPs.
Red dots represent the adsorption of BSA measured on MNPs, black line represents the non-linear fitting of Langmuir isotherm (n=1, all Langmuir fitted isotherms are presented in Figure 8.12*).*

Table 8 Average Langmuir parameters for BSA adsorption on MNPs **(n=6, Langmuir parameters for each independent replicate are displayed on Table 15 Langmuir** constants for PR adsorption on MNPs.

	S_{max} (µg/mg)	K (ml/µg)
BSA-MNPs	318 ± 48	0.02 ± 0.008

3.3.8.2 PR-MNPs delivery to cells in plasma

MNPs and PR-MNPs uptake in serum free media (none), 5% plasma and 10% FCS media by NIH3t3 cells was assessed by ICP-MS and Prussian Blue staining of iron (Figure 3.18 B and C). PR significantly and consistently enhances particle uptake regardless of the protein content in the media. Importantly, PR-MNPs cell uptake in the presence of plasma is significantly lower than in serum free media or in serum (10% FCS). It was hypothesized that proteins present in plasma and not in serum (clotting factors) will have an effect on the protein corona and affect particle uptake.

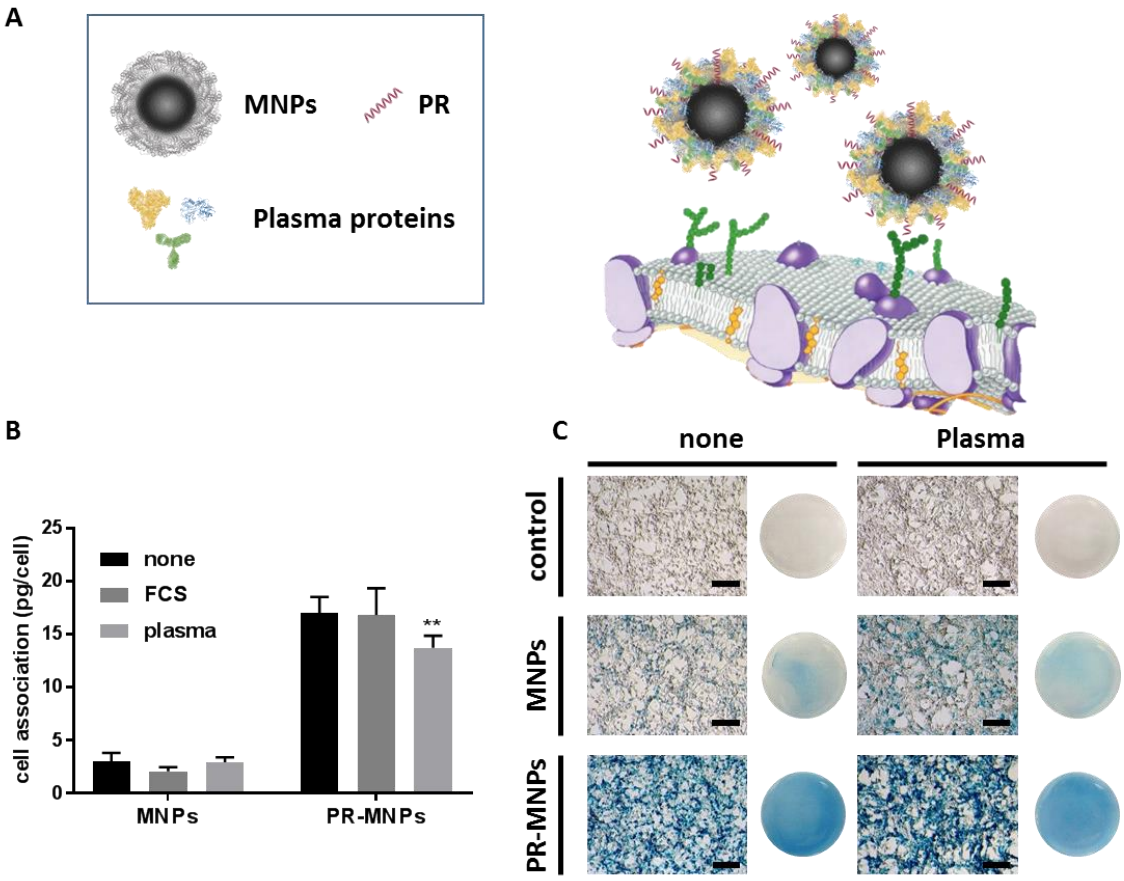

Figure 3.18 Plasma does not prevent PR mediated enhanced MNPs

*A) Schematic of PR-MNPs interaction in the presence of plasma proteins. B) Iron content per cell after overnight delivery of MNP and PR-MNPs in serum free media (none), 10% FCS media (FCS) and 5% plasma (plasma). Iron content was analysed using ICP-MS. Values represent mean iron per cell (pg/cell) ± s.d. (n=6 biological repeats, 2 technical replicates, significant difference between FCS and plasma**p< 0.01, Tukey's multiple comparisons test) C) Representative light microscopy images of Prussian blue iron-stained NIH3t3 cells treated with 50 µg MNPs or 50 µg PR-MNPs (4 nmol/mg MNPs) for 12 hours in SFM (left) and at 5% plasma (right). MNPs are taken into NIH3t3 cells most efficiently when delivered with PR (PR-MNPs) irrespective of the presence of plasma (circular image is of entire well). (Scale bar = 50 µm).*

3.3.8.3 PR-MNPs characterisation in plasma

Significant emphasis is placed on the full characterisation of nanoparticles prior to delivery but very little work has been done in characterizing particles in a cell culture environment where the proteins and ions present in the media have the potential to alter the particles properties: the ions might decrease the strength of charged

chemical groups on the particle surface; the molecules in solution might replace the surface associated molecules. Physicochemical properties of the particles in plasma were analysed and compared to particles in water. In terms of particle stability, there weren't any significant changes on particle size or size distribution when the particles are incubated in plasma compared to water (Figure 3.19 A). Similarly to what was previously observed in serum, the presence of plasma proteins and ions significantly affect the particle charge, giving both MNPs and PR-MNPs identical negative charges (around -10 mV) (Figure 3.19 B).

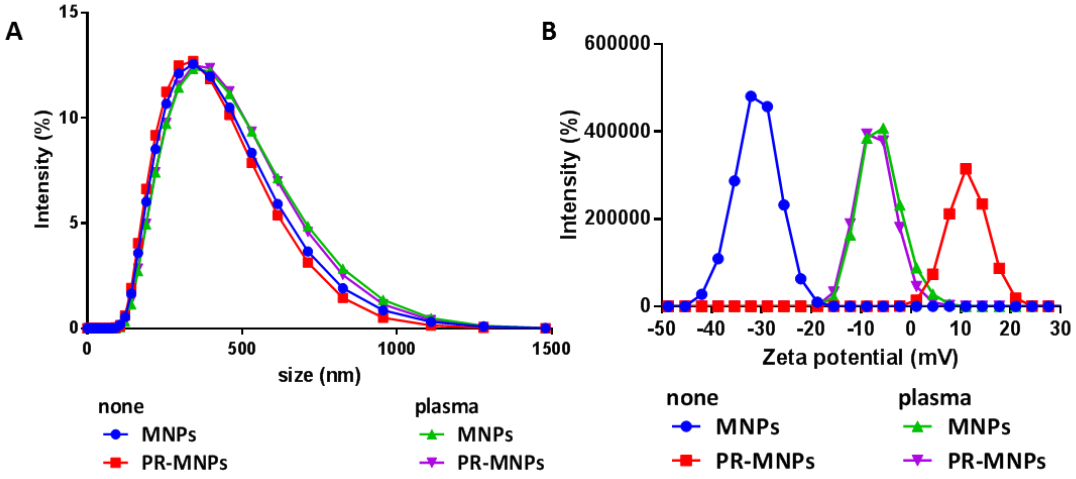

Figure 3.19 Plasma adsorption on MNPs and PR-MNPs does not affect particle size but it changes zeta potential.
A) DLS assessment of PR binding to MNPs in the presence of plasma proteins overtime. A slight increase in the diameter size is observed when the particles were incubated with plasma proteins. The apparent diameter of MNPs and PR-MNPs in water is shown for reference (n=6 independent repeats, 3 subruns per repeat). B) Zeta potential of MNPs and PR-MNPs in 5% plasma v/v in water. The zeta potential of MNPs and PR-MNPs in water is shown for reference. MNPs and PR-MNPs present similar negative charge in the presence of plasma. (n=6 independent repeats, 3 subruns per repeat).

When looking at aggregate formation in the presence of plasma (Figure 3.20), a significant increase in MNPs aggregation was observed on day 2, however there are

no significant differences in aggregation between MNPs and PR-MNPs that could account for the differences in uptake.

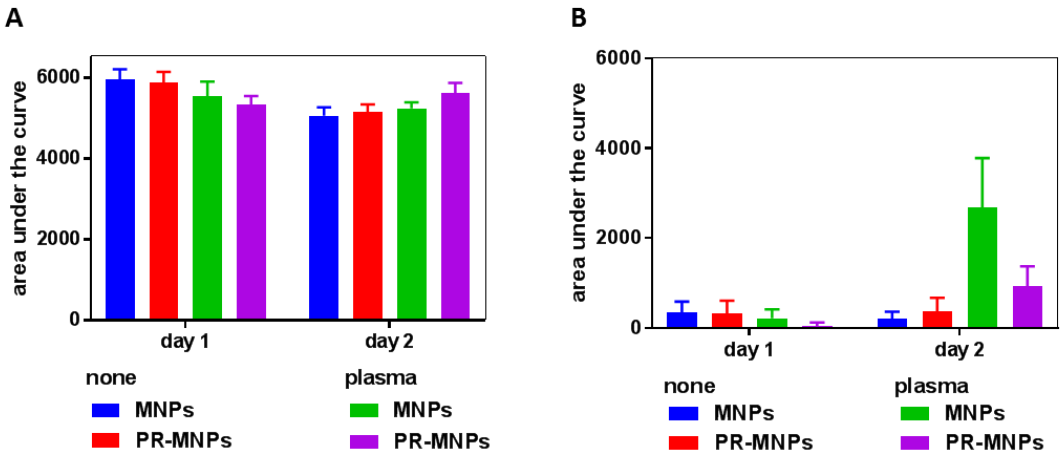

Figure 3.20 Plasma proteins do not contribute to particle aggregation.
*Area under the curve (AUC) for the size distribution of MNPs and PR-MNPs of the main peak (A) and aggregates (B). Main peak area calculated between 0-1600 nm. Aggregate area calculated between 3000-7000 nm. AUC was calculated in water (none) and 5% plasma v/v in water (plasma) on day 1 (particle formation and delivery) and day 2 (end of particle delivery) looking to most accurately reproduce particle delivery to cells in vitro. Size distribution plots (*Figure 8.13*))*

These results suggest that regardless of the evident interaction of plasma proteins with the nanoparticles and the consequent changes in the physicochemical properties, PR activity is not completely negated by the proteins in solution and is still able to mediate and enhance particle uptake.

3.3.9 Rapid, stable and specific protein corona formation on PR-MNPs

In order to assess protein profile of the protein corona formed on MNPs and PR-MNPs, the particles were incubated with plasma for 10 mins. Adsorbed proteins were digested by trypsin and separated by gel electrophoresis. SDS-Page gel demonstrated a complex protein corona was formed for MNPs and PR-MNPs with a major band of

around 68 KDa corresponding to albumin.[222] Similar protein bands were observed for both particles. (Figure 3.21)

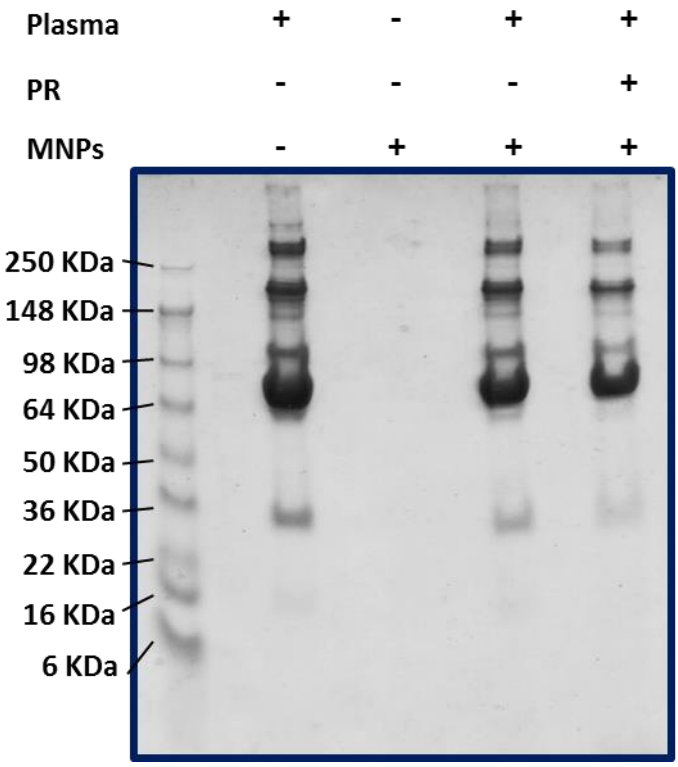

Figure 3.21 There are no significant differences in the protein bands observed after incubation of MNPs and PR-MNPs with plasma.
Separation of plasma proteins adsorbed on MNPs and PR-MNPs after 30 min incubation on 12% SDS-PAGE gel. Molecular mass and sample characteristics are indicated.

3.3.9.1 Protein corona composition in MNPs and PR-MNPs

To gain further insight on the effect of PR on the protein corona formation, label-free snapshot proteomics (LC-MS) was used. The composition of the protein corona was assessed at two different time points to determine whether exposure time (acute, 1min and chronic, 30min) had an effect on the protein profile. 167 proteins were identified after incubation of the MNPs in human plasma for a minute, this was the same for the longer exposure time (30 minutes). This finding agrees with previously published research on protein corona that reported that out of the thousands of

proteins present in plasma only a few tens of proteins bind to nanoparticles at significant quantities (>1 molecule per MNP).[196], [202]

Further analysis showed that negatively charged proteins at physiological pH (isoelectric point between 5-7) represent the majority of the corona components for MNPs and PR-MNPs, irrespective of the particles' initial surface charge or plasma exposure time (Figure 3.22 A). This is also reflected by zeta potential results that show that nanoparticles exposed to plasma present an overall negative charge irrespective of their original charge (Figure 3.19 B). These results have been previously reported in the literature, and point towards the possibility that positive charge might not be absolutely required for the enhanced uptake mediated by PR.[200], [202], [223]

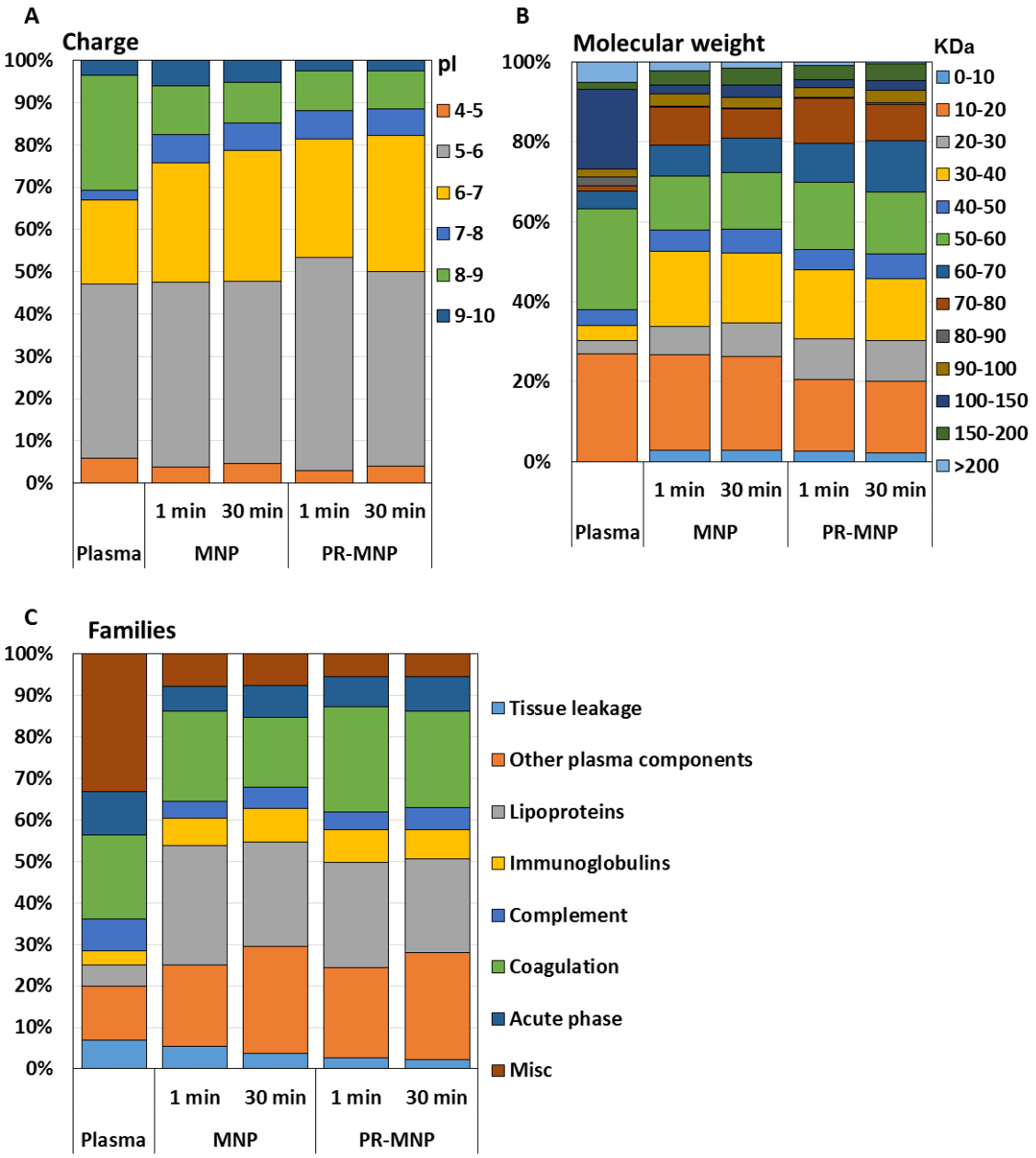

Figure 3.22 Rapid formation of protein corona (1 min) that remains stable over time.

Classification of corona proteins identified by LC-MS on MNPs and PR-MNPs after 1 min and 30 min exposure to plasma. Proteins were classified according to A) calculated molecular weight, B) isoelectric point and C) protein family. Relative percentages of protein abundance are shown (n=2, independent repeats).

Evolution of proteins overtime follows similar patterns in naked MNPs and PR-MNPs (Figure 3.22) suggesting a strong interaction of the proteins with the dextran on the particle surface. [224] The kinetics of those interactions is not affected by the presence of PR.

It is important to mention, however, there are some interesting differences amongst the top 15 most abundant proteins present in MNPs and PR-MNPs coronas after 1 min incubation (Table 8) For example, glycoproteins are seen to be more commonly abundant in PR-MNPs than in MNPs. Looking at the same most abundant corona proteins after 30 minutes exposure to plasma (Table 9), most proteins were present in both particles with only one protein differing between the two. These observations agree with previous reports that suggest that protein corona formation is a two-step process that involves first, the build-up of an inner layer of biomolecules that are more tightly bound to the particle ('hard corona') and an outer layer that interacts more loosely with the particle surface and more readily with the environment ('soft corona') [202]. Looking at the most abundant proteins at the two different time points, it can be seen that while the initial corona presents more specific proteins to each particle's formulation, after a longer incubation time in plasma the two corona become more uniform, potentially due to prolonged exposure to the same proteins in the media.

Overall the results thus far show that there are very minimal differences in the protein corona between naked MNPs and PR-coated MNPs. Plasma proteins have dedicated cells surface receptors in order to carry out their biological functions. [200]

The successful enhancement on nanoparticle uptake in the presence of PR could potentially suggest that the affinity of PR for glycosaminoglycans in the cell membrane is greater than any other interaction possibly elicited by the plasma proteins and their respective cell surface receptors.

Table 9 Top 15 most-abundant corona proteins (NSAF) after 1 min of plasma exposure.

No	MNPs	PR-MNPs
1	Apolipoprotein A-I	Apolipoprotein A-I
2	Serum albumin	Prothrombin*
3	Fibrinogen gamma chain	Serum albumin
4	Transthyretin	Serotransferrin
5	Fibrinogen beta chain	Fibrinogen gamma chain
6	Serotransferrin	Transthyretin
7	Apolipoprotein A-II	Apolipoprotein A-II
8	Apolipoprotein C-III	Fibrinogen beta chain
9	Kininogen-1	Apolipoprotein C-III
10	Apolipoprotein C-I (Fragment)	Apolipoprotein C-I (Fragment)
11	Apolipoprotein E	Hemopexin*
12	Fibrinogen alpha chain	Apolipoprotein E
13	Angiogenin	Hyaluronan-binding protein 2*
14	Tetranectin	Fibrinogen alpha chain
15	Apolipoprotein A-IV	Apolipoprotein A-IV

*Proteins highlighted in grey are common for MNPs and PR-MNPs. * Most abundant proteins in PR-MNPs that are not present in MNPs are glycoproteins.*

Table 10 Top 15 most-abundant corona proteins (NSAF) after 30 min of plasma exposure.

No	MNPs	PR-MNPs
1	Apolipoprotein A-I	Apolipoprotein A-I
2	Serum albumin	Serum albumin
3	Transthyretin	Transthyretin
4	Serotransferrin	Serotransferrin
5	Fibrinogen beta chain	Hyaluronan-binding protein
6	Fibrinogen gamma chain	Prothrombin*
7	Apolipoprotein C-III	Fibrinogen gamma chain
8	Apolipoprotein A-II	Fibrinogen beta chain
9	Apolipoprotein C-I	Apolipoprotein C-III
10	Hemopexin	Apolipoprotein A-II
11	Apolipoprotein E	Hemopexin
12	Complement C3	Apolipoprotein CI
13	Angiogenin	Haptoglobin
14	Haptoglobin	Fibrinogen alpha chain
15	Fibrinogen alpha chain	Complement C3

Proteins highlighted in grey are common for MNPs and PR-MNPs.

3.3.10 PR-MNP corona prevents haemotoxicity and aggregation

The biological effects of the protein corona on PR-MNPs were demonstrated on human erythrocytes since they are present in high concentrations in blood and are likely to be one of the first cell types that come in contact with nanoparticles as they enter the blood system in several biotherapeutic applications.[225]

3.3.10.1 Effect of PR-MNPs on red blood cell morphology and aggregation

Human blood was purchased from the NHS. Human erythrocyte (red blood cell) aggregation and cell morphology were assessed after exposure to PR-MNPs for 5, and 30 mins in PBS or human plasma. Red blood cells were also incubated with PR alone and Lipofectamine 2000 (commercial transfection agents). A representative sample of aggregation results at time points 5 and 30 mins are shown in Figures 3.23 and 3.24. Red blood cell morphology was immediately (<5 min) affected after incubation with Lipofectamine 2000 in PBS. PR peptide alone in high concentration progressively induced cell morphology changes over time in PBS (Figure 8.14). No significant changes in cell morphology were observed with MNPs or PR-MNPs (higher doses of MNPs were not possible to image under a standard microscope due to the high density of particles in solution). PR-induced cell morphology could potentially be mediated by the interaction of the peptide with glycoproteins present in the cell membrane[226]. Change in morphology is not observed when PR is adsorbed onto the nanoparticles (PR-MNPs) or in the presence of plasma. Additionally the difference in osmolality between the plasma and PBS could account for this morphological changes.[227]

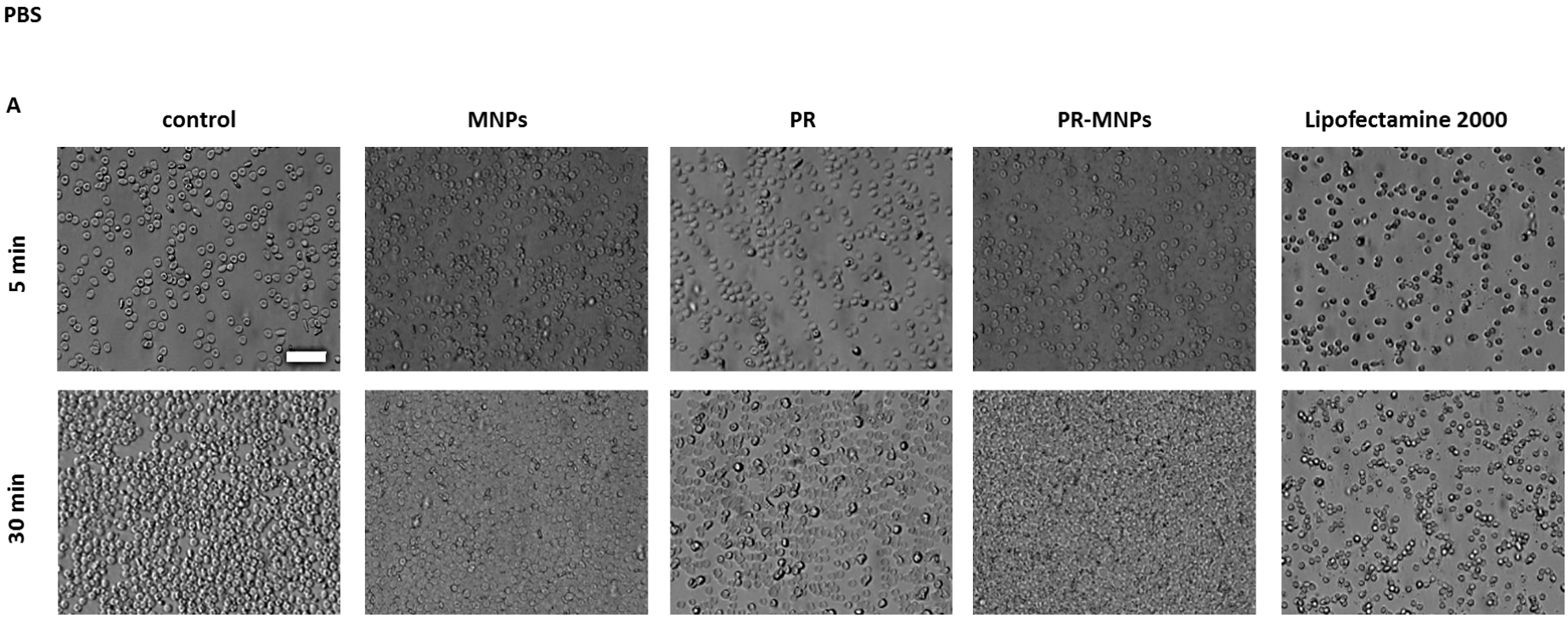

Figure 3.23 PR-MNPs exposure does not trigger changes in erythrocyte morphology in PBS compared to control.

Freshly isolated human erythrocytes were exposed to 100 µg/ml MNPs (MNPs), 0.4 nmol/ml PR (PR) and 100 µg/ml PR-MNPs (4 nmol PR/mg MNPs) in PBS for 5 min and 30 mins and analysed on a microscope. Untreated erythrocytes were used as control for aggregation. Lipofectamine 2000 was used as comparison for commercially available transfection reagent. Scale bar 20 µm.

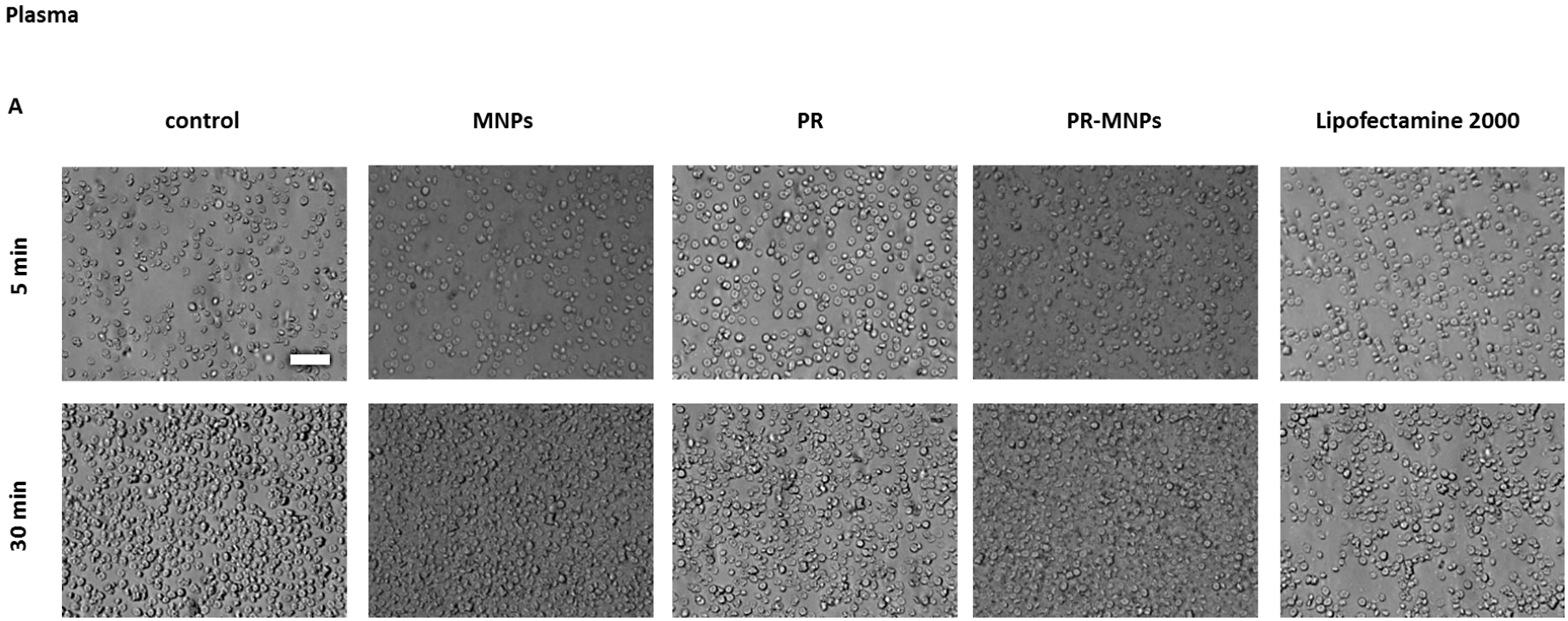

Figure 3.24 PR-MNPs exposure does not trigger changes in erythrocyte morphology in plasma compared to control.

Freshly isolated human erythrocytes were exposed to 100 µg/ml MNPs (MNPs), 0.4 nmol/ml PR (PR) and 100 µg/ml PR-MNPs (4 nmol PR/mg MNPs) in PBS for 5 min and 30 mins and analysed on a microscope. Untreated erythrocytes were used as control for aggregation. Lipofectamine 2000 was used as comparison for commercially available transfection reagent. Scale bar 20 µm.

3.3.10.2 Effect of PR-MNPs on haemolysis

The effect of the PR and MNPs in erythrocyte cell lysis was further investigated. The percentage of erythrocyte lysis was calculated compared to the effect of Triton-X 100 (1% v/v) which permeabilises and ruptures the cell membrane. Lipofectamine 2000 was analysed as a control for commercially available transfection reagents. After 30 minutes, MNPs, PR and PR-MNPs have similar low effect on haemolysis in PBS. Rapid corona formation in plasma efficiently prevented haemolysis in MNPs and PR-MNPs (Figure 3.26). PR or PR-MNPs do not create aggregation or lysis of erythrocytes in the presence of the endogenous blood corona provided by serum or plasma.

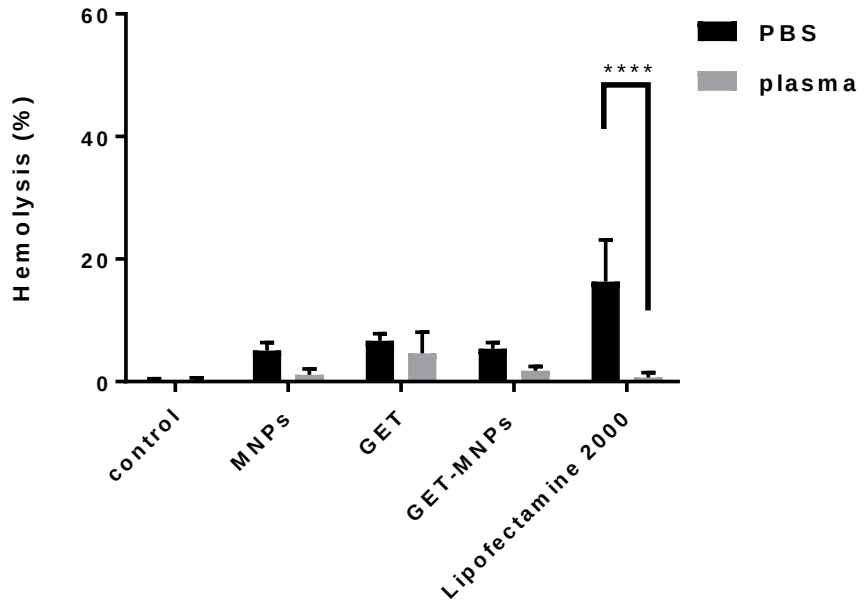

Figure 3.25 Plasma prevents haemolysis.

*Erythrocytes were exposed to 100 µg/ml MNPs (MNPs), 0.4 nmol/ml PR (PR) and 100 µg/ml PR-MNPs (4 nmol PR/mg MNPs) in PBS or plasma. Erythrocytes were also treated with Triton-x 100 (positive control for lysis) and Lipofectamine as comparison for transfection reagent. All treatments were performed in PBS and plasma. Haemolysis was quantified by spectrophotometric assay after 30 mins. PBS and plasma were used as controls. Values are mean ± s.d. from 4 independent repeats from the same donor. Results are expressed as percentage lysis taking Triton-x 100 as complete lysis (100%). Haemolysis was significantly affected by rapid protein corona formation in particles (n=4, independent repeats, **** p<0.0001, Sidak's multiple comparisons test)*

3.4 Conclusions

PR functionalised MNPs are capable of significantly enhancing MNPs uptake in the presence of serum and plasma proteins (up to 8 fold). This increase in uptake was not due to aggregate formation and preliminary experiments in the presence of heparin suggested the possibility that the interaction between PR and heparan sulphates on the cell membrane could potentially be involved in the uptake mechanism. Furthermore, in a physiological relevant environment, highly complex protein coronas are rapidly formed in PR-MNPs. This corona does not quantitatively change overtime. Additionally, it was found that even if most corona proteins on MNPs and PR-MNPs are the same there are differences in the relative abundance of the proteins present as well as a small number of specific proteins both on MNPs and PR-MNPs, which suggests a specific role of PR on the protein corona formation.

Since previous publications had described the impairment of targeted delivery in biologically relevant environments, the previous findings that confirm the presence of a protein corona on PR-MNPs but also the significant enhancement on particle uptake in the presence of plasma proteins represent a stepping stone to further develop PR-MNPs into a platform technology for future applications in nanomedicine.

This study presents various limitations that have already been discussed. In order to better understand the mechanism through which PR enhances MNPs uptake, future work should include the assessment of the potential of the individual components of the peptide, P (P21) and R (8R) for MNPs delivery, as well as their delivery efficiency in the presence of heparin or in the absence of GAGs to stablish their specific role in the delivery process. More in depth analysis of the protein corona development

overtime would be needed in order to better predict the behaviour of the particles *in vivo* as well as further understanding of the role of heparin in particle delivery and the protein corona. Further work should also consider whether the effect of plasma on preventing erythrocyte lysis is due to the presence of extra proteins in the media tailoring the protein corona or whether plasma proteins play a specific role on erythrocyte protection as well as the effect of the particles on the different components in blood (i.e. thrombocytes). Finally, future work should include the demonstration of the application of PR-MNPs for targeted delivery, both *in vitro* and *in vivo*.

4 Optimisation of GET-MNPs for magnetically mediated gene delivery *in vitro*

4.1 Introduction

Non-viral vectors are an attractive gene delivery method due to their safety, high gene carrying capacity and easy mass production.[99], [228] Unfortunately, non-viral vectors are in general less efficient compared to viral alternatives. This has been attributed amongst other reasons, to their inability to overcome extra and intracellular barriers. In order for a vector to efficiently deliver a gene both *in vitro* and *in vivo*, it has to first come in contact with the cell membrane, enter the cell, in case of endosomal entrapment, avoid lysosomal and cytosolic degradation and enter the cell nucleus. [229]

There are ongoing efforts to design non-viral vectors capable of efficiently overcoming all these limitations. Slow vector accumulation and therefore low DNA concentration on the cell membrane is a major barrier for most gene delivery methods therefore, any approach capable of accelerating the DNA-vector interaction with the target cells should result in enhanced gene delivery.[230], [231] Furthermore a vector accumulation method that could be remotely controlled would be desirable. All these requirements gave rise to a relatively new technology termed “magnetofection”.[232] The acronym magnetofection was first mentioned in the scientific literature in 2000 and it loosely refers to any magnetically guided or enhanced nucleic acid delivery, the most common approach involves the association of vectors (viral and non-viral) with magnetic carriers that are accumulated on the cells by the application of magnetic

gradient fields. In the past years, magnetofection has shown very promising results both *in vivo* and *in vitro.*[126], [233]–[236]

One of the most common non-viral vectors used for magnetofection is polyethylenimine (PEI). [118], [191], [203], [237]–[239] PEI is a branch polymer containing primary, secondary and tertiary amines capable of complexing plasmid DNA and delivering it *in vitro* and *in vivo*. Its amine groups are believed to interact with protons, preventing acidification in the endosomes, promoting vesicle swelling and endosomal escape, increasing gene transfection ability. PEI is one of the most investigated vectors for non-viral gene delivery *in vitro* and *in vivo.* [99], [101], [240]

Previous work in the group used a modified GET peptide termed FLR for efficient gene delivery *in vitro* and *in vivo* with superior transfection efficiencies to current gold standard PEI.[167] FLR stands for FGF2B-LK15-8R and is formed of three different domains: fibroblast growth factor, FGF2B, (TYRSRKYTSWYVALKR) a 16 amino acid peptide that has affinity for heparin/heparan sulphate proteoglycans present on the cell surface and acts as a membrane docking domain[241]; LK15 (KLLKLLLKLLLKLLK) an amphipathic region able to complexate DNA[242] and a cell penetrating peptide 8R (RRRRRRRR)[163] (Figure 4.1).

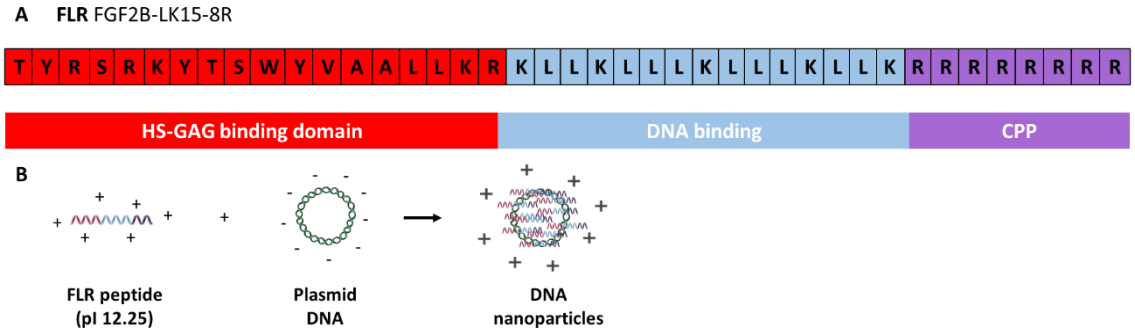

Figure 4.1 FLR peptide and FLR-DNA nanoparticle formation.

A. FLR is a multi-domain peptide formed of a heparan sulphate glycosaminoglycan binding domain (red), an amphipathic region (blue) able to condense DNA and a cell penetrating peptide CPP (purple). FLR amino acid sequence and chemical structure. B. When mixed with DNA, the positively charged residues in the FLR peptide sequence interact electrostatically with the negatively charged phosphate groups of the plasmid DNA forming nanoparticles (NP). Full Amino acid sequence displayed in Figure 8.7.

4.1.1 Aims

This thesis chapter is focused on the development of a FLR-MNPs formulation for efficient magnetically mediated gene delivery. Understanding the advantages and limitations of magnetofection is key for the development of better magnetofection vectors.

Cellular entry mechanism for the vectors with and without the presence of a magnetic field was determined through the inhibition of specific uptake pathways: macropinocytosis, clathrin or caveolae mediated endocytosis. Uptake kinetics, endosomolysis, intracellular DNA degradation and confocal microscopy were also assessed. The ultimate aim of this section was to better understand the mechanisms underlying non-viral magnetically mediated gene transfer.

4.2 Chapter experimental review

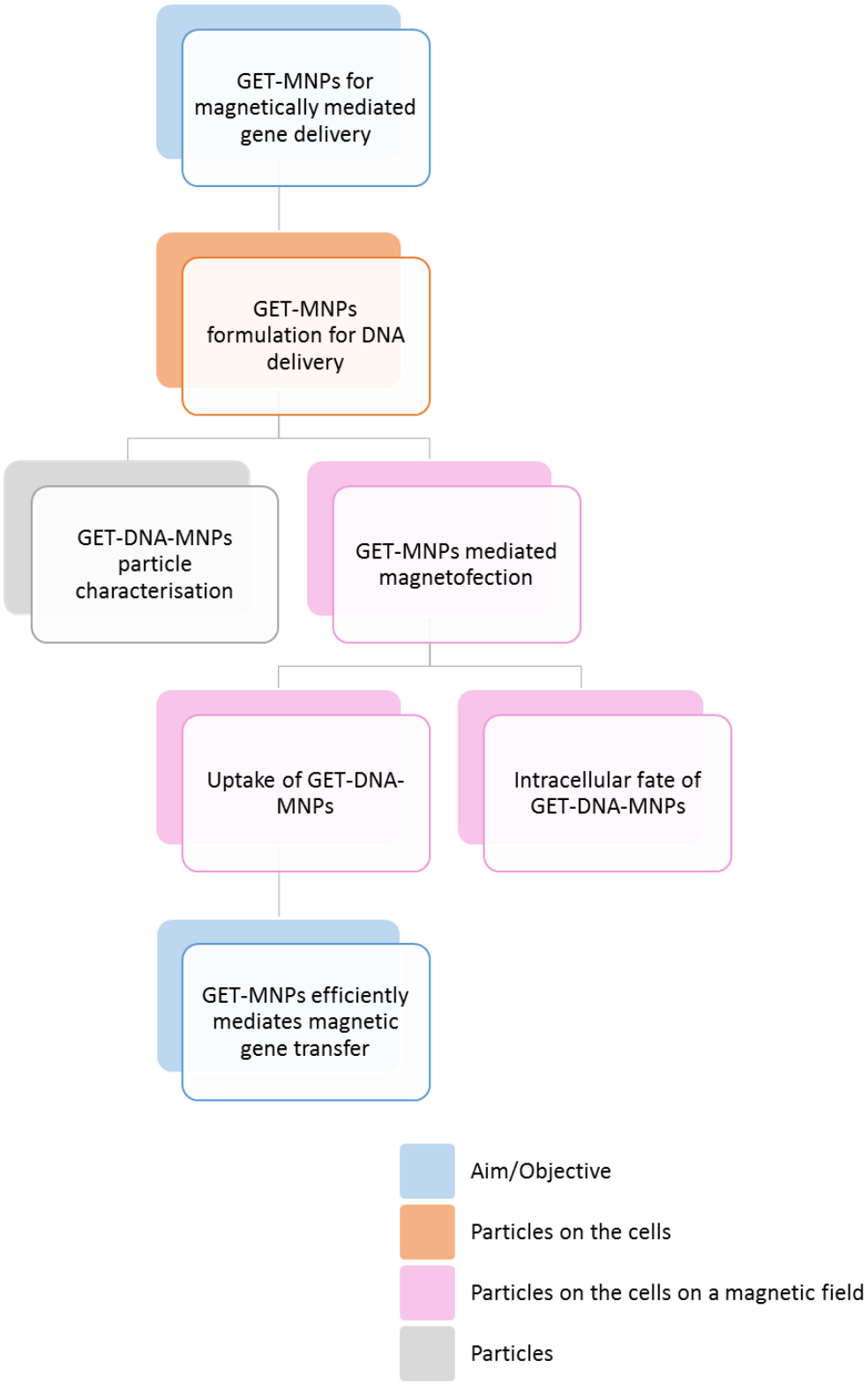

4.3 Results

4.3.1 Particle characterisation

In order to develop a FLR-MNPs based gene delivery vector, a step by step formulation process adapted from Mykhaylyk et al. was followed[231] (Figure 4.2).

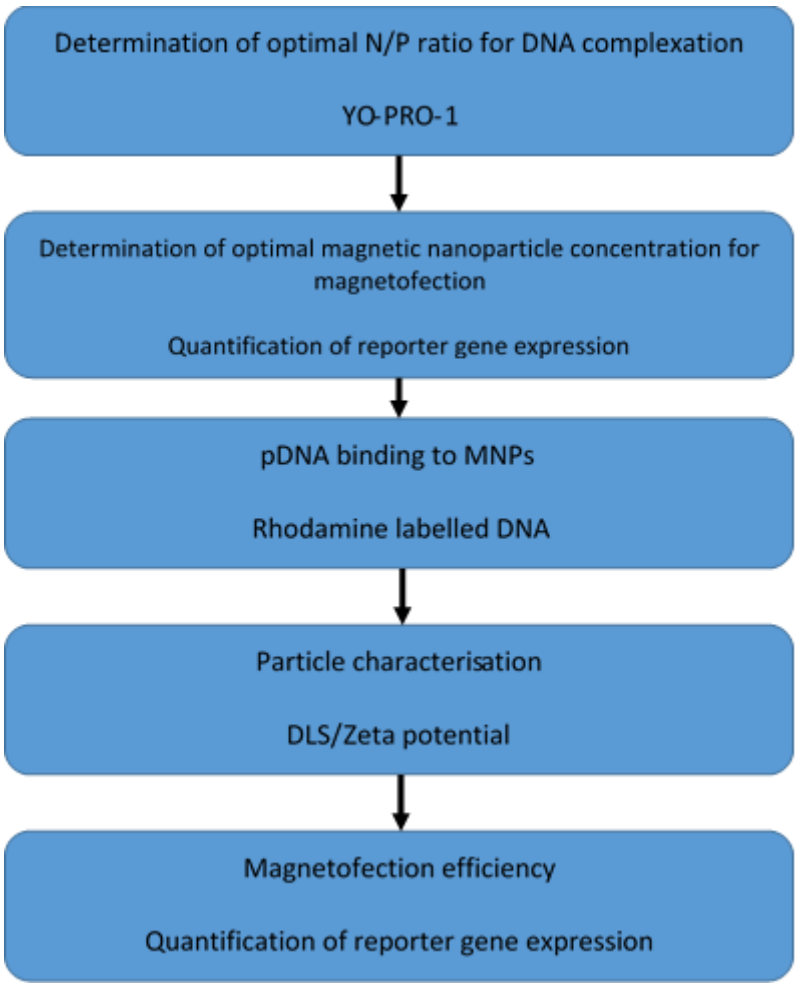

Figure 4.2 Stages of the formulation and characterisation of FLR-DNA-MNPs for gene delivery.

4.3.1.1 Determination of optimal FLR DNA N/P ratio for DNA complexation

The optimal amount of FLR needed to complex DNA was determined using the YO-PRO-1 fluorescent-based assay. Briefly, YO-PRO-1 is a carbocyanine that becomes fluorescent when it binds DNA through its positive side chain. The amount of

fluorescence is proportional to the amount of free DNA. When DNA is complexed or interacts with other molecules in the media, the YO-PRO-DNA interaction becomes unstable and therefore YO-PRO-1 loses its fluorescence proportionally to the amount of DNA complexed. This assay is used to study optimal N/P ratio for DNA complexation. [167] A more detailed explanation on YO-PRO-1 and its complexation with DNA as well as the calculation of the charge ratio (N/P) is provided in section *2.5.2 YO-PRO-1 fluorescence quenching assay.* Briefly, increasing concentrations of FLR were added to a mix of fluorescent DNA-YO-PRO-1 complex. As the concentration of FLR increases, the fluorescence in the media decreases, indicating the interaction of FLR-DNA, outcompeting YO-PRO-1, which in turn loses its fluorescence (Figure 4.3). Total DNA complexation starts occurring at N/P ratio 4 (7.4 ± 5.6% of fluorescence left).

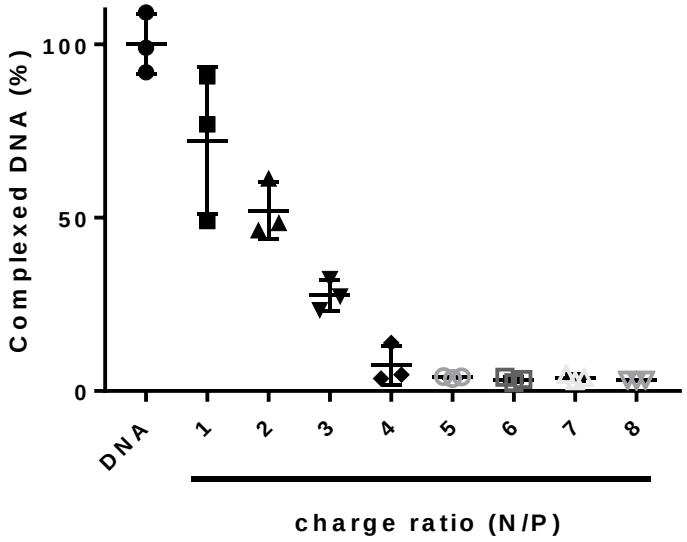

Figure 4.3 FLR efficiently complexes plasmid DNA at N/P ratio 4 and higher.
The graph shows a decrease in the percentage YO-PRO-1 fluorescence as the peptide out competes the dye by complexing DNA at different tested charge ratios (N/P). Graph represent mean ± s.d. (n= 3 technical replicates).

4.3.1.2 Determination of optimal magnetic nanoparticle concentration for magnetofection

To determine optimal MNP concentration for gene delivery, cells were transfected with pCMV-GLuc 2 for 24 hours using a FLR-DNA formulation at N/P 4, 5 and 6 and increasing concentrations of MNPs (5, 10, 25 and 50 µg MNPs/µg DNA). Cells transfected with FLR-DNA alone at N/P ratios 4, 5 and 6 were used as control and labelled 0 µg MNPs/µg. (Figure 4.4). Gene transfer efficiency was measured by Gaussia luciferase expression in the media. N/P ratio 6 showed significantly enhanced protein expression overall compared with 5 and 4.

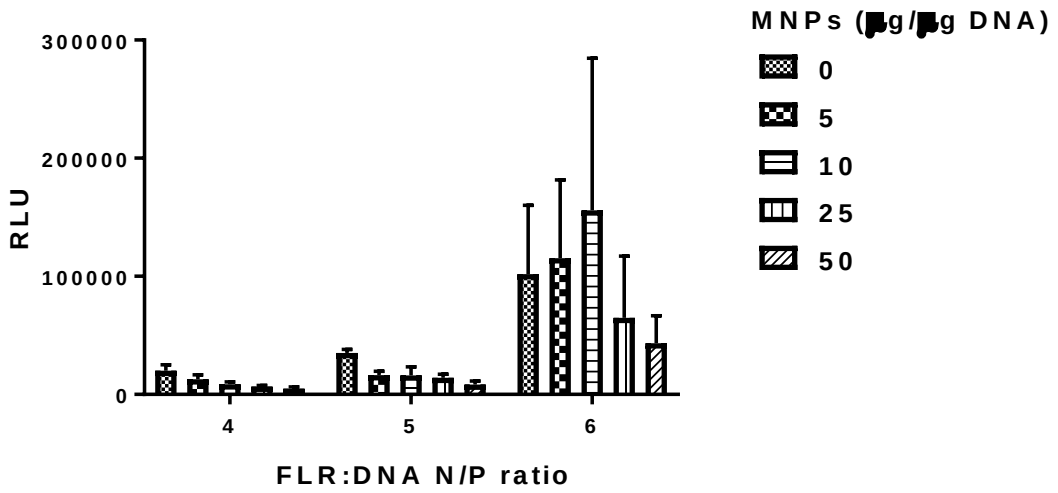

Figure 4.4 Determination of optimal magnetic nanoparticle concentration for magnetofection.

Gaussia luciferase expression in NIH3t3 cells after overnight incubation with FLR-DNA-MNPs at N/P 4, 5 and 6 at increasing concentrations of MNPs (5, 10, 25 and 50 µg per µg of DNA). Cells treated with FLR-DNA only at N/P 4, 5 and 6 were used as control and labelled 0 µg MNPs/µg. All transfections were carried out at same DNA concentration (0.5 µg DNA per transfection). Bars represent luminescence expressed as Relative Light Units, RLU ± s.d. (n=6 biological repeats, 2 technical replicates).

4.3.1.3 Plasmid DNA binding to MNPs

To confirm that DNA was incorporated into the magnetic vector complex, rhodamine labelled DNA (Rh-DNA) was used for vector formation at increasing concentrations of MNPs. After particle assembly, MNPs were separated using a magnetic field and the unbound DNA was measured from the supernatant. (Figure 4.5, A).

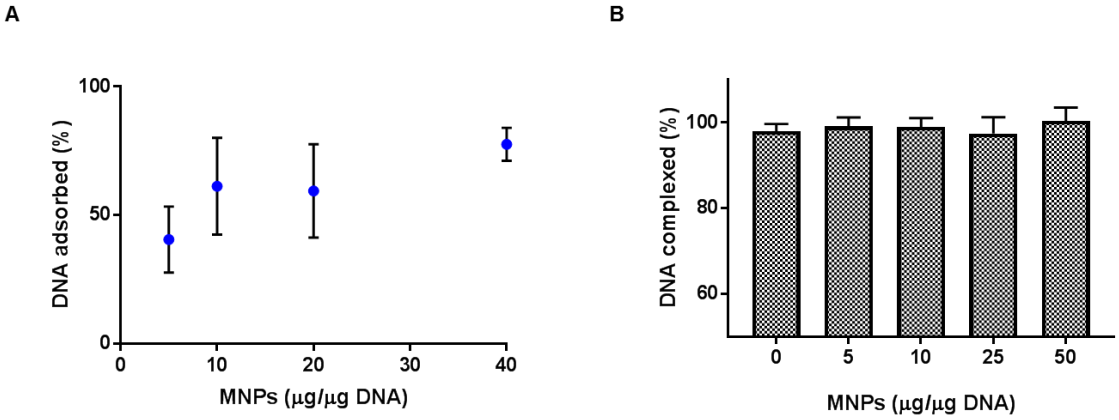

Figure 4.5 FLR-DNA electrostatically interacts with dextran coated MNPs.

A) FLR-DNA adsorbed onto MNPs. Rh- DNA conjugated with FLR at N/P ratio 6 was incubated with increasing amounts of MNPs (5, 10, 20 and 40 µg MNPs/ 1 µg DNA) in water. Percentage of DNA absorbed was calculated relative to the total amount of DNA and plotted against MNPs concentration. Dots represent mean percentage of DNA adsorbed ± s.d. (n=9 technical repeats). B) FLR-DNA binding to MNPs does not affect DNA complexation. Plasmid DNA was incubated with YO-PRO-1 and FLR and then incubated with increasing amounts of MNPs (5, 10, 25 and 50 µg MNPs/ 1 µg DNA). Percentage of complexed DNA was calculated based on the fluorescence of DNA-YO-PRO-1. The fluorescence of FLR-DNA-YO-PRO-1 was taken as 100% complexation. Bars represent mean complexed DNA ± s.d. (n=3 technical repeats).

In order to assess whether plasmid DNA remained complexed after incorporation into the MNPs vector, YO-PRO-1 assay was used. The same principle described before applied here. The fluorescent DNA-YO-PRO complex was incubated with FLR at a N/P ratio of 6 and then incubated with increasing amounts of MNPs. Percentage of complexed DNA was calculated as a function of the loss in fluorescence in solution

compared to DNA-YO-PRO. Figure 4.5 B shows the percentage of complexed DNA against increasing concentrations of MNPs (5, 10, 25 and 50 µg MNPs/ 1 µg DNA).

There is no significant difference in DNA complexation in the presence of MNPs, which indicates that binding of the FLR-DNA complex to the MNPs does not disturb the FLR-DNA interactions, or at least, not enough to allow YO-PRO to bind the DNA.

4.3.1.4 Particle characterisation

Table 11 Physical characterisation of FLR-MNPs vectors for DNA delivery

	D_H (nm)*	**PDI¥**	**Zeta potential (mV)**
MNPs	225.1 ± 4.4	0.18 ± 0.03	-20.7 ± 0.5
FLR-DNA	124.6 ± 2.9	0.24 ± 0.002	49.8 ± 1.1
MNPs-FLR	228 ± 4.6	0.16 ± 0.02	35.3 ± 0.8
MNPs-DNA	239.1 ± 3.9	0.24 ± 0.01	-31.6 ± 0.8
FLR-DNA-MNPs	244.7 ± 8.5	0.21 ± 0.01	34 ± 1

Apparent diameter of the particles obtained by DLS for 20 µg/ml of MNPs incubated with DNA (4 µg/ml), FLR (4.08 µM) or a combination of both formulated according to previously described and resuspended in a total volume of 1 ml of dH_2O. Z-average hydrodynamic diameter extracted by cumulant analysis of the data. Polydispersity index (PDI) from cumulant analysis. Values represent mean ± s.d. (n=1-2 independent repeats, 3 runs per repeat, 15 subruns per run).
Zeta potential, measurements consisted of 3 repeats (12 subruns per repeat). Smoluchowski approximation was used to calculate the zeta potentials from the measured electrophoretic motilities. Values represent mean ± s.d. All measurements were done with Malvern Nanosizer Nano ZS.

Table 11 summarises the physical characteristics, dynamic light scattering (DLS) and zeta potential of MNP and FLR vectors. In the presence of FLR all MNP vectors are positively charged, indicating the disposition of FLR on the outer layer of the MNP complex. In contrast, when MNPs were incubated with just DNA, the particle charge

became significantly lower to that of the particles alone (-31.6 ± 0.8 and -20.7 ± 0.5 mV respectively).

Particle size measurement by DLS suggested particles mostly in the monodisperse range after functionalisation with FLR and DNA-FLR.[204] FLR-DNA-MNPs (244.7 ± 8.5 nm) are significantly larger than MNPs and MNPs-FLR (225.1 ± 4.4 nm and 228 ± 4.6 nm respectively), and comparable to MNPs-DNA (239.1 ± 3.9 nm).

Because the size of the FLR-DNA-MNPs did not account to the addition of FLR-DNA and MNPs, it was hypothesized that upon encounter with the MNPs the FLR-DNA nanoparticles interact with the functional groups in the magnetic particle surface and rearrange seeking to find the most stable conformation. [177] The positive zeta potential of the particles suggests that positively charged FLR is arranged in the outer layer of the particle shielding the negative charge of the plasmid DNA. In order to confirm this hypothesis, future work should include the use of FTIR and CD to gain further understanding on the structural changes on DNA and FLR upon interaction between them and with the dextran surface of the MNPs.[243]

4.3.1.5 Magnetofection with FLR-DNA-MNPs significantly enhances transfection speed

In order to determine whether magnetofection increased overall transfection efficiency or like previously suggested in the literature, just transfection speed, protein expression mediated by FLR-DNA-MNPs was assessed. [123], [162], [238], [239], [244]

Cells were transfected for 1 hour or 24 hours with and without an external magnetic field (Figure 4.6). MNPs-DNA and FLR-DNA were used as controls. FLR-DNA-MNPs

mediated transfection was significantly enhanced by the presence of a magnetic field during 1 hour transfection (2.09 ± 0.45 x 10^7 RLU with a magnet compared to 1.13 ± 0.6 x 10^7 RLU without a magnet). Interestingly, in one hour FLR-DNA-MNPs without an external magnetic field induced similar protein expression as FLR-DNA (0.80 ± 0.76 x 10^7 RLU), suggesting MNPs are not hampering the gene transfer process. After 24 hours transfection, cells transfected with both FLR-DNA and FLR-DNA-MNPs showed comparable levels of protein expression independent of the magnetic field. Protein expression after 24 hours was comparable to that of FLR-DNA-MNPs in 1 hour under a magnetic field.

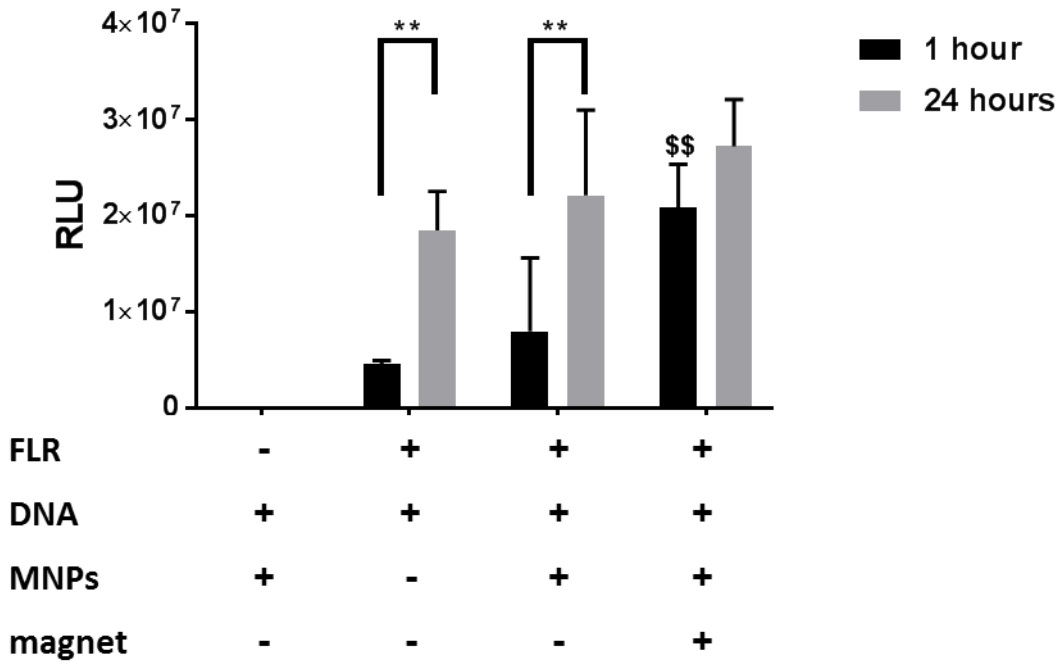

Figure 4.6. Magnetofection increases the speed and enhances protein expression over short incubation times in NIH3t3 cells.

*Gaussia luciferase expression on NIH3t3 cells after 1 hour or 24 hours delivery. DNA was delivered with MNPs, FLR and FLR and MNPs in the presence or absence of a magnet. For all formulations 0.5 µg of DNA were delivered, MNPs complexes were formulated at 5 µg MNPs/ 1 µg of DNA. FLR-DNA ratio was constant at N/P 6. (n=4 biological replicates, 2 technical repeats ** p>0.01, comparison between transfection at 1 hour and 24 hours, Sidak's multiple comparisons test; $$ p>0.01, comparison between transfection at 1 hour, Tukey's multiple comparisons test).*

In summary, in this section, a FLR-DNA-MNPs formulation has been optimised and characterised. FLR-DNA-MNPs induced comparable protein expression to its non-magnetic counterpart FLR-DNA in the absence of a magnetic field. Importantly, under the influence of a magnetic field FLR-DNA-MNPs were able to achieve maximal protein expression after 1 hour transfection.

4.3.1.6 Magnetofection mediated by FLR-DNA-MNPs does not affect cell viability

The cytotoxic effect of magnetofection on growth of NIH3t3 cells was assessed by trypan blue (Figure 4.7). Cells were transfected for 1 hour with pCMV-GLuc 2 with FLR (FLR-DNA) and FLR-MNPs (FLR-DNA-MNPs) with or without an external magnetic field (magnet). Cells were counted 24 hours post transfection (day 1) and every 24 hours for 7 days. There were no significant differences in cell proliferation or viability across all treatment groups compared to control (untreated). These results indicate that regardless of the rapid accumulation of vector complex on the cell membrane mediated by magnetofection, the dosages of plasmid, peptide and MNPs were not harmful for NIH3t3 cells.

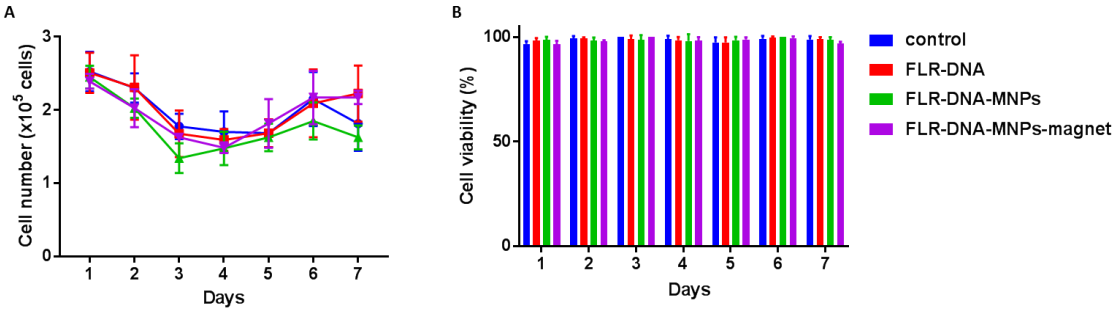

Figure 4.7. Cell proliferation and viability after incubation with FLR based vectors.

NIH3t3 cells were treated with FLR-DNA and FLR-DNA-MNPs with and without the presence of an external magnetic field (magnet). After 1 hour cells were washed with PBS to remove any unbound vector. A) Cell number represent the number of viable cells. B) Cell viability was measured by the intake of trypan blue by dead cells. Live and dead cells were counted. Percentage of cell viability was calculated based on the total number of viable and unviable cells for each group. *n=3, biological replicates.*

4.3.2 Transfection kinetics

In order to gain further understanding on magnetofection, transfection kinetics mediated by FLR and FLR-MNPs with and without an external magnetic field were assessed in NIH3t3 cells. Cells were transfected/magnetofected for increasing amounts of time (from 5 min to 60 min). Transfection kinetics were assessed by: reporter gene expression (Gaussia Luciferase), percentage of DNA labelled cells as well as the amount of DNA per cell (intensity mean).

4.3.2.1 Reporter gene expression at increasing transfection time points

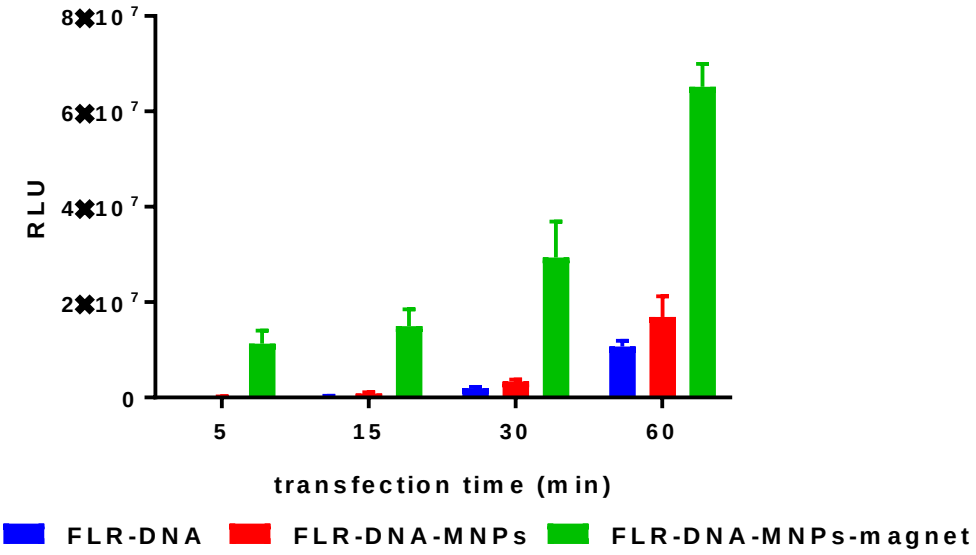

Figure 4.8 Efficient and fast (less than 5 min) DNA delivery using magnetofection with FLR-DNA-MNPs.
Gaussia luciferase expression after 5, 15, 30 and 60 min transfection/magnetofection. After transfection cells were washed with PBS to remove any unbound DNA complex. 0.5 µg of DNA were delivered with FLR (FLR-DNA) and FLR and MNPs, FLR-DNA-MNPs with/without the application of a magnetic field. MNPs complexes were formulated at 5 µg MNPs/ 1 µg of DNA. FLR-DNA ratio was constant at N/P 6. n=3 biological repeats, 1 technical replicates.

FLR-DNA-MNPs in an external magnetic field were able to generate significant levels of reporter gene expression after just 5 minutes, which was comparable to gene expression mediated by FLR and FLR-DNA-MNPs after 60 mins delivery (Figure 4.8).

4.3.2.2 DNA uptake at increasing transfection time points

Labelled plasmid DNA (Rh-DNA) was used to quantify DNA uptake in the cells with FLR-DNA and FLR-DNA-MNPs with/without a magnet at increasing time points. Prior to performing the inhibitory studies the effect of pDNA labelling with rhodamine on transfection efficiency and cell viability were assessed (Figure 4.9). Labelling of the plasmid pCMV-GLuc 2 did not have an effect on cell metabolic activity or protein expression activity on NIH3t3 cells.

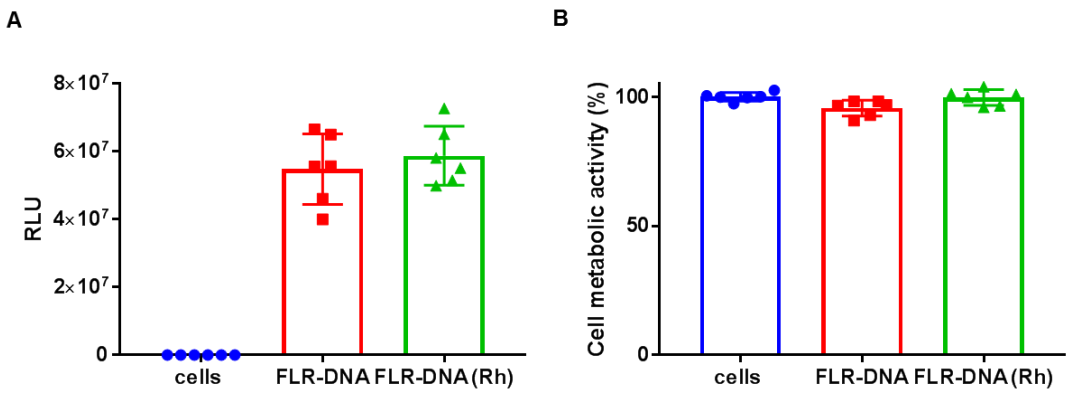

Figure 4.9 Rhodamine labelling of pCMV-GLuc 2 plasmid does not affect protein expression or cell viability in NIH3t3 cells.
A) Gaussia luciferase expression on NIH3t3 cells after 24 hours transfection with FLR and unlabelled DNA (FLR-DNA) or FLR and Rh- DNA. B) Relative cell metabolic activity of NIH3t3 cells after 24 transfection with FLR and unlabelled DNA (FLR-DNA) vs FLR and Rh-DNA (FLR-Rh-DNA) measured by Alamar Blue. Untreated cells were taken as a control for 100% cell metabolic activity. n=6, biological repeats, 2 technical replicates.

Flow cytometry quantification of percentage of rhodamine positive cells confirmed the association of Rh-DNA to the cell as early as 5 minutes (70 ± 12% of positive cells with FLR-DNA-MNPs-magnet compared with 4 ± 2% and 6.4 ± 2% for FLR-DNA and FLR-DNA-MNPs respectively) (Figure 4.10).

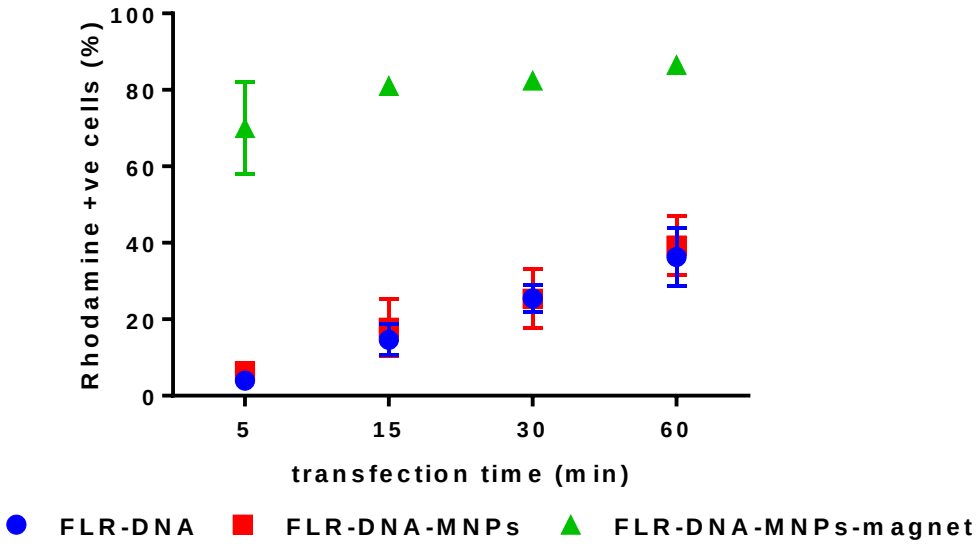

Figure 4.10 Percentage of rhodamine positive cells after Rh-DNA delivery for increasing amounts of time.
Rh-DNA-cell membrane association in NIH3t3 cells after 5, 15, 30 and 60 min transfection/magnetofection. After transfection cells were washed with PBS. 0.5 µg of Rh-DNA were delivered with FLR (FLR-DNA) and FLR and MNPs, FLR-DNA-MNPs with/without the application of a magnetic field. MNPs complexes were formulated at 5 µg MNPs/ 1 µg of DNA. FLR-DNA ratio was constant at N/P 6. Values represent mean ± s.d. n=6 biological repeats, 2 technical replicates.

DNA association over time followed two different trends when the magnetic vectors are delivered with or without the magnet. The percentage of rhodamine positive cells remained almost constant over 60 minutes (at around 80%) when Rh-DNA was delivered with MNPs in the presence of a magnetic field, whereas without a magnet Rh-DNA association increases progressively overtime.

Mean fluorescent intensity per cell, remained constant or increased minimally over time (Figure 4.11), suggesting that a similar amount of DNA gets bound or uptaken by the cells in the same experimental conditions and longer exposure times increased the percentage of labelled cells (Figure 4.10) but not necessarily the amount of DNA per cell.

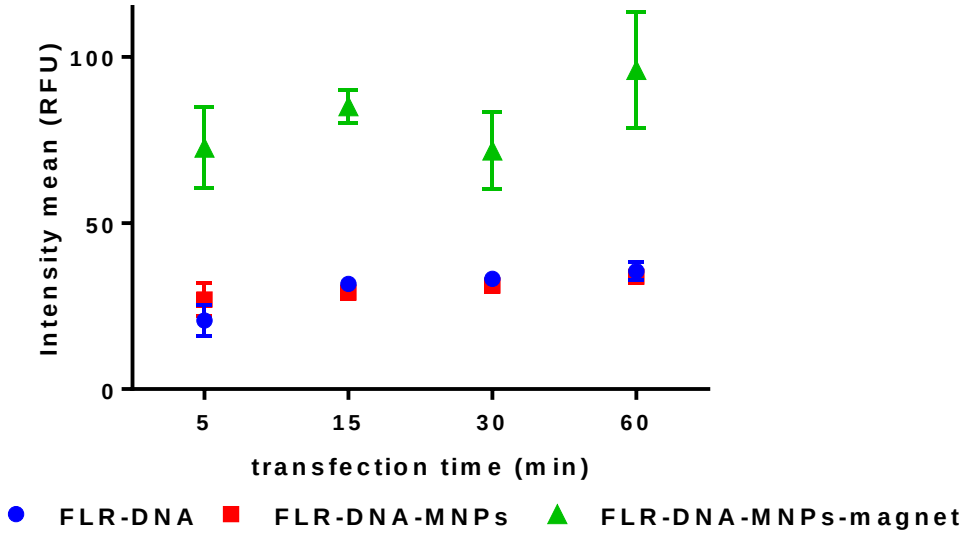

Figure 4.11 Mean intensity rhodamine positive cells after Rh-DNA delivery for increasing amounts of time.
Mean intensity of Rh-DNA loaded NIH3t3 cells after 5, 15, 30 and 60 min transfection/magnetofection. After transfection cells were washed with PBS to remove any unbound DNA complex. 0.5 µg of Rh-DNA were delivered with FLR (FLR-DNA) and FLR and MNPs, FLR-DNA-MNPs with/without the application of a magnetic field. MNPs complexes were formulated at 5 µg MNPs/ 1 µg of DNA. FLR-DNA ratio was constant at N/P 6. Values represent mean ± s.d. n=6 biological repeats, 2 technical replicates.

The application of an external magnetic field on FLR-DNA-MNPs allows for rapid concentration of DNA on the cells. In the absence of any magnetic forces, the magnetic vectors progressively accumulate on the cells over time.

4.3.2.3 MNPs uptake at increasing transfection times

Similarly to previously described, NIH3t3 cells were incubated with FLR-DNA-MNPs for increasing amounts of time: 5, 15, 30 and 60 mins with and without an external

magnetic field (magnet). After delivery, cells were washed with PBS to remove any unbound vector/complex. The amount of iron per cell was quantified 24 hours post-delivery by ICP-MS. Figure 4.12 shows that significantly more iron was associated in the cells in the presence of a magnetic field. Importantly, iron content progressively increased with prolonged incubation times when the particles were delivered in the presence of a magnetic field.

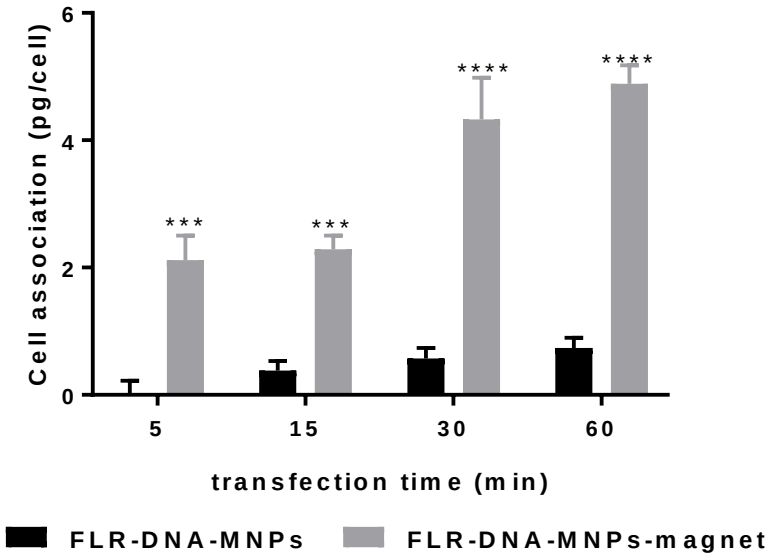

Figure 4.12 MNPs uptake in the cells over time.
*Iron cell association in NIH3t3 cells after 5, 15, 30 and 60 min transfection/magnetofection. After transfection cells were washed with PBS to remove any unbound DNA complex. 0.5 µg of DNA were delivered with FLR (FLR-DNA) and FLR and MNPs, FLR-DNA-MNPs with/without the application of a magnetic field. For all formulations MNPs complexes were formulated at 5 µg MNPs/ 1 µg of DNA. FLR-DNA ratio was constant at N/P 6. Bars represent mean values ± s.d. n=6 biological repeats, 2 technical replicates (*** p<0.001, **** p<0.0001, Sidak's multiple comparison's test).*

4.3.3 Endocytosis inhibitors

Most non-viral vectors are hydrophilic, which greatly inhibits their ability to passively traverse the hydrophobic cell membrane. Therefore, these vectors require active,

energy dependent endocytosis processes to cross the cell membrane. There is some evidence of lipoplex mediated DNA delivery through fusion with the cell membrane and direct release to the cytoplasm but there is no confirmation that this is the case for cationic peptides/polymers.[98], [245]–[247]

The most widely researched endocytic pathways are clathrin or caveolae mediated endocytosis and macropinocytosis (Figure 4.13). Clathrin mediated endocytosis (CME) is the major and best-characterised pathway. CME starts by the interaction of a ligand with a cell receptor, the receptor-ligand complexes then cluster on clathrin coated pits on the cell membrane. These pits then invaginate and separate from the plasma membrane forming vesicles that mature into early endosomes. These vesicles can take particle sizes of up to 200 µm.

Caveolae are defined as small hydrophobic invaginations that get internalised and form intracellular organelles, different to the previously mentioned endosomes. Caveolae endocytosis is highly dependent on cholesterol. Regular caveolae size ranges from 50-60 nm, although, recent literature has suggested that larger molecules (500 nm) are preferentially taken up by this pathway.[195]

Macropinocytosis describes the formation of large vesicles generated by the actin mediated invagination of the cell membrane. These vesicles are irregular in shape and size (they can be up to 5 µm). Most of the cargoes taken up by this route get recycled back to the cell membrane but macropinosomes do not fuse into lysosomes so they mostly avoid lysosomal degradation. GET mediated gene delivery has been associated

with this endocytic pathway, however it is likely that changes in cargo size, charge and payload could change the mode of uptake. [163]

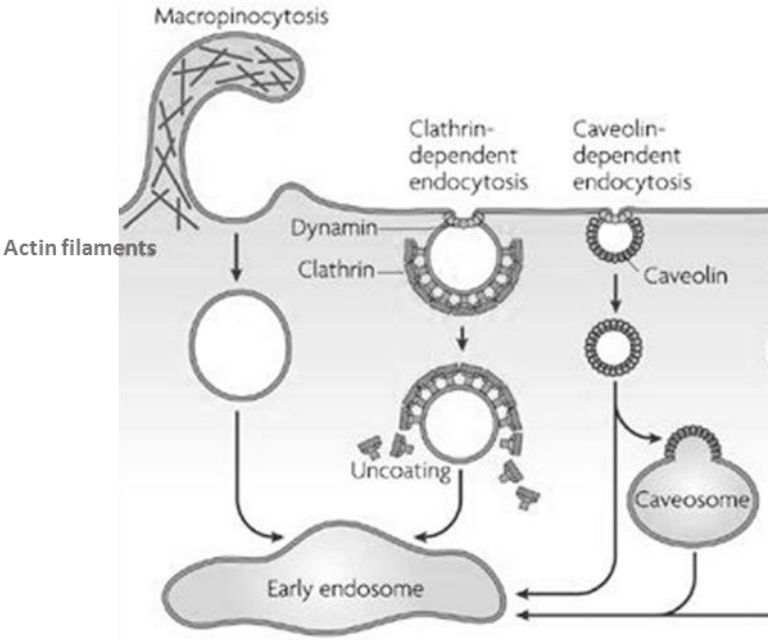

Figure 4.13 Schematic of endocytic pathways.
Adapted from Mayor et al.[248]

4.3.3.1 DNA uptake

Labelled plasmid DNA (Rh-DNA) was used to quantify DNA uptake in the cells with FLR-DNA and FLR-DNA-MNPs with/without a magnet under four different conditions that are known to be inhibitory to cellular uptake through endocytosis: low temperature (4^{o}C) rigidifies the cell membrane affecting both passive and active uptake[191], hypertonic (sucrose) to hinder clathrin lattice formation[192], methyl-B-cyclodextrin (MBCD) an inhibitor of caveolae mediated endocytosis through complexation of cholesterol[194] and amiloride, an inhibitor of Na+/H+ exchange required for micropinocytosis.[249] Cells incubated with the vectors at 37^{o}C without any inhibitors were identified as “control” treatment. Experimental conditions including effective concentrations and treatment times of low temperature (4^{o}C) MBCD and amiloride

had been previously validated when assessing the mechanism of internalisation of GET peptides using a cAMP response element (CRE) assay system. [163] It has been previously reported that the treatment of NIH3t3 cells with methyl- β-cyclodextrin (0-5 mM) or amiloride (0-5 mM) did not negatively affect cell viability. [249]

The aim of this experiment was to assess the effect of different endocytosis inhibitors on the uptake of Rh-DNA mediated by FLR-MNPs and to determine whether the fast accumulation of magnetic vector on the cell membrane mediated by an external magnetic field had an effect on the uptake mechanism. It was therefore very important to differentiate between Rh-DNA uptake (internalisation) and Rh-DNA-cell association (Rh-DNA bound to the cell membrane but not internalised). In order to do so, after transfection, cells were washed with either PBS (removes unbound or loosely bound transfection complex) or heparin, known to destabilise DNA-FLR interaction, preventing further gene transfer.[163] Evidence of FLR-DNA particle destabilisation in the presence of heparin is provided in Figure 8.15.

Figure 4.14 A shows that, hypertonic media (sucrose) which is known to disrupt clathrin lattices, significantly decreases overall DNA cell association in all three treatment groups. None of the other inhibitors have a significant effect on DNA-cell association.

All inhibitors significantly decrease DNA internalisation for all vectors in NIH3t3 cells (Figure 4.14 B). FLR-DNA and FLR-DNA-MNPs without a magnet showed similar DNA uptake patterns in response to the different inhibitors. Low temperature (4^{o}C) known to rigidify the cell and hypertonic media (sucrose), reported to disrupt clathrin lattices have the most significant effect on DNA internalisation, suggesting a heavy

contribution of clathrin mediated endocytosis in the process. Clathrin mediated uptake of similar size particles and magnetofection complexes has been previously reported in the literature.[191], [195], [244]

Interestingly, when FLR-DNA-MNPs were delivered in the presence of a magnetic field, MBCD, which has been suggested to inhibit caveolae mediated endocytosis, had a greater effect on DNA uptake compared to sucrose (Figure 4.14 B).

In the presence of a magnetic field magnetic vectors are rapidly attracted towards the cell surface increasing DNA concentration on the cell membrane (Figure 4.11). High concentrations of vector on the cell membrane have been previously reported to saturate binding sites specific to a particular uptake mechanism.[250]–[252] It could therefore be hypothesised that the saturation of the CME (previously suggested mechanism of FLR and FLR-MNPs mediated DNA uptake), triggered the rerouting of the cargo towards different endocytic pathways, in this case, caveolae mediated endocytosis.

It is important to note that FLR-DNA and FLR-DNA-MNPs in the absence of a magnetic field showed comparable uptake mechanisms. These results are in agreement with data previously presented on transfection kinetics that indicated that reporter gene expression and DNA uptake profiles over time were similar for the two vectors. These findings suggests that the incorporation of MNPs into the FLR-DNA does not prevent efficient gene delivery mediated by FLR.

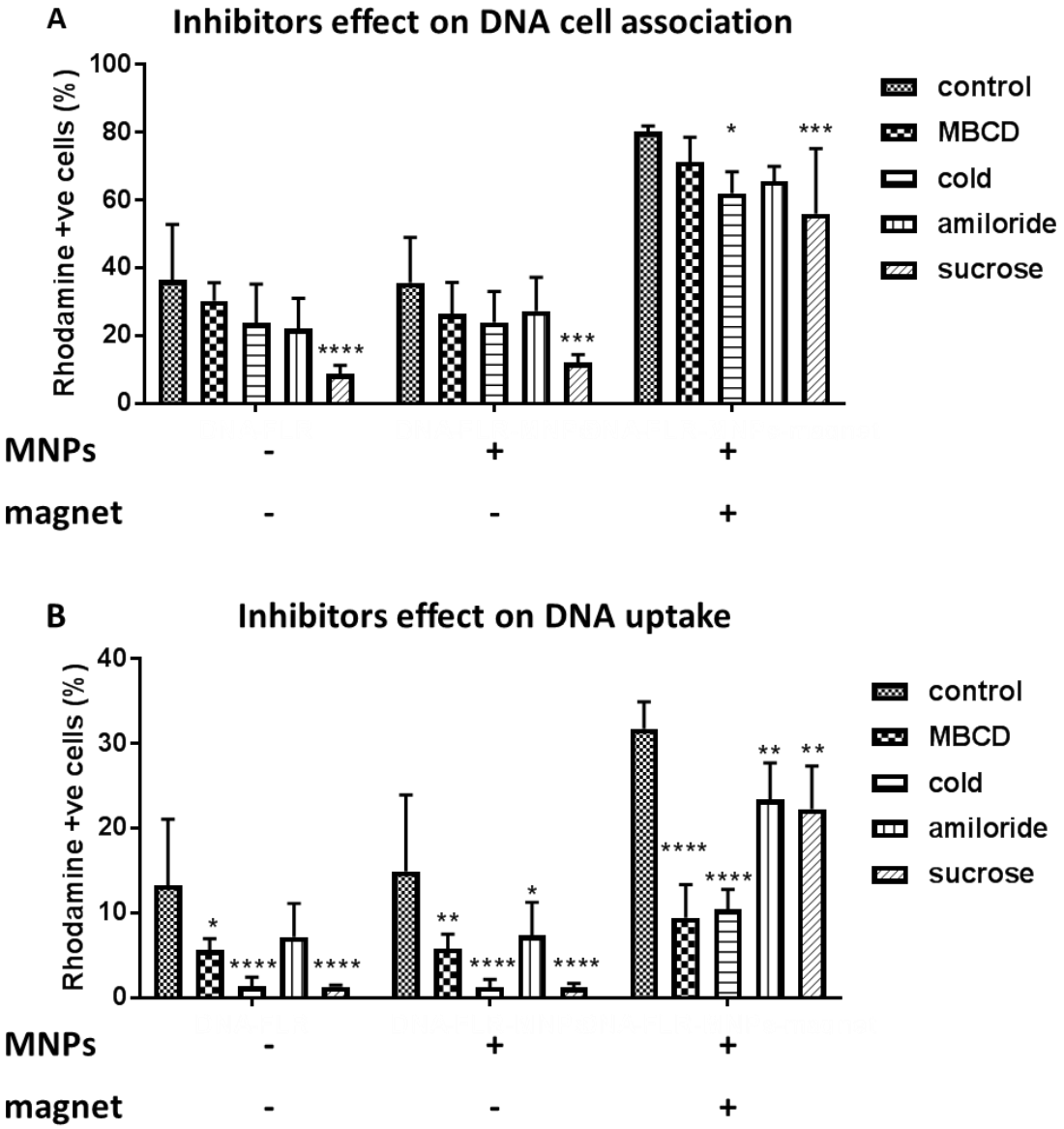

Figure 4.14 Effect of endocytosis inhibitors on Rh- DNA cell association and uptake in NIH3t3 cells.

*Final concentration of inhibitors: methyl-B-cyclodextrin (MBCD) 5 mM, 5(N-ethyl-N-isopropyl) amiloride 100 µM and sucrose 0.45 M. Cells were transfected with 0.5 µg DNA per well, FLR N/P 6 and 5 µg of MNPs/µg DNA for magnetic vectors. Magnetic vectors were delivered with/without a magnetic field. Cells were exposed to the inhibitors/4°C for 1 hour. The effect of inhibitors was tested on DNA cell association (A) and DNA cell uptake (B) 24 hours post-delivery. Bars represent average percentage of rhodamine labelled cells ± s.d. n= 6 biological repeats, 2 technical replicates. (*p<0.05, **p<0.01, ***p<0.001, ****p<0.0001, Tukey's multiple comparisons test).*

4.3.4 Membrane rupturing activity of FLR based complexes

After being internalised by the cell, endocytosed DNA must be released into the cytosol and access the cell nucleus in order to express the desired gene. Endosome membrane rupturing activity of FLR and FLR-MNPs vectors was assessed through haemolysis assay, in which erythrocyte membranes serve as a surrogate for the lipid bilayer membrane in the endo-lysosomal vesicles.[253]–[256]

Membrane disruption activity was assessed at physiological pH (7.5) and late endosome/lysosome pH (5). Haemolytic activity was calculated as a percentage of total haemolysis mediated by detergent Triton-x 100 (Figure 4.15).

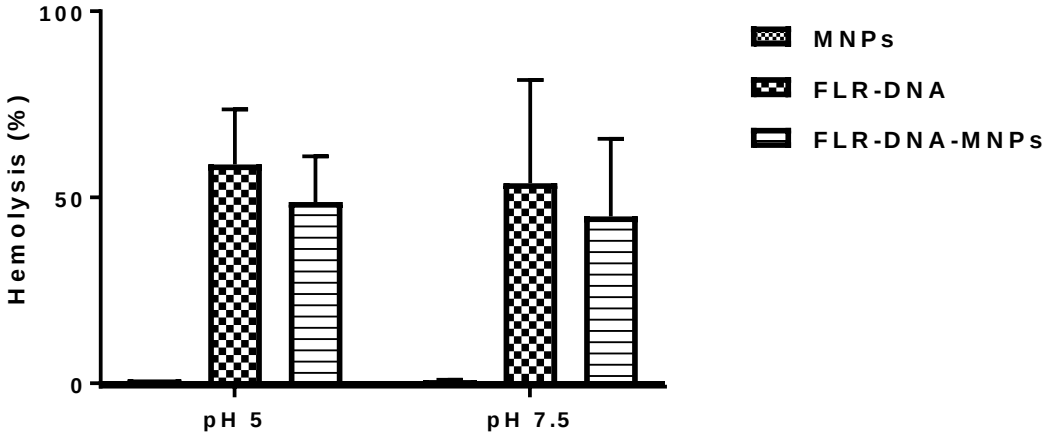

Figure 4.15 Membrane rupturing activity is mediated by FLR and independent of pH. *Freshly isolated human erythrocytes were exposed to 0.5 µM of FLR. For FLR-DNA, N/P ratio 6 between peptide and DNA. 5 µg of MNPs/µg of DNA were added to form the FLR-DNA-MNPs. Haemolysis experiments were performed in PBS for 30 min at physiological pH (7.5) and late endosome pH (5). Haemolysis was quantified by spectrophotometric assay. Results are expressed as percentage lysis taking Triton-x 100 as complete lysis (100%). Bars represent mean ± s.d. from 7 independent repeats from the same donor.*

There were not significant differences between the haemolytic activity of FLR-DNA and FLR-DNA-MNPs independent of the pH (58.8 ± 14.8% and 48.7 ± 12.3%

respectively at pH 7.5 and 53.8 ± 27.8% and 44.8 ± 20.8% respectively at pH 5). Dextran coated MNPs alone did not show any significant membrane rupturing activity. These results could suggest that if there was to be endosomal escape activity, triggered by the complex, part of it would be mediated by FLR. Additionally, FLR membrane disruptive activity is pH independent, which is consistent with the lack of carboxylic side chains on FLR molecule (Figure 8.7) known to mediate pH dependant endosomal disruptive activity.[253] The membrane disruptive activity of FLR could then potentially be explained by physical interaction between the peptide and the lipid bilayer, like it has been previously reported for similar peptides.[257]

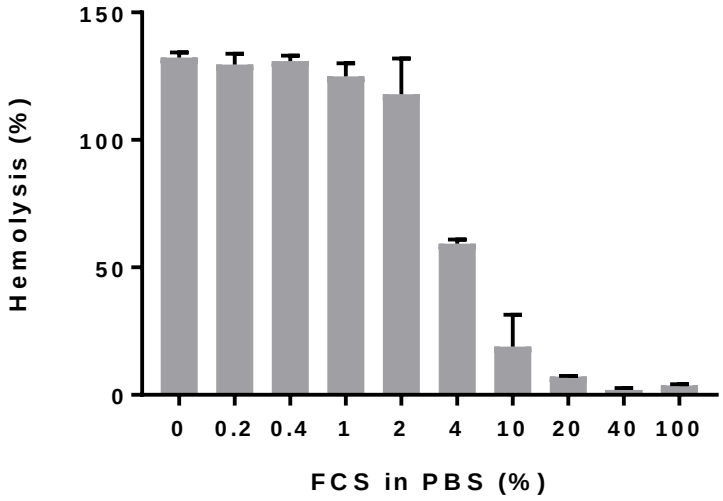

Figure 4.16 FLR minimally affects membrane integrity in cell culture conditions.
Freshly isolated human erythrocytes were exposed to 1 μM of FLR at increasing concentrations of FCS (0-100% v/v in PBS). Haemolysis experiments were performed for 30 min at physiological pH (7.5). Haemolysis was quantified by spectrophotometric assay. Results are expressed as percentage lysis taking Triton-x 100 as complete lysis (100%). Bars represent mean ± s.d. from 2 independent repeats from the same donor.

Membrane disruptive activity of FLR decreases in the presence of serum and it drops down to approximately 20% (19 ± 12.6 % hemolysis) at 10% FCS (*in vitro* experimental

conditions) (Figure 4.16). Indicating FLR would not significantly affect the cell plasma membrane integrity during transfection.

It is important to note that haemolysis assay only assesses for membrane rupturing activity due to chemical interactions with the cell membrane, however it does not account for endosome swelling or physical alterations of the loaded endosome. Additionally, this assay is performed in PBS or FCS, which do not accurately represent the intracellular environment (i.e. cytosol or endosome composition). Finally, in this assay, red blood cells are used as a surrogate for endosomal membranes, however, the lipid content and exact composition of the endosomal membranes varies between cells and might not always be adequately recapitulated by the red blood cell membranes. Isolation and analysis of the internal structure of the magnetically labelled endosomes would provide more information on endosomal membrane composition.[255], [258]

4.3.5 Stability of extrachromosomal DNA over time

To evaluate the ability of FLR-MNPs vectors and magnetofection conditions to deliver intact DNA inside the cells as well as its stability overtime, pCMV-GLuc 2 plasmid DNA was delivered with FLR-DNA, FLR-DNA-MNPs and FLR-DNA-MNPs-magnet for 5 min. Extrachromosomal DNA was isolated and quantified at different time points post-delivery.[259] Percentage of cell bound DNA was calculated compared to total amount of DNA delivered (Figure 4.17).

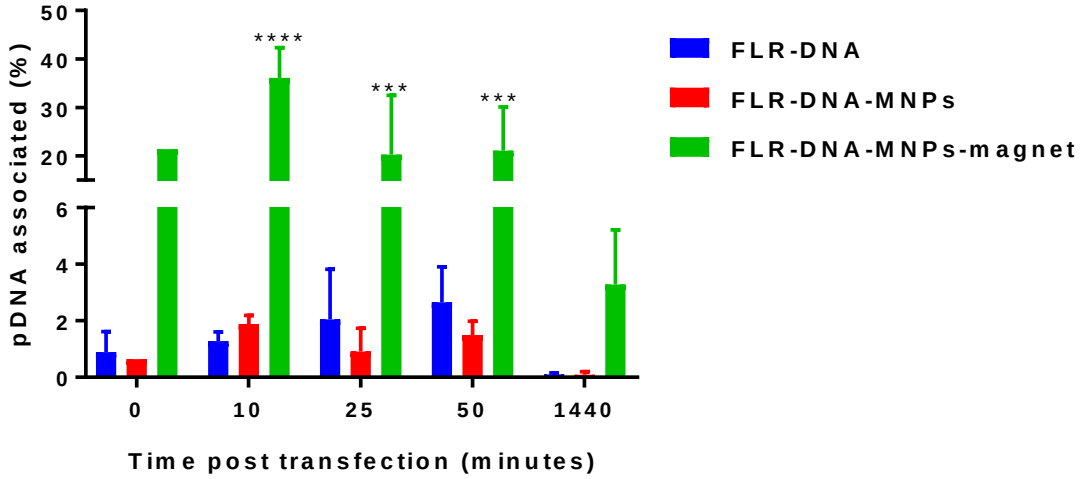

Figure 4.17 Stability of extrachromosomal DNA over time.
Percentage of intact plasmid DNA associated with NIH3t3 cells after 5 minutes transfection/magnetofection. Unbound DNA was washed with PBS. Collection points were: immediately after (0 min), 10, 25, 50 and 1440 min. 0.5 µg of DNA were delivered with FLR (FLR-DNA) and FLR and MNPs, FLR-DNA-MNPs with/without the application of a magnetic field. MNPs complexes were formulated at 5 µg MNPs/ 1 µg of DNA. FLR-DNA ratio was constant at N/P 6. Extrachromosomal DNA was extracted, purified and quantified by bacterial transformation. Percentage of pDNA associated was calculated from the total amount of DNA delivered. Bars represent mean percentage of cell associated DNA ± s.d. n= 3 technical repeats.

A significantly higher percentage of functional DNA was associated to NIH3t3 cells when DNA was delivered with FLR-DNA-MNPs in a magnetic field compared to FLR-

DNA and FLR-DNA-MNPs in the absence of a magnetic field. The percentage of cell bound DNA remained constant during the first 60 mins and decreased significantly after 24 hours. Interestingly, the percentage of extrachromosomal DNA degraded over 24 hours was comparable in all transfection groups (around 10% of the DNA present immediately post-delivery). Since all vectors were taken up through endocytosis, it is most likely that degradation is due to either to the entrapment of the complexes in the lysosomal compartment or degradation by cytosolic nucleases.[260]

In this context, DNA degradation depends largely on the presentation of the plasmid where naked DNA is more susceptible to degradation compared to encapsulated, and is proportional to the amount of DNA delivered independent of specific uptake route.[261]

The results here presented support data previously reported on Rh-DNA uptake mediated by FLR-DNA-MNPs (*4.3.3 Uptake kinetics*). A repeat of the experiment in the presence of heparin to assess for internalised DNA would provide more information regarding the intracellular concentration of the DNA and degradation profiles over time. Additionally, measurement of extrachromosomal DNA in the nucleus would provide additional information on DNA localization.[99]

4.3.6 Intracellular localization of Rh-DNA

Intracellular localization of Rh-DNA was imaged after delivery with FLR (FLR-DNA) or FLR-MNPs on a magnetic field (FLR-DNA-MNPs) after 30 min (Figure 4.18), 60 min (Figure 4.19) and 24 hours (Figure 4.20) transfection. At the end of each incubation time, cells were washed with PBS and fixed with 3.7% PFA, actin cytoskeleton was

stained with Alexa Fluor 488 Phalloidin (cytoskeleton) and the nucleus was stained with DAPI (nucleus). pCMV-GLuc 2 was labelled with rhodamine (Rh-DNA).[262]

Merged fluorescent images showed little to no fluorescence after 30 min when Rh-DNA was delivered with FLR, however, when the DNA is delivered with MNPs on a magnetic field, large numbers of fluorescent particles could be observed localized around the boundaries of the cell and attached to the cell surface. After 1 hour delivery, discrete fluorescent units could already be detected on the cells treated with FLR-DNA, however these were less frequent compared FLR-DNA-MNPs.

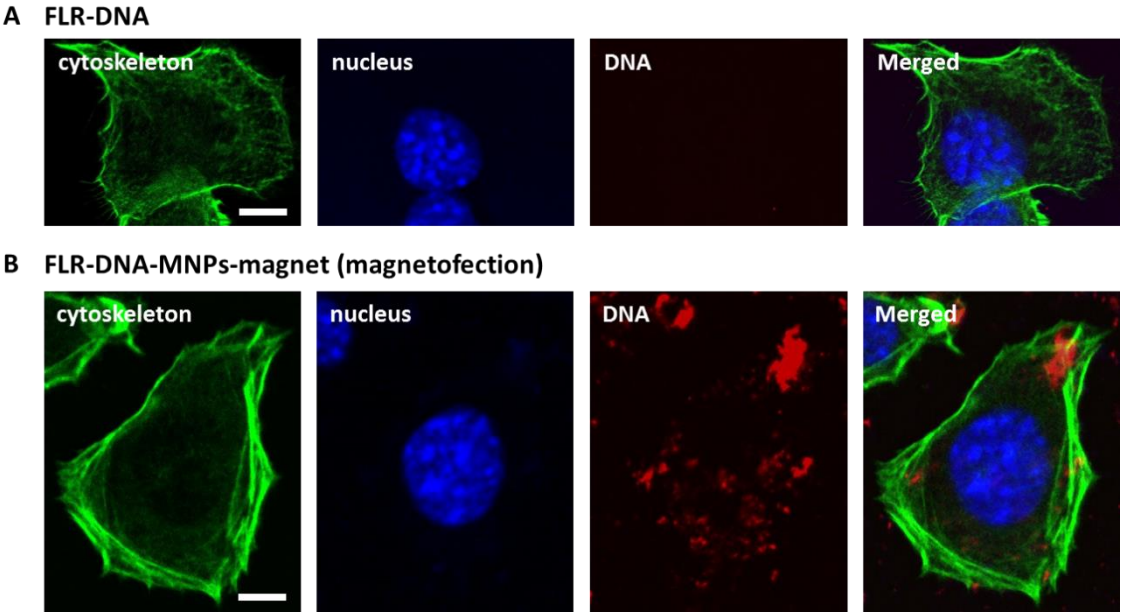

Figure 4.18 Representative Confocal Laser Scanning Microscopy (CLSM) images of Rho-labelled DNA in NIH3t3 cells after 30 min delivery.
Cells were transfected with FLR-DNA (A) and FLR-DNA-MNPs in the presence of a magnetic field (B). Cells were treated with 1 µg of Rh-DNA at N/P ratio 6 and optimal MNPs mass ratio 5 µg MNPs / 1 µg DNA for 30 min. After incubation, unbound complex was removed with PBS and cells were fixed with 3.7% PFA. pCMV-GLuc 2 was stained with rhodamine (red), nucleus was stained with DAPI (blue) and actin cytoskeleton was stained with Alexa Fluor 488 Phalloidin (green). Scale bar 2 µm.

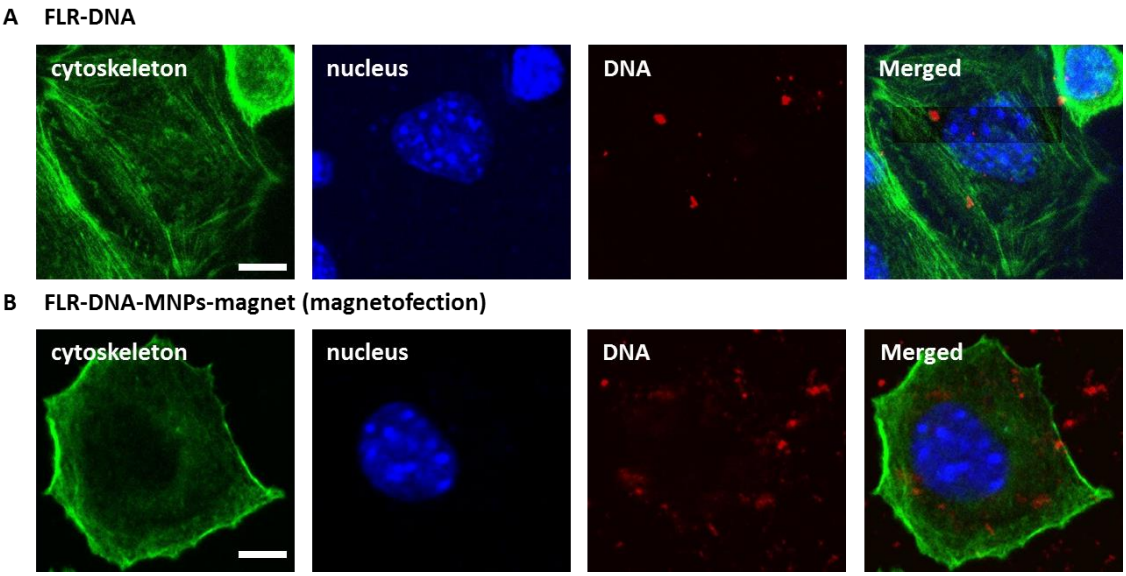

Figure 4.19 Representative Confocal Laser Scanning Microscopy (CLSM) images of Rho-labelled DNA in NIH3t3 cells after 60 min delivery.

Cells were transfected with FLR-DNA (A) and FLR-DNA-MNPs in the presence of a magnetic field (B). Cells were treated with 1 µg of Rh-DNA at N/P ratio 6 and optimal MNPs mass ratio 5 µg MNPs/ 1 µg DNA for 60 min. After incubation, unbound complex was removed with PBS and cells were fixed with 3.7% PFA. pCMV-GLuc 2 was stained with rhodamine (red), nucleus was stained with DAPI (blue) and actin cytoskeleton was stained with Alexa Fluor 488 Phalloidin (green). Scale bar 2 µm.

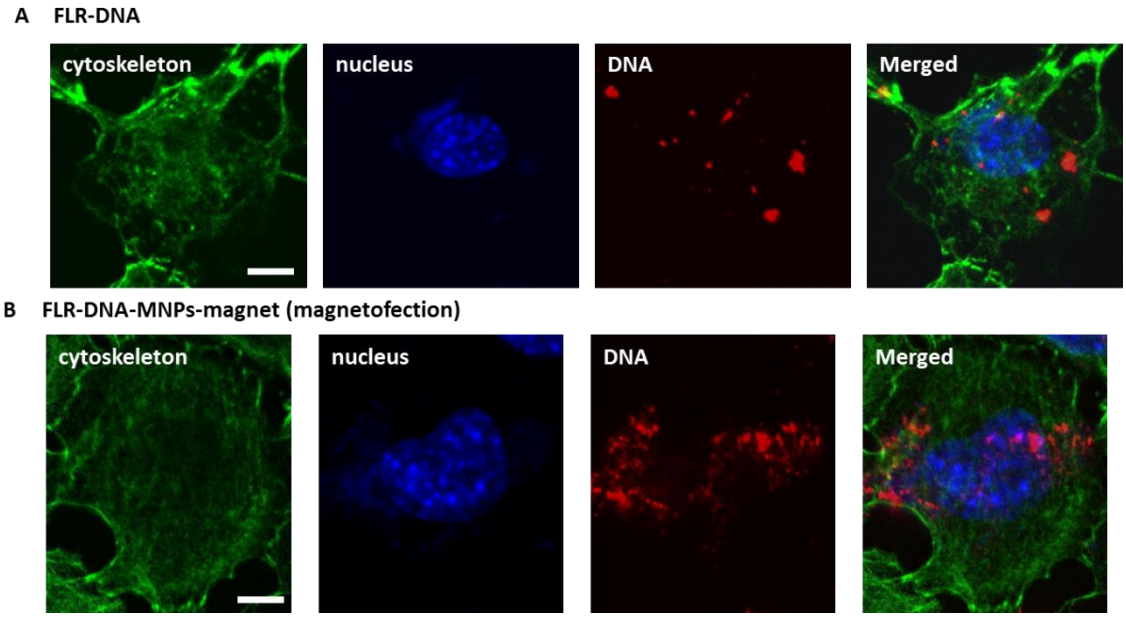

Figure 4.20 Representative Confocal Laser Scanning Microscopy (CLSM) images of Rho-labelled DNA in NIH3t3 cells after 24 hours delivery.

Cells were transfected with FLR-DNA (A) and FLR-DNA-MNPs in the presence of a magnetic field (B). Cells were treated with 1 µg of Rh-DNA at N/P ratio 6 and optimal MNPs mass ratio 5 µg MNPs/ 1 µg DNA for 24 hours. After incubation, unbound complex was removed with PBS and cells were fixed with 3.7% PFA. pCMV-GLuc 2 was stained with rhodamine (red), nucleus was stained with DAPI (blue) and actin cytoskeleton was stained with Alexa Fluor 488 Phalloidin (green). Scale bar 2 µm.

After 24 hours, most of the fluorescence in the cell is concentrated around the nucleus and confined to localized and discrete compartments/vesicles suggesting degradation and recycling by the endosomes. This observation is common for both treatment groups.[260]

Colocalisation analysis of DNA in intracellular vesicles (i.e. Lisotracker Blue for lysosomes) and the cell nucleus would provide further information on DNA trafficking.

Finally, implementation and optimization of dual labelling methods like the one described by Srinivasan et al.[262] could be useful to determine MNP-DNA and DNA-FLR interactions as well as DNA stability.

4.4 Conclusions

In this work, the use of GET peptide, FLR, to efficiently deliver DNA on a MNP based vector under the influence of a magnetic field has been optimised and characterised. FLR-DNA-MNPs were able to significantly improve reporter gene expression after 1 hour incubation in the presence of a magnetic field compared with no magnetic field or FLR-DNA alone. Effect of magnetofection on cellular entry mechanism, DNA stability inside the cell and cellular viability have also been assessed.

Importantly nearly all cells could be loaded with detectable amounts of DNA within 5 mins with FLR-MNPs in the presence of a magnetic field, however delivery of DNA with FLR or FLR-MNPs in the absence of a magnetic field required 15-30 mins of delivery.

When treated with endocytosis inhibitors DNA-FLR and DNA-FLR-MNPs showed significantly lower DNA uptake in hypertonic media compared to the other inhibitors,

suggesting a significant contribution of CME on DNA uptake. Interestingly, MBCD, which is involved in cholesterol depletion from the cell membrane, significantly affected DNA uptake during magnetofection in the presence of a magnetic field, more so than the other inhibitors, suggesting a more important role of caveolae mediated endocytosis.

The difference in uptake mechanism could be attributed on the one hand to a change in size due to the aggregation of the MNPs in the presence of a magnetic field. Bigger particles would require different uptake pathways. Future work should include physicochemical characterisation and TEM images of FLR-DNA-MNPs after exposure to a magnetic field in order to determine whether there are any significant changes in particle size and morphology.[195] Alternatively, quantification of DNA uptake at increasing transfection times, showed a very rapid increase in cell mean intensity (less than 5 mins), that did not significantly increase at longer transfection times, suggesting a saturation of the cells' ability to take any more pDNA. Based on the available experimental evidence it was hypothesized that the saturation of CME by the fast increase in DNA concentration in the cell membrane mediated by the magnetic field triggered alternative endocytosis mechanisms.

Finally a combination of particle aggregation in the presence of the magnetic field and CME saturation should also be considered.

Membrane rupturing activity in the endosomes is driven by FLR with minimal contribution from the MNPs.

Degradation of delivered DNA seems to be consistent across the different vectors over a 24 hour period suggesting that the delivery vector or uptake mechanism do not play

a significant role on DNA intracellular trafficking, more likely, DNA degradation rate is proportional to intracellular concentration.

Finally, confocal imaging confirmed the presence of DNA localized around the boundaries of the cell as well as some degree of internalisation at early time points (30 and 60 min) using magnetofection, but very little uptake for FLR-DNA. After 24 hours DNA could be seen internalised around the cell nucleus or confined to vesicles in the cytoplasm.

The principle behind magnetofection is the concentration of the DNA vector to the cell population either *in vitro* or *in vivo*. The findings here presented suggest, that, indeed, MNPs vectors under a magnetic field quickly concentrate the plasmid DNA onto the cell surface and by doing so, alter to a certain degree the uptake mechanism, however, there is no evidence that MNPs play any further role in gene transfer.

In summary, these results show that GET system can efficiently be used for magnetofection. Furthermore, an insight into mechanisms of uptake during magnetofection is provided. This information could help improve the design of future magnetic gene vectors.

5 Use of GET-MNPs and Magnefect-nano™ for enhanced gene delivery in dendritic cells.

5.1 Introduction

It has been previously demonstrated and greatly discussed in the literature that the application of a static magnetic field enhanced magnetic mediated transfection in short periods of time.[230], [231], [244], [263] Additionally, recent work has reported that the mechanic oscillation of the magnetic vectors mediated by the oscillation of the magnetic source or by application of an electric pulse improves transfection efficiency when compared with static magnetofection. [172], [187], [264], [265]

5.1.1 Magnefect-Nano™

In order to further exploit and characterise gene delivery mediated by oscillating magnetic field, in 2012 Prof. Jon Dobson and Dr Christopher D Batich patented a new device based on the oscillation of NdFeB permanent magnetic arrays.[184] The frequency and amplitude of the oscillation of the magnet array was controlled by a computerized motor system. The culture plate is fixed on top of the magnet array, which is developed in a way such that each well in the culture plate is subjected to identical magnetic fields with minimal interferences between them. Field strength was of 320 ± 25 mT on the magnet surface, field gradient ranges from 100-200 T/m on the cell surface (from the centre to the edge of the well).[185] They termed the device Magnefect-nano™ (Figure 5.1).

When a magnetic nanoparticle is exposed to an external magnetic field gradient, its magnetic moment orientates parallel to the applied magnetic field (spin rotation,

physical or mechanical). By oscillating the magnet arrays in the x plane, the source of the field is effectively being displaced, introducing a lateral component of motion superimposed to the z-axis motion of the particles imposed by the permanent magnetic field gradient. [9], [266] The hypothesis is that mechanical stimulation of the cell surface caused by oscillating motion of the magnetic nanoparticle's vectors stimulates endocytosis.[173], [185], [188], [267]–[270]

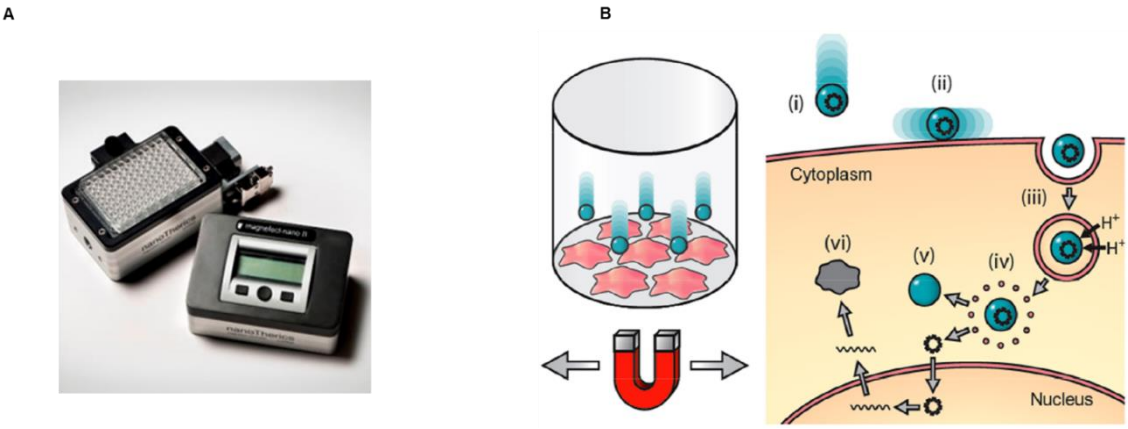

Figure 5.1 Magnefect-nano^{TM} design and proposed mechanism of action.
A) Magnefect-nano^{TM} (top) and controller unit (bottom) by nanoTherics Ltd. The device is pictured here with a 96-well magnetic array and culture plate. B) Proposed mechanism of oscillating nanomagnetic transfection by nanoTherics Ltd. Plasmid DNA encoding the protein of interest is attached to MNPs and concentrated on the cell surface by the application of a magnetic field (i), the oscillating magnetic field drags the particles on the horizontal lane on the cell membrane (ii), mechanical movement of the particles triggers endocytosis of the magnetic vector (iii), once inside the cell the vector escapes to the cytoplasm (iv) plasmid DNA is dissociated from the magnetic vector (v), in order to be able to be transcribed into the protein of interest the plasmid DNA must first enter the nucleus (vi).[267]

5.1.2 Dendritic cells in immunotherapy

Dendritic cells (DCs) are potent antigen presenting cells, both endogenous and exogenous. In their immature form DCs are found in non-lymphoid tissues and are very proficient in capturing antigens derived from infections or cancer. After antigen acquisition DCs start a maturation process through which they are able to migrate to

the draining lymph nodes and express the acquired antigens together with other cytokines that they present to T cells that become then activated.[271] This is one of the mechanisms of the immune system in response to foreign organisms in the body. The immune system, however, is not very efficient at eradicating tumours, due to the low tumour antigenicity, in other words, the immune system does not easily detect tumour cells and therefore, does not react against them. A way to improve the immune response against tumours is by inducing active antigen presenting cells such as DCs to present tumour associated antigens to induce a tumour specific response from the T lymphocytes. This particular treatment is known as “Dendritic cell vaccine”[186] A schematic of the process of cell extraction and manipulation involved in dendritic cell vaccines is presented in Figure 5.2.[272]

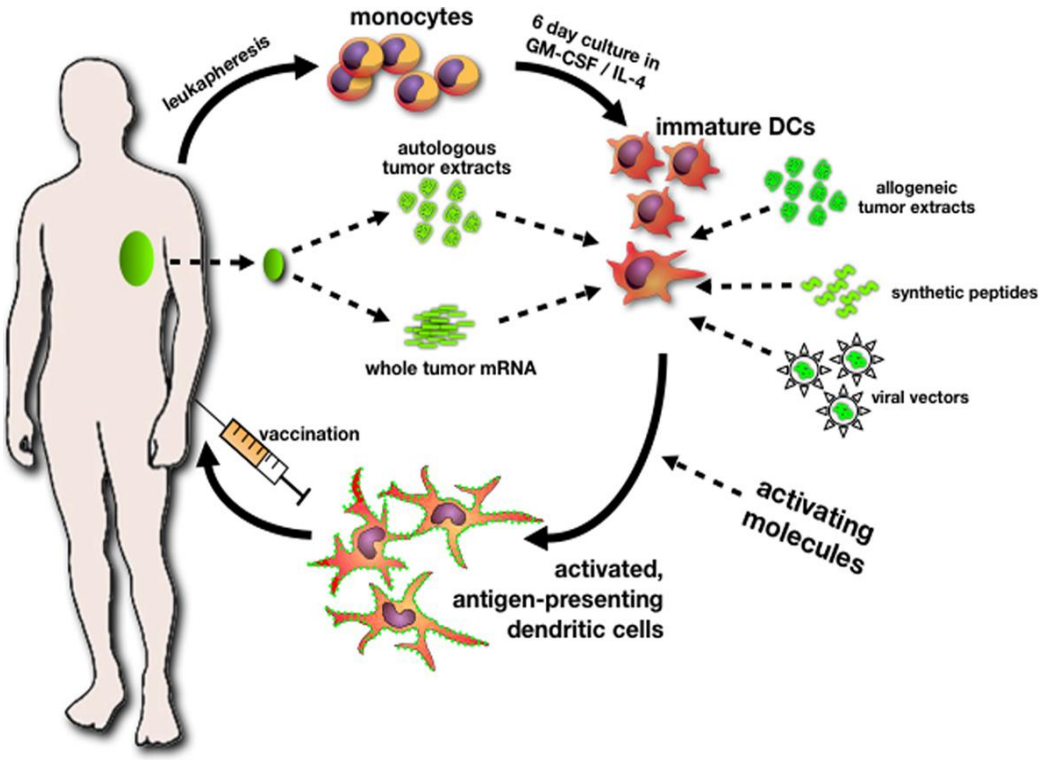

Figure 5.2 DC vaccine.
Schematic of dendritic cell vaccine for cancer treatment. Briefly, cells (monocytes or more recently isolated DCs) are extracted from the patient and get transduced with tumour extracts, mRNA, DNA encoding for tumour antigen production (human prostatic acid phosphatase, p53, MART-1[273]*). Activated DCs are injected back into the patient Schematic downloaded from open source superstarfloraluk.com/7623164-Immature-Dendritic-Cells.html*

Initially, DCs were differentiated from patient monocytes and induced with tumour peptides, however, these approaches were met with limitations such as short term expression of antigens and resistance to self-antigens.[274] Since then, transfection of DCs with transgenes encoding for tumour-associated antigens has proven to be a better alternative for antigen presentation in DCs, although gene transfer on DCs still remains a challenge due to significant barriers of phagosomal and endosomal degradation in antigen presenting cells.[183] Various vehicles have been tested and developed for gene transfer in DCs, including both viral and non-viral vectors. Viral vectors present higher transfection efficiencies, however, the incorporation of the

virus genome in the host cells inducing an immunologic response represents a major concern. On the other hand, safer non-viral methods are not able to achieve successful transfection efficiencies.

To date, there is only one FDA approved dendritic cell vaccine for metastatic prostate cancer.[275], [276] However, since its approval in 2011, no more DC based treatments have been approved. New generation DC immunotherapy approaches are attempting to overcome the limitation presented by the first generation of cell vaccines, by improving DC isolation and manipulation with minimal effect on its phenotype and also by improving antigen expression.[273]

Once the antigen is expressed, DCs start undergoing a maturation process and migrate to the T-cell zone of the lymphoid tissue, where they activate antigen specific T cells.[277] Ensuring migration of DCs to the lymph nodes is another hurdle to overcome in the development of DC vaccines.[278] The ability to non-invasively assess DC migration to the lymph nodes *in vivo* would facilitate the assessment of the efficacy of the therapy and allow to gain better understanding of the treatment. Magnetic resonance imaging (MRI) presents one of the highest spatial resolution with high anatomical contrast of the non-invasive imaging techniques for *in vivo* cell tracking. MRI tracking of cells requires previous labelling of the cells with a MR contrast agent such as biocompatible and biodegradable iron oxide MNPs.[43] SPIONs have been successfully used for tracking ex vivo labelled DCs *in vivo.*[44], [45], [53] They present an ideal platform to integrate a gene delivery system to achieve efficient gene expression and easy evaluation of therapeutic success. There has been some degree

of success in the past implementing this multimodal technology for dendritic vaccines, however, viral vectors still remain superior in transfection efficiency.[279], [280]

5.1.3 Aims

This results chapter is divided in three main objectives: to optimise FLR-DNA-MNPs formulation for gene delivery in DCs and compare with previously published PEI coated MNPs (PEI-MNPs)[182] developed in Prof Jon Dobson's group. To assess the effect of an oscillating magnetic field during delivery of FLR-DNA-MNPs on transfection efficiency on DCs compared with a static magnetic field ("magnetofection"). Finally, evaluate whether the application of an oscillating magnetic field after delivery of DNA could further enhance transfection efficiency in DCs.

5.2 Chapter experimental overview

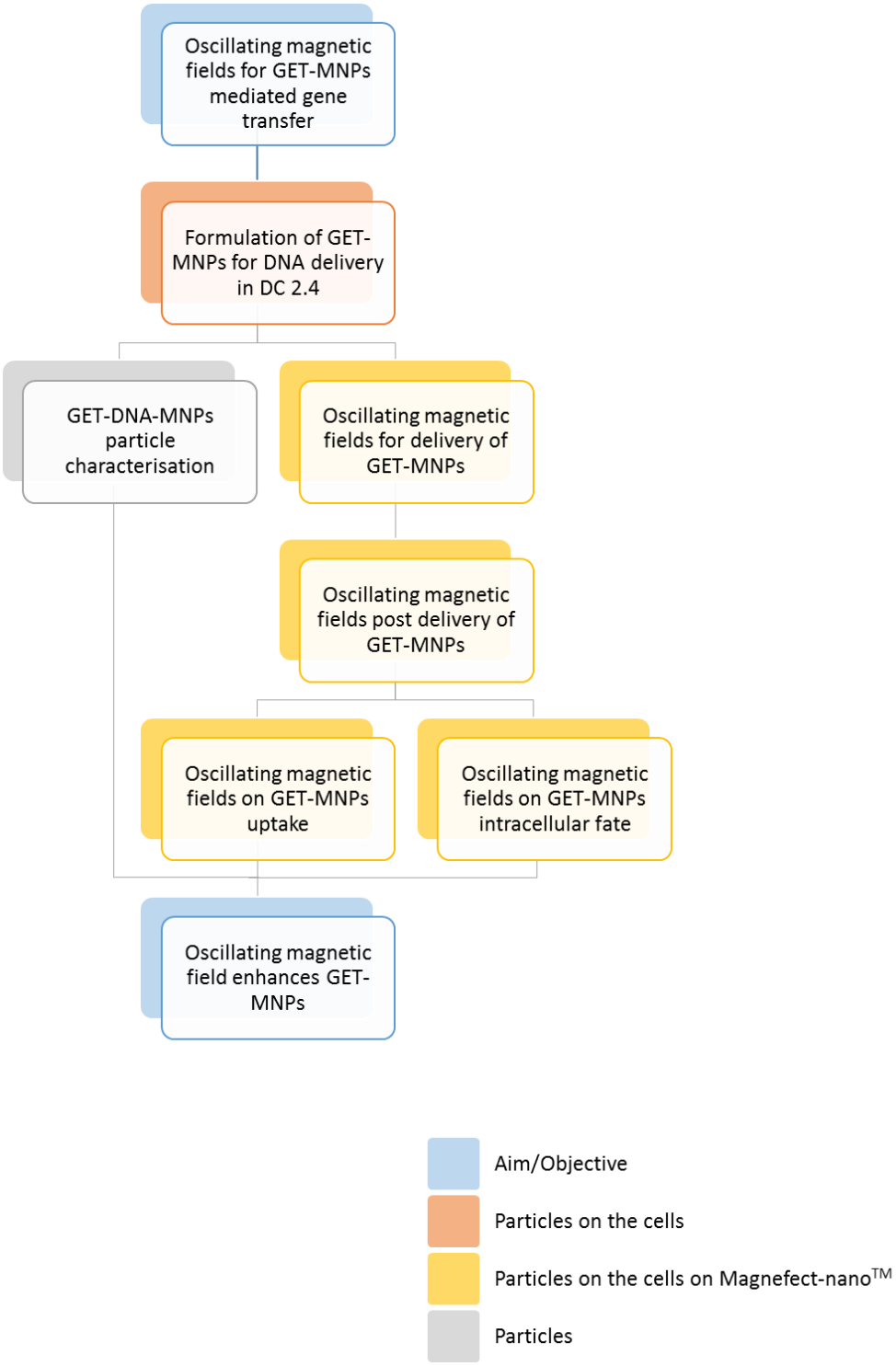

5.3 Results

5.3.1 Particle optimisation

The formulation of two different magnetic vectors (FLR-DNA-MNPs and PEI-MNPs) was optimised in order to find the most suitable candidate for magnetofection in DC 2.4.

Previous work had already determined full PEI-MNPs and DNA complexation at N/P ratio 3.[182] The same publication had reported that high N/P ratios were more efficient at gene transfer in HeLa. The authors attributed this to the increased positive charge of the vector. N/P ratios 2.5, 5 and 10 were tested.

FLR-DNA-MNPs are formed by the combination of three different components. FLR:DNA N/P ratio was set at 10 (comparable to the highest N/P ratio selected for PEI-MNPs). DNA:MNPs mass ratios were optimised (10, 20 and 40 μg MNPs per 1 μg of DNA). FLR-DNA was used as control for transfection (0 μg MNPs per 1 μg of DNA)

DNA concentration was also optimised for both vectors: 0.06, 0.125, 0.25, 0.5, 1 and 2 μg of Firefly Luciferase plasmid pGL4.51 per transfection.

Gene transfer efficiency was measured by Firefly luciferase expression in the cells after 24 hours and normalised to protein content in the sample measured by BCA assay (Figure 5.3).

PEI-MNPs mediated protein expression was higher at the higher DNA concentrations 1μg and 2 μg per transfection. N/P ratios 5 and 10 were mostly comparable to each other.

For FLR-DNA-MNPs, maximal reporter gene expression was achieved from 0.25 to 1 μg of DNA/transfection. Unfortunately the wide variability of the results did not allow for significant differences between the different DNA:MNPs on each group, however 20 μg MNPs/ 1 μg of DNA seemed to be consistently efficient across the groups.

FLR-DNA-MNPs were overall significantly better at gene transfer in DC 2.4 compared with PEI-MNPs (Figure 5.3).

In order to move forward with the characterisation of the magnetic vectors, the formulation of 20 μg MNPs/1 μg of DNA was chosen.

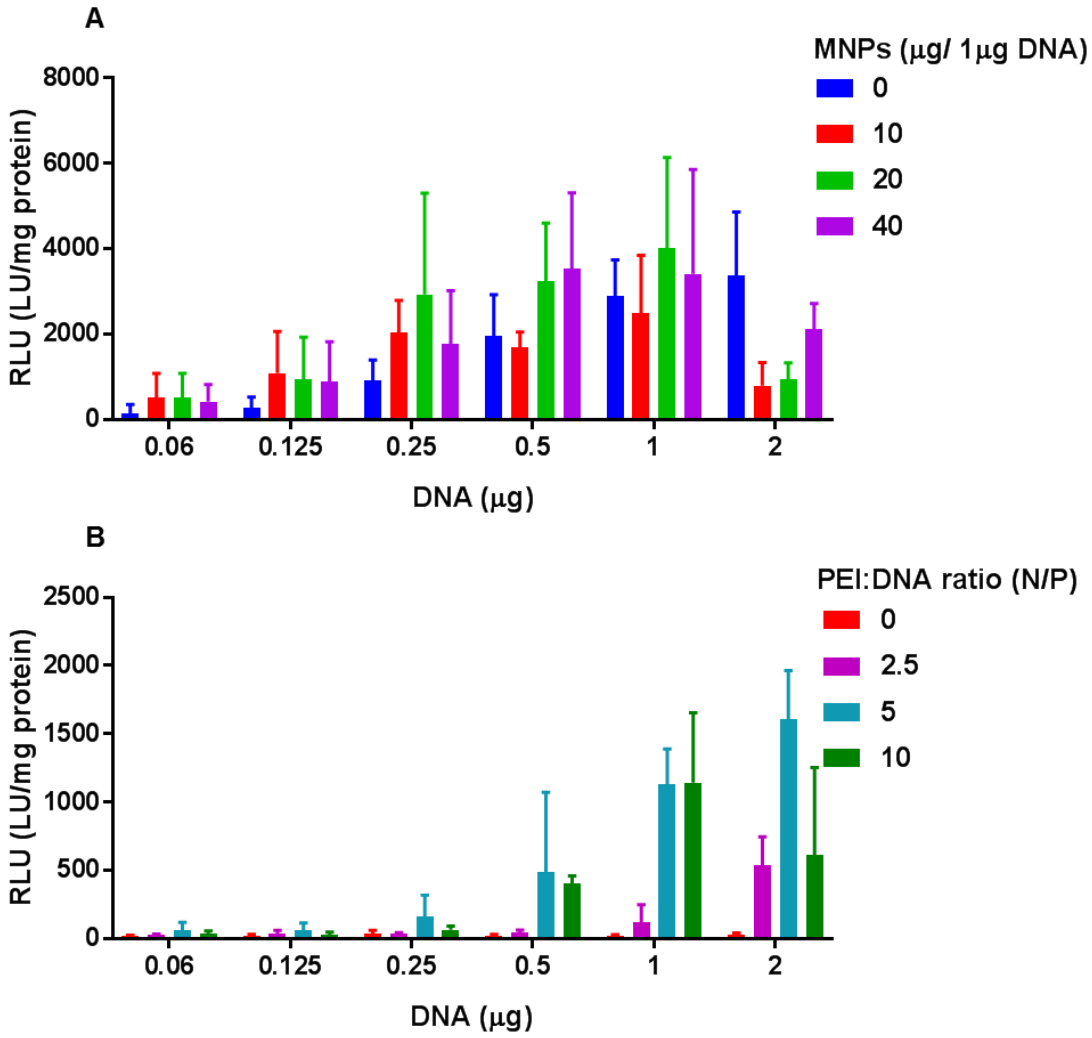

Figure 5.3 Optimisation of magnetic vector formulation with FLR-MNPs and PEI-MNPs.

Cells were treated with FLR-DNA-MNPs and PEI -MNPs at increasing concentrations of DNA (0.06, 0.125, 0.25, 0.5, 1 and 2 µg of DNA/well). A) FLR-DNA N/P ratio was kept constant at 10. MNPs concentrations were calculated as a mass ratio to DNA (10, 20 and 40 µg/ 1 µg of DNA). Cells were treated with FLR-DNA without MNPs as a control. B) DNA particle ratio was calculated based on estimated PEI functional groups on the particle surface (N/P). Cells were treated with DNA alone as a control. All treatment groups were transfected for 1 hour in the presence of a magnetic field. Unbound transfection complexes were washed. Cells were harvested for luciferase analysis 24 hours post transfection. Relative Luminescence Units (RLU) were calculated as a ratio between luminescence units and mg of protein per sample. Bars represent mean ± s.d. n=4 biological repeats, 2 technical replicates.

5.3.1.1 Optimal DNA concentration for FLR-DNA-MNPs gene transfer on DC 2.4

Cell metabolic activity was assessed on DC 2.4 in order to determine optimal DNA concentration for FLR-DNA-MNPs mediated delivery. FLR-DNA-MNPs were formed at a N/P ratio of 10 and MNPs to DNA ratio of 20 µg of MNPs per 1 µg of DNA. Cells were transfected for 24 hours with 0.5 µg or 1 µg of DNA. Cell metabolic activity was assessed by resazurin (Figure 5.4 DC 2.4 metabolic activity after transfection with FLR-DNA-MNPs

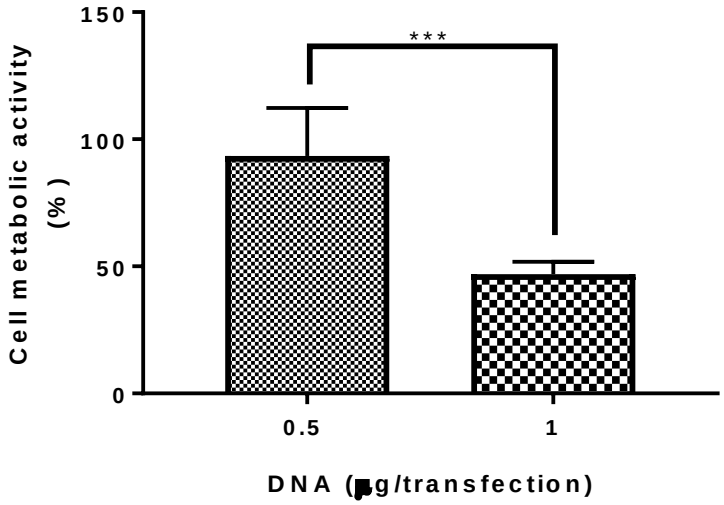

Figure 5.4 DC 2.4 metabolic activity after transfection with FLR-DNA-MNPs

*Cells were transfected with 0.5 µg or 1 µg of pGL4.51 plasmid with FLR-MNPs for 24 hours. Cell metabolic activity was measured with resazurin. Percentage metabolic activity was calculated with metabolic activity of untreated cells. n=6 biological repeats, from at least 2 technical replicates (***p<0.001, Sidak's multiple comparisons test).*

DC 2.4 were significantly affected by the delivery of 1 µg of pGL4.51 plasmid but remained unaltered when transfected with 0.5 µg of plasmid. The DNA concentration for FLR-DNA-MNPs mediated transfection was stabilised as 0.5 µg per transfection.

5.3.2 Particle characterisation

Table 12 summarises the physical characteristics, dynamic light scattering (DLS) and zeta potential of FLR-MNPs based vectors. Dextran coated MNPs are negatively charged in water (-7.6 ± 3.7 mV). In the presence of FLR all MNP vectors become positively charged (25.5 ± 6.6 mV FLR-MNPs and 21.4 ± 5.1 mV FLR-DNA-MNPs).

Table 12 Physical characterisation of GET-MNPs vectors for DNA delivery

	DH (nm)*	**PDI¥**	**Zeta potential (mV)**
MNPs	274.7 ± 3.8	0.12 ± 0.02	-7.6 ± 3.7
FLR-DNA	84.15 ± 0.4	0.24 ± 0.01	56 ± 2.2
FLR-MNPs	308.4 ± 28.2	0.13± 0.03	25.5 ± 6.6
FLR-DNA-MNPs	287.9 ± 6.5	0.14 ± 0.02	21.4 ± 5.1

Apparent diameter of the particles obtained by DLS for 80 µg/ml of MNPs incubated with DNA (4 µg/ml), FLR at N/P ratio 10 in a total volume of 1 ml of dH_2O. Z-average hydrodynamic diameter extracted by cumulant analysis of the data. Polydispersity index (PDI) from cumulant analysis. Values represent mean ± s.d. (technical repeats n=1-3 independent repeats, 3 runs per repeat, 15 subruns per run).
Zeta potential, measurements consisted of 3 repeats (12 subruns per repeat). Smoluchowski approximation was used to calculate the zeta potentials from the measured electrophoretic motilities. Values represent mean ± s.d. (Technical repeats n=1-3).
All measurements were done with Malvern Nanosizer Nano ZS.

Particle size measurement by DLS suggested particles mostly in the monodisperse range after functionalisation with FLR and FLR-DNA, (PDI<0.2), except for FLR-DNA nanoparticles that were significantly more polydisperse (0.24 ± 0.01).[204] FLR-DNA-MNPs (277.6 ± 0.99 nm) and FLR-MNPs (308.4 ± 28.2 nm) were significantly bigger than naked MNPs (274.7 ± 3.8 nm).

As in the previous chapter, based on the particle's zeta potential and size it was hypothesized that upon encounter with the MNPs, FLR-DNA nanoparticles interact with the functional groups on the dextran surface of the magnetic particle seeking to

find the most stable conformation, with the FLR on the outer surface of the particle providing it with the positive charge.

5.3.3 Magnetically mediated gene delivery in DC 2.4 with FLR-DNA-MNPs was efficient and faster than commercial standard FuGENE.

Cells were treated with 0.5 μg of pCMV-eGFP-SV40-noDTS plasmid with FLR-DNA, FLR-DNA-MNPs without a magnetic field (FLR-DNA-MNPs). FLR-DNA-MNPs were formed at a N/P ratio of 10 and MNPs to DNA ratio of 20 μg of MNPs per 1 μg of DNA. FLR-DNA-MNPs delivery was carried out on a static magnet array (static) and on an oscillating magnet array with an amplitude of 0.2 mm and frequency of 2 Hz (oscillating) for 1 hour.[182], [187], [188] Cells were also transfected with FuGENE 6 in order compare to commercially available transfection reagent.[281] FLR-DNA, FLR-DNA-MNPs and FuGENE were delivered for 1 hour and 24 hours. Transfection efficiency was measured by flow cytometry 24 hours post transfection (Figure 5.5).

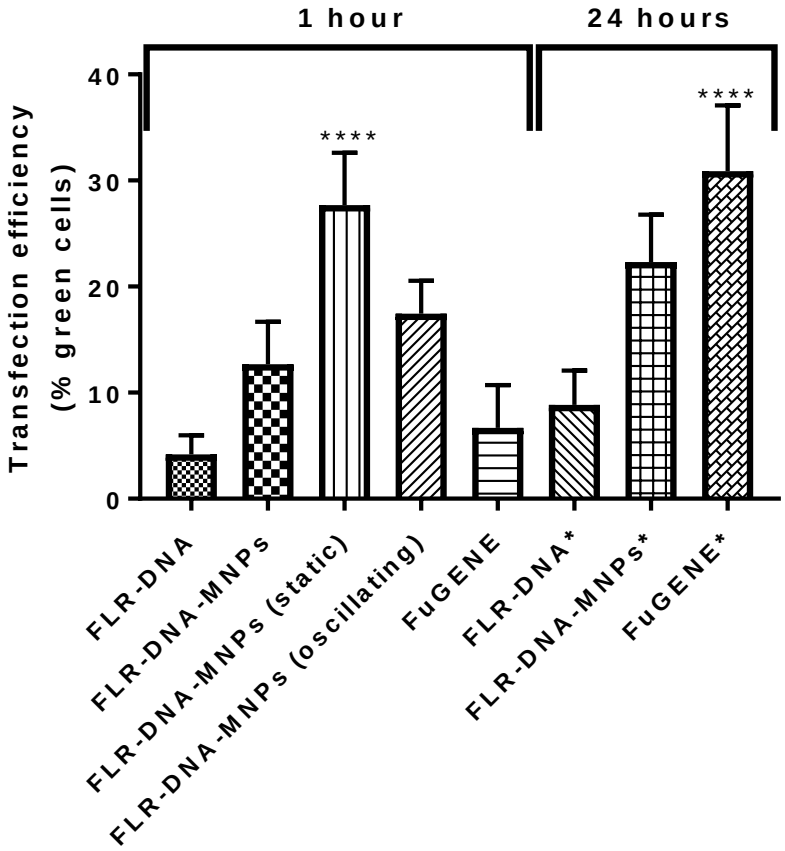

Figure 5.5 Transfection efficiency with FLR-DNA-MNPs on a static magnetic field is comparable to FuGENE's transfection efficiency after 24 hours in DC 2.4.

*Cells were transfected with 0.5 µg of pCMV-eGFP-SV40-noDTS plasmid with FLR (FLR-DNA) or FLR-MNPs (FLR-DNA-MNPs) for 1 hour and 24 hours. Treatment groups that were transfected for 24 hours are marked with * on the graph. FLR:DNA N/P 10, MNPs:DNA mass ratio 20 µg MNPs/ 1 µg of DNA. Cells treated with FLR-DNA-MNPs were separated in three groups, no magnet (control), placed on a static magnetic array (static) or an oscillating magnet array (200 µm displacement, 2.0 Hz, Magnefect-nano™) for 1 hour, excess transfection reagent was washed with PBS. GFP transfection efficiency was measured by flow cytometry 24 hours post-transfection and reported as percentage of GFP positive cells. FuGENE was used as a transfection standard according to manufacturer's instructions: 3:1 ratio FuGENE: DNA Bar charts represent mean ± s.d. n=9 biological repeats, 3 technical replicates (****p<0.0001, Tukey's multiple comparisons test).*

Transfection efficiency was reported as percentage of GFP positive cells. Best transfection efficiencies were achieved with FLR-DNA-MNPs under a static magnetic field for 1 hour (27.7 ± 4.9% of GFP positive cells) and FuGENE after 24 hours (30.9 ±

6.2% of GFP positive cells). Transfection efficiency obtained in 1 hour with FLR-DNA-MNPs was significantly better than that previously reported for DC 2.4 using non-viral vectors. Yuba et al. reported 25% of GFP expressing cells after a 4 hour delivery period with a novel formulation combining liposomes and lipoplexes with pH-sensitive fusogenic polymers.[282]

Interestingly, after 24 hours transfection efficiency with FLR-DNA-MNPs in the absence of a magnetic field is comparable to that of FLR-DNA-MNPs under a static field for 1 hour (22.3 ± 4.4% of GFP positive cells). This finding reinforces the previously reported hypothesis (*Results II*) that magnetofection does not improve overall transfection efficiency, rather it enhances gene delivery speed by quickly concentrating the nucleic acid cargo on the cell membrane.

Surprisingly, when FLR-DNA-MNPs were delivered on an oscillating magnetic field transfection efficiency was significantly worse than that on a static magnetic field (17.4 ± 3.1% of GFP positive cells) which is contrary to previous published work, that reported that the application of an oscillating field enhanced gene transfer on different cell lines significantly better than a static magnetic field or the absence of it. [173], [182], [187], [188], [268], [269]

The exact mechanism through which oscillation of the external magnetic field during particle delivery promotes gene transfer still remains unknown. As previously mentioned in the introduction of this chapter, the main hypothesis is that the oscillation of the MNPs on the cell membrane, triggers or enhances particle endocytosis. With this in mind two possible explanations were proposed to explain the lack on enhanced gene transfer with FLR-DNA-MNPs. On the one hand, it is

important to note that the particles used in these publications were in general smaller (~ 100 nm diameter), than the ones used on the current study (~250 nm). It is possible that different mechanisms are involved in the uptake of smaller particles. These uptake pathways could be more susceptible to mechanical activation generated by the oscillation of the MNPs.[195]

Additionally, as it has been previously discussed (*Results I*) and reported by Dixon et al.[163] the interaction of the GET with heparan sulphate glycosaminoglycans on the cell membrane plays a key role on the uptake of the therapeutic cargo. It was hypothesized that mechanical oscillation of the particles on the cell membrane could potentially disrupt GET-GAG interaction hampering particle transduction.

5.3.4 Magnefect-nano™ enhances transfection efficiency post-delivery

5.3.4.1 Application of a magnetic field after delivery further enhances gene transfer

There are several steps involved in protein expression mediated by an exogenous gene. More specifically, efficient plasmid DNA expression requires for: plasmid DNA accumulation on the cell membrane, uptake, intracellular trafficking, access to the cell nucleus, gene transcription and protein production and finally gene expression. Vector accumulation on the cell membrane is defined by the delivery system. The main mechanisms through which magnetofection has been reported to enhance gene transfer are so far either through increased accumulation of the magnetic vector on the cell membrane, enhanced endocytosis or facilitating intracellular trafficking of the DNA.[126], [238], [283], [284]

Magnefect-nano™ was used to assess whether application of additional magnetic forces on the MNPs could further enhance FLR-DNA-MNPs mediated gene transfer by either inducing additional stress on the cell membrane and mediate endocytosis or by altering intracellular structures (i.e. vesicles).

The timing of the application of the oscillating magnetic field was established aiming to differentiate between endocytosis (immediately post-delivery) and intracellular trafficking (6 hours post-delivery).[223], [285], [286] It was suggested that the nature and the timing of the applied magnetic field would play an important role in gene transfer.

pCMV-eGFP-SV40-noDTS plasmid was delivered to DC 2.4 using FLR-MNPs. FLR-DNA-MNPs were formed at a N/P ratio of 10 and MNPs to DNA ratio of 20 μg of MNPs per 1 μg of DNA. FLR-DNA-MNPs delivery was carried out on a static magnetic array for 1 hour, excess transfection reagent was washed and cells were placed on an oscillating magnet array (STATIC-OSCILLATING, 200 μm displacement, 2.0 Hz, Magnefect-nano™) immediately after (0 hours) and 6 hours post-delivery (6 hours) for 1 hour. To control for the magnetic forces induced by the magnetic field alone (without oscillation) the cells were also placed on a static magnet array (STATIC-STATIC) for the same amount of time at the same time points. After exposure to the magnetic field cells were incubated at 37°C and 5% CO_2 for 24 hours. Transfection efficiency was measured using flow cytometry (Figure 5.6).

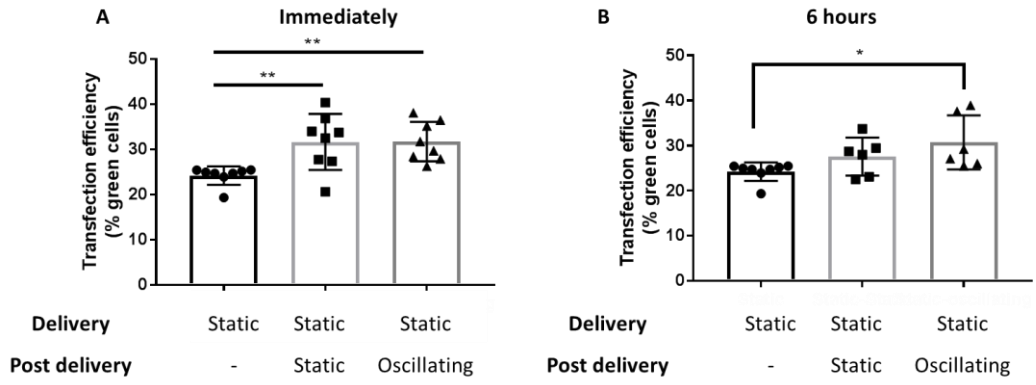

Figure 5.6 Transfection efficiency with FLR-DNA-MNPs is enhanced by further exposure to a static or oscillating magnetic field in DC 2.4.

*Cells were transfected with 0.5 µg of pCMV-eGFP-SV40-noDTS plasmid with FLR-MNPs on a static magnetic array for 1 hour, excess transfection reagent was washed and cells were placed back on the incubator (**circle**) on a static magnet array (**square**) or on an oscillating magnet array (200 µm displacement, 2.0 Hz, Magnefect-nano™, **triangle**) for another hour either immediately post-delivery (A) or 6 hours post-delivery (B). Transfection efficiency was measured by flow cytometry and reported as percentage of GFP positive cells. At least n= 6 biological repeats, minimum of 2 technical replicates. ** p<0.01, Tukey's multiple comparison's test)*

The application of a magnetic field immediately post-delivery significantly enhanced transfection efficiency compared to control (no magnetic field after delivery). Interestingly, there were no significant differences between the groups exposed to an oscillating or a static field with 31.8 ± 4.4 and 31.7 ± 6.2 % of GFP positive cell respectively compared with 24.2 ± 2.0 for control. Interestingly, when the magnetic field was applied 6 hours post transfection only the cells on an oscillating field showed significantly enhanced transfection efficiency compared to the absence of the field.

5.3.4.1.1 Cell metabolic activity

Cell metabolic activity was assessed 24 hours and 48 hours after gene transfer mediated by FLR-DNA-MNPs (Figure 5.7). pCMV-eGFP-SV40-noDTS plasmid was delivered to DC 2.4 using FLR-MNPs (formulated as previously described in section 5.3.3) on a static magnetic array for 1 hour, excess transfection reagent was washed

and cells were placed on an oscillating magnet array (200 μm displacement, 2.0 Hz, Magnefect-nano^{TM}) immediately after (0 H) and 6 hours post-delivery (6 H) for 1 hour. Cell metabolic activity was significantly affected in all treatment groups compared to control (untreated cells). Interestingly, in all groups, metabolic activity increased on day 2 post transfection (72.3 ± 3.7% for static transfection alone, 79.8 ± 16.5% and 76.1 ± 8.7% for cells exposed to a static magnetic field or oscillating magnetic field immediately post transfection respectively and 64.8 ± 10.4% and 77.9 ± 7.9% for cells exposed to a static magnetic field or oscillating magnetic field 6 hours post transfection). It was hypothesized that the main cause in metabolic activity decrease in magnetofection is induced by the rapid concentration of positively charged FLR-DNA-MNPs clusters on the cell membrane mediated by the static field. [282], [287], [288]

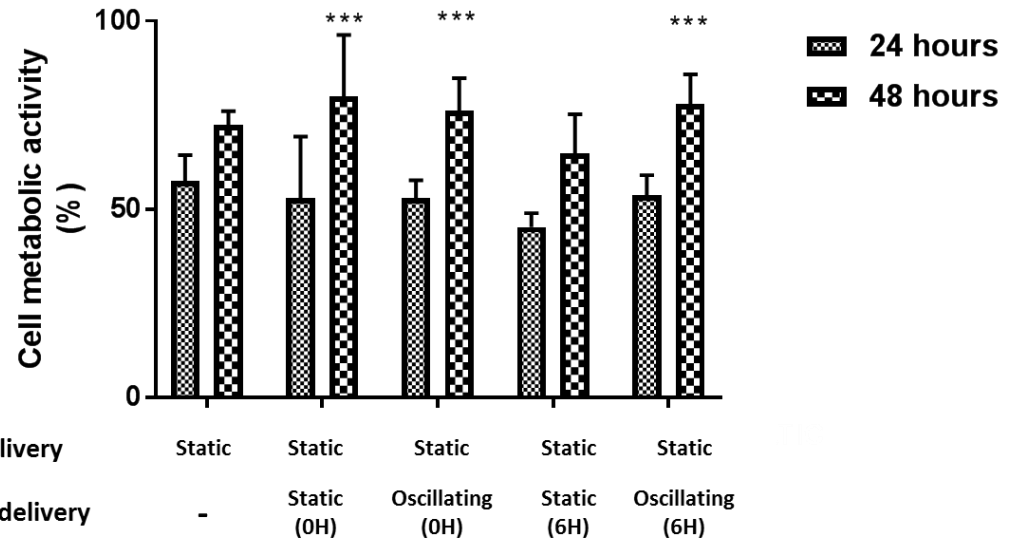

Figure 5.7 DC 2.4 metabolic activity is not affected by exposure to external magnetic fields post magnetofection.

*Cells were transfected with 0.5 µg of pCMV-eGFP-SV40-noDTS plasmid with FLR-MNPs on a static magnetic array for 1 hour, excess transfection reagent was washed and cells were placed back on the incubator on a static magnet array or on an oscillating magnet array (200 µm displacement, 2.0 Hz, Magnefect-nano^{TM}) for another hour immediately post-delivery and 6 hours post transfection. Cell metabolic activity was measured with resazurin 24 and 48 hours post transfection. Percentage metabolic activity was calculated with metabolic activity of untreated cells. n at least 6 biological repeats, from at least 2 technical replicates (***p<0.001, Sidak's multiple comparisons test)*

Further analysis on the effect of cell viability after magnetofection should include cell cycle analysis with propidium iodide (PI) stain and cell proliferation assays (trypan blue). These assays would allow to determine whether magnetofection is inducing an acute toxic effect causing cell death or alternatively, affecting cell metabolism that then recovers over time. However, current data indicates that the differences in GFP expression between groups could not be attributed to the difference in cell viability between the groups.

5.3.4.2 Transfection efficiency and reporter gene expression over time

To gain further understanding into the nature of magnetically mediated transfection, GFP expression in DC 2.4 was measured over time. Cells were transfected with pCMV-eGFP-SV40-noDTS plasmid using FLR-MNPs on a static magnetic array for 1 hour, excess transfection reagent was washed and cells were placed on a static magnet array (STATIC-STATIC as control for magnetic force) or on an oscillating magnet array (STATIC-OSCILLATING, 200 µm displacement, 2.0 Hz, Magnefect-nano^{TM}) for 1 hour immediately post-delivery and 6 hours post-transfection. Transfection efficiency was assessed both as percentage of GFP positive cells and also at mean fluorescent intensity on day 1, 2 and 3 post transfection (Figure 5.8 and Figure 5.9).

On day 1, percentage of GFP positive cells was comparable across all the treatment groups (Figure 5.8 A). When looking at fluorescent intensity, however, cells exposed to a static magnetic field 6 hours post transfection showed significantly lower fluorescent intensity compared to the other treatment groups (Figure 5.9 A).

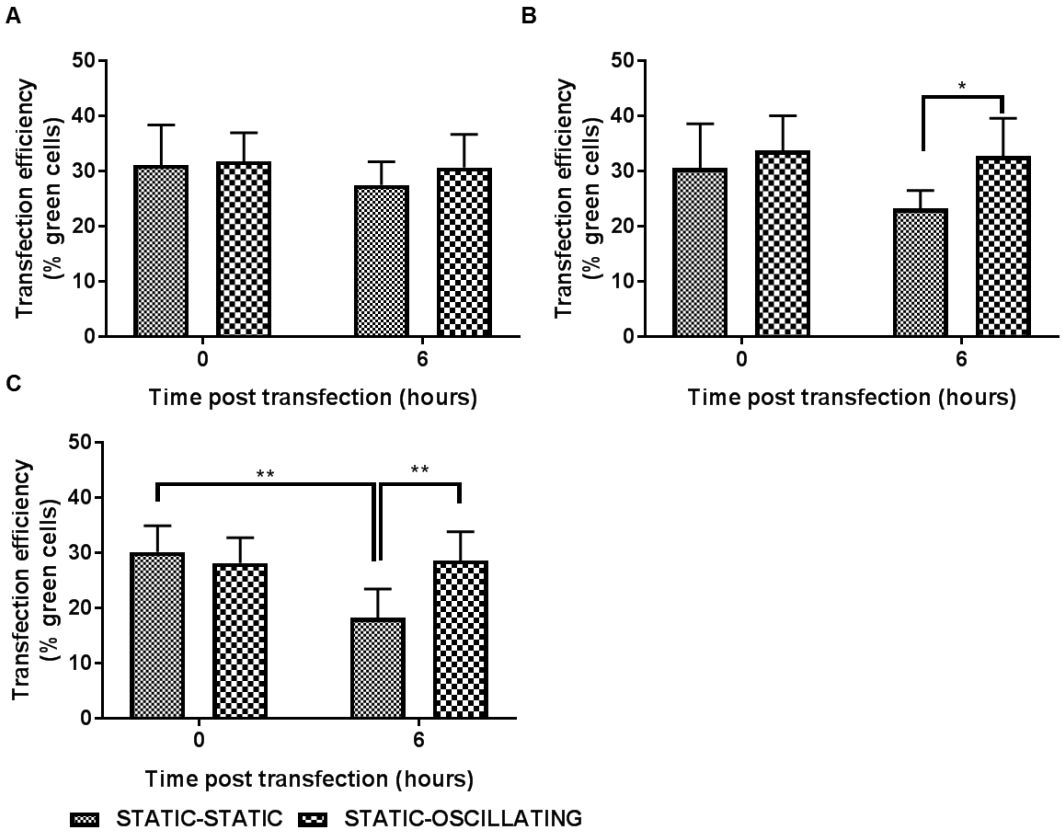

Figure 5.8 Over time transfection efficiency in DC 2.4 expressed as percentage of GFP positive cells.

DC 2.4 cells were transfected with pCMV-eGFP-SV40-noDTS plasmid using FLR-MNPs on a static magnetic array for 1 hour, excess transfection reagent was washed and cells were placed on a static magnet array (STATIC-STATIC as control) or on an oscillating magnet array (STATIC-OSCILLATING, 200 µm displacement, 2.0 Hz, Magnefect-nano™) for 1 hour. The cells were exposed to the oscillating field immediately (0 hours) or 6 hours post-delivery. GFP transfection efficiency was measured by flow cytometry 24 (A), 48 hours (B) and 72 hours (C) post-transfection. Bar charts represent mean percentage of GFP positive cells ± s.d. n=6 biological repeats, 2 technical replicates. (p<0.05, ** p<0.01, Tukey's multiple comparisons test).*

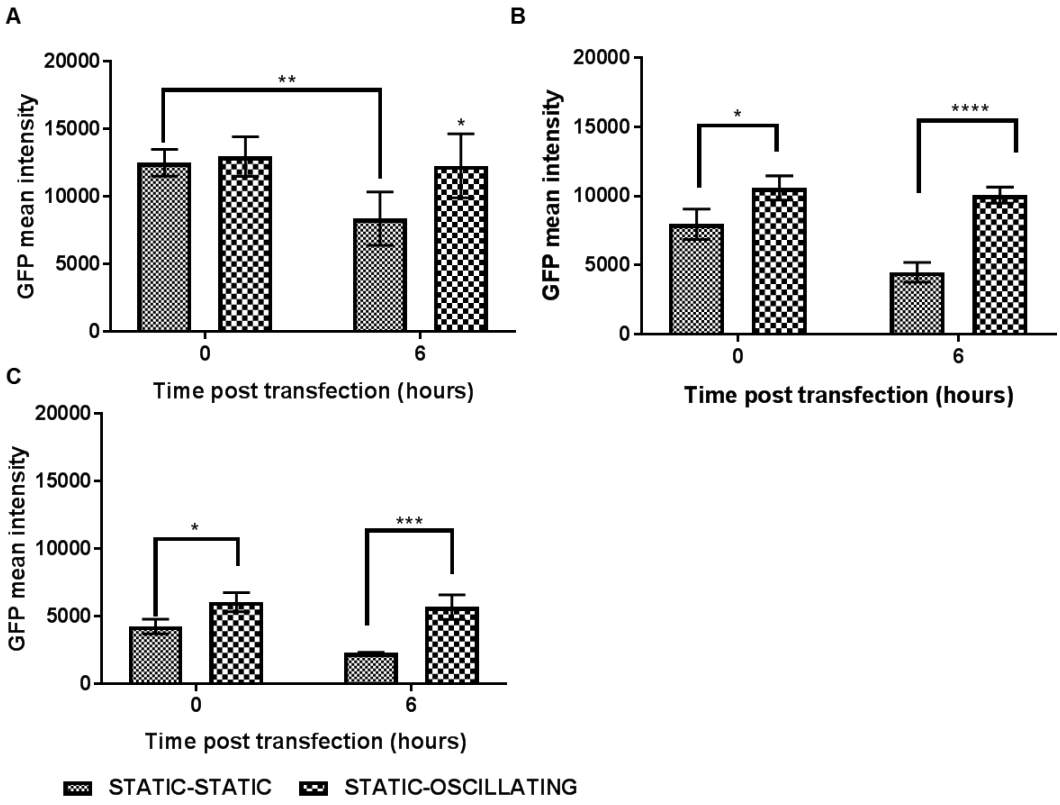

Figure 5.9 Overtime transfection efficiency in DC 2.4 expressed as GFP mean intensity.

*DC 2.4 cells were transfected with pCMV-eGFP-SV40-noDTS plasmid using FLR-MNPs on a static magnetic array for 1 hour, excess transfection reagent was washed and cells were placed on a static magnet array (STATIC-STATIC as control) or on an oscillating magnet array (STATIC-OSCILLATING, 200 µm displacement, 2.0 Hz, Magnefect-nanoTM) for 1 hour. The cells were exposed to the oscillating field immediately (0 hours) or 6 hours post-delivery. GFP transfection efficiency was measured by flow cytometry 24 (A), 48 hours (B) and 72 hours (C) post-transfection. Bar charts represent mean GFP mean intensity ± s.d. n=3, 1 technical replicate. * p<0.05, ** p<0.01, **** p<0.0001, Sidak's multiple comparisons test.*

Transfection efficiency, expressed as percentage of GFP positive cells, on days 2 and 3 is comparable to day 1 for cells that had been exposed to an oscillating magnetic field post transfection. However, cells that had been exposed to a static magnetic field 6 hours post transfection showed lower transfection efficiency compared to their oscillating counterparts on day 3 (18.2 ± 5.2% GFP positive cells on a static field and

28.6 ± 5.2% GFP positive cells on an oscillating at 6 hours post-transfection) (Figure 5.8 B and C).

GFP mean intensity on days 2 and 3 is consistently and significantly lower in cells exposed to a static magnetic field compared to an oscillating field, independent of the treatment time (Figure 5.9 B and C).

GFP half-life is estimated to be around 26 hours and its expression has been reported to be maximal between 24 and 48 hours, depending on the cell line.[289] In this particular case, GFP expression in DC 2.4 peaks at some point between 24 and 36 hours (Figure 5.9). Posterior decrease in fluorescence intensity has been previously attributed to a combination of factor including: partitioning of protein and plasmid at cell division and protein degradation in the cytoplasm.[290] Additionally, other factor affecting transient gene expression are the plasmid vector, cell type, delivery vector used for gene delivery, all those variables are the same for all the treatment groups here presented. A possible explanation to the differences observed on GFP expression on days 2 and 3 between the different treatment groups (STATIC-STATIC and STATIC-OSCILLATING) could be attributed to a more efficient delivery of GFP plasmid to the cell nucleus induced by the mechanical oscillation of the magnetic nanoparticles in an oscillating magnetic field, reducing the loss on plasmid copies in the nucleus with each cell division and allowing a more sustained GFP expression over time.

5.3.4.3 The distribution of plasmid DNA after magnetofection on DC 2.4

In order to confirm DNA delivery to DC 2.4, cells were transfected with Rh-DNA using FLR-MNPs on a static magnetic array for 1 hour. Cells were washed with PBS and

imaged using bright field and fluorescent microscope immediately after transfection (Figure 5.10).

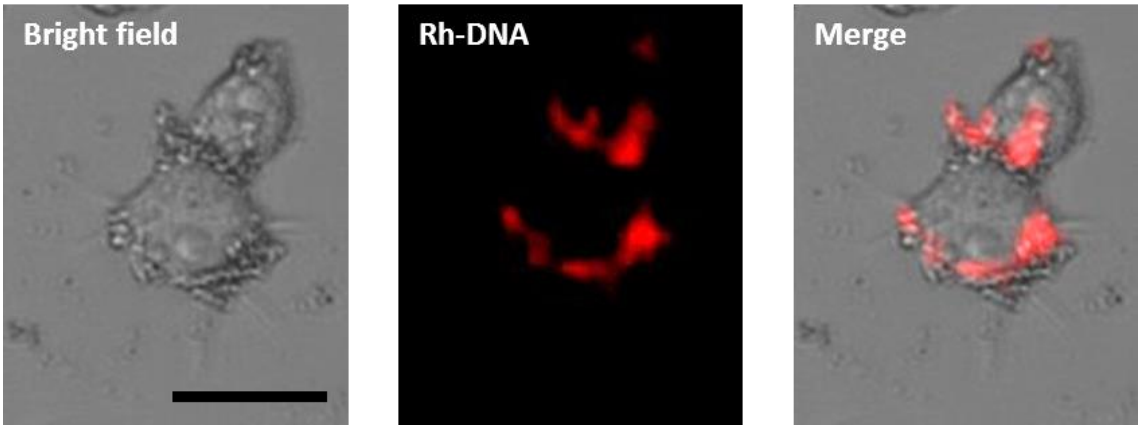

Figure 5.10 Representative bright field and fluorescent image of DC 2.4.
Cells were treated with 0.5 µg of DNA at N/P ratio 10 and 20 µg MNPs/ 1 µg DNA. Magnetofection was performed for 1 hour. After transfection, unbound complex was removed with PBS. pCMV-GLuc 2 was stained with rhodamine (Rh-DNA). Cells were imaged immediately post transfection using EVOS®FL Digital Fluorescent microscope (Transfection toolbar function: RFP light cube excitation source). Images were overlaid using ImageJ version 4.0J. Scale bar 10 µm.

Bright field images showed large clusters of MNPs around the cell or on the cell membrane. These clusters colocalised with the signal generated by Rh-DNA (Merge). These images suggest that FLR-DNA-MNPs form clusters on the cell membrane that were not removed after washing with PBS. A similar observation has been previously reported by Safi et al.[189] who showed that upon delivery, MNPs can either adsorb onto the cell membrane forming a stable layer of deposited particles of up to 500 nm.

To further assess DNA localization after FLR-DNA-MNPs delivery to DC 2.4, cells were transfected with Rh-DNA using FLR-MNPs on a static magnetic array for 1 hour, excess transfection reagent was washed and cells were placed on a static magnet array (Static as control for the magnetic field) or on an oscillating magnet array (Oscillating, 200 µm displacement, 2.0 Hz, Magnefect-nano^{TM}) for 1 hour, post-transfection (Figure 5.11).

Cells were imaged using a Leica TCS SP8 confocal laser microscope. In both magnetic field regimes discrete individual dots localized in the peripheral cytoplasmic compartment (white circles) can be observed as well as large formations of aggregated dots on the outer side of the cell (white arrows), corresponding to the previously mentioned MNPs clusters adsorbed onto the cell membrane.

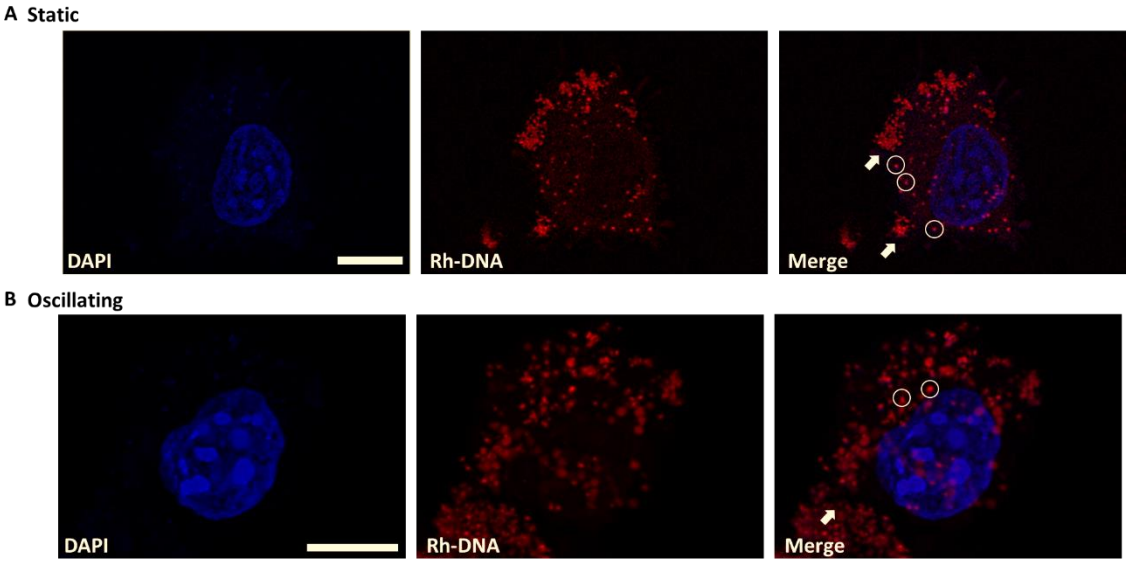

Figure 5.11 Visualisation of Rh-DNA in DC 2.4 transfected with FLR-DNA-MNPs on a static field and further exposed to Magnefect-nano^{TM}.
Cells were seeded onto tissue culture treated glass coverslips, then treated with 0.5 µg of DNA at N/P ratio 10 and 20 µg MNPs/ 1 µg DNA. Magnetofection was performed for 1 hour. After transfection, unbound complex was removed with PBS and then placed over a static magnet array (Static) or an oscillating magnet array (Oscillating, 200 µm displacement, 2.0 Hz, Magnefect-nano^{TM}) for 1 hour. Cells were fixed with 3.7% PFA. Images were acquired with Leica TCS SP8. pCMV-GLuc 2 was stained with rhodamine (Rh-DNA) and nucleus was stained with DAPI (DAPI) Scale bar 2 µm. Small arrows on "Merge" images indicate FLR-DNA-MNPs aggregation. White circles represent single individual vesicles loaded with Rho labelled DNA.

5.3.4.4 MNP uptake does not necessarily correlate with gene transfer efficiency

The amount of iron uptaken by the cells was measured by ICP-MS as an indicator of MNP uptake (Figure 5.12). DCs 2.4 were transfected with FLR-DNA-MNPs on a static magnetic field for 1 hour as previously described (Sections 5.3.4.1 and 5.3.4.2). After delivery, unbound MNPs were washed with PBS and replaced with normal growth media. MNP uptake significantly increases when DC 2.4 were placed on an oscillating magnetic field immediately post-delivery (25.8 ± 7 percentage of total iron associated) compared with cells that had not been exposed to any magnetic field post-delivery

(13.8 ± 4.4 percentage of total iron associated). When the oscillating field was applied 6 hours post transfection, iron cell association was slightly higher than in the absence of any oscillating magnetic field but the difference was not significant (17.6 ± 6.0 percentage of total iron associated in cells).

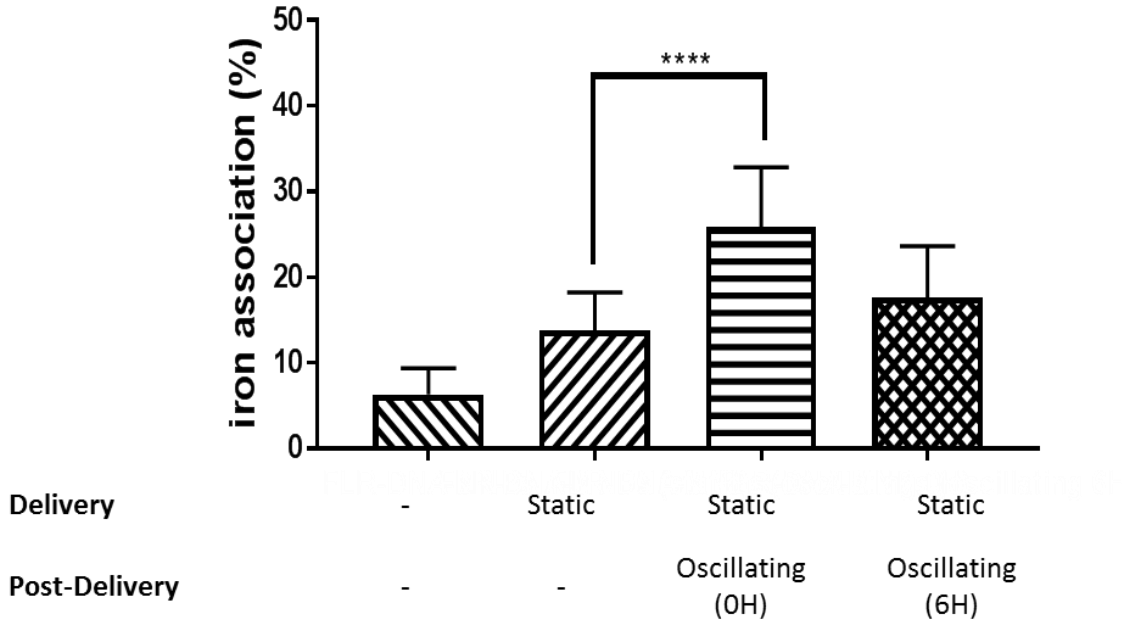

Figure 5.12 Application of an oscillating magnetic field after delivery enhances MNPs uptake on DC 2.4.

*Cells were transfected with pCMV-eGFP-SV40-noDTS plasmid using FLR-MNPs with or without a magnetic field for 1 hour. After delivery cells were washed with PBS. Cells were exposed to an oscillating magnetic field for a further hour, immediately post-delivery (0H) and 6 hours (6 H). Iron content was quantified by ICP-MS. Percentage of iron association was calculated on iron content of 10 µg of MNPs. Bars show mean percentage of iron cell association ± s.d. n=9 biological repeats, 3 technical replicates. **** p<0.0001, Tukey's multiple comparison's test.*

Enhanced MNPs uptake upon application of an oscillating field immediately post-delivery, suggests that mechanical oscillating of the particles on the cell membrane facilitates further particle uptake that does not occur when the particles are just left unaltered on the cell membrane (FLR-DNA-MNPs delivered on a static field).

Additionally, these results indicate that the timing of the application of the oscillating magnetic field significantly affects its effect on MNPs cellular uptake.

5.4 Conclusions

In this chapter the formulation of FLR-DNA-MNPs for gene delivery in immortalized murine DC 2.4 has been optimised. FLR-DNA-MNPs significantly enhanced transfection efficiency compared with PEI-MNPs.[182] Furthermore, FLR-DNA-MNPs magnetofection in 1 hour was comparable with the transfection efficiency of commercially available transfection reagent FuGENE in 24 hours.

The final aim of this section was to assess the effect of the application of a horizontal oscillating magnetic field on the magnetic vectors post-delivery. In order to distinguish between the effect of a magnetic field on uptake and intracellular trafficking two different time points were assessed (immediately post-delivery and six hours post-delivery).[195], [291] Transfection efficiency was significantly enhanced when an oscillating magnetic field was applied post-delivery which was accompanied by an increase on MNPs uptake (compared to control, when FRL-DNA-MNPs were delivered on a static field but no additional field was applied).

Similar observations have been reported by Kamau et al. who showed significantly enhanced transfection efficiency when magnetically loaded cells were subjected to a pulsed magnetic field immediately post-delivery.[264] Additionally, Zhou et al. showed that mechanic oscillations on the cell membrane enhanced transfection efficiency. Further computational modelling of the cell cytoskeleton under the

oscillating mechanic forces showed increased pore area on the cytoskeleton cortex. [292]

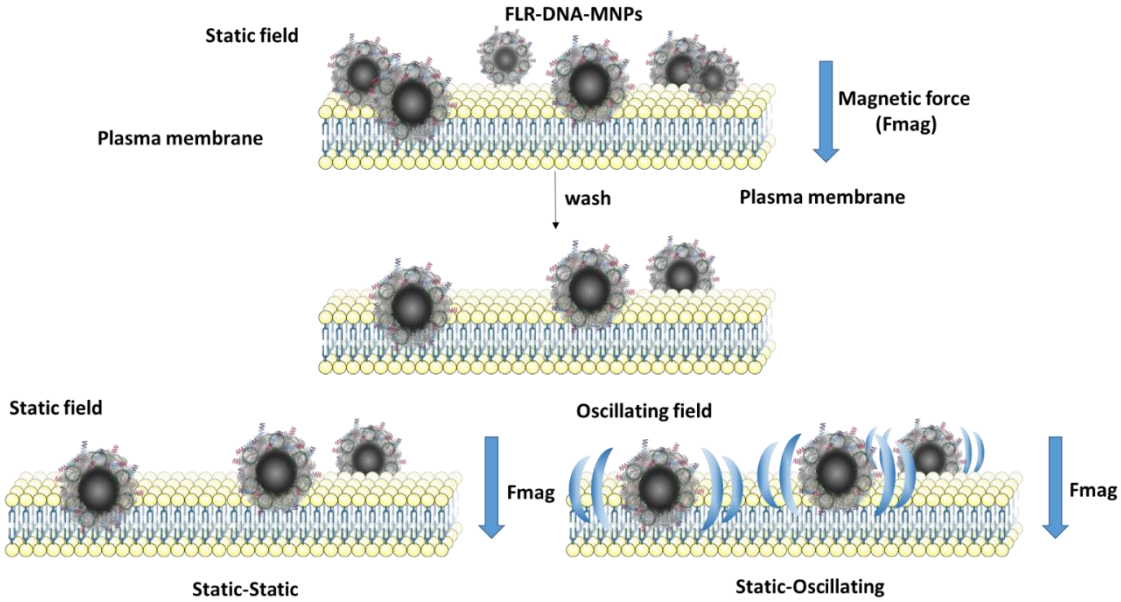

Figure 5.13 Proposed mechanism on the effect of static and oscillating magnetic fields on magnetic nanoparticle uptake.

The mechanical force of a single MNPs on the cell membrane was calculated to be in the piconewton (pN) range, which is the same order of magnitude required to deform the cytoskeleton particle uptake (*8.1.1 Calculation of magnetic force of MNPs on the cell membrane*). It was therefore hypothesized that the mechanic oscillation of the MNPs during particle uptake (immediately post-transfection) could lead to further deformation of the actin cytoskeleton (added to the deformation already mediated by the magnetic force acting on the MNPs) and further enhance DNA uptake (Figure 5.13).

This is the first time that the enhanced transfection efficiency mediated by Magnefect-nano^{TM} has been characterised by looking at MNPs uptake.

The rationale behind choosing a later time point post transfection was to ensure that the particle uptake process was minimal and therefore the application of an external magnetic field would mostly mediate processes related with the intracellular trafficking of the DNA. The specific time point of 6 hours was based on the kinetics of uptake of PR-MNPs previously described in this thesis (*3.3.5 PR mediated enhanced particle uptake is a rapid and not cell-type specific*) and the available literature.[223], [285], [286] The hypothesis was confirmed by enhanced transfection efficiency observed on application of an external magnetic field 6 hours post-delivery which was not related to enhanced particle uptake.

It has been previously reported that the application of a static field to endosomes loaded with MNPs, alters the morphology and orientation of the vesicle, although membrane rupture was never reported.[293], [294] Interestingly, when magnetically loaded endosomes were subjected to external magnetic oscillating fields, endosomal membrane integrity was significantly affected by mechanical oscillation.[68], [283], [284], [295], [296] It is important to note that the frequencies of oscillation/rotation applied on these experiments were higher than the ones applied in this experimental section (20Hz-100Hz, compared to 2 Hz from Magnefect-nano^{TM}). However, based on the available literature and the results previously presented, it was hypothesized that whereas the application of a static field would only induce the reorientation of the MNPs inside the intracellular vesicle as they align with the magnetic field, with no significant effect on the membrane integrity, mechanical oscillation of the MNPs could trigger rupture of the intracellular vesicles liberating more plasmid into the cytoplasm, resulting in enhanced reporter gene expression (Figure 5.14).

In order to test this hypothesis, future work should include endosome membrane labelling and colocalisation studies using confocal microscopy. Furthermore, TEM image analysis would also provide evidence of the cell and endosome membrane integrity.

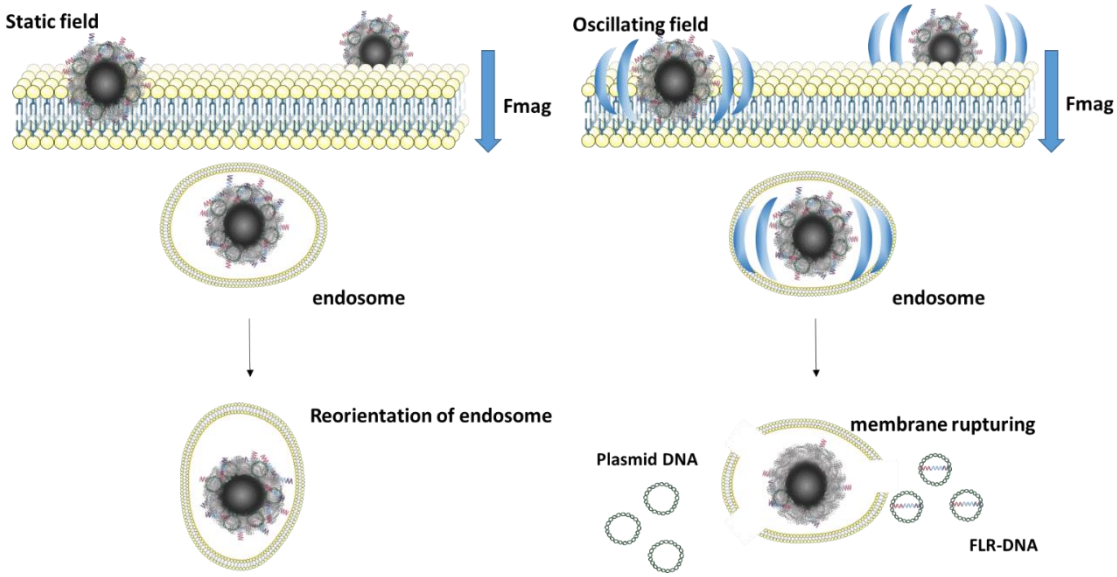

Figure 5.14 Proposed mechanism on the effect of static and oscillating magnetic fields on magnetically loaded endosomes.

To more efficiently isolate intracellular trafficking from particle uptake and gain better understanding in the role of Magnefect-nano^{TM} on the gene transfer process, future work should include a protocol similar to the one described in *Results II* (section Endocytosis inhibitors), completely removing the DNA that has not been uptaken from the cell membrane post-delivery by thoroughly washing with molecules such as DNase or heparin, this step would ensure that any alteration on transfection efficiency from that point onwards would be mediated by the intracellular fate of the DNA.

DCs were selected for this experimental section because they provided a clinically relevant model for the application of a multimodal technology such as FLR-DNA-MNPs, capable of fast and efficient gene delivery with the possibility of further manipulation and tracking in the context of immune cancer therapy. The formulation optimised in this results section has provided a platform to better understand the mechanism of Magnefect-nano^{TM} in this difficult to transfect cells. However, if FLR-DNA-MNPs was to be further developed for its application as platform technology in the context of dendritic cell vaccine, more exhaustive optimisation would be required in order to ensure safe, fast and efficient transfection in a short period of time.

6 Conclusions and Future Work

Successful application of MNPs *in vivo* depends on the efficient uptake of the particles by the target cells/organs.[297] To date, most therapeutic applications of MNPs rely on passive biodistribution (clearance from the blood and accumulation in the liver or the spleen) or on the uptake by phagocytic cells part of the immune system (i.e. macrophages).[298]

This project was focused on the development of two delivery platforms by combination of MNPs and newly discovered multi-domain delivery system, GET.

The first delivery system aimed to increase MNPs accumulation on the cells looking to provide a robust and efficient system capable of overcoming problems encountered by NPs when they are delivered *in vivo*, such as aggregation, clot formation or loss of activity upon protein corona formation. The delivery system developed on the first results chapter (*Results I)* consists on the incorporation of GET peptide P21-8R (PR) to dextran coated MNPs for delivery to mammalian cells *in vitro*. PR efficiently delivered MNPs to a range of different cell lines in the presence of serum with insignificant effect on cell viability and proliferation. PR mediated enhanced MNPs uptake was negated by the addition of heparin to the system, suggesting that interaction of PR and heparan sulphates in the cell membrane plays a very important role on PR enhanced particle uptake. Furthermore, PR was able to efficiently deliver MNPs to cells in the presence of plasma. Analysis of the protein corona revealed fast adsorption of plasma proteins to the particle surface that was only partially affected by the presence of PR. These results indicated that PR is capable of efficiently delivering MNPs even after protein corona formation. This presents an advantage of PR compared to other

delivery systems that lose their targetability/efficacy in the presence of plasma proteins and are therefore not suitable for their use *in vivo*. Additionally, PR-MNPs did not cause changes on erythrocyte morphology or cell lysis in the presence of plasma, suggesting PR-MNPs could be a good candidate for its application *in vivo*. Further work could be carried out *in vivo* to determine biodistribution of the particles and possible ways to benefit from their enhanced uptake for clinical applications (i.e. MRI or hyperthermia).

The second delivery system was developed with the aim to exploit the already optimised GET-MNPs platform for magnetically mediated gene delivery. Another variant of GET, FGF2B-LK15-8R (FLR), that had been previously demonstrated to efficiently deliver DNA *in vitro* and *in vivo,* was incorporated into the same dextran coated MNPs and assessed for gene delivery in the presence of a magnetic field.[167] *Results II* is dedicated to the optimisation and characterisation of the FLR-DNA-MNPs for gene delivery on a mouse fibroblast cell line. FLR formed stable complexes with DNA and MNPs. In the presence of an external magnetic field FLR-DNA-MNPs significantly increased transfection speed compared with FLR-DNA, achieving significant gene expression levels in just 5 minutes. Interesting, FLR-DNA and FLR-DNA-MNPs showed comparable gene expression and uptake kinetics suggesting MNPs do not hamper FLR mediated gene transfer.

Importantly, enhanced gene transfer by FLR-DNA-MNPs in the presence of an external magnetic field had minimal effect on cell viability and proliferation.

Endocytosis inhibition studies indicated that plasmid DNA uptake happened mainly through CME when mediated by FLR-DNA and FLR-DNA-MNPs. Interestingly, delivery of FLR-DNA-MNPs in the presence of a magnetic field was more affected by the

presence of MCBD, a molecule known to deplete cholesterol from the cell membrane, disrupting CME. It was hypothesised that the rapid concentration of DNA mediated by the magnetic sedimentation of FLR-DNA-MNPs on the cell membrane, caused the saturation of clathrin receptors, triggering the activation of alternative endocytosis mechanisms.

DNA degradation rate after delivery was proportional to the amount of internalised DNA and was not affected by the delivery vector or the speed of gene transfer. Endosomal escape study on a haemolysis model revealed that membrane rupturing activity was mainly mediated by FLR.

The mechanism through which magnetofection enhanced plasmid DNA delivery was mostly related to the rapid concentration of the magnetic vector on the cell membrane. No other effects on intracellular trafficking were observed.

One of the advantages of the use of MNPs for biomedical applications is their ability to be externally manipulated by the application of a magnetic field or magnetic resonance.[171]

The incorporation of an oscillating dimension to the external magnetic field applied had previously shown significant improved transfection levels in difficult to transfect cell lines.[172], [264], [270]

Results III was focused on the use of Magnefect-nano^{TM} to assess the effect of a controlled external oscillating magnetic field on FLR-DNA-MNPs mediated gene transfer in difficult to transfect DC 2.4. The rationale behind choosing these cells for this particular application stems from the recently increased interest on the use of cells for immunotherapy. These therapies require, ideally, fast and efficient

manipulation of the patients cells (gene modification) but also benefit from multimodal systems that allow non-invasive manipulation and traceability.

Optimised FLR-DNA-MNPs was able to achieve transfection efficiencies comparable to commercial standard FuGENE in a fraction of the time (1 hour verses 24 hours).

The application of an oscillating external magnetic field after delivery of FLR-DNA-MNPs complexes to the cells significantly enhanced gene expression. This was observed when the oscillating magnetic field was applied up to 6 hours post-delivery. Interestingly, enhanced gene expression mediated by oscillating magnetic field at this point was not related to enhance on FLR-DNA-MNPs uptake. It was therefore hypothesized that the oscillating magnetic field was mediating intracellular processes (i.e. mechanical oscillation of MNPs in intracellular compartments) that resulted on increased concentration of plasmid DNA into the cytoplasm.

Even if the application of an oscillating magnetic field to FLR-DNA-MNPs could trigger both enhanced uptake and endosomal escape, the two effects represent only a fraction of the initial gene expression achieved by magnetofection. Future steps in order to further enhance gene transfer mediated with Magnefect-nano^{TM} should include application of more oscillating regimes, oscillation pulses[264] and optimisation of frequency and amplitude for endosomal escape.

6.1 Future directions

Focusing on magnetofection, the results here presented and literature on the topic[126], [244], suggest that the main limitation of this technique still remains the lack of ability to specifically promote DNA transfer into the cell nucleus. In this context, delivery of nucleic acids that could exert their function in the cytoplasm such as small interfering RNA (siRNA) and microRNA (miRNA) (as opposed to DNA that requires entry to the nucleus in order to be transcribed) complement better the current state of the art of magnetically mediated gene delivery. *In vitro* and preclinical testing of magnetofection with siRNA and miRNA have shown promising results.[105], [299], [300], [235], [301]

The main advantage of magnetofection still remains it's fast and safe gene transfer capacity. With the added bonus of providing a platform for particle/cell manipulation and non-invasive imaging *in vivo.* Incorporation of molecules capable of promoting intracellular trafficking and nuclear translocation of nucleic acids into the current MNPs based formulations for magnetofection will provide a very powerful tool for more efficient gene transfer.

In conclusion, both GET-MNPs delivery systems here described, present the advantage that their formulations rely on electrostatic interactions between their different components which makes them: easy to tailor to specific needs and easy to translate to the clinic, as long as the individual components can be manufactured under Good Manufacturing Practise (GMP) conditions.

Magnetofection represents a promising strategy for therapies that require rapid, safe and or localised gene delivery and with further development of the magnetic vectors, could be used for the delivery of state of art therapeutics to treat a variety of

conditions, with particular interest in localised tumours [116],[119], [302] or disorders that are mainly present or originated in a particular region of the body, including examples like the striatum in Parkinson's disease [299] or the lung for inherited (cystic fibrosis) or acquired (asthma) diseases [303], [304].

7 References

[1] R. Duncan and R. Gaspar, “Nanomedicine(s) under the microscope,” *Mol. Pharm.*, vol. 8, no. 6, pp. 2101–2141, 2011.

[2] C. Sun, J. S. H. Lee, and M. Zhang, “Magnetic nanoparticles in MR imaging and drug delivery ☆,” *Adv. Drug Deliv. Rev.*, vol. 60, no. 11, pp. 1252–1265, 2008.

[3] L. Corchero and A. Villaverde, “Biomedical applications of distally controlled magnetic nanoparticles,” *Trends Biotechnol.*, vol. 27, no. 8, pp. 468–476, 2009.

[4] R. K. Gilchrist, R. Medal, W. D. Shorey, R. C. Hanselman, J. C. Parrott, and C. B. Taylor, “Selective inductive heating of lymph nodes,” *Ann. Surg.*, vol. 146, no. 4, p. 596, 1957.

[5] J. Estelrich, E. Escribano, J. Queralt, and M. A. Busquets, “Iron oxide nanoparticles for magnetically-guided and magnetically-responsive drug delivery,” *Int. J. Mol. Sci.*, vol. 16, no. 4, pp. 8070–8101, 2015.

[6] D. J. Craik, *Magnetism: principles and applications*. Wiley-VCH, 2003.

[7] U. Jeong, X. Teng, Y. Wang, H. Yang, and Y. Xia, “Superparamagnetic colloids: controlled synthesis and niche applications,” *Adv. Mater.*, vol. 19, no. 1, pp. 33–60, 2007.

[8] M. Arruebo, R. Fernández-pacheco, M. R. Ibarra, and J. Santamaría, “Magnetic nanoparticles Controlled release of drugs from nanostructured functional materials ,” *Magn. nanoparticles drug Deliv.*, vol. 2, no. 3, pp. 22–32, 2007.

[9] Q. A. Pankhurst, J. Connolly, S. K. Jones, and J. Dobson, “Applications of magnetic nanoparticles in biomedicine,” *J. Phys. D. Appl. Phys.*, vol. 36, no. 13, p. 167, 2003.

[10] L. Mohammed, H. G. Gomaa, D. Ragab, and J. Zhu, “Magnetic nanoparticles for environmental and biomedical applications : A review,” *Particuology*, vol. 30, pp. 1–14, 2017.

[11] N. Lee, D. Yoo, D. Ling, M. H. Cho, T. Hyeon, and J. Cheon, “Iron Oxide Based Nanoparticles for Multimodal Imaging and Magnetoresponsive Therapy,” *Chem. Rev.*, vol. 115, no. 19, pp. 10637–10689, 2015.

[12] C. Riggio, M. P. Calatayud, M. Giannaccini, B. Sanz, T. E. Torres, R. Fernández-pacheco, A. Ripoli, M. R. Ibarra, L. Dente, A. Cuschieri, G. F. Goya, and V. Raffa, “The orientation of the neuronal growth process can be directed via magnetic nanoparticles under an applied magnetic field,” *Nanomedicine Nanotechnology, Biol. Med.*, vol. 10, no. 7, pp. 1549–1558, 2014.

[13] S. C. Mcbain, H. H. Yiu, and J. Dobson, “Magnetic nanoparticles for gene and drug delivery,” *Int. J. Nanomedicine*, vol. 3, no. 2, pp. 169–180, 2008.

[14] K. Schulze, A. Koch, A. Petri-Fink, B. Steits, S. Kamau, M. Hottiger, and B. Von Rechenberg, “Uptake and Biocompatibility of Functionalized Poly(vinylalcohol) Coated Superparamagnetic Maghemite Nanoparticles by Synoviocytes In Vitro,” *J. nanocience Nanotechnol.*, vol. 6, no. 9–10, pp. 2829–2840, 2006.

[15] P. Tartaj, P. Morales, S. Veintemillas-verdaguer, and T. Gonz, “The preparation of magnetic nanoparticles for applications in biomedicine,” *J. Phys. D. Appl. Phys.*, vol. 36, no. 13, p. R182, 2003.

[16] S. Sun, “Recent Advances in Chemical Synthesis , Self-Assembly , and Applications of FePt Nanoparticles,” *Adv. Mater.*, vol. 18, no. 4, pp. 393–403, 2006.

[17] C. C. Berry and A. S. G. Curtis, “Functionalisation of magnetic nanoparticles for applications in biomedicine,” *J. Phys. D. Appl. Phys.*, vol. 36, no. 13, p. R198, 2003.

[18] S. Li and L. Huang, “Pharmacokinetics and Biodistribution of Nanoparticles,” *Mol. Pharm.*, vol. 5, no. 4, pp. 496–504, 2008.

[19] O. L. Lanier, A. G. Monsalve, P. S. Mcfetridge, J. Dobson, O. L. Lanier, A. G. Monsalve, P. S. Mcfetridge, and J. Dobson, “Magnetically triggered release of biologics,” *Int. Mater. Rev.*, pp. 1–28, 2018.

[20] A. J. M. D. Souza, R. L. Schowen, and E. M. Topp, “Polyvinylpyrrolidone – drug conjugate : synthesis and release mechanism,” *J. Control. Release*, vol. 94, no. 1, pp. 91–100, 2004.

[21] E. Khor and L. Yong, “Implantable applications of chitin and chitosan,” *Biomaterials*, vol. 24, no. 13, pp. 2339–2349, 2003.

[22] D. Olsen, C. Yang, M. Bodo, R. Chang, S. Leigh, J. Baez, D. Carmichael, M. Pera, M. Jarvinen, and J. Polarek, “Recombinant collagen and gelatin for drug delivery,” *Adv. Drug Deliv. Rev.*, vol. 55, no. 12, pp. 1547–1567, 2003.

[23] Q. Feng, Y. Liu, J. Huang, K. Chen, J. Huang, and K. Xiao, “Uptake , distribution , clearance , and toxicity of iron oxide nanoparticles with different sizes and coatings,” *Sci. Rep.*, vol. 8, no. 1, p. 2082, 2018.

[24] J. R. Mccarthy and R. Weissleder, “Multifunctional magnetic nanoparticles for targeted imaging and therapy ☆,” *Adv. Drug Deliv. Rev.*, vol. 60, no. 11, pp. 1241–1251, 2008.

[25] C. Tassa, S. Y. Shaw, and R. Weissleder, “Dextran-Coated Iron Oxide

Nanoparticles: a Versatile Platform for Targeted Molecular Imaging, Molecular Diagnostics and Therapy," *Acc. Chem. Res.*, vol. 44, no. 10, pp. 842–852, 2011.

[26] Y. J. Wang, "Superparamagnetic iron oxide based MRI contrast agents : Current status of clinical application," *Quant. imagine Med. Surg.*, vol. 1, no. 1, p. 35, 2011.

[27] V. P. Torchilin, "Recent advances with liposomes as pharmaceutical carriers," *Nat. Rev. Drug Discov.*, vol. 4, no. 2, p. 145, 2005.

[28] N. Nasongkla, E. Bey, J. Ren, H. Ai, C. Khemtong, J. S. Guthi, S. Chin, A. D. Sherry, D. A. Boothman, and J. Gao, "Multifunctional Polymeric Micelles as cancer-targeted, MRI-ultrasensitive drug delivery systems," *Nano Lett.*, vol. 6, no. 11, pp. 2427–2430, 2006.

[29] S. Santra, R. Tapec, N. Theodoropoulou, J. Dobson, A. Hebard, and W. Tan, "Synthesis and Characterization of Silica-Coated Iron Oxide Nanoparticles in Microemulsion : The Effect of Nonionic Surfactants," *Langmuir*, vol. 17, no. 10, pp. 2900–2906, 2001.

[30] J. Lin, W. Zhou, A. Kumbhar, J. Wiemann, J. Fang, E. E. Carpenter, and C. J. O. Connor, "Gold-Coated Iron (Fe @ Au) Nanoparticles : Synthesis , Characterization , and Magnetic Field-Induced Self-Assembly," *J. Solid State Chem.*, vol. 159, no. 1, pp. 26–31, 2001.

[31] A. K. Gupta and V. D. Vaidya, "Recent advances on surface engineering of magnetic iron oxide nanoparticles and their biomedical applications," *Futur. Med.*, vol. 2, no. Ii, pp. 23–39, 2007.

[32] Y. Lu, E. Sega, C. P. Leamon, and P. S. Low, "Folate receptor-targeted

immunotherapy of cancer : mechanism and therapeutic potential," *Adv. Drug Deliv. Rev.*, vol. 56, no. 8, pp. 1161–1176, 2004.

[33] F. Sonvico, C. Dubernet, D. Jaillard, J. Degrouard, J. Hoebeke, E. Duguet, P. Colombo, and P. Couvreur, "Folate-Conjugated Iron Oxide Nanoparticles for Solid Tumor Targeting as Potential Specific Magnetic Hyperthermia Mediators : Synthesis , Physicochemical Characterization , and in Vitro Experiments," *Bioconjug. Chem.*, vol. 16, no. 5, pp. 1181–1188, 2005.

[34] K. Bhadriraju and L. K. Hansen, "Hepatocyte adhesion , growth and di ! erentiated function on RGD-containing proteins," *Biomaterials*, vol. 21, no. 3, pp. 267–272, 2000.

[35] J. Zhou, C. Leuschner, C. Kumar, J. F. Hormes, and W. O. Soboyejo, "Sub-cellular accumulation of magnetic nanoparticles in breast tumors and metastases," *Biomaterials*, vol. 27, no. 9, pp. 2001–2008, 2006.

[36] P. Yang, X. Sun, J. Chiu, H. Sun, and Q. He, "Transferrin-Mediated Gold Nanoparticle Cellular Uptake," *Bioconjug. Chem.*, vol. 16, no. 3, pp. 494–496, 2005.

[37] A. K. Gupta and A. S. G. Curtis, "Lactoferrin and ceruloplasmin derivatized superparamagnetic iron oxide nanoparticles for targeting cell surface receptors," *Biomaterials*, vol. 25, no. 15, pp. 3029–3040, 2004.

[38] E. J. Sayers, J. P. Magnusson, P. R. Moody, F. Mastrotto, C. Conte, C. Brazzale, P. Borri, P. Caliceti, P. Watson, G. Mantovani, J. Aylott, S. Salmaso, A. T. Jones, and C. Alexander, "Switching of Macromolecular Ligand Display by Thermoresponsive Polymers Mediates Endocytosis of Multiconjugate

Nanoparticles," *Bioconjug. Chem.*, vol. 29, no. 4, pp. 1030–1046, 2018.

[39] A. Khurana, H. Nejadnik, F. Chapelin, O. Lenkov, S. Lee, S. N. Gupta, N. Aflakian, N. Derugin, S. Messing, G. Lin, T. F. Lue, L. Pisani, and H. E. Daldrup-link, "Ferumoxytol: a new, clinically applicable label for stem-cell tracking in arthritic joints with MRI," *Nanomedicine*, vol. 8, no. 12, pp. 1969–1983, 2013.

[40] R. E. Lauffer, "Paramagnetic Metal Complexes as Water Proton Relaxation Agents for NMR Imaging : Theory and Design," *Chem. Rev.*, vol. 87, no. 5, pp. 901–927, 1987.

[41] A. D. Elster and J. H. Burdette, "Questions and Answers in Magnetic Resonance Imaging , 2e." 2001.

[42] M. D. Budde and J. A. Frank, "Magnetic tagging of therapeutic cells for MRI," *J. Nucl. Med. Off. Publ.*, vol. 50, no. 2, pp. 171–174, 2010.

[43] D. Baumjohann and M. B. Lutz, "Non-invasive imaging of dendritic cell migration in vivo," *Immunobiology*, vol. 211, no. 6–8, pp. 587–597, 2006.

[44] C. M. Long, H. W. M. Van Laarhoven, and J. W. M. Bulte, "Magnetovaccination as a Novel Method to Assess and Quantify Dendritic Cell Tumor Antigen Capture and Delivery to Lymph Nodes," *Cancer Res.*, vol. 69, no. 7, pp. 3180–3188, 2009.

[45] E. T. Ahrens, R. Flores, H. Xu, and P. A. Morel, "In vivo imaging platform for tracking immunotherapeutic cells," *Nat. Biotechnol.*, vol. 23, no. 8, pp. 983–987, 2005.

[46] H. Markides, O. Kehoe, R. H. Morris, and A. J. El Haj, "Whole body tracking of superparamagnetic iron oxide nanoparticle-labelled cells--a rheumatoid arthritis mouse model.," *Stem Cell Res. Ther.*, vol. 4, no. 5, p. 126, 2013.

[47] R. Harrison, H. Markides, R. H. Morris, P. Richards, A. J. El Haj, and V. Sottile, "Autonomous magnetic labelling of functional mesenchymal stem cells for improved traceability and spatial control in cell therapy applications," *J. Tissue Eng. Regen. Med.*, vol. 11, no. 8, pp. 2333–2348, 2017.

[48] Q. A. Pankhurst, N. T. K. Thanh, S. K. Jones, and J. Dobson, "Progress in applications of magnetic nanoparticles in biomedicine," *J. Phys. D. Appl. Phys.*, vol. 42, no. 22, p. 224001, 2009.

[49] M. Srinivas, A. Heerschap, E. T. Ahrens, C. G. Figdor, and I. J. M. de Vries, "19F MRI for quantitative in vivo cell tracking," *Trends Biotechnol.*, vol. 28, no. 7, pp. 363–370, 2010.

[50] C. Toso, J. Vallee, P. Morel, and F. Ris, "Clinical Magnetic Resonance Imaging of Pancreatic Islet Grafts After Iron Nanoparticle Labeling," *Am. J. Transplant.*, vol. 8, no. 3, pp. 701–706, 2008.

[51] J. Zhu, L. Zhou, and F. XingWu, "Tracking Neural Stem Cells in Patients with Brain Trauma," *N. Engl. J. Med.*, vol. 355, no. 22, pp. 2376–2378, 2006.

[52] J. W. M. Bulte, "In Vivo MRI Cell Tracking: Clinical Studies," *Am. J. Roentgenol.*, vol. 193, no. 2, pp. 314–325, 2009.

[53] I. J. M. De Vries, W. J. Lesterhuis, J. O. Barentsz, P. Verdijk, J. H. Van Krieken, O. C. Boerman, W. J. G. Oyen, J. J. Bonenkamp, J. B. Boezeman, G. J. Adema, J. W. M. Bulte, T. W. J. Scheenen, C. J. A. Punt, A. Heerschap, and C. G. Figdor, "Magnetic resonance tracking of dendritic cells in melanoma patients for monitoring of cellular therapy," *Nat. Biotechnol.*, vol. 23, no. 11, pp. 1407–1413, 2005.

[54] F. Callera and C. M. de Melo, “Magnetic resonance tracking of magnetically labeled autologous bone marrow CD34+ cells transplanted into the spinal cord via lumbar puncture technique in patients with chronic spinal cord injury: CD34+ cells’ migration into the injured site.,” *Stem Cells Dev.*, vol. 16, no. 3, pp. 461–466, 2007.

[55] A. F. Hersi, S. Eriksson, J. Ramos, S. Abdsaleh, F. Warnberg, and A. Karakatsanis, “A combined, totally magnetic technique with a magnetic marker for non-palpable tumour localization and superparamagnetic iron oxide nanoparticles for sentinel lymph node detection in breast cancer surgery,” *Eur. J. Surg. Oncol.*, 2018.

[56] D. Karussis, C. Karageorgiou, A. Vaknin-dembinsky, B. Gowda-kurkalli, J. M. Gomori, I. Kassis, J. W. M. Bulte, P. Petrou, T. Ben-hur, O. Abramsky, and S. Slavin, “Safety and Immunological Effects of Mesenchymal Stem Cell Transplantation in Patients With Multiple Sclerosis and Amyotrophic Lateral Sclerosis,” *Arch. Neurol.*, vol. 67, no. 10, pp. 1187–1194, 2010.

[57] “19F Hot Spot MRI of Human Adipose-derived Stem Cells for Breast Reconstruction.” ClinicalTrials.gov, p. NCT02035085, 2018.

[58] “Dendritic Cell Vaccination in Melanoma Patients Scheduled for Regional Lymph Node Dissection.” ClinicalTrials.gov, p. NCT00243594, 2009.

[59] “Tracking Peripheral Immune Cell Infiltration of the Brain in Central Inflammatory Disorders Using [Zr-89]Oxinate-4-labeled Leukocytes.” ClinicalTrials.gov, p. NCT03807973, 2019.

[60] “Safety of Labeled Dendritic Cell (DC) Vaccines and Feasibility of Tracking by

Magnetic Resonance Imaging (MRI).” ClinicalTrials.gov, p. NCT01671592, 2017.

[61] “Mesenchymal Stem Cells for the Treatment of MS.” ClinicalTrials.gov, p. NCT00781872, 2008.

[62] Y. X. J. Wáng and J. Idée, “A comprehensive literatures update of clinical researches of superparamagnetic resonance iron oxide nanoparticles for magnetic resonance imaging,” *Quant. imagine Med. Surg.*, vol. 7, no. 1, pp. 88–122, 2017.

[63] R. Hergt, S. Dutz, R. Müller, and M. Zeisberger, “Magnetic particle hyperthermia: nanoparticle magnetism and materials development for cancer therapy,” *J. Phys. Condens. Matter*, vol. 18, no. 38, pp. S2919–S2934, 2006.

[64] R. Hergt, S. Dutz, M. Robert, and M. Zeisberger, “Magnetic particle hyperthermia : nanoparticle magnetism and materials development for cancer therapy,” vol. 18, pp. 2919–2934, 2006.

[65] J. M. Byrne, V. S. Coker, E. Cespedes, P. L. Wincott, D. J. Vaughan, R. A. D. Pattrick, G. Van Der Laan, E. Arenholz, F. Tuna, M. Bencsik, J. R. Lloyd, and N. D. Telling, “Biosynthesis of zinc substituted magnetite nanoparticles with enhanced magnetic properties,” *Adv. Funct. Mater.*, vol. 24, no. 17, pp. 2518–2529, 2014.

[66] G. F. Goya, E. Lima, A. D. Arelaro, T. Torres, H. R. Rechenberg, L. Rossi, C. Marquina, M. R. Ibarra, I. D. F. D. S. Paulo, S. Paulo, I. De Química, U. De São, S. Paulo, and A. S. Preparation, “Magnetic Hyperthermia With Fe 3 O 4 Nanoparticles : The Influence of Particle Size on Energy Absorption,” *IEEE Trans. Nanobioscience*, vol. 44, no. 11, pp. 4444–4447, 2008.

[67] B. Sanz, M. P. Calatayud, E. De Biasi, E. Lima Jr, M. Mansilla, and G. F. Goya, “In Silico before In Vivo : how to Predict the Heating Efficiency of Magnetic Nanoparticles within the Intracellular Space,” *Sci. Rep.*, vol. 6, no. November, p. 38733, 2016.

[68] B. Sanz, M. P. Calatayud, T. E. Torres, M. L. Fanarraga, M. R. Ibarra, and G. F. Goya, *Magnetic hyperthermia enhances cell toxicity with respect to exogenous heating*, vol. 114. 2017, pp. 62–70.

[69] B. Thiesen and A. Jordan, “Clinical applications of magnetic nanoparticles for hyperthermia,” *Int. J. hyperthermia2*, vol. 24, no. 6, pp. 467–474, 2008.

[70] K. J. Widder, A. E. Senyei, and D. G. Scarpelli, “Magnetic microspheres: a model system for site specific drug delivery in vivo,” *Proc. Natl. Acad. Sci.*, vol. 158, no. 2, pp. 141–146, 1978.

[71] C. Mah, I. Zolotukhin, T. J. Fraites, J. Dobson, C. Batich, and B. J. Byrne, “Microsphere-mediated delivery of recombinant AAV vectors in vitro and in vivo,” *Mol. Ther.*, vol. 1, p. S239, 2000.

[72] C. Chiang, Y. Lin, R. Lee, Y. Lai, H. Cheng, C. Hsieh, W. Shyu, and S. Chen, “Combination of fucoidan-based magnetic nanoparticles and immunomodulators enhances tumour-localized immunotherapy,” *Nat. Nanotechnol.*, p. 1, 2018.

[73] O. Mykhaylyk, A. Cherchenko, A. Ilkin, N. Dudchenko, V. Ruditsa, M. Novoseletz, and Y. Zozulya, “Glial brain tumor targeting of magnetite nanoparticles in rats,” *J. Magn. Magn. Mater.*, vol. 225, no. 1–2, pp. 241–247, 2001.

[74] B. Chertok, B. A. Moffat, A. E. David, F. Yu, C. Bergemann, B. D. Ross, and V. C.

Yang, “Iron oxide nanoparticles as a drug delivery vehicle for MRI monitored magnetic targeting of brain tumors,” *Biomaterials*, vol. 29, no. 4, pp. 487–496, 2008.

[75] B. Chertok, A. E. David, and V. C. Yang, “Biomaterials Polyethyleneimine-modi fi ed iron oxide nanoparticles for brain tumor drug delivery using magnetic targeting and intra-carotid administration,” *Biomaterials*, vol. 31, no. 24, pp. 6317–6324, 2010.

[76] A. J. Cole, A. E. David, J. Wang, C. J. Galbán, and V. C. Yang, “Biomaterials Magnetic brain tumor targeting and biodistribution of long-circulating PEG-modi fi ed , cross-linked starch-coated iron oxide nanoparticles,” *Biomaterials*, vol. 32, no. 26, pp. 6291–6301, 2011.

[77] Y. Qiu, S. Tong, L. Zhang, Y. Sakurai, D. R. Myers, L. Hong, W. A. Lam, and G. Bao, “Magnetic forces enable controlled drug delivery by disrupting endothelial cell-cell junctions,” *Nat. Commun.*, vol. 8, p. 15594, 2017.

[78] A. S. Lãbbe, H. Riess, F. Schriever, P. Reichardt, K. Possinger, M. Matthias, B. Dã, F. Herrinann, R. Gurtler, P. Hohenberger, N. Haas, R. Sohr, B. Sander, A. Lemke, D. Ohlendorf, W. Huhnt, and D. Huhn, “Clinical Experiences with Magnetic Drug Targeting : A Phase Epidoxorubicin in 14 Patients with Advanced Solid Tumors1,” *Cancer Res.*, vol. 56, no. 20, pp. 4686–4693, 1996.

[79] K. El-boubbou, “Magnetic iron oxide nanoparticles as drug carriers : Clinical relevance Magnetic iron oxide nanoparticles as drug carriers : clinical relevance,” *Nanomedicine*, vol. 13, no. 8, pp. 953–971, 2018.

[80] K. Cheng, T.-S. Li, K. Malliaras, D. Davis, Y. Zhang, and E. Marban, “Magnetic

Targeting Enhances Engraftment and Functional Benefit of Iron-Labeled Cardiosphere-Derived Cells in Myocardial," *Circ. Res.*, vol. 106, no. 10, pp. 1570–1581, 2011.

[81] M. Bietenbeck, A. Florian, and C. Faber, "Remote magnetic targeting of iron oxide nanoparticles for cardiovascular diagnosis and therapeutic drug delivery : where are we now ?," *Int. J. Nanomedicine*, vol. 11, pp. 3191–3203, 2016.

[82] A. L. I. S. Arbab, E. K. Jordan, L. B. Wilson, G. T. Yocum, B. K. Lewis, and J. A. Frank, "In Vivo Trafficking and Targeted Delivery of Magnetically Labeled Stem Cells," *Hum. Gene Ther.*, vol. 15, no. 4, pp. 351–360, 2004.

[83] J. Riegler, J. A. Wells, P. G. Kyrtatos, A. N. Price, Q. A. Pankhurst, and M. F. Lythgoe, "Targeted magnetic delivery and tracking of cells using a magnetic resonance imaging system," *Biomaterials*, vol. 31, no. 20, pp. 5366–5371, 2010.

[84] M. Muthana, A. J. Kennerley, R. Hughes, E. Fagnano, J. Richardson, M. Paul, C. Murdoch, F. Wright, C. Payne, M. F. Lythgoe, N. Farrow, J. Dobson, J. Conner, J. M. Wild, and C. Lewis, "Directing cell therapy to anatomic target sites in vivo with magnetic resonance targeting," *Nat. Commun.*, vol. 6, no. August, p. 8009, 2015.

[85] J. Dobson, "Remote control of cellular behaviour with magnetic nanoparticles," *Nat. Nanotechnol.*, vol. 3, no. 3, pp. 139–143, 2008.

[86] H. Markides, J. S. McLaren, and A. J. El Haj, "Overcoming translational challenges - The delivery of mechanical stimuli in vivo," *Int. J. Biochem. Cell Biol.*, vol. 69, pp. 162–172, 2015.

[87] D. W. Coyne, "Ferumoxytol for treatment of iron deficiency anemia in patients

with chronic kidney disease," *Expert Opin. Pharmacother.*, vol. 10, no. 15, pp. 2563–2568, 2009.

[88] C. L. Ventola, "Progress in Nanomedicine : Approved and Investigational Nanodrugs," *Pharm. Ther.*, vol. 42, no. 12, pp. 742–755, 2017.

[89] P. K. Nguyen, J. Riegler, and J. C. Wu, "Stem Cell Imaging : From Bench to Bedside," *Cell Stem Cell*, vol. 14, no. 4, pp. 431–444, 2014.

[90] D. Bobo, K. J. Robinson, J. Islam, K. J. Thurecht, S. R. Corrie, and S. R. Corrie, "Nanoparticle-Based Medicines : A Review of FDA-Approved Materials and Clinical Trials to Date," *Pharm. Res.*, vol. 33, no. 10, pp. 2373–2387, 2016.

[91] A. C. Anselmo and S. Mitragotri, "Nanoparticles in the clinic," *Bioeng. Transl. Med.*, vol. 1, no. 1, pp. 10–29, 2016.

[92] "Clinical Trials." [Online]. Available: https://clinicaltrials.gov/.

[93] T. Neuberger, B. Scho, M. Hofmann, and B. Von Rechenberg, "Superparamagnetic nanoparticles for biomedical applications : Possibilities and limitations of a new drug delivery system," *J. Magn. Magn. Mater.*, vol. 293, no. 1, pp. 483–496, 2005.

[94] L. H. Reddy, J. L. Arias, J. Nicolas, and P. Couvreur, "Magnetic Nanoparticles : Design and Characterization , Toxicity and Biocompatibility , Pharmaceutical and Biomedical Applications," 2012.

[95] S. E. Barry, "Challenges in the development of magnetic particles for therapeutic applications," *Int. J. Hyperth.*, vol. 24, no. 6, pp. 451–466, 2008.

[96] M. Ramamoorth and A. Narvekar, "Non Viral Vectors in Gene Therapy- An Overview," *J. Clin. Diagnostic Res.*, vol. 9, no. 1, p. GE01, 2015.

[97] R. M. Raftery, D. P. Walsh, I. M. Castaño, A. Heise, G. P. Duffy, S. Cryan, and F. J. O. Brien, “Delivering Nucleic-Acid Based Nanomedicines on Biomaterial Scaffolds for Orthopedic Tissue Repair : Challenges , Progress and Future Perspectives,” *Adv. Mater.*, vol. 28, no. 27, pp. 5447–5469, 2016.

[98] I. A. Khalil, K. Kogure, H. Akita, and H. Harashima, “Uptake Pathways and Subsequent Intracellular Trafficking in Nonviral Gene Delivery,” *Pharmacol. Rev.*, vol. 58, no. 1, pp. 32–45, 2006.

[99] C. M. Varga, N. C. Tedford, M. Thomas, A. M. Klibanov, L. G. Griffith, and D. A. Lauffenburger, “Quantitative comparison of polyethylenimine formulations and adenoviral vectors in terms of intracellular gene delivery processes,” *Gene Ther.*, vol. 12, no. 13, pp. 1023–1032, 2005.

[100] D. J. Glover, G. W. Moseley, and D. A. Jans, “The efficiency of nuclear plasmid DNA delivery is a critical determinant of transgene expression at the single cell level,” no. November 2009, pp. 77–85, 2010.

[101] H. Yin, R. L. Kanasty, A. A. Eltoukhy, A. J. Vegas, J. R. Dorkin, and D. G. Anderson, “Non-viral vectors for gene-based therapy,” *Nat. Rev. Genet.*, vol. 15, no. 8, pp. 541–555, 2014.

[102] N. Somia and I. M. Verma, “Gene therapy: trials and tribulations,” *Nat. Rev. Genet.*, vol. 1, no. 2, p. 91, 2000.

[103] K. Lundstrom, “Viral Vectors in Gene Therapy,” *Diseases*, vol. 6, no. 42, pp. 1–20, 2018.

[104] S. G. Stolberg, “The Biotech Death of Jesse Gelsinger,” *The New York Times Magazine*, 1999.

[105] S. L. Ginn, A. K. Amaya, M. R. Abedi, I. E. Alexander, and M. Edelstein, “Gene therapy clinical trials worldwide to 2017 : An update,” *J. Gene Med.*, vol. 20, no. 5, p. e3015, 2018.

[106] US Food and Drug Administration., “FDA Approval Brings First Gene Therapy to the United States. CAR T-Cell Therapy Approved to Treat Certain Children and Young Adults with B-Cell Acute Lymphoblastic Leukemia.,” 2017. [Online]. Available: https://www.fda.gov/NewsEvents/Newsroom/PressAnnouncements/ucm574058.htm.

[107] D. L. Porter, B. L. Levine, M. Kalos, A. Bagg, and C. H. June, “Chimeric Antigen Receptor–Modified T Cells in Chronic Lymphoid Leukemia,” *N. Engl. J. Med.*, vol. 365, no. 8, pp. 725–733, 2011.

[108] D. M. O. Rourke, M. P. Nasrallah, A. Desai, J. J. Melenhorst, K. Mansfield, J. J. D. Morrissette, M. Martinez-lage, S. Brem, E. Maloney, A. Shen, R. Isaacs, S. Mohan, G. Plesa, S. F. Lacey, J. Navenot, Z. Zheng, B. L. Levine, H. Okada, C. H. June, J. L. Brogdon, and M. V Maus, “A single dose of peripherally infused EGFRvIII-directed CAR T cells mediates antigen loss and induces adaptive resistance in patients with recurrent glioblastoma,” *Sci. Transl. Med.*, vol. 9, no. 399, p. 0984, 2017.

[109] US Food and Drug Administration., “Luxturna Statistical Review. US Food and Drug Administration Center for Drug Evaluation and Research.,” 2017.

[110] C. Morrison, “$ 1-million price tag set for Glybera gene therapy,” *Nat. Publ. Gr.*, vol. 33, no. 3, pp. 217–218, 2015.

[111] N. Touchot and M. Flume, “Early Insights from Commercialization of Gene,” *Genes (Basel).*, vol. 8, no. 2, p. 78, 2017.

[112] A. Zhang, “Market Access of Advanced Therapy Medicinal Product (ATMP) in Europe: Lessons Learnt And Key Considerations for Future Success,” *Value Heal.*, vol. 20, no. 9, p. A696, 2017.

[113] N. Nayerossadat, T. Maedeh, and P. A. Ali, “Viral and nonviral delivery systems for gene delivery,” *Adv. Biomed. Res.*, vol. 1, 2012.

[114] A. Hacobian and D. Hercher, “Pushing the Right Buttons : Improving Efficacy of Therapeutic DNA Vectors,” *Tissue Eng. Part B Rev.*, vol. 24, no. 3, pp. 226–239, 2018.

[115] E. P. Papapetrou, P. G. Ziros, I. D. Micheva, N. C. Zoumbos, and A. Athanassiadou, “Gene transfer into human hematopoietic progenitor cells with an episomal vector carrying an S / MAR element,” *Gene Ther.*, vol. 13, no. 1, pp. 40–51, 2006.

[116] D. J. Glover, H. J. Lipps, and D. A. Jans, “TOWARDS SAFE , NON-VIRAL THERAPEUTIC GENE EXPRESSION IN HUMANS,” *Nat. Rev. Genet.*, vol. 6, no. 4, p. 299, 2005.

[117] E. W. F. W. Alton, D. K. Armstrong, D. Ashby, K. J. Bayfi, D. Bilton, E. V Bloomfi, A. C. Boyd, J. Brand, R. Buchan, R. Calcedo, P. Carvelli, M. Chan, S. H. Cheng, D. D. S. Collie, S. Cunningham, H. E. Davidson, G. Davies, J. C. Davies, L. A. Davies, M. H. Dewar, A. Doherty, J. Donovan, N. S. Dwyer, H. I. Elgmati, R. F. Featherstone, J. Gavino, S. Gea-sorli, D. M. Geddes, J. S. R. Gibson, D. R. Gill, A. P. Greening, U. Griesenbach, D. M. Hansell, K. Harman, T. E. Higgins, S. L.

Hodges, S. C. Hyde, L. Hyndman, J. A. Innes, J. Jacob, N. Jones, B. F. Keogh, M. P. Limberis, P. Lloyd-evans, A. W. Maclean, M. C. Manvell, G. D. Murray, A. G. Nicholson, T. Osadolor, J. Parra-leiton, D. J. Porteous, I. A. Pringle, E. K. Punch, K. M. Pytel, A. L. Quittner, G. Rivellini, C. J. Saunders, R. K. Scheule, S. Sheard, N. J. Simmonds, K. Smith, S. N. Smith, N. Soussi, S. Soussi, E. J. Spearing, B. J. Stevenson, S. G. Sumner-jones, M. Turkkila, R. P. Ureta, and M. D. Waller, "Repeated nebulisation of non-viral CFTR gene therapy in patients with cystic fi brosis : a randomised , double-blind , placebo-controlled , phase 2b trial," *Lancet Respir Med*, vol. 3, no. 9, pp. 684–691, 2015.

[118] F. Scherer, M. Anton, U. Schillinger, J. Henke, C. Bergemann, A. Kruger, B. Gansbacher, and C. Plank, "Magnetofection: enhancing and targeting gene delivery by magnetic force in vitro and in vivo," *Gene Ther.*, vol. 9, pp. 102–109, 2002.

[119] H. Cornelia, K. Roberto, T. Brill, C. Plank, K. Helmut, S. Krieger, and U. Schillinger, "Neoadjuvant gene delivery of feline granulocyte-macrophage colony-stimulating factor using magnetofection for the treatment of feline fibrosarcomas : a phase I trial," *J. Gene Med. a cross-disciplinary J. Res. Sci. gene Transf. its Appl.*, vol. 10, no. 6, pp. 655–667, 2008.

[120] S. Xenariou, U. Griesenbach, S. Ferrari, P. Dean, R. K. Scheule, S. H. Cheng, and D. M. Geddes, "Using magnetic forces to enhance non-viral gene transfer to airway epithelium in vivo," *Gene Ther.*, vol. 13, no. 21, pp. 1545–1552, 2006.

[121] L. Prosen, S. Hudoklin, M. Cemazar, M. Stimac, U. Lampreht Tratar, M. Ota, and G. Sersa, "Magnetic field contributes to the cellular uptake for effective therapy with magnetofection using plasmid DNA encoding against Mcam in B16F10

melanoma in vivo," *Nanomedicine*, vol. 11, no. 6, pp. 627–641, 2016.

[122] A. Jahnke, J. Hirschberger, C. Fischer, T. Brill, R. Köstlin, C. Plank, and U. Schillinger, "Intra-tumoral Gene Delivery of feIL-2 , feIFN- c and feGM-CSF using Magnetofection as a Neoadjuvant Treatment Option for Feline Fibrosarcomas : A Phase-I Study," *J. Vet. Med. Ser. A*, vol. 54, no. 10, pp. 599–606, 2007.

[123] H. Peng, J. Ye, S. Loong, Y. Wang, W. Min, X. Sheng, J. Min, and S. Wang, "Gene transfer using self-assembled ternary complexes of cationic magnetic nanoparticles , plasmid DNA and cell-penetrating Tat peptide," *Biomaterials*, vol. 31, no. 4, pp. 769–778, 2010.

[124] C. Soto-sánchez, G. Martínez-Navarrete, L. Humphreys, G. Puras, J. Zarate, J. L. Pedraz, and E. Fernández, "Enduring high-efficiency in vivo transfection of neurons with non-viral magnetoparticles in the rat visual cortex for optogenetic applications," *Nanomedicine Nanotechnology, Biol. Med.*, vol. 11, no. 4, pp. 835–843, 2015.

[125] M. Dowaidar, H. N. Abdelhamid, M. Hällbrink, and K. Freimann, "Magnetic Nanoparticle Assisted Self-assembly of Cell Penetrating Complexes for Gene Delivery," *Sci. Rep.*, vol. 7, no. 1, p. 9159, 2017.

[126] C. Plank, O. Zelphati, and O. Mykhaylyk, "Magnetically enhanced nucleic acid delivery. Ten years of magnetofection-Progress and prospects," *Adv. Drug Deliv. Rev.*, vol. 63, no. 14–15, pp. 1300–1331, 2011.

[127] G. Guidotti, L. Brambilla, and D. Rossi, "Cell-Penetrating Peptides : From Basic Research to Clinics," *Trends Pharmacol. Sci.*, vol. 38, no. 4, pp. 406–424, 2017.

[128] S. Reissmann, "Cell penetration : scope and limitations by the application of

cell-penetrating peptides," *J. Pept. Sci.*, vol. 20, no. 10, pp. 760–784, 2014.

[129] M. Green and P. M. Loewenstein, "Autonomous Functional Domains of Chemically Synthesized Human lmmunodeficiency Virus Tat Trans-Activator Protein," *Cell*, vol. 55, no. 6, pp. 1179–1188, 1988.

[130] A. D. Frankel and C. O. Pabo, "Cellular Uptake of the Tat Protein from Human lmmunodeficiency Virus," *Cell*, vol. 55, no. 6, pp. 1189–1193, 1988.

[131] L. D. Vasconcelos and U. Langel, "Therapeutic potential of cell-penetrating peptides," *Ther. Deliv.*, vol. 4, no. 5, pp. 573–591, 2013.

[132] J. B. Rothbard, S. Garlington, Q. Lin, T. Kirschberg, E. Kreider, McGrane, and P. A. Khavari, "Conjugation of arginine oligomers to cyclosporin A facilitates topical delivery and inhibition of inflammation," *Nat. Med.*, vol. 6, no. 11, pp. 1253–1257, 2000.

[133] E. Koren and V. P. Torchilin, "Cell-penetrating peptides : breaking through to the other side," *Trends Mol. Med.*, vol. 18, no. 7, pp. 386–394, 2012.

[134] L. B. Lopes, E. J. Furnish, P. Komalavilas, C. R. Flynn, A. Panitch, and C. M. Brophy, "Cell permeant peptide analogues of the small heat shock protein, HSP20, reduce TGF-beta1induced CTGF expression in keloid fibroblasts," *J. Invest. Dermatol.*, vol. 129, no. 3, pp. 590–598, 2009.

[135] M. A. Warso, J. M. Richards, D. Mehta, K. Christov, C. Schaeffer, L. R. Bressler, T. Yamada, D. Majumdar, S. A. Kennedy, C. W. Beattie, and T. K. Das Gupta, "A first-in-class , first-in-human , phase I trial of p28 , a non-HDM2-mediated peptide inhibitor of p53 ubiquitination in patients with advanced solid tumours," *Br. J. Cancer*, vol. 108, no. 5, pp. 1061–1070, 2013.

[136] S. S. Usmani, G. Bedi, J. S. Samuel, S. Singh, S. Kalra, P. Kumar, A. A. Ahuja, M. Sharma, A. Gautam, and G. P. S. Raghava, "THPdb : Database of FDA-approved peptide and protein therapeutics," *PLoS One*, vol. 12, no. 7, pp. 1–12, 2017.

[137] M. S. Wadhwa, W. T. Collard, R. C. Adami, D. L. Mckenzie, and K. G. Rice, "Peptide-Mediated Gene Delivery : Influence of Peptide Structure on Gene Expression," *Bioconjug. Chem.*, vol. 8, no. 1, pp. 81–88, 1997.

[138] A. Eguchi, T. Akuta, H. Okuyama, T. Senda, H. Yokoi, H. Inokuchi, S. Fujita, T. Hayakawa, K. Takeda, M. Hasegawa, and M. Nakanishi, "Protein Transduction Domain of HIV-1 Tat Protein Promotes Efficient Delivery of DNA into Mammalian Cells *," vol. 276, no. 28, pp. 26204–26210, 2001.

[139] A. F. Saleh, H. Aojula, Y. Arthanari, S. Offerman, M. Alkotaji, and A. Pluen, "Improved Tat-mediated plasmid DNA transfer by fusion to LK15 peptide ARTICLE IN PRESS ARTICLE IN PRESS," *J. Control. Release*, vol. 143, no. 2, pp. 233–242, 2010.

[140] A. F. A. Saleh, H. S. Aojula, and A. Pluen, "Enhancement of gene transfer using YIGSR analog of Tat-derived peptide," *Biopolym. Orig. Res. Biomol.*, vol. 89, no. 1, pp. 17–21, 2007.

[141] I. A. Ignatovich, E. B. Dizhe, A. V Pavlotskaya, B. N. Akifiev, S. V Burov, S. V Orlov, and A. P. Perevozchikov, "Complexes of Plasmid DNA with Basic Domain 47 – 57 of the HIV-1 Tat Protein Are Transferred to Mammalian Cells by Endocytosis-mediated Pathways *," *J. Biol. Chermistry*, vol. 278, no. 43, pp. 42625–42636, 2003.

[142] I. A. Khalil, S. Kimura, Y. Sato, and H. Harashima, "Synergism between a cell

penetrating peptide and a pH-sensitive cationic lipid in e ffi cient gene delivery based on double-coated nanoparticles," *J. Control. Release*, vol. 275, no. February, pp. 107–116, 2018.

[143] Y. Hu, B. Xu, Q. Ji, D. Shou, X. Sun, J. Xu, J. Gao, and W. Liang, "A mannosylated cell-penetrating peptide-graft-polyethylenimine as a gene delivery vector," *Biomaterials*, vol. 35, no. 13, pp. 4236–4246, 2014.

[144] J. Nguyen, R. Reul, J. Sitterberg, T. Schmehl, T. Gessler, W. Seeger, and T. Kissel, "Effects of cell-penetrating peptides and pegylation on transfection efficiency of polyethylenimine in mouse lungs," *J. Gene Med. a cross-disciplinary J. Res. Sci. gene Transf. its Appl.*, vol. 10, no. 11, pp. 1236–1246, 2008.

[145] S. Yamano, J. Dai, S. Hanatani, K. Haku, T. Yamanaka, M. Ishioka, T. Takayama, C. Yuvienco, S. Khapli, A. M. Moursi, and J. K. Montclare, "Long-term efficient gene delivery using polyethylenimine with modi fi ed Tat peptide," *Biomaterials*, vol. 35, no. 5, pp. 1705–1715, 2014.

[146] L. Peng, J. Niu, C. Zhang, W. Yu, J. Wu, Y. Shan, and J. Gao, "TAT conjugated cationic noble metal nanoparticles for gene delivery to epidermal stem cells," *Biomaterials*, vol. 35, no. 21, pp. 5605–5618, 2014.

[147] D. Rahmat, M. I. Khan, G. Shahnaz, D. Sakloetsakun, G. Perera, and A. Bernkop-schnürch, "Synergistic effects of conjugating cell penetrating peptides and thiomers on non-viral transfection ef fi ciency," *Biomaterials*, vol. 33, no. 7, pp. 2321–2326, 2012.

[148] K. Veiman, K. Künnapuu, T. Lehto, K. Kiisholts, K. Pärn, Ü. Langel, and K. Kurrikoff, "PEG shielded MMP sensitive CPPs for ef fi cient and tumor speci fi c

gene delivery in vivo," *J. Control. Release*, vol. 209, pp. 238–247, 2015.

[149] V. P. Torchilin, T. S. Levchenko, R. Rammohan, N. Volodina, B. Papahadjopoulos-sternberg, and G. G. M. D. Souza, "Cell transfection in vitro and in vivo with nontoxic TAT peptide-liposome – DNA complexes," *Proc. Natl. Acad. Sci.*, vol. 100, no. 4, pp. 1972–1977, 2003.

[150] Q. Jiang, L. Lai, J. Shen, Q. Wang, F. Xu, and G. Tang, "Gene delivery to tumor cells by cationic polymeric nanovectors coupled to folic acid and the cell-penetrating peptide octaarginine," *Biomaterials*, vol. 32, no. 29, pp. 7253–7262, 2011.

[151] S. Mussa, A. Valizadeh, H. Karami, and S. Mohammadi, "Cell penetrating peptides : Efficient vectors for delivery of nanoparticles , nanocarriers , therapeutic and diagnostic molecules," *Peptides*, vol. 57, pp. 78–94, 2014.

[152] H. W. Child, P. A. Pino, J. M. D. La Fuente, A. S. Hursthouse, D. Stirling, M. Mullen, G. M. Mcphee, C. Nixon, V. Jayawarna, and C. C. Berry, "Working Together : The Combined Application of a Magnetic Field and Penetratin for the Delivery of Magnetic Nanoparticles to Cells in 3D," *ACS Nano*, vol. 5, no. 10, pp. 7910–7919, 2011.

[153] C. Wang, L. Qiao, Q. Zhang, H. Yan, and K. Liu, "Enhanced cell uptake of superparamagnetic iron oxide nanoparticles through direct chemisorption of FITC-Tat-PEG 600 - b -poly (glycerol monoacrylate)," *Int. J. Pharm.*, vol. 430, no. 1–2, pp. 372–380, 2012.

[154] A. K. Hauser, M. I. Mitov, E. F. Daley, R. C. Mcgarry, K. W. Anderson, and J. Z. Hilt, "Targeted iron oxide nanoparticles for the enhancement of radiation

therapy," *Biomaterials*, vol. 105, pp. 127–135, 2016.

[155] L. Josephson, C. Tung, A. Moore, and R. Weissleder, "High-Efficiency Intracellular Magnetic Labeling with Novel Superparamagnetic-Tat Peptide Conjugates," *Bioconjug. Chem.*, vol. 10, no. 2, pp. 186–191, 1999.

[156] M. Zhao, M. F. Kircher, L. Josephson, and R. Weissleder, "Differential Conjugation of Tat Peptide to Superparamagnetic Nanoparticles and Its Effect on Cellular Uptake," *Bioconjug. Chem.*, vol. 13, no. 4, pp. 840–844, 2002.

[157] E. Perillo, K. Hervé-aubert, E. Allard-vannier, A. Falanga, S. Galdiero, and I. Chourpa, "Synthesis and in vitro evaluation of fluorescent and magnetic nanoparticles functionalized with a cell penetrating peptide for cancer theranosis," *J. Colloid Interface Sci.*, vol. 499, pp. 209–217, 2017.

[158] K. Koutsiouki, A. Angelopoulou, E. Ioannou, E. Voulgari, A. Sergides, G. E. Magoulas, A. Bakandritsos, and K. Avgoustakis, "Research Article TAT Peptide-Conjugated Magnetic PLA-PEG Nanocapsules for the Targeted Delivery of Paclitaxel : In Vitro and Cell Studies," *AAPS PharmSci Tech*, vol. 18, no. 3, pp. 769–781, 2017.

[159] M. Lewin, N. Carlesso, C. Tung, X. Tang, D. Cory, D. T. Scadden, and R. Weissleder, "Tat peptide-derivatized magnetic nanoparticles allow in vivo tracking and recovery of progenitor cells," *Nat. Biotechnol.*, vol. 18, no. 4, pp. 410–414, 2000.

[160] C. H. Dodd, H. Hsu, W. Chu, P. Yang, H. Zhang, J. D. Mountz, K. Zinn, J. Forder, L. Josephson, R. Weissleder, J. M. Mountz, and J. D. Mountz, "Normal T-cell response and in vivo magnetic resonance imaging of T cells loaded with HIV

transactivator-peptide-derived superparamagnetic nanoparticles," *J. Immunol. Methods*, vol. 256, no. 1–2, pp. 89–105, 2001.

[161] P. Wunderbaldinger, L. Josephson, and R. Weissleder, "Tat Peptide Directs Enhanced Clearance and Hepatic Permeability of Magnetic Nanoparticles," *Bioconjug. Chem.*, vol. 13, no. 2, pp. 264–268, 2002.

[162] H. P. Song, J. Ye, S. Loong, Y. Wang, W. Min, X. Sheng, J. Min, and S. Wang, "Gene transfer using self-assembled ternary complexes of cationic magnetic nanoparticles , plasmid DNA and cell-penetrating Tat peptide," *Biomaterials*, vol. 31, pp. 769–778, 2010.

[163] J. E. Dixon, G. Osman, G. E. Morris, H. Markides, M. Rotherham, Z. Bayoussef, A. J. El Haj, and K. M. Shakesheff, "Highly efficient delivery of functional cargoes by the synergistic effect of GAG binding motifs and cell-penetrating peptides," *Proc. Natl. Acad. Sci.*, vol. 113, no. 3, pp. E291–E299, 2016.

[164] H. M. Eltaher, J. Yang, K. M. Shakesheff, and J. E. Dixon, "Highly efficient intracellular transduction in three-dimensional gradients for programming cell fate," *Acta Biomater.*, pp. 1–12, 2016.

[165] L. Thiagarajan, H. A. M. Abu-awwad, and J. E. Dixon, "Osteogenic Programming of Human Mesenchymal Stem Cells with Highly Efficient Intracellular Delivery of RUNX2," *Stem Cells Transl. Med.*, vol. 6, no. 12, pp. 2146–2159, 2017.

[166] H. A. M. Abu-awwad, L. Thiagarajan, and J. E. Dixon, "Controlled release of GAG-binding enhanced transduction (GET) peptides for sustained and highly efficient intracellular delivery," *Acta Biomater.*, vol. 57, pp. 225–237, 2017.

[167] G. Osman, J. Rodriguez, S. Yan, J. Chisholm, G. Duncan, N. Kim, A. L. Tatler, K.

M. Shakeshe, J. Hanes, J. Soo, and J. E. Dixon, “PEGylated enhanced cell penetrating peptide nanoparticles for lung gene therapy,” *J. Control. Release*, vol. 285, pp. 35–45, 2018.

[168] A. Salvati, A. S. Pitek, M. P. Monopoli, K. Prapainop, F. B. Bombelli, D. R. Hristov, P. M. Kelly, C. Åberg, E. Mahon, and K. a Dawson, “Transferrin-functionalized nanoparticles lose their targeting capabilities when a biomolecule corona adsorbs on the surface.,” *Nat. Nanotechnol.*, vol. 8, no. 2, pp. 137–43, 2013.

[169] C. J. Cheng, G. T. Tietjen, J. K. Saucier-sawyer, and W. M. Saltzman, “A holistic approach to targeting disease with polymeric nanoparticles,” *Nat. Rev.*, vol. 14, no. April, 2015.

[170] L. B. Kim E. Sapsford, W. Russ Algar, “Functionalizing Nanoparticles with Biological Molecules: Developing Chemistries that Facilitate Nanotechnology,” *Chem. Rev.*, vol. 113, no. 3, p. 1904−2074, 2013.

[171] M. Muthana, A. J. Kennerley, R. Hughes, E. Fagnano, J. Richardson, M. Paul, C. Murdoch, F. Wright, C. Payne, M. F. Lythgoe, N. Farrow, J. Dobson, J. Conner, J. M. Wild, and C. Lewis, “Directing cell therapy to anatomic target sites in vivo with magnetic resonance targeting,” *Nat. Commun.*, vol. 6, p. 8009, 2015.

[172] C. F. Adams, M. R. Pickard, and D. M. Chari, “Magnetic nanoparticle mediated transfection of neural stem cell suspension cultures is enhanced by applied oscillating magnetic fields,” *Nanomedicine Nanotechnology, Biol. Med.*, vol. 9, no. 6, pp. 737–741, 2013.

[173] M. Pickard and D. Chari, “Enhancement of magnetic nanoparticle-mediated gene transfer to astrocytes by ‘ magnetofection ’: effects of static and oscillating

fields R esearch A rticle," *Nanomedicine*, vol. 5, no. 2, pp. 217–232, 2010.

[174] M. Subramanian, J. Lim, and J. Dobson, "Enhanced Nanomagnetic Gene Transfection of Human Prenatal Cardiac Progenitor Cells and Adult Cardiomyocytes," *PLoS One*, vol. 8, no. 7, 2013.

[175] P. Roach, D. Farrar, and C. C. Perry, "Surface Tailoring for Controlled Protein Adsorption : Effect of Topography at the Nanometer Scale and Chemistry," *J. Am. Chem. Soc.*, vol. 17, no. 7, pp. 617–621, 2006.

[176] G. Kemmer and S. Keller, "Nonlinear least-squares data fitting in Excel spreadsheets," *Nat. Protoc.*, vol. 5, no. 2, pp. 267–281, 2010.

[177] R. A. Latour, "The Langmuir isotherm : A commonly applied but misleading approach for the analysis of protein adsorption behavior," *J. Biomed. Mater. Res. Part A,* vol. 103, no. 3, pp. 949–958, 2015.

[178] H. Markides, K. J. Newell, H. Rudorf, L. B. Ferreras, J. E. Dixon, R. H. Morris, M. Graves, J. Kaggie, F. Henson, and A. J. El Haj, "Ex vivo MRI cell tracking of autologous mesenchymal stromal cells in an ovine osteochondral defect model," *Stem Cell Res. Ther.*, vol. 10, no. 1, p. 25, 2019.

[179] Y. Murayama and M. Sano, "Exchange of Counterions in," *Biopolymers*, vol. 77, pp. 354–360, 2005.

[180] D. Marie, D. Vaulot, R. I. C. Partensky, S. Biologique, C. National, D. Recherche, M. E. T. Al, and A. P. P. L. E. N. M. Icrobiol, "Application of the Novel Nucleic Acid Dyes YOYO-1 , YO-PRO-1 , and PicoGreen for Flow Cytometric Analysis of Marine Prokaryotes," *Appl. Environ. Microbiol.*, vol. 62, no. 5, pp. 1649–1655, 1996.

[181] First4Magnets, “First4Magnets.” [Online]. Available: https://www.first4magnets.com/circular-disc-rod-magnets-c34/10mm-dia-x-5mm-thick-ultra-high-performance-n52-neodymium-magnet-3-2kg-pull-p3591#ps_1-3119.

[182] M. Cruz-acuna, L. Maldonado-camargo, J. Dobson, and C. Rinaldi, “From oleic acid-capped iron oxide nanoparticles to polyethyleneimine-coated single-particle magnetofectins,” *J. Nanoparticle Res.*, vol. 18, no. 9, p. 268, 2016.

[183] O. A. Ali and D. J. Mooney, “Sustained GM-CSF and PEI condensed pDNA presentation increases the level and duration of gene expression in dendritic cells,” *J. Control. Release*, vol. 132, no. 3, pp. 273–278, 2008.

[184] J. Dobson and C. D. Batich, “US8232102_Gene_Delivery.pdf,” 2012.

[185] M. Subramanian, A. Tyler, E. M. Luther, E. Di Daniel, J. Lim, and J. Dobson, “Oscillating Magnet Array − Based Nanomagnetic Gene Transfection : A Valuable Tool for Molecular Neurobiology Studies,” *Nanomaterials*, vol. 7, no. 2, p. 28, 2017.

[186] I. Strobel, S. Berchtold, A. Gotze, U. Schulze, G. Schuler, and A. Steinkasserer, “Human dendritic cells transfected with either RNA or DNA encoding influenza matrix protein M1 differ in their ability to stimulate cytotoxic T lymphocytes,” *Gene Ther.*, vol. 7, no. 23, pp. 2028–2035, 2000.

[187] S. C. Mcbain, U. Griesenbach, S. Xenariou, A. Keramane, C. D. Batich, E. W. F. W. Alton, and J. Dobson, “Magnetic nanoparticles as gene delivery agents : enhanced transfection in the presence of oscillating magnet arrays,” *Nanotechnology*, vol. 19, no. 40, p. 405102, 2008.

[188] A. Fouriki, N. Farrow, M. A. Clements, and J. Dobson, “Evaluation of the magnetic field requirements for nanomagnetic gene transfection,” *Nano Rev.*, vol. 1, no. 1, p. 5167, 2010.

[189] M. Safi, J. Courtois, M. Seigneuret, H. Conjeaud, and J. Berret, “The effects of aggregation and protein corona on the cellular internalization of iron oxide nanoparticles,” *Biomaterials*, vol. 32, no. 35, pp. 9353–9363, 2011.

[190] M. F. C. C. Facility, “Autofluorescence.” .

[191] M. Arsianti, M. Lim, C. P. Marquis, and R. Amal, “Polyethylenimine Based Magnetic Iron-Oxide Vector : The Effect of Vector Component Assembly on Cellular Entry Mechanism , Intracellular Localization , and Cellular Viability,” pp. 2521–2531, 2010.

[192] R. G. W. A. J. E. Heuser, “Hypertonic Media Inhibit Receptor-mediated Endocytosis by Blocking Clathrin-coated Pit Formation,” *J. Cell Biol.*, vol. 108, no. February, pp. 389–400, 1989.

[193] B. R. Liu, Y. Huang, and H. Lee, “Mechanistic studies of intracellular delivery of proteins by cell-penetrating peptides in cyanobacteria Mechanistic studies of intracellular delivery of proteins by cell-penetrating peptides in cyanobacteria,” *BMC Microbiol.*, vol. 13, no. 57, pp. 1471–2180, 2013.

[194] I. S. Zuhorna, R. Kalicharanb, and D. Hoekstraa, “Lipoplex-mediated transfection of mammalian cells occurs through the cholesterol-dependent clathrin-mediated pathway of endocytosis,” *J. Biol. Chermistry*, pp. 31–50, 2002.

[195] J. Rejman, V. Oberle, I. S. Zuhorn, and D. Hoekstra, “Size-dependent internalization of particles via the pathways of clathrin- and caveolae-mediated

endocytosis," vol. 169, pp. 159–169, 2004.

[196] S. Tenzer, D. Docter, J. Kuharev, A. Musyanovych, V. Fetz, R. Hecht, F. Schlenk, D. Fischer, K. Kiouptsi, C. Reinhardt, K. Landfester, H. Schild, M. Maskos, S. K. Knauer, and R. H. Stauber, "Rapid formation of plasma protein corona critically affects nanoparticle pathophysiology," *Nat. Nanotechnol.*, vol. 8, no. 10, pp. 772–781, 2013.

[197] A. Lesniak, A. Salvati, Santos-Martinez, R. M. J., D. M. W., and C. K. A., & Åberg, "Nanoparticle Adhesion to the Cell Membrane and Its E ff ect on Nanoparticle Uptake E ffi ciency," *J. Am. Chem. Soc.*, vol. 135, no. 4, pp. 1438–1444, 2013.

[198] M. P. Monopoli, D. Walczyk, A. Campbell, G. Elia, I. Lynch, F. Baldelli Bombelli, and K. A. Dawson, "Physical-Chemical aspects of protein corona: Relevance to in vitro and in vivo biological impacts of nanoparticles," *J. Am. Chem. Soc.*, vol. 133, no. 8, pp. 2525–2534, 2011.

[199] L. Treuel, S. Brandholt, P. Maffre, S. Wiegele, L. Shang, and G. U. Nienhaus, "Impact of protein modification on the protein corona on nanoparticles and nanoparticle-cell interactions," *ACS Nano*, vol. 8, no. 1, pp. 503–513, 2014.

[200] C. C. Fleischer and C. K. Payne, "Nanoparticle − Cell Interactions: Molecular Structure of the Protein Corona and Cellular Outcomes," 2014.

[201] D. Docter, D. Westmeier, M. Markiewicz, S. Stolte, and S. K. Knauer, "The nanoparticle biomolecule corona : lessons learned – challenge accepted ?," *Chem. Soc. Rev.*, vol. 44, no. 17, pp. 6094–6121, 2015.

[202] M. P. Monopoli, C. Åberg, A. Salvati, and K. A. Dawson, "Biomolecular coronas provide the biological identity of nanosized materials," *Nat. Nanotechnol.*, vol.

7, no. 12, pp. 779–786, 2012.

[203] S. C. McBain, H. H. P. Yiu, A. El Haj, and J. Dobson, “Polyethyleneimine functionalized iron oxide nanoparticles as agents for DNA delivery and transfection,” *J. Mater. Chem.*, vol. 17, no. 24, p. 2561, 2007.

[204] J. Stetefeld, S. A. Mckenna, and T. R. Patel, “Dynamic light scattering : a practical guide and applications in biomedical sciences,” *Biophys. Rev.*, pp. 409–427, 2016.

[205] C. M. Alves, R. L. Reis, and J. A. Hunt, “The competitive adsorption of human proteins onto natural-based biomaterials,” no. February, pp. 1367–1377, 2010.

[206] M. Rabe, D. Verdes, and S. Seeger, “Understanding protein adsorption phenomena at solid surfaces,” *Adv. Colloid Interface Sci.*, vol. 162, no. 1–2, pp. 87–106, 2011.

[207] P. Roach, “Interpretation of Protein Adsorption : Surface- Induced Conformational Changes,” no. July, 2005.

[208] I. Amenabar, S. Poly, W. Nuansing, E. H. Hubrich, A. A. Govyadinov, F. Huth, R. Krutokhvostov, L. Zhang, M. Knez, J. Heberle, A. M. Bittner, and R. Hillenbrand, “Structural analysis and mapping of individual protein complexes by infrared nanospectroscopy.,” *Nat. Commun.*, vol. 4, p. 2890, 2013.

[209] B. S. Kendrick, A. Dong, S. D. Allison, M. C. Manning, and J. F. Carpenter, “Quantitation of the area of overlap between second-derivative amide I infrared spectra to determine the structural similarity of a protein in different states,” *J. Pharm. Sci.*, vol. 85, no. 2, pp. 155–158, 1996.

[210] W. Cui, J. Li, Y. Zhang, H. Rong, W. Lu, and L. Jiang, “Effects of aggregation and

the surface properties of gold nanoparticles on cytotoxicity and cell growth," *Nanomedicine Nanotechnology, Biol. Med.*, vol. 8, no. 1, pp. 46–53, 2012.

[211] D. Press, "Endocytosis and exocytosis of nanoparticles in mammalian cells," pp. 51–63, 2014.

[212] A. Albanese and W. C. W. Chan, "Effect of gold nanoparticle aggregation on cell uptake and toxicity," *ACS Nano*, vol. 5, no. 7, pp. 5478–5489, 2011.

[213] C. Marty, "Antennapedia and HIV Transactivator of Transcription (TAT) ' Protein Transduction Domains ' Promote Endo .... University of Zurich Zurich Open Repository and Archive," no. October, 2003.

[214] J. R. Fromm, R. E. Hileman, E. E. O. Caldwell, J. M. Weiler, and R. J. Linhardt, "Differences in the Interaction of Heparin with Arginine and Lysine and the Importance of these Basic Amino Acids in the Binding of Heparin to Acidic Fibroblast Growth Factor 1," *Arch. Biochem. Biophys.*, vol. 323, no. 2, pp. 279–287, 1995.

[215] C. Huang, T. Ger, Z. Wei, and M. Lai, "Compare Analysis for the Nanotoxicity Effects of Different Amounts of Compare Analysis for the Nanotoxicity Effects of Different Amounts of Endocytic Iron Oxide Nanoparticles at Single Cell Level," *PLoS One*, vol. 9, no. 5, p. e96550, 2014.

[216] X. Wang, X. Hu, J. Li, A. C. M. Russe, N. Kawazoe, Y. Yang, and G. Chen, "Influence of cell size on cellular uptake of gold nanoparticles," *Biomater. Sci.*, vol. 4, no. 6, pp. 970–978, 2016.

[217] M. R. Birtwister and B. N. Kholodenko, "Endocytosis and signalling : a meeting with mathematics," vol. 3, no. 4, pp. 308–320, 2010.

[218] C. C. Fleischer and C. K. Payne, “Nanoparticle − Cell Interactions: Molecular Structure of the Protein Corona and Cellular Outcomes,” *Acc. Chem. Res.*, vol. 47, no. 8, pp. 2651–2659, 2014.

[219] M. Lundqvist, C. Augustsson, M. Lilja, and K. Lundkvist, “The nanoparticle protein corona formed in human blood or human blood fractions,” *PLoS One*, pp. 1–15, 2017.

[220] C. Biology, V. Mirshafiee, R. Kim, M. Mahmoudi, and M. L. Kraft, “The importance of selecting a proper biological milieu for protein corona analysis in vitro : Human plasma versus human serum,” *Int. J. Biochem. Cell Biol.*, vol. 75, pp. 188–195, 2016.

[221] A. Farrugia, “Albumin Usage in Clinical Medicine: Tradition or Therapeutic?,” *Transfus. Med. Rev.*, vol. 24, no. 1, pp. 53–63, 2010.

[222] B. Meloun, L. Moravek, and V. Kostka, “Complete amino acid sequence of human serum albumin,” *FEBS Lett.*, vol. 58, no. 1–2, pp. 134–137, 1975.

[223] A. Salvati, C. Åberg, T. Santos, J. Varela, P. Pinto, I. Lynch, and K. A. Dawson, “Experimental and theoretical comparison of intracellular import of polymeric nanoparticles and small molecules : toward models of uptake kinetics,” *Nanomedicine Nanotechnology, Biol. Med.*, vol. 7, no. 6, pp. 818–826, 2011.

[224] L. VROMAN, “Effect of Adsorbed Proteins on the Wettability of Hydrophilic and Hydrophobic Solids,” *Nature*, vol. 196, no. 4853, pp. 476–477, 1962.

[225] M. A. Dobrovolskaia, D. R. Germolec, and J. L. Weaver, “Evaluation of nanoparticle immunotoxicity,” *Nat. Nanotechnol.*, vol. 4, no. 7, pp. 411–414, 2009.

[226] J. D. Moyer, R. B. Nowak, N. E. Kim, S. K. Larkin, L. L. Peters, J. Hartwig, F. A. Kuypers, and V. M. Fowler, “Tropomodulin 1-null mice have a mild spherocytic elliptocytosis with appearance of Tropomodulin 3 in red blood cells and disruption of the membrane skeleton,” *RED CELLS, IRON, Erythrop.*, vol. 116, no. 14, pp. 2590–2600, 2010.

[227] M. Friebel, J. Helfmann, and M. Meinke, “Influence of osmolarity on optical properties of human erythrocytes,” *J. Biomed. Opt.*, vol. 15, no. 5, p. 055005, 2010.

[228] C. Tros, D. Ilarduya, Y. Sun, and N. Düzgünes, “Gene delivery by lipoplexes and polyplexes,” *Eur. jounal Pharm. Sci.*, vol. 40, no. 3, pp. 159–170, 2010.

[229] C. M. Varga, T. J. Wickham, and D. A. Lauffenburger, “Receptor-Mediated Targeting of Gene Delivery Vectors : Insights from Molecular Mechanisms for Improved Vehicle Design,” *Biotechnol. Bioeng.*, vol. 70, no. 6, pp. 563–605, 2000.

[230] C. Plank, U. Schillinger, C. Bergemann, F. Krötz, M. Anton, and J. Rosenecker, “The Magnetofection Method : Using Magnetic Force to Enhance Gene Delivery,” *Biol. Chem.*, vol. 384, no. 5, pp. 737–747, 2003.

[231] O. Mykhaylyk, Y. Sanchez Antequera, D. Vlaskou, and C. Plank, “Generation of magnetic nonviral gene transfer agents and magnetofection in vitro,” *Nat. Protoc.*, vol. 2, no. 10, pp. 2391–2411, 2007.

[232] C. Plank, F. Scherer, U. Schillinger, and M. Anton, “Magnetofection: enhancement and localization of gene delivery with magnetic particles under the influence of a magnetic field,” *J Gene Med,* vol. 2, no. 5, p. S24, 2000.

[233] S. Titze de Almeida, C. Horst, C. Soto-Sánchez, E. Fernandez, and R. Titze de Almeida, “Delivery of miRNA-Targeted Oligonucleotides in the Rat Striatum by Magnetofection with Neuromag®,” *Molecules*, vol. 23, no. 7, p. 1825, 2018.

[234] S. Smolders, S. Kessels, S. M. Smolders, F. Poulhes, O. Zelphati, C. Sapet, and B. Brône, “Magnetofection is superior to other chemical transfection methods in a microglial cell line,” *J. Neurosci. Methods*, vol. 293, pp. 169–173, 2018.

[235] Z. Pan, Z. Shi, H. Wei, F. Sun, J. Song, Y. Huang, and T. Liu, “Magnetofection Based on Superparamagnetic Iron Oxide Nanoparticles Weakens Glioma Stem Cell Proliferation and Invasion by Mediating High Expression of MicroRNA-374a,” *J. cancer*, vol. 7, no. 11, p. 1487, 2016.

[236] J. Singh, I. Mohanty, and X. S. Rattan, “In vivo magnetofection : a novel approach for targeted topical delivery of nucleic acids for rectoanal motility disorders,” *Am. J. Physiol. Liver Physiol.*, vol. 314, no. 1, pp. G109–G118, 2018.

[237] R.-X. Z. and S.-W. H. Wen-Ming Liu, Ya-Nan Xue, Na Peng, Wen-Tao He, “Dendrimer modified magnetic iron oxide nanoparticle / DNA / PEI ternary magnetoplexes : a novel strategy for magnetofection,” *j. mater. chem*, vol. 21, pp. 13306–13315, 2011.

[238] Y. Ma, Z. Zhang, X. Wang, W. Xia, and H. Gu, “Insights into the mechanism of magnetofection using MNPs-PEI / pDNA / free PEI magnetofectins,” *Int. J. Pharm.*, vol. 419, no. 1–2, pp. 247–254, 2011.

[239] S. Sun, Y. Lo, H. Chen, and L. Wang, “Hybrid Polyethylenimine and Polyacrylic Acid-Bound Iron Oxide as a Magnetoplex for Gene Delivery,” *Langmuir*, vol. 7, no. 28, pp. 3542–3552, 2012.

[240] L. Jin, C. Zhang, Y. Deng, Q. Jia, Y. Liu, N. He, L. Wang, and M. Weng, "Polyethylenimine and Chitosan-Based Non-Viral Carriers for Gene Delivery," *Nanosci. Nanotechnol. Lett.*, vol. 10, no. 7, pp. 908–912, 2018.

[241] J. Lee, J. Choo, Y. Choi, K. Lee, D. Min, S. Pi, Y. Seol, S. Lee, I. Jo, C. Chung, and Y. Park, "Characterization of the surface immobilized synthetic heparin binding domain derived from human fibroblast growth factor-2 and its effect on osteoblast differentiation," *J. Biomed. Mater. Res. Part A an Off. J. Soc. Biomater. Japanese Soc. Biomater. Aust. Soc. Biomater. Korean Soc. Biomater.*, vol. 83, no. 4, pp. 970–979, 2007.

[242] A. F. Saleh, H. Aojula, Y. Arthanari, S. Offerman, M. Alkotaji, and A. Pluen, "Improved Tat-mediated plasmid DNA transfer by fusion to LK15 peptide," *J. Control. Release*, vol. 143, no. 2, pp. 233–242, 2010.

[243] H. A. Tajmir-Riahi, C. N. N'Soukpoe-Kossi, and D. Joly, "Structural analysis of protein – DNA and protein – RNA interactions by FTIR , UV-visible and CD spectroscopic methods," *J. Spectrosc.*, vol. 23, no. 2, pp. 81–101, 2009.

[244] S. Huth, J. Lausier, C. Rudolph, C. Plank, U. Welsch, and J. Rosenecker, "Insights into the mechanism of magnetofection using PEI-based magnetofectins for gene transfer," no. December 2003, pp. 923–936, 2004.

[245] R. Wattiaux, N. Laurent, S. W. Coninck, and M. Jadot, "Endosomes, lysosomes: their implication in gene transfer," *Adv. Drug Deliv. Rev.*, vol. 41, no. 2, pp. 201–208, 2000.

[246] L. K. Medina-kauwe and J. Xie, "Intracellular trafficking of nonviral vectors," *Gene Ther.*, vol. 12, no. 24, pp. 1734–1751, 2005.

[247] D. Lechardeur, A. S. Verkman, and G. L. Lukacs, “Intracellular routing of plasmid DNA during non-viral gene transfer,” *Adv. Drug Deliv. Rev.*, vol. 57, no. 5, pp. 755–767, 2005.

[248] S. Mayor and R. E. Pagano, “Pathways of clathrin-independent endocytosis,” *Nat. Rev. Mol. cell Biol.*, vol. 8, no. 8, pp. 603–612, 2007.

[249] J. S. Wadia, R. V Stan, and S. F. Dowdy, “Transducible TAT-HA fusogenic peptide enhances escape of TAT-fusion proteins after lipid raft macropinocytosis,” *Nat. Med.*, vol. 10, no. 3, pp. 310–315, 2004.

[250] G. J. Doherty and H. T. Mcmahon, “Mechanisms of Endocytosis,” *Annu. Rev. Biochem.*, vol. 78, no. March, pp. 857–902, 2009.

[251] C. Wilhelm, F. Gazeau, J. Roger, J. N. Pons, J. Bacri, and M. Curie, “Interaction of Anionic Superparamagnetic Nanoparticles with Cells : Kinetic Analyses of Membrane Adsorption and Subsequent Internalization,” *Langmuir*, vol. 18, no. 21, pp. 8148–8155, 2002.

[252] A. V Weigel, M. M. Tamkun, and D. Krapf, “Quantifying the dynamic interactions between a clathrin-coated pit and cargo molecules,” *Proc. Natl. Acad. Sci.*, vol. 110, no. 48, pp. E4591–E4600, 2013.

[253] N. Murthy, J. R. Robichaud, D. A. Tirrell, P. S. Stayton, and S. Hoffman, “The design and synthesis of polymers for eukaryotic membrane disruption,” *J. Control. Release*, vol. 61, pp. 137–143, 1999.

[254] C. Plank, B. Oberhauser, K. Mechtler, C. Koch, and E. Wagner, “The Influence of Endosome-disruptive Peptides on Gene Transfer Using Synthetic Virus-like Gene Transfer Systems *,” *JBC*, vol. 269, no. 17, pp. 12918–12924, 1994.

[255] B. C. Evans, C. E. Nelson, S. S. Yu, K. R. Beavers, A. J. Kim, H. Li, H. M. Nelson, and C. L. Duvall, “Ex Vivo Red Blood Cell Hemolysis Assay for the Evaluation of pH-responsive Endosomolytic Agents for Cytosolic Delivery of Biomacromolecular Drugs,” *J. Vis. Exp. JoVE*, vol. 73, no. March, 2013.

[256] Y. Lee, G. Johnson, and J. Pellois, “Modeling of the Endosomolytic Activity of HA2-TAT Peptides with,” *Biochemistry*, vol. 49, no. 36, pp. 7854–7866, 2010.

[257] A. Won, A. Ruscito, and A. Ianoul, “Imaging the membrane lytic activity of bioactive peptide latarcin 2a,” *BBA - Biomembr.*, vol. 1818, no. 12, pp. 3072–3080, 2012.

[258] C. et al Riviere, “Internal structure of magnetic endosomes,” *Eur. Phys. J. E*, vol. 22, no. 1, pp. 1–10, 2007.

[259] B. Hirt, “Selective Extraction of Polyoma DNA from Infected Mouse Cell Cultures,” *J. Mol. Biol.*, vol. 26, no. 2, pp. 365–369, 1967.

[260] D. Lechardeur, K. Sohn, M. Haardt, P. B. Joshi, M. Monck, R. W. Graham, B. Beatty, and J. Squire, “Metabolic instability of plasmid DNA in the cytosol : a potential barrier to gene transfer,” *Gene Ther.*, vol. 6, no. 4, pp. 482–497, 1999.

[261] A. Kichler, C. Leborgne, E. Coeytaux, and O. Danos, “Polyethylenimine-mediated gene delivery : a mechanistic study,” *J. Gene Med.*, no. 3, pp. 135–144, 2001.

[262] C. Srinivasan, S. Siddiqui, L. K. Silbart, F. Papadimitrakopoulos, and D. J. Burgess, “Dual Fluorescent Labeling Method to Visualize Plasmid DNA Degradation,” *Bioconjug. Chem.*, vol. 20, no. 1, pp. 163–169, 2008.

[263] U. Schillinger, T. Brill, C. Rudolph, S. Huth, F. Kro, J. Hirschberger, C. Bergemann, and C. Plank, “Advances in magnetofection — magnetically guided nucleic acid

delivery," *J. Magn. Magn. Mater.*, vol. 293, pp. 501–508, 2005.

[264] S. W. Kamau, P. O. Hassa, B. Steitz, A. Petri-fink, H. Hofmann, M. Hofmann-amtenbrink, B. Von Rechenberg, and M. O. Hottiger, "Enhancement of the efficiency of non-viral gene delivery by application of pulsed magnetic field," *Nucleic Acids Res.*, vol. 34, no. 5, pp. e40–e40, 2006.

[265] R. J. Mannix, S. Kumar, F. Cassiola, M. Montoya-Zavala, E. Feinstein, M. Prentiss, and D. E. Ingber, "Nanomagnetic actuation of receptor- mediated signal transduction," *Nat. Nanotechnol.*, vol. 3, no. 1, p. 36, 2008.

[266] E. Tombácz, R. Turcu, V. Socoliuc, and L. Vékás, "Magnetic iron oxide nanoparticles : Recent trends in design and synthesis of magnetoresponsive nanosystems," *Biochem. Biophys. Res. Commun.*, vol. 468, no. 3, pp. 442–453, 2015.

[267] M. P. Range, "Magnefect Product Range," *nanoTherics Ltd*, vol. High Perfo.

[268] S. I. Jenkins, M. R. Pickard, N. Granger, and D. M. Chari, "Magnetic Nanoparticle-Mediated Gene Transfer to Oligodendrocyte Precursor Cell Transplant Populations Is Enhanced by Magnetofection Strategies," *ACS Nano*, vol. 5, no. 8, pp. 6527–6538, 2011.

[269] A. Fouriki and J. Dobson, "Oscillating magnet array-based nanomagnetic gene transfection of human mesenchymal stem cells," *Nanomedicine*, vol. 9, no. 7, pp. 989–997, 2014.

[270] M. Uzhytchak, A. Lynnyk, V. Zablotskii, N. M. Dempsey, A. L. Dias, M. Bonfim, M. Lunova, M. Jirsa, Š. Kubinová, O. Lunov, A. Dejneka, M. Uzhytchak, A. Lynnyk, V. Zablotskii, N. M. Dempsey, A. L. Dias, and M. Bonfim, "The use of pulsed

magnetic fields to increase the uptake of iron oxide nanoparticles by The use of pulsed magnetic fields to increase the uptake of iron oxide nanoparticles by living cells," *Appl. Phys. Lett.*, vol. 111, no. 24, p. 243703, 2017.

[271] S. Garg, A. Oran, J. Wajchman, S. Sasaki, C. H. Maris, J. A. Kapp, and J. Jacob, "Genetic tagging shows increased frequency and longevity of antigen-presenting , skin-derived dendritic cells in vivo," *Nat. Immunol.*, vol. 4, no. 9, pp. 907–912, 2003.

[272] B. K. Inaba, J. P. Metlay, M. T. Crowley, and R. M. Steinman, "Dendritic Cells Pulsed with Protein Antigens In Vitro Can Prime Antigen-specific, MHC-restricted T Cells In Situ," *J. Exp. Med.*, vol. 172, no. 2, pp. 631–640, 1990.

[273] M. Saxena and N. Bhardwaj, "Re-Emergence of Dendritic Cell Vaccines for Cancer Treatment," *Trends in Cancer*, vol. 4, no. 2, pp. 119–137, 2018.

[274] Y. Chen, X. Yao, Y. Tabata, S. Nakagawa, and J. Gao, "Gene Carriers and Transfection Systems Used in the Recombination of Dendritic Cells for Effective Cancer Immunotherapy," *Clin. Dev. Immunol.*, vol. 2010, 2010.

[275] E. J. Small, P. F. Schellhammer, C. S. Higano, C. H. Redfern, J. J. Nemunaitis, F. H. Valone, S. S. Verjee, L. A. Jones, and R. M. Hershberg, "Placebo-Controlled Phase III Trial of Immunologic Therapy with Sipuleucel-T (APC8015) in Patients with Metastatic , Asymptomatic Hormone Refractory Prostate Cancer," *J. Clin. Oncol.*, vol. 24, no. 19, pp. 3089–3094, 2006.

[276] M. A. Cheever and C. S. Higano, "PROVENGE (Sipuleucel-T) in Prostate Cancer : The First FDA-Approved Therapeutic Cancer Vaccine," *Clin. Cancer Res.*, 2011.

[277] R. Ridolfi, A. Riccobon, R. Galassi, G. Giorgetti, M. Petrini, L. Fiammenghi, M.

Stefanelli, L. Ridolfi, A. Moretti, G. Migliori, and G. Fiorentini, “Evaluation of in vivo labelled dendritic cell migration in cancer patients,” *J. Transl. Med.*, vol. 2, no. 1, p. 1, 2004.

[278] H. Jin, Y. Qian, Y. Dai, S. Qiao, C. Huang, L. Lu, and Q. Luo, “Magnetic Enrichment of Dendritic Cell Vaccine in Lymph Node with Fluorescent-Magnetic Nanoparticles Enhanced Cancer Immunotherapy,” *Theranostics*, vol. 6, no. 11, p. 2000, 2016.

[279] J. A. Frank, B. R. Miller, A. S. Arbab, H. A. Zywicke, E. K. Jordan, B. K. Lewis, L. H. Bryant, and J. W. M. Bulte, “Clinically Applicable Labeling of Mammalian and Stem Cells by Combining Radiology of Mammalian and Stem Cells by Combining Superparamagnetic Iron Oxides and Transfection Agents 1,” *Radiology*, vol. 228, no. 2, pp. 480–487, 2003.

[280] A. S. Arbab, G. T. Yocum, H. Kalish, E. K. Jordan, S. A. Anderson, A. Y. Khakoo, E. J. Read, and J. A. Frank, “Efficient magnetic cell labeling with protamine sulfate complexed to ferumoxides for cellular MRI,” *Blood*, vol. 104, no. 4, pp. 1217–1224, 2018.

[281] A. Rughetti, M. Biffoni, M. Sabbatucci, H. Rahimi, I. Pellicciotta, A. Fattorossi, and L. Pierelli, “Transfected human dendritic cells to induce antitumor immunity,” *Gene Ther.*, vol. 7, no. 17, pp. 1458–1466, 2000.

[282] E. Yuba, C. Kojima, N. Sakaguchi, A. Harada, K. Koiwai, and K. Kono, “Gene delivery to dendritic cells mediated by complexes of lipoplexes and pH-sensitive fusogenic polymer-modi fi ed liposomes,” *J. Control. Release*, vol. 130, no. 1, pp. 77–83, 2008.

[283] Y. Shen, C. Wu, T. Q. P. Uyeda, G. R. Plaza, B. Liu, Y. Han, and S. Maciej, "Elongated Nanoparticle Aggregates in Cancer Cells for Mechanical Destruction with Low Frequency Rotating Magnetic Field," *Theranostics*, vol. 7, no. 6, p. 1735, 2017.

[284] Y. Cheng, M. E. Muroski, D. C. M. C. Petit, R. Mansell, T. Vemulkar, R. A. Morshed, Y. Han, I. V Balyasnikova, C. M. Horbinski, X. Huang, L. Zhang, R. P. Cowburn, and M. S. Lesniak, "Rotating magnetic field induced oscillation of magnetic particles for in vivo mechanical destruction of malignant glioma," *J. Control. Release*, vol. 223, pp. 75–84, 2016.

[285] S. L. Schmid and L. L. Carter, "ATP Is Required for Receptor-mediated Endocytosis in Intact Cells," vol. 111, no. 6, pp. 2307–2318, 1989.

[286] V. Zablotskii, O. Lunov, A. Dejneka, L. Jastrabík, T. Polyakova, T. Syrovets, T. Simmet, V. Zablotskii, O. Lunov, A. Dejneka, and L. Jastrabı, "Nanomechanics of magnetically driven cellular endocytosis," *Appl. Phys. Lett.*, vol. 99, no. 18, p. 183701, 2011.

[287] Y. Zhu, X. Yao, X. Chen, and L. Chen, "PH-sensitive hydroxyethyl starch-doxorubicin conjugates as antitumor prodrugs with enhanced anticancer efficacy," *J. Appl. Polym. Sci.*, vol. 132, no. 45, pp. 1–7, 2015.

[288] S. Awasthi and R. A. Cox, "Transfection of murine dendritic cell line (JAWS II) by a nonviral transfection reagent," *Biotechniques*, vol. 35, no. 3, pp. 600–605, 2003.

[289] P. Corish and C. Tyler-smith, "Attenuation of green fluorescent protein half-life in mammalian cells," *Protein Eng.*, vol. 12, no. 12, pp. 1035–1040, 1999.

[290] S. Subramanian and F. Srienc, “Quantitative analysis of transient gene expression in mammalian cells using the green fluorescent protein,” *J. Biotechnol.*, vol. 49, no. 1–3, pp. 137–151, 1996.

[291] A. P. F. et al. Trombone, “Endocytosis of DNA-Hsp65 Alters the pH of the Late Endosome / Lysosome and Interferes with Antigen Presentation,” *PLoS One*, vol. 2, no. 9, p. e923, 2007.

[292] Z. L. Zhou, X. X. Sun, J. Ma, C. H. Man, A. S. T. Wong, A. Y. Leung, and A. H. W. Ngan, “Mechanical oscillations enhance gene delivery into suspended cells,” *Sci. Rep.*, vol. 6, p. 22824, 2016.

[293] C. Wilhelm, A. Cebers, J. C. Bacri, and F. Gazeau, “Deformation of intracellular endosomes under a magnetic field,” *Eur. Biophys. J.*, vol. 32, no. 7, pp. 655–660, 2003.

[294] C. Wilhelm and F. Gazeau, “Magnetic nanoparticles : Internal probes and heaters within living cells,” *Magn. Magn. Mater.*, vol. 321, no. 7, pp. 671–674, 2009.

[295] L. Chen, C. Chen, P. Wang, and T. Song, “Mechanisms of Cellular Effects Directly Induced by Magnetic Nanoparticles under Magnetic Fields,” *J. nanopmaterials*, vol. 2017, 2017.

[296] T. Yue, X. Zhang, and F. Huang, “Molecular modeling of membrane responses to the adsorption of rotating nanoparticles: Promoted cell uptake and mechanical membrane rupture,” *Soft Matter*, vol. 11, no. 3, pp. 456–465, 2014.

[297] M. Colombo, S. Carregal-Romero, M. F. Casula, L. Gutierrez, M. P. Morales, I. B. Bohm, J. T. Heverhagen, D. Prosperi, and W. J. Parak, “Biological applications of

magnetic nanoparticles," *Chem. Soc. Rev.*, vol. 41, no. 11, pp. 4306–4334, 2012.

[298] C. Corot, P. Robert, J. Idée, and M. Port, "Recent advances in iron oxide nanocrystal technology for medical imaging ☆," *Adv. Drug Deliv. Rev.*, vol. 58, no. 14, pp. 1471–1504, 2006.

[299] S. S. T. de Almeida, C. H. Horst, C. Soto-Sánchez, E. Fernandez, and R. T. de Almeida, "Delivery of miRNA-Targeted Oligonucleotides in the Rat Striatum by Magnetofection with Neuromag ®," *Molecules*, vol. 23, p. 1825, 2018.

[300] V. V. Mody, A. Cox, S. Shah, A. Singh, W. Bevins, and H. Parihar, "Magnetic nanoparticle drug delivery systems for targeting tumor," *Appl. Nanosci.*, vol. 4, no. 4, pp. 385–392, 2014.

[301] R. Ensenauer, D. Hartl, J. Vockley, A. A. Roscher, and U. Fuchs, "Efficient and gentle siRNA delivery by magnetofection," *Biotech. Histochem.*, vol. 86, no. 4, pp. 226–231, 2011.

[302] Z. Wang and A. Cuschieri, "Tumour cell labelling by magnetic nanoparticles with determination of intracellular iron content and spatial distribution of the intracellular iron," *Int. J. Mol. Sci.*, vol. 14, no. 5, pp. 9111–9125, 2013.

[303] U. Griesenbach and E. W. Alton, "Gene transfer to the lung: Lessons learned from more than 2 decades of CF gene therapy," *Adv. Drug Deliv. Rev.*, vol. 61, no. 2, pp. 128–139, 2009.

[304] S. Castellani, C. Orlando, A. Carbone, S. Di Giogia, and M. Conese, "Magnetofection Enhances Lentiviral-Mediated Extracellular and Cellular Barriers," *Genes (Basel).*, vol. 7, no. 11, p. 103, 2016.

[305] Micromod, "Technical data sheet," p. 2017, 2017.

[306] M. M. Vernon, “ENHANCING MAGNETIC NANOPARTICLE-BASED DNA TRANSFECTION: INTRACELLULAR-ACTIVE CASSETTE FEATURES,” University of Florida, 2014.

8 Appendix

8.1 Methods

8.1.1 Calculation of magnetic force of MNPs on the cell membrane

A system based on the forces acting on the cell membrane was proposed to estimate the order of magnitude of the forces exerted by a magnetic nanoparticle on the cell surface in the presence of a magnetic field and assess whether that order of magnitude is comparable to those required to deform the cell cytoskeleton.[286]

The force exerted on a magnetic nanoparticle on a non-uniform magnetic field (magnetic field gradient) with a magnetic force *m* is described by the following equation:

$$F = (m \cdot \nabla) B \qquad (5)$$

The only magnetic field in the system is the one produced by Magnefect-nano™ (dB/dz) and ranges from 100 to 200 Tm^{-1}. The value of saturation magnetization (M_S) provided by the manufacturer is 63 Am^2kg^{-1} of iron (H > 800 kAm^{-1})[305]. Eq. 5 can be expressed as[12]:

$$F = M M_S \frac{dB}{dr} \qquad (6)$$

M being the estimated mass of Fe_3O_4 per particle.

TEM analysis has previously confirmed that the magnetic core of the Micromod-Nanomag-D nanoparticles is formed of a cluster of individual Fe_3O_4 nanocrystals (9 nm diameter) embedded on a dextran matrix (Figure 8.1).

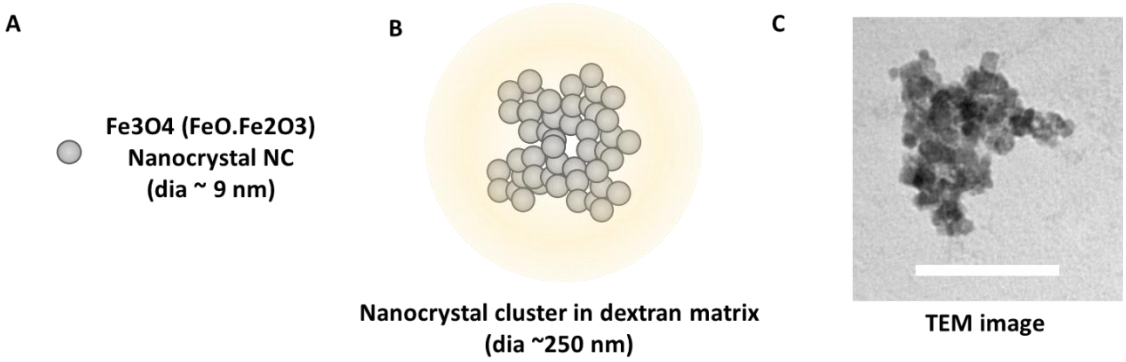

Figure 8.1 Schematic of Micromod-dextran COOH 250 nm MNPs.
Fundamental magnetic unit in Micromod-iron oxide-dextran coated particles. Iron oxide nanocrystals (NC) of approximately 9 nm diameter. B. Schematic representation of 250 nm Micromod-iron oxide-dextran coated particles magnetic core formed of clustered iron oxide NC (Cluster). C) Representative TEM image of 250 nm Micromod-iron oxide core (NC cluster). Scale bar 100 nm.

Those nanocrystals are the fundamental unit of magnetic material in the particles, in other words, the units experiencing the magnetic force exerted by the magnetic field and their volume was approximated to that of a sphere of 9 nm diameter. Table 13 summarises the calculation of the magnetic force exerted by a single Fe_3O_4 NC.

Table 13 Calculation of magnetic force experienced on a single Fe_3O_4 nanocrystal (NC) of 9 nm.

density Fe_3O_4	Diameter	Volume	Mass	Ms	dB/dx	F
kg/m^3	m	m^3	kg	Am^2/kg	T/m	pN
5170	$9.00x10^{-9}$	$3.82x10^{-25}$	$1.78\ x10^{-29}$	63	200	$2.49\ x10^{-5}$

The total number of NC per cluster was calculated based on the following approximations:

1- NC cluster was approximated to a sphere of 100 nm diameter (Figure 3.2).

2- Approximately 70% of the weight of the particles corresponds to Fe_3O_4, the remaining 30% being dextran (measured by Thermogravimetric analysis Figure 8.2).

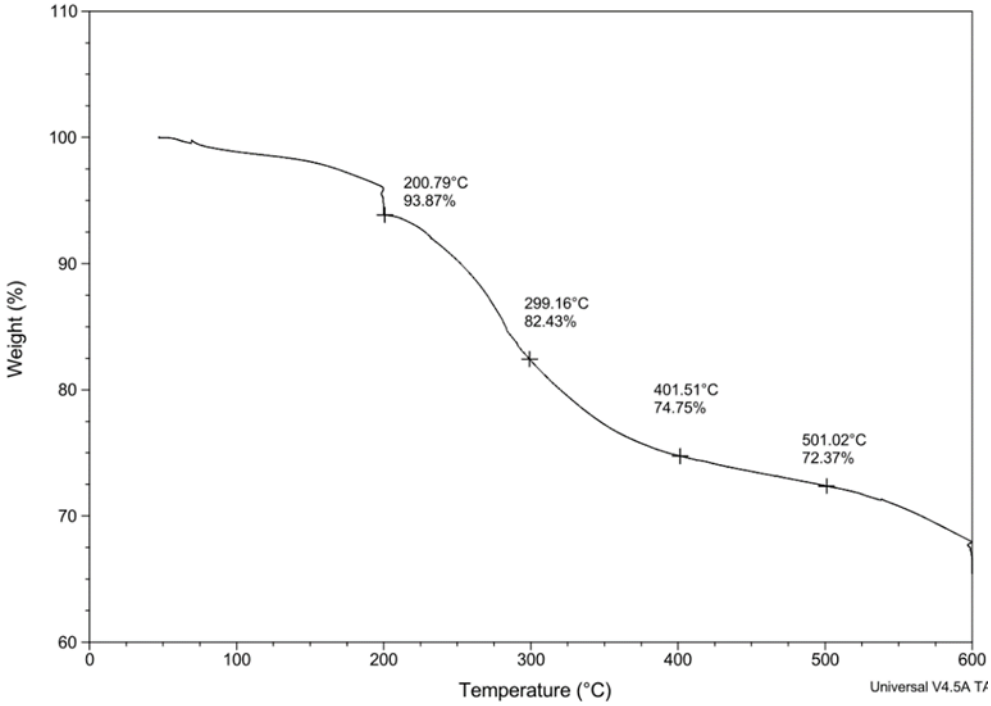

Figure 8.2 Representative TGA curve of Micromod-dextran COOH 250 nm MNPs.
72% w/w of dry sample corresponds to the inorganic core. The remaining 28% of the sample corresponds to the dextran matrix.

Table 14 Calculation of magnetic force experienced on a single Micromod-dextran COOH 250 nm magnetic nanoparticle, with a magnetic core of 100 nm.

Size NC	**Vol NC**	**Size Cluster**	**Vol Cluster**	**density dextran**	**density Fe_3O_4**	**Cluster mass***	**NCs in cluster (number)§**	**F cluster†**
m	m^3	m	m^3	kg/m^3	kg/m^3	kg		pN
9.00×10^{-9}	3.82×10^{-25}	1.00×10^{-7}	5.24×10^{-22}	1100	5170	1.28294×10^{-18}	2.35×10^{6}	5.85

**The mass of the magnetic cluster was calculated according to the previously stablished 70:30 ratio Fe_3O_4:dextran.*

§The number of NC per cluster was calculated by dividing the total mass of the cluster by the individual mass of one NC (NC in cluster).

†The force exerted by all the NC in a cluster (F cluster), was determined by multiplying the number of NC per cluster by the force exerted by a single NC (table 13)

8.2 Figures

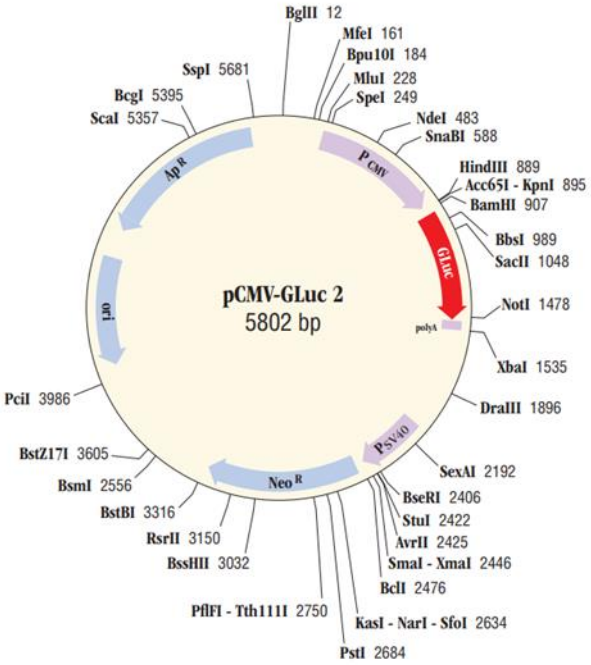

Figure 8.4 Annotated plasmid map of pCMV-Gluc 2. Plasmid map obtained from NEB.

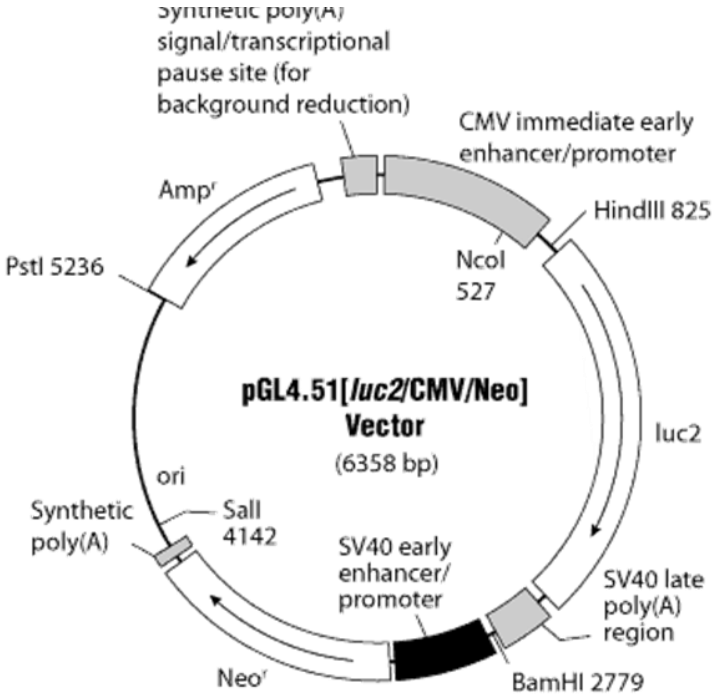

Figure 8.3 Annotated plasmid map of pGL4.51. Plasmid map obtained from Promega.

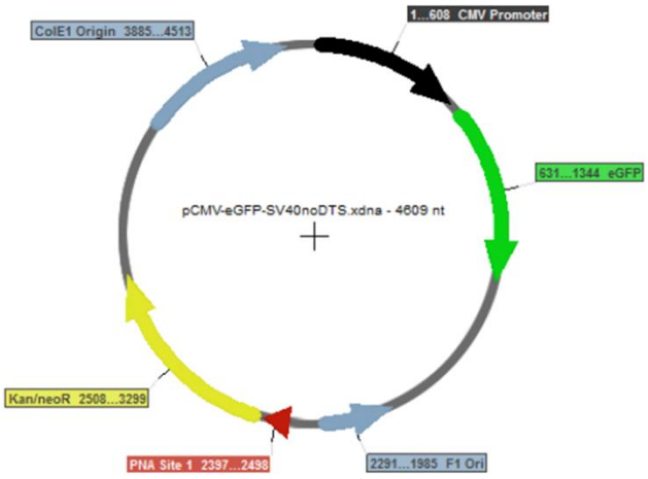

Figure 8.5 Annotated plasmid map of pCMV-eGFP-SV40noDTS. Plasmid map generated using Serial Cloner version 2.6 on a PC running Windows 7.[306]

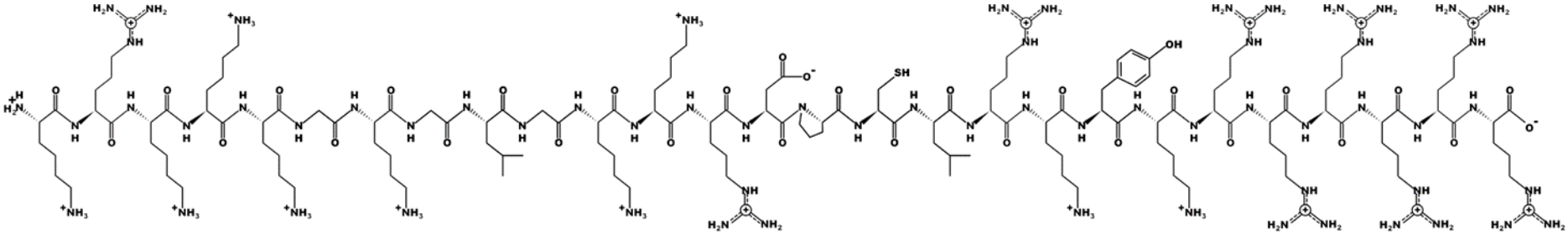

Figure 8.6 Amino acid sequence of GET peptide P21-8R (PR).

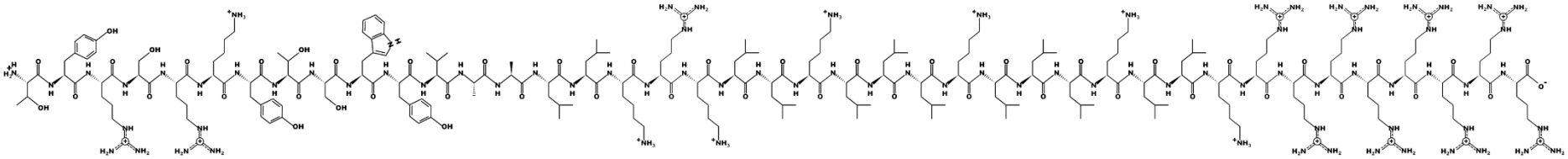

Figure 8.7 Amino acid sequence of GET peptide FLR-LK15-8R (FLR).

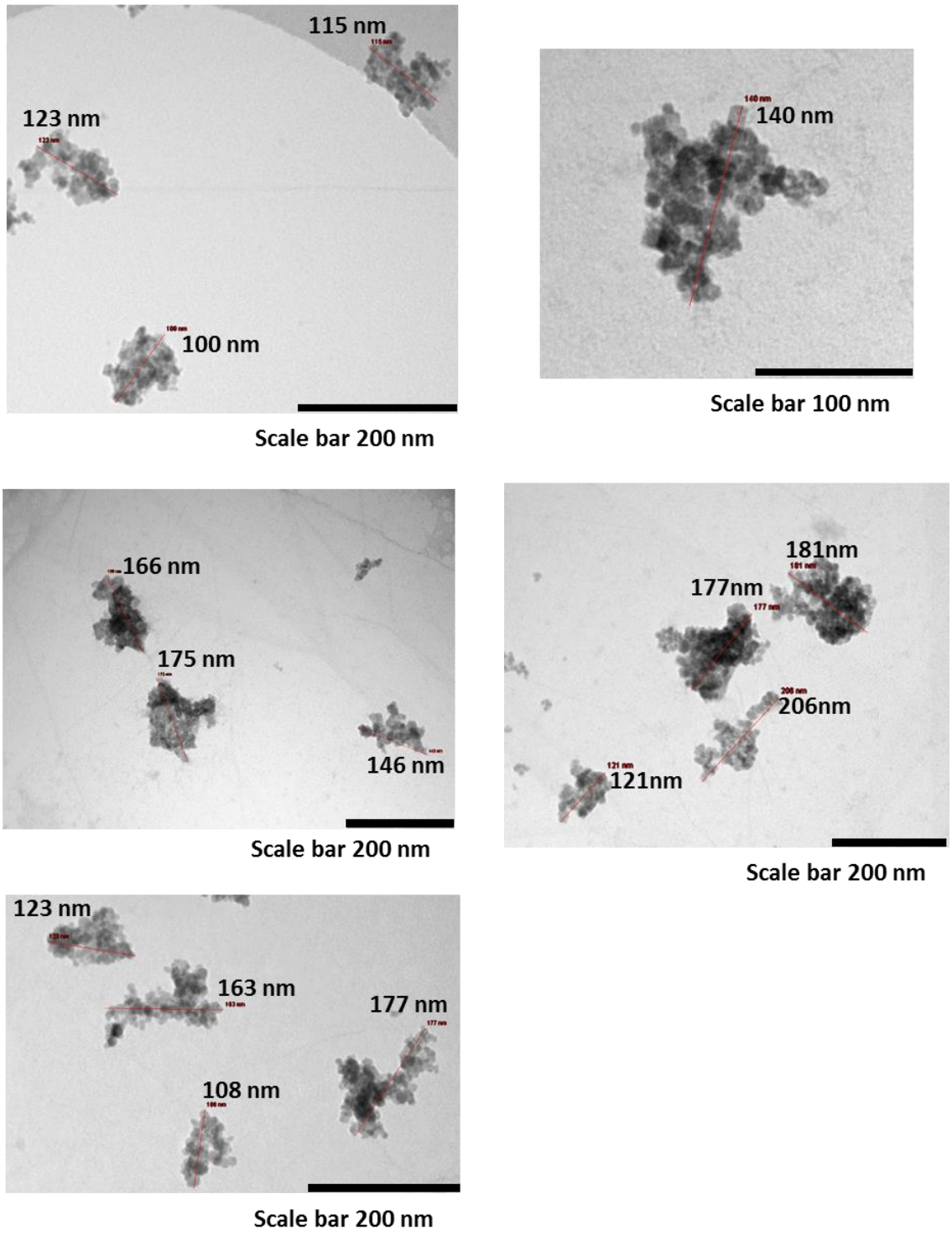

Figure 8.8 Representative TEM images of dextran coated Micromod COOH 250 nm magnetic core. Core diameter was measured in situ (red labelling) and then confirmed by ImageJ analysis (black font).

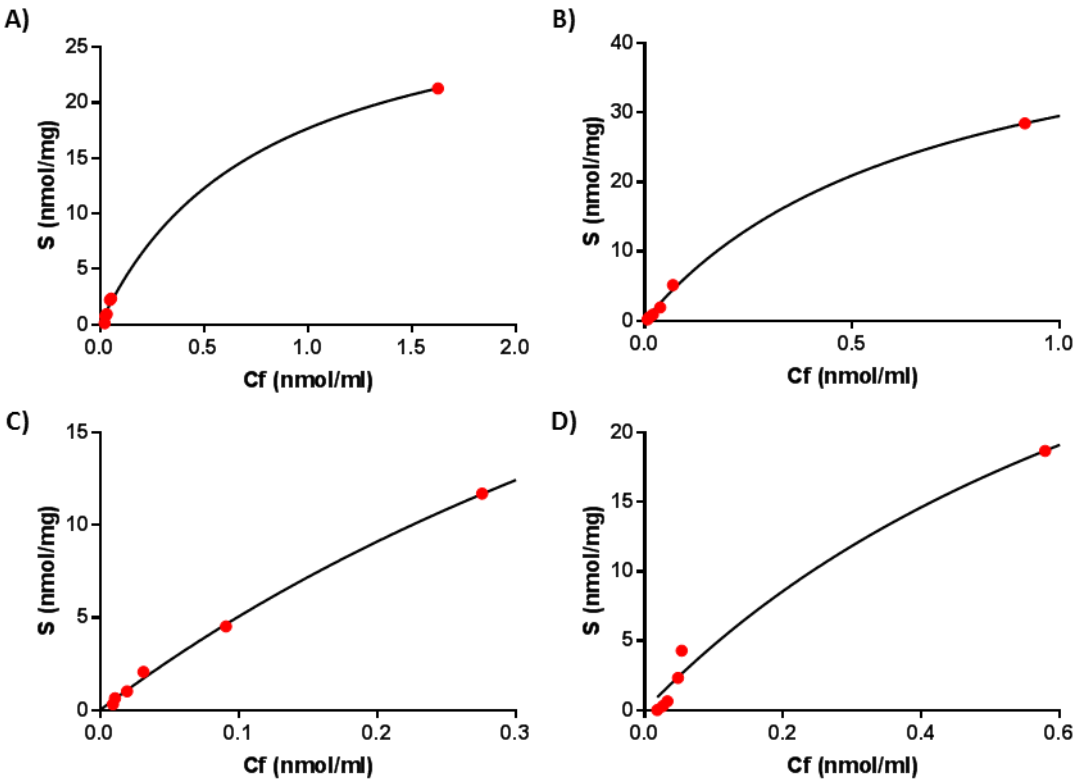

Figure 8.9 Langmuir fitting curve for PR adsorption on MNPs.
Red dots represent the adsorption of PR-T measured on MNPs, black line represents the non-linear fitting of Langmuir isotherm. Each graph represents an independent experiment. Each individual data point represents the mean of three instrumental repeats.

Table 15 Langmuir constants for PR adsorption on MNPs.

	S_{max} (nmol/mg)	K (ml/nmol)	SSR (nmol²/mg²)
PR-T-MNPs (A)	31.6	1.3	1.03
PR-T-MNPs (B)	50	1.44	1.27
PR-T-MNPs (C)	46.1	1.24	0.19
PR-T-MNPs (D)	49.5	1.05	5.69

Table shows parameters of adsorption S_{max} (maximum concentration of PR that can adsorb onto 50 µg of MNPs) as well as the constant of adsorption K and the sum of squared residuals (SSR) corresponding to the Langmuir fitting curves displayed on Figure 8.9.

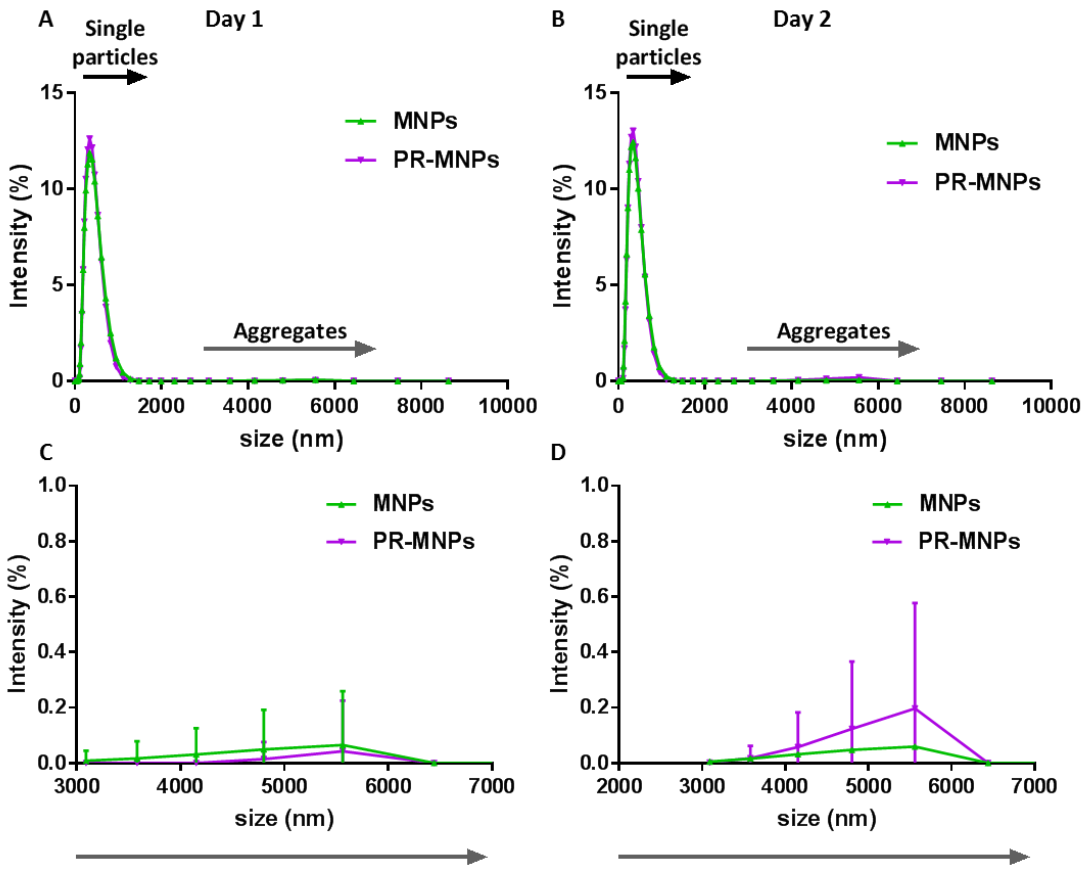

Figure 8.10 MNPs and PR-MNPs size distribution in FCS.
Apparent diameter of the particles obtained by DLS for 50 µg/ml of MNPs and 50 µg/ml MNPs incubated with 4 nmol/mg MNPs in 10% FCS v/v in water. DLS was measured on day 1 (particle formation) and day 2 (24 hours after particle formation) looking to most accurately reproduce particle delivery to cells in vitro. Plots A and B represent full size distribution. Black arrow represents single particles size distribution area (0-1500 nm). Grey arrow represents aggregates size distribution (2000-7000 nm). Values represent mean intensity. Plots C and D represent aggregate size distribution plot (3000-7000 nm). Values represent mean ± s.d. intensity (n=6 technical repeats).

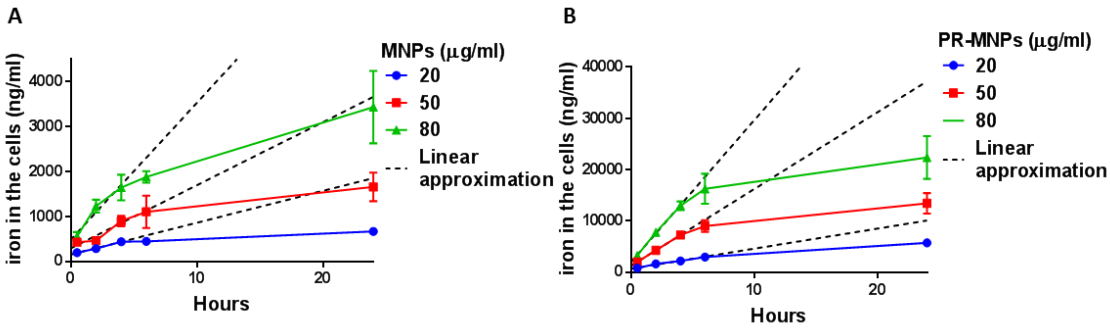

Figure 8.11 MNPs concentration in the cells increases linearly during the first 4 hours of uptake.

Total concentration of iron in the cells for naked MNPs delivery (A) and PR-MNPs (B) over time in NIH3t3s. Increasing dosages of MNPs (20 µg, 50 µg and 80 µg) were delivered in order to assess effect of concentration on uptake. PR-MNPs were delivered at 4 nmol/mg MNPs. Iron content in the cells was analysed 0.5, 1, 2, 4, 6 and 24 hours post-delivery using Inductively Coupled Plasma (ICP). Linear approximation was calculated using the iron uptake interval between 0.5 and 4. Linear regression was adjusted to the iron uptake mean by GraphPad Prism.

Table 16 Linear fit for MNPs concentration in the cells during the first 4 hours of uptake.

	MNPs			PR-MNPs		
Concentration (µg/ml)	**Slope**	**Intercept**	**R^2**	**Slope**	**Intercept**	**R^2**
20	70.88 ± 4.869	154.4 ± 12.65	0.9953	391.4 ± 79.11	709.3 ± 205.5	0.9607
50	140.3 ± 55.19	294.4 ± 143.4	0.8661	1499 ± 2.575	1276 ± 6.691	1
80	304.5 ± 68.95	484.8 ± 179.1	0.9512	2765 ± 125.4	2050 ± 325.8	0.9979

Slope, Intercept and R square of the linear approximation in the linear range of particle uptake for Figure 8.11. Linear approximation was calculated using the iron uptake interval between 0.5 and 4. Linear regression was adjusted to the iron uptake mean by GraphPad Prism.

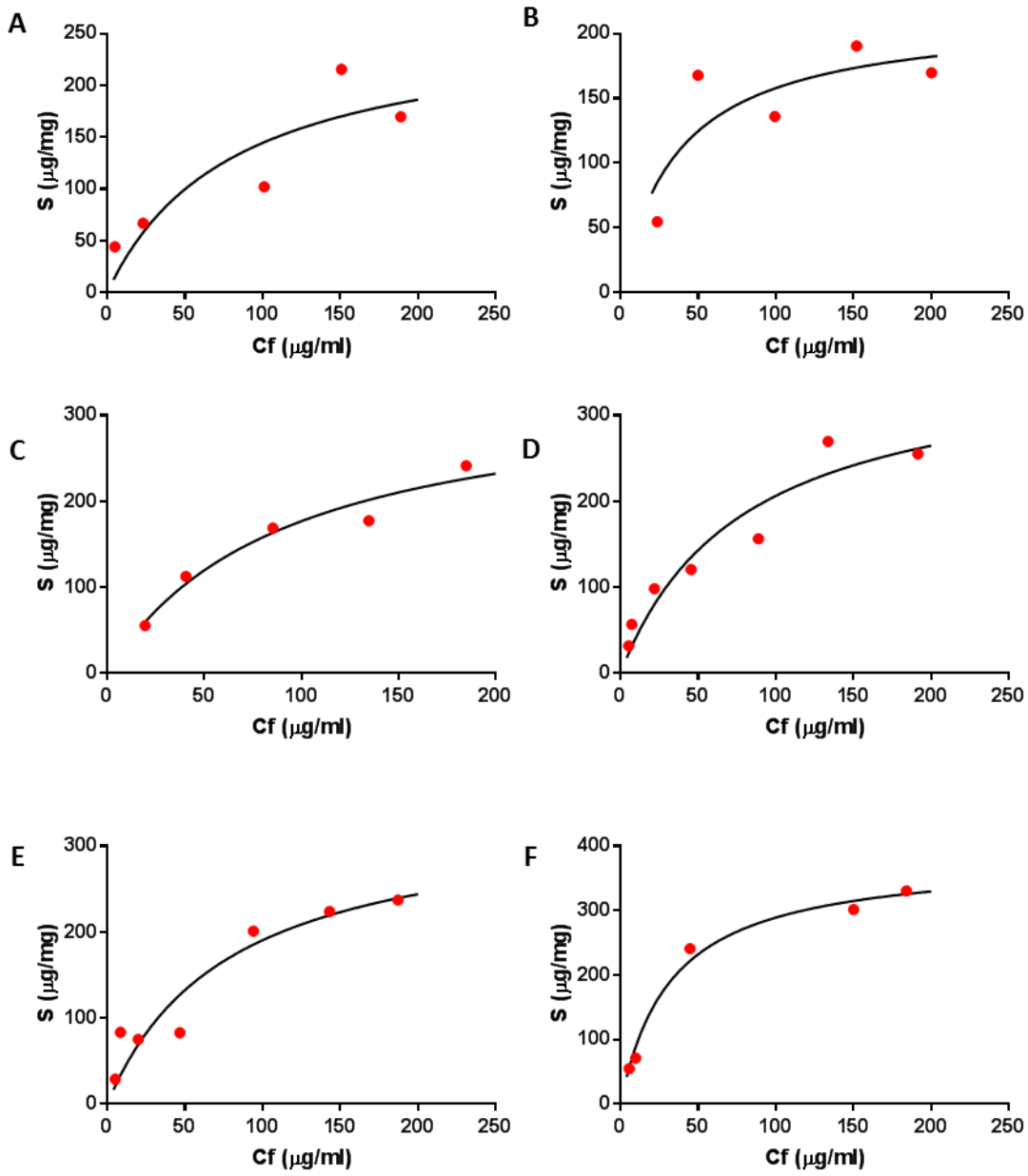

Figure 8.12 Langmuir fitting curve for BSA adsorption on MNPs.

Red dots represent the adsorption of PR measured on MNPs, black line represents the non-linear fitting of Langmuir isotherm. Each graph represents an independent experiment. Each individual data point represents the mean of three instrumental repeats.

Table 17 Langmuir constants for BSA adsorption on MNPs.

	S_{max} (µg/mg)	K (ml/µg)	SSR ($µg^2/mg^2$)
GET-BSA (A)	262	0.012	5027.5
GET-BSA (B)	215.4	0.027	3696.75
GET-BSA (C)	337.6	0.012	938.01
GET-BSA (D)	339.3	0.013	4798.82
GET-BSA (E)	368.9	0.013	4243.52
GET-BSA (F)	383.1	0.031	855.64

Table shows parameters of adsorption S_{max} (maximum concentration of BSA that can adsorb onto 50 µg of MNPs) as well as the constant of adsorption K and the sum of squared residuals (SSR) corresponding to the Langmuir fitting curves displayed on Figure 8.12.

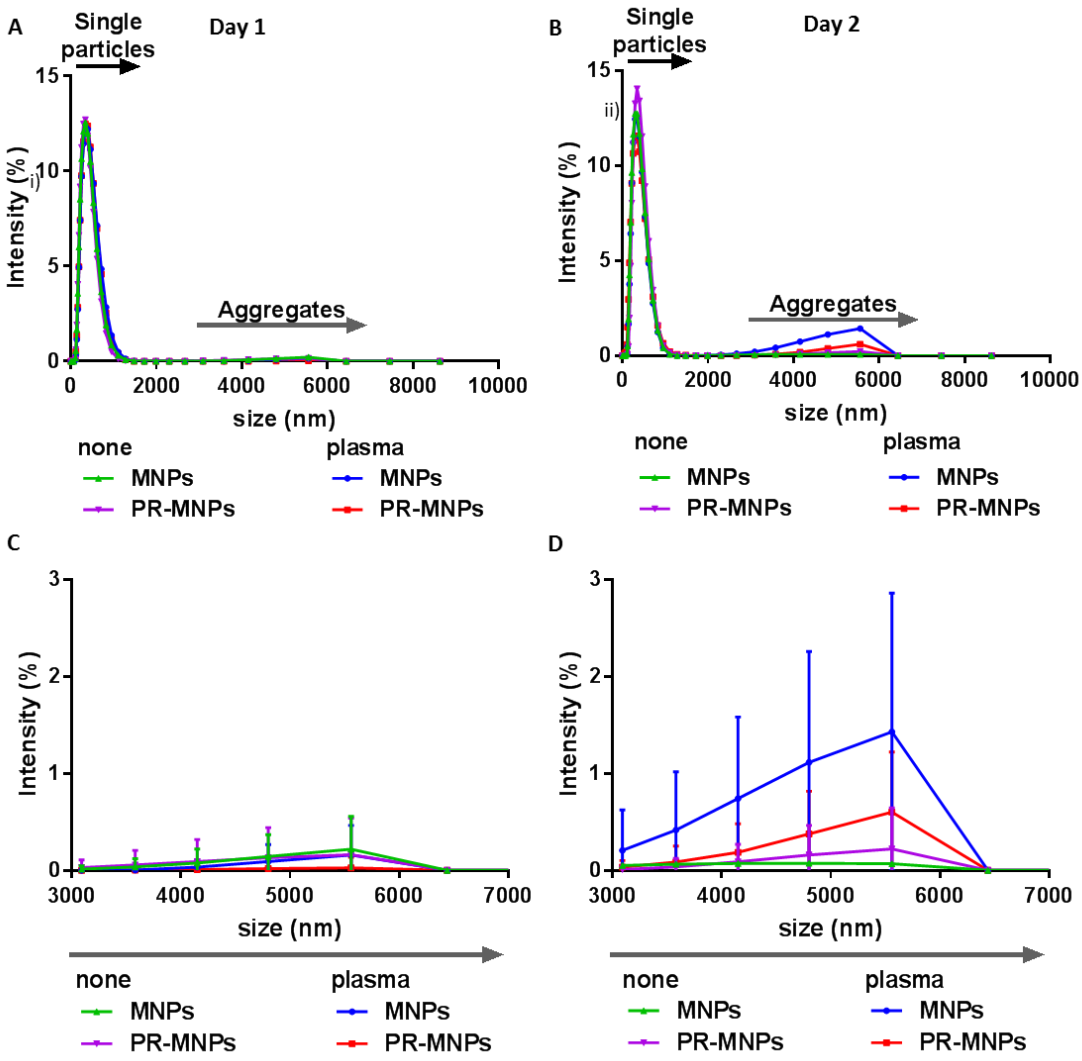

Figure 8.13 MNPs and PR-MNPs size distribution in water and plasma.

Apparent diameter of the particles obtained by DLS for 50 µg/ml of MNPs and 50 µg/ml MNPs incubated with 4 nmol/mg MNPs in water (none) and 5% plasma v/v in water (plasma). DLS was measured on day 1 (particle formation) and day 2 (24 hours after particle formation) looking to most accurately reproduce particle delivery to cells in vitro. Plots A and B represent full size distribution. Black arrow represents single particles size distribution area (0-1500 nm). Grey arrow represents aggregates size distribution (2000-7000 nm). Values represent mean intensity. Plots C and D represent aggregate size distribution plot (3000-7000 nm). Values represent mean ± s.d. intensity (n=6 technical repeats).

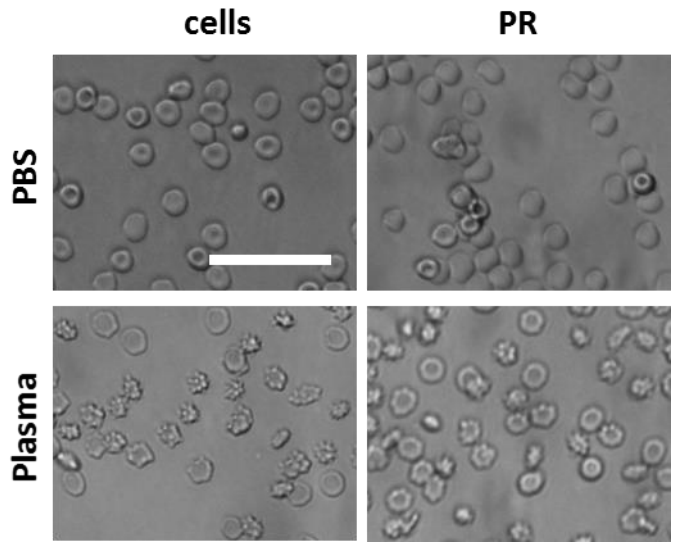

Figure 8.14 PBS triggers minor changes in erythrocyte morphology, independent of the presence of PR.

Close up image of effect of PR on erythrocytes after 5 mins and 30 mins. Scale bar 20 µm.

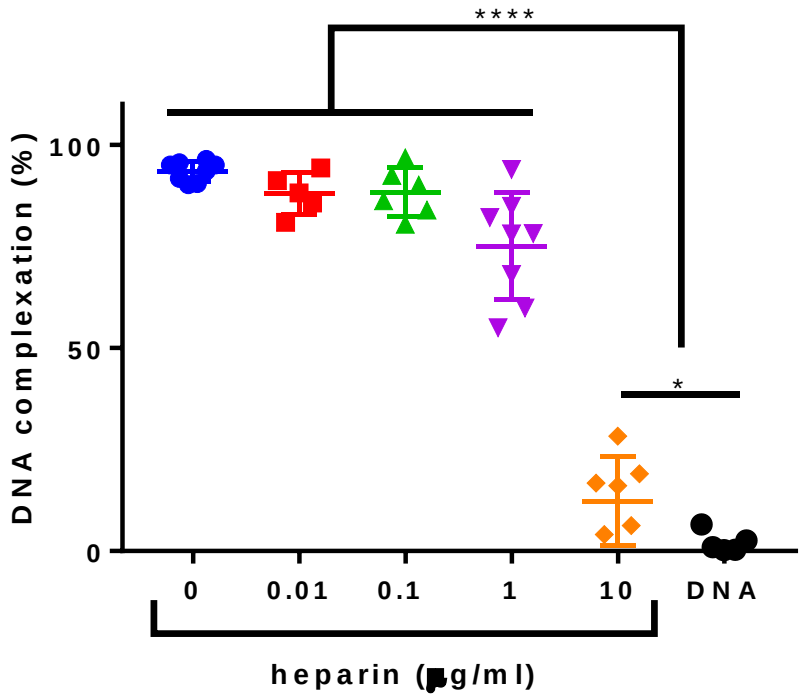

Figure 8.15 High concentrations of heparin destabilize the FLR-DNA complex.

*Percentage of DNA complexation was measured by using YO-PRO-1. As previously described, first of all DNA was incubated with YO-PRO-1 to form the fluorescent complex DNA-YO-PRO. Then, the DNA-YO-PRO complex was incubated with FLR. The significant reduction on fluorescence indicated complete DNA complexation by FLR. Finally, FLR-DNA was incubated with increasing concentrations of heparin: 0, 0.01, 0.1, 1 and 10 µg/ml in water for 15 min. FLR has a strong affinity for heparin and binds preferentially to it. As a result, DNA molecules become available to interact with YO-PRO-1 producing a fluorescent signal proportional to the amount of free DNA. DNA alone was used to calculate 100% of free DNA (0% complexed DNA). n=3 technical repeats, 1-3 replicates per repeat. *p<0.05, **** p<0.0001, Tukey's multiple comparisons test.*